Stellingen

behorenden bij het proefschrift

Tweede-orde sluitingsmodellering van transitionele en instationaire turbulente stromingen

van

Ibrahim Hadžić

1. Turbulentie die wordt onderworpen aan alleen cyclische compressie en expansie kan niet in stand blijven en zal onafhankelijk van de begintoestand uitsterven.

2. Een kleine verandering van een modelcoëfficiënt van een lage-Reynolds tweede-orde sluitingsmodel leidt vaak tot een aanzienlijke verandering in de voorspelde resultaten.

3. Instabiliteit van een numerieke rekencode kan ook veroorzaakt worden door dat het fysische model ofwel de implementatie hiervan incorrect is.

4. Het hebben van een groot aantal ideeën over een bepaald onderzoeksonderwerp hoeft nog niet te betekenen dat daar ook goede ideeën bijzitten.

5. De directe numeriek simulatie van een volledige vliegtuig blijft gedurende vele tientallen jaren nog onbereikbaar. We mogen ons gelukkig prijzen dat we Reynolds-gemiddelde turbulentiemodellen tot onze beschikking hebben.

6. Omdat sommige wiskundige modellen vele jaren geleden, toen de oplosmethodes waren besmet door numerieke fouten vanwege de geringe computerkracht, zijn ontwikkeld zouden deze opnieuw moeten worden bekeken en herzien.

7. Bij de productie van hand-geknoopte tapijten is kinderarbeid een direct resultaat van de wens van de aankopers om deze producten zo voordelig mogelijk te krijgen.

8. De term 'etnische zuivering' is uitgevonden om de ware betekenis van de daad te verbergen.

9. Met het oog op de grote vooruitgang in treinreizen, informatie- en computertechnologie is het verbluffend dat het onlangs onmogelijk is geworden om op het treinstation van Delft en andere kleine steden in Nederland een kaartje te kopen voor een internationale bestemming.

10. Terwijl we op zoek zijn naar oplossingen voor een probleem, stuiten we vaak op andere onverwachte problemen, die eerst opgelost moeten worden.

Propositions

belonging to the dissertation

Second-Moment Closure Modelling of Transitional and Unsteady Turbulent Flows

by

Ibrahim Hadžić

1. Turbulence subjected to only cyclic compression and expansion cannot sustain and it will die out irrespective of the initial state.

2. A slight change in a model coefficient of low-Re-number second-moment closure models often leads to a notable change in the prediction results.

3. Instability of a numerical code indicates also that either the physical model or its implementation is incorrect.

4. Having a large number of ideas about a particular research subject can mean having no good ideas.

5. The direct numerical simulation of an entire aircraft is inconceivable and will remain so for many decades to come. We are fortunate to have Reynolds-averaged turbulence closures at our disposal.

6. Since some mathematical models were developed many years ago, when the solution methods were contaminated by numerical errors because of small computer power, they should be revisited and revised.

7. In the manufacturing of hand-knotted carpets, child labour is a direct result of the purchasers' desire to have these products as cheap as possible.

8. The term 'ethnic cleansing' was invented to conceal the true meaning of the deed.

9. Despite great advancement in train transportation, informatics and computer technologies, it is surprising that it has recently become impossible to buy a ticket for an international destination at the train stations in Delft and others small cities in the Netherlands.

10. While we seek solutions of a problem, other unexpected problems often appear and have to be solved first.

Second-Moment Closure Modelling of Transitional and Unsteady Turbulent Flows

Second-Moment Closure Modelling of Transitional and Unsteady Turbulent Flows

Proefschrift

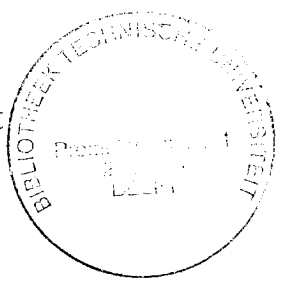

ter verkrijging van de graad van doctor
aan de Technische Universiteit Delft,
op gezag van de Rector Magnificus prof. ir. K. F. Wakker
in het openbaar te verdedigen ten overstaan van een commissie,
door het College voor Promoties aangewezen,
op maandag 8 februari 1999 te 13.30 uur

door

Ibrahim HADŽIĆ
Diplomirani mašinski inženjer, Univerzitet u Sarajevu
geboren te Dubrave Donje, Bosnië en Herzegovina

Dit proefschrift is goedgekeurd door de promotor:
Prof. Dr. Dipl.-Ing. K. Hanjalić

Samenstelling promotiecommissie:

Rector Magnificus	voorzitter
Prof. Dr. Dipl.-Ing. K. Hanjalić	Technische Universiteit Delft, promotor
Prof. Dr. Dr. h.c. F. Durst	Friedrich-Alexander-Universität Erlangen-Nürnberg, Deutschland
Prof. Dr. D. Laurence	Ecole Centrale de Lyon, France
Prof. dr. ir. H. W. M. Hoeijmakers	Universiteit Twente
Prof. dr. ir. F. T. M. Nieuwstadt	Technische Universiteit Delft
Prof. dr. ir. H. E. A. van den Akker	Technische Universiteit Delft
Dr. ir. R. A. W. M. Henkes	Shell International, Amsterdam

ISBN 90-6464422-5
Printed by Ponsen & Looijen bv, Wageningen.

Contents

CHAPTER 1

Introduction

This thesis deals with computational modelling of the wall-bounded fluid flows in arbitrary geometries at transitional and higher Re-numbers using second-moment closure statistical turbulence models. Accurate prediction of these flows is of vital importance for design of many engineering devices. Examples of situations where such predictions are needed are numerous and include external and internal aerodynamics. Of particular importance are the flows in turbines, compressors, pumps, heat exchangers, internal combustion engines, as well as flows around vehicles. Transitional flows are important also in bio-engineering and in mammal organisms (air flow in lungs, blood in vanes and arteries).

Besides experiments, several computational techniques are nowadays in use for research and design purposes concerning turbulent fluid flows. Direct Numerical Simulation (DNS) solves the Navier-Stokes equations, which describe the fluid flow, with appropriate boundary conditions on a such fine numerical grid and with a such small time step so that all eddy scales in turbulent motions of fluid are resolved. The only uncertainty involved is the numerical error. Since DNS requires a very large computer power and time, it is nowadays limited only to flows at relatively small Reynolds numbers and in simple geometries. The number of grid points used is up to tens of millions and such computations last for months on the massively parallel computers. DNS provides a great deal of information on turbulence phenomena enabling a deep insight into it. It also supplies essential information for the turbulence modelling. For these reasons, DNS is gaining on importance, but mainly as a research tool.

An increasingly popular technique for simulation of turbulent flows is the Large Eddy Simulation (LES). It is also an unsteady approach which solves Navier-Stokes equations on a coarser mesh and with a larger time step than DNS but which are still fine enough to resolve large scale motions. The effects of the unresolved small scale motions are modelled. LES has been, with moderate to large success, already applied to computations of turbulent flows at relatively complex conditions. However, LES requires also significant computer resources and long time computations. Spalart *et al.* (1997) estimated, highly optimistically, as they said, that for a LES of an airplane wing one needs about 10^{11} grid points and 5×10^6 time steps on unstructured adaptive grids. With current trend of increase in computer power (a factor of 5 every 5 years) they foresee that resolving this task only may become feasible in the forth decade of the next century!

Single-point statistical modelling of turbulence is nowadays the most widely spread approach for predicting turbulent flows. It is based on Reynolds averaging (Reynolds 1894) of the instantaneous fluctuating quantities. This approach involves modelling of the second-moment correlation of the fluctuating velocity, which appear in the Reynolds averaged Navier-Stokes (RANS) equations. Depending on the level at which the modelling is applied, several different approaches of the statistical modelling of turbulence are to be distinguished. Eddy-viscosity model (EVM) is an algebraic representation of the second-moment correlation where the needed velocity-, time- and length-scales of turbulence are supplied usually by transport equations for two of the scales or any combinations of them. Although numerous shortcomings of the EVM approach have been well documented in the literature, this approach is still the most widely used turbulence model for engineering design. Non-linear eddy-viscosity models, currently under development and investigation, are a possible route to overcome the defects of conventional linear EVMs. A mathematically and physically better founded approach with the framework of RANS modelling is the second-moment closure (SMC) which seeks solution of the differential transport equations for the second-moment correlations of the fluctuating quantities. Some terms in the exact equations have to be modelled. Solving the transport equations for turbulence quantities offers a large potential because all particular phenomena which drive these quantities are separately accounted for.

Computations of turbulent wall flows in the framework of RANS modelling are carried out with either solving the model equations up to the wall (low-Re-number approach) or applying the wall functions (high-Re-number approach) which utilise some empirical laws to set boundary conditions for the mean flow and turbulence quantities relatively far from the wall (outside the viscous region). Essential difference between these two approaches is that the low-Re-number approach requires a more sophisticated turbulence model and demands a much finer numerical mesh in the wall vicinity than the wall function approach. It is argued, however, that the low-Re-number approach may be unavoidable if transition phenomena and accurate wall friction and heat transfer are in focus. Successful reproduction of the near wall second-moment statistics qualifies this approach for computations of a variety of engineering flows.

DNS of turbulent wall flows performed in the last decade and the databases they provided, made a large impact on the development of turbulence models for the prediction of wall turbulent flows. These data were especially useful for the development and validation of the SMC models on the basis of the term-by-term modelling and particularly for the low-Re-number models. The mathematical models aimed at the computation of turbulent flows are usually developed and tuned to satisfy the most basic flows such as homogeneous shear flows and channel and boundary layer flows and only occasionally are tested in more complex cases with separation, though restricted to rectangular geometries (e.g. back-step flows). In order to be applied to the prediction of complex flows, as needed in engineering and industrial applications, turbulence models have to be tested in more severe geometrical and physical conditions. Arbitrary shape of the wall boundary imposes a large deal of physical complexity and requires advanced numerical solvers.

1.1 The scope of the research

The present work has two main objectives:

- to investigate possibilities for modelling of transitional wall flows by second-moment closure modelling and to provide a comparative and critical analysis of the existing models, and to contribute to their improvement and validation
- to establish a reliable, accurate and efficient numerical solution procedure for solving the second-moment closure transport models for arbitrary two-dimensional flow domains with applying both the wall functions and integration of the model equations up to the wall with applying the exact wall boundary conditions.

Prior to this work, another PhD thesis (Jakirlić 1997) under supervision of Professor K. Hanjalić was aimed to model development in the framework of the low-Re-number second-moment closure. In the course of that work several different modelling strategies were investigated. The model emerged was first tested in several equilibrium and non-equilibrium attached, separating and rotating flows in a broad range of Re numbers and compared with a variety of experimental and DNS results (Jakirlić 1997). Considered were: channel flows, strongly accelerated boundary layers and sink flows including also cases with laminarisation, strongly decelerated boundary layers with increasingly adverse pressure gradient leading to separation, three-dimensional boundary layers subjected to traverse shear and stream-wise acceleration, flow over surface mounted fence and rib, backward facing step flow and pipe expansion at low and high Re numbers, and swirling and rotating flows. Being focussed on model development and validation this analysis was restricted to orthogonal flow domains.

The present author was partly involved in the joint research and contributed to the final formulation of the model coefficients by expanding the optimisation process to a class of transitional flows which included oscillating boundary layers and by-pass transition on the flat plate with a sharp leading edge.

Subsequently, the present author explored some alternative approaches to modelling some of the crucial terms in the transport equation for Reynolds-stresses as well as possible model improvements. Specifically, a new approach to providing an alternative and a new general derivation of the pressure-strain model was proposed. Also, a new model for stress dissipation rate tensor is derived which does not use the wall topology parameters. Finally, a critical analysis of conventional models of dissipation rate ε equation is proposed with suggestion for possible improvement for non-equilibrium flows. Further, the model validation was expanded to a broader range of non-equilibrium flows. In contrast to the work of Dr. S. Jakirlić, this thesis focusses on the flows with transitional phenomena and flows with more complex irregular boundaries, using non-orthogonal block-structured grids. The flows considered in the course of this thesis cover:

- oscillating boundary layers at transitional and higher Re numbers;
- oscillating finite length pipe flows;
- pulsating flows;
- by-pass transition on flat plate with sharp leading edge;

- separation induced transition on flat plate with circular leading edge;
- separation induced transition on flat plate with virtually laminar incoming boundary layer;
- flow around an airfoil (NACA 4412) at high-Re-number;
- developed and developing Couette flows at various pressure gradients;
- channel and Couette flows with a wavy fixed wall;
- a number of high-Re-number flows in complex geometries applying high- and low-Re-number models such as: the staggered tube bundle flows, back-step flows with different pressure gradient imposed by inclination of opposite wall, the hill and stenosis flows, etc.

The latter class of flows (high-Re-number flows), although interesting, are not discussed in this thesis as they are not relevant to the topic.

1.2 Outline of thesis

This thesis is divided in six chapters. Chapter 2 presents the rational of high- and low-Re-number second-moment closure models with some critical observations. It also provides some novel ideas aimed at removing some known difficulties and at broadening the width of model application. Chapter 3 presents the essential features of the numerical approach used towards solving the second moment closure turbulence models with the wall functions and with the exact wall boundary conditions. Special attention is given to obtaining accurate solution and providing sufficient stability of the numerical solver in order to enable application of the second-moment closure models in geometrically and physically complex flows. In addition to geometric complexity, a particular challenge here was the solution of high-Re-number flows using the model with low-Re-number modifications which allowed integration up to wall. Subsequent two chapters present applications and model validation in two major classes of transitional flows. In Chapter 4 attention is focussed on the oscillating and pulsating flows at transitional and higher Re-numbers. Optimisation of model coefficients was done using available DNS and experimental data. Chapter 5 presents results of the model validation and its application to transitional flows involving bypass transition and the separation induced transition with a range of conditions. Finally, conclusions drawn from the range of studies performed in the course of the present work as well as some recommendations for the future work are given in Chapter 6.

CHAPTER 2

The Second-Moment Turbulence Closure

This chapter contains an outline of the turbulence models considered and used in the present study. Several models for high-Re number flows, especially the linear and quasi-linear ones, are discussed in more depth as they form the basis on which the model refinement and extension are founded. Special attention is given to the models which allow integration of the equations up to the wall with the use of exact wall boundary conditions. Some modelling issues, together with some proposals for their improvement, such as modelling of the pressure-strain correlation and dissipation rate tensor are discussed in more details. Performances of two low-Re-number Reynolds-stress models in a channel flow and some non-equilibrium flows are presented and discussed.

2.1 Introduction

The Reynolds-stress tensor has the greatest influence on the mean velocity and pressure in a turbulent flow, which in turn are of primary interest for engineering purposes. Therefore, the proper modelling of this tensor is essential for ensuring satisfactory predictive capability of a CFD code. A number of modelling approaches for determining the Reynolds-stress tensor in the framework of the Reynolds-averaging exists in the literature. These approaches differ in the physical background, complexity and success in predicting modelled quantities. The most popular one, primarily because of its simplicity and computational convenience, is the *eddy-viscosity model* (EVM) by which the Reynolds-stress tensor is assumed to be proportional to the mean flow rate of strain. The turbulent viscosity ν_t, is determined from algebraic formulae in terms of a time (or velocity) and length scales, which are usually provided from transport equations for these variables or any linearly independent combination of them. Whereas the turbulence kinetic energy is generally accepted as a good representation of the velocity scale, the choice of the second variable, providing the time or length scale is more uncertain. The $k-\varepsilon$, $k-l$ and $k-\omega$ are the most popular models for determination of the time and length scale. Although very popular and widely used, the eddy-viscosity approach suffers from several weaknesses which are rooted in the linear stress-strain relation as well as in the model equations, particularly the one which provides the length or time scale. The basic shortcomings of the eddy-viscosity based models are: *i)* unrealistic representation of the diagonal components of the Reynolds-stress tensor; *ii)*

the history and non-local effects on the Reynolds-stresses tensor cannot be well predicted. These shortcomings affect overall model performances especially in flows in which the gradients of normal stresses contribute significantly to the momentum equations. Such are flows with separation and recirculation, flows with strong normal straining (stagnation and impinging regions); swirling and rotating flows, secondary motion and three-dimensional flows in general. A number of corrections to the model equations of eddy-viscosity approach has been proposed aimed at eliminating some of the above mentioned deficiencies, though, most such remedies work only in the specific class of flows for which they are tuned.

Due to the fact that the shortcomings of this approach are rooted primarily in the linear relation between the stress and the mean flow strain rate, a way to improve performance of eddy-viscosity type of models, which has become popular in the last decade, is to use a non-linear constitutive relation (e. g. Gatski and Speziale 1993; Craft *et al.* 1997). Thus, the Reynolds-stress tensor is expressed in terms of the mean flow strain rate and vorticity, where the time and length scales are provided by the transport equations as in linear eddy-viscosity models. Better performances of some quadratic and cubic forms of non-linear eddy-viscosity models over a linear eddy-viscosity model in several complex flows including separation from smooth surfaces and by-pass transition flows were reported recently by for example Craft *et al.* (1997), Suga (1997), Apsley *et al.* (1997).

The second-moment closure (SMC) models (also called the Reynolds-stress models, RSM, when applied only to the dynamic field) are based on the exact transport equations for the Reynolds-stress tensor components and are, therefore, the first natural step towards overcoming the oversimplified idea behind the algebraic representation of the Reynolds-stress tensor. The SMC model equations account separately for all physical mechanisms which drive the Reynolds-stress tensor and, therefore, are capable of capturing the nonlocal and history effects. Some terms in these equations (i.e. convection and production) do not need modelling and therefore preserve the natural type of equations which might be of significant importance in many flows. Major problem, encountered in SMC is a need to model a number of extra terms, primarily these including pressure fluctuations, which are either absent or not dominant in eddy viscosity models. While providing better physical basis, these terms in the SMC model equations pose new challenges and may, if modelled incorrectly, cancel the natural advantages of SMC models.

2.2 Reynolds-averaged Navier-Stokes equations

The instantaneous velocity and pressure fields in an incompressible turbulent flow under isothermal conditions are solutions of the instantaneous continuity and Navier-Stokes equations, for a Newtonian fluid given by

$$\frac{\partial \mathcal{U}_i}{\partial x_i} = 0 \tag{2.1}$$

$$\frac{\partial \mathcal{U}_i}{\partial t} + \mathcal{U}_k \frac{\partial \mathcal{U}_i}{\partial x_k} = -\frac{1}{\rho}\frac{\partial \mathcal{P}}{\partial x_i} + \nu \frac{\partial^2 \mathcal{U}_i}{\partial x_k \partial x_k} \tag{2.2}$$

where ρ and ν are density and kinematic viscosity of the fluid, $\mathcal{U}_i$ are instantaneous velocity vector components and and $\mathcal{P}$ is instantaneous pressure. According to the Reynolds-averaging approach, the instantaneous variables are decomposed into an ensemble mean and a fluctuating part given by

$$\mathcal{U}_i = U_i + u_i, \quad \mathcal{P} = P + p, \tag{2.3}$$

where the capital letters (U_i, P) represent an ensemble mean and the lower-case letters (u_i, p) represent the fluctuating part. This averaging leads to the Reynolds-averaged continuity equation and the Reynolds-averaged Navier-Stokes (RANS) equations for incompressible isothermal turbulent flow of a Newtonian fluid, which can be written as

$$\frac{\partial U_i}{\partial x_i} = 0, \tag{2.4}$$

$$\frac{DU_i}{Dt} = -\frac{1}{\rho}\frac{\partial P}{\partial x_i} + \nu\frac{\partial^2 U_i}{\partial x_k x_k} - \frac{\partial \overline{u_i u_k}}{\partial x_k}. \tag{2.5}$$

Here the operator $\dfrac{D}{Dt}$ is

$$\frac{D}{Dt} = \frac{\partial}{\partial t} + U_k\frac{\partial}{\partial x_k}, \tag{2.6}$$

and $\overline{u_i u_k}$ are the one-point second-moment correlations of the fluctuating velocities which are usually called the *turbulent* or *Reynolds stresses*. The system of equations (2.4) and (2.5) is not closed, as $\overline{u_i u_j}$ is a new variable (second order tensor) which emerges as a consequence of the averaging. The task of RANS modelling is to provide the value of $\overline{u_i u_j}$ in order to close and solve the system of equations (2.4) and (2.5).

The corresponding continuity and transport equations for the fluctuating variables are also a direct consequence of Reynolds-averaging and read

$$\frac{\partial u_i}{\partial x_i} = 0, \tag{2.7}$$

$$\frac{Du_i}{Dt} + \frac{\partial U_i}{\partial x_k}u_k + \frac{\partial u_i}{\partial x_k}u_k - \overline{\frac{\partial u_i}{\partial x_k}u_k} = -\frac{1}{\rho}\frac{\partial p}{\partial x_i} + \nu\frac{\partial^2 u_i}{\partial x_k\,\partial x_k}. \tag{2.8}$$

Fluctuating velocity u_i and pressure p are the solution of equations (2.7) and (2.8) and depend on the history of the velocity field, initial and boundary conditions. These equations are the basis for deriving the exact transport equations for turbulence quantities, used for turbulence modelling.

2.3 Modelling Reynolds-stress transport equation

2.3.1 Exact Reynolds-stress transport equation

The exact transport equation for the Reynolds-stress tensor components $\overline{u_i u_j}$ is derived by multiplication of the transport equation for the fluctuating velocity u_i (2.8) with u_j and vice versa, adding these two expressions and taking the Reynolds-average. For an isothermal incompressible flow of Newtonian fluid the equation can be written as

$$\frac{D\overline{u_i u_j}}{Dt} = P_{ij} - \varepsilon_{ij} + \Pi_{ij} + \mathcal{D}^{\mathrm{t}}_{ij} + \mathcal{D}^{\mathrm{v}}_{ij}\,, \tag{2.9}$$

where

$P_{ij} = -\left(\overline{u_i u_k}\frac{\partial U_j}{\partial x_k} + \overline{u_j u_k}\frac{\partial U_i}{\partial x_k}\right)$ - production of Reynolds-stresses,

$\varepsilon_{ij} = 2\nu\overline{\frac{\partial u_i}{\partial x_k}\frac{\partial u_j}{\partial x_k}}$ - dissipation rate tensor,

$\Pi_{ij} = -\overline{\frac{1}{\rho}\left(u_i\frac{\partial p}{\partial x_j} + u_j\frac{\partial p}{\partial x_i}\right)}$ - velocity-pressure/gradient correlation,

$\mathcal{D}^{\mathrm{t}}_{ij} = -\frac{\partial\overline{u_i u_j u_k}}{\partial x_k}$ - turbulent velocity diffusion of Reynolds-stresses,

$\mathcal{D}^{\mathrm{v}}_{ij} = \frac{\partial}{\partial x_k}\nu\frac{\partial\overline{u_i u_j}}{\partial x_k}$ - viscous diffusion of Reynolds-stresses.

The term in which the fluctuating pressure appears (Π_{ij}) is for the modelling purposes usually decomposed into two terms:

$$\Pi_{ij} = \Phi^{\mathrm{x}}_{ij} + D^{\mathrm{x}}_{ij}, \tag{2.10}$$

where Φ^{x}_{ij} is a traceless tensor which does not contribute to the turbulence kinetic energy budget ($k = \overline{u_l u_l}/2$) and, therefore, is interpreted as a stress redistribution, and D^{x}_{ij} is a corresponding deviatoric tensor which represents turbulent transport of $\overline{u_i u_j}$ by pressure fluctuations. It is possible to form more traceless tensors out of the Π_{ij}. Some possibilities for decomposition of Π_{ij} are given in Table (2.1).

Groth (1991) argued that of all decompositions listed only the classical one (with the pressure-strain correlation) is justified since all others yield non-zero diffusion in all directions even if the flow is homogeneous in some directions. For example, in a two-dimensional flow which is homogeneous in x_3 direction, only the classical decomposition will lead to $D_{33} = 0$, whereas all other alternatives give non-zero D^{x}_{33}. It should be noted that in most models the pressure diffusion is lumped together with triple velocity correlation and modelled jointly so that, in fact, the models do not distinguish Φ_{ij} and Π_{ij}.

Table 2.1: Decomposition of the velocity-pressure/gradient correlation Π_{ij} into a traceless tensors ($\Phi^{\mathtt{x}}_{ij}$) and corresponding deviatoric tensor ($D^{\mathtt{x}}_{ij}$).

Proposal	$\Phi^{\mathtt{x}}_{ij}$	$D^{\mathtt{x}}_{ij}$
Pressure-strain correlation	$\overline{\frac{1}{\rho}p\left(\frac{\partial u_i}{\partial x_j}+\frac{\partial u_j}{\partial x_i}\right)}$	$-\frac{1}{\rho}\left(\frac{\partial \overline{pu_i}}{\partial x_j}+\frac{\partial \overline{pu_j}}{\partial x_i}\right)$
Lumley (1975)	$-\frac{1}{\rho}\left(\overline{u_i\frac{\partial p}{\partial x_j}}+\overline{u_j\frac{\partial p}{\partial x_i}}-\frac{2}{3}\frac{\partial \overline{pu_k}}{\partial x_k}\delta_{ij}\right)$	$-\frac{1}{\rho}\frac{2}{3}\frac{\partial \overline{pu_k}}{\partial x_k}\delta_{ij}$
Mansour et al. (1988)	$-\frac{1}{\rho}\left(\overline{u_i\frac{\partial p}{\partial x_j}}+\overline{u_j\frac{\partial p}{\partial x_i}}-\frac{\overline{u_iu_j}}{k}\frac{\partial \overline{pu_k}}{\partial x_k}\right)$	$-\frac{1}{\rho}2\frac{\overline{u_iu_j}}{k}\frac{\partial \overline{pu_k}}{\partial x_k}$
Durbin (1993)	$\Pi_{ij}-\frac{1}{3}\Pi_{kk}\delta_{ij}-\varepsilon_{ij}+\frac{\overline{u_iu_j}}{k}\varepsilon$	$\frac{1}{3}\Pi_{kk}\delta_{ij}+\varepsilon_{ij}-\frac{\overline{u_iu_j}}{k}\varepsilon$

In the framework of the second-moment closure modelling, terms in equation (2.9) denoted as ε_{ij}, $\mathcal{D}^{\mathtt{t}}_{ij}$ and Π_{ij}, which are the higher order correlations, have to be modelled.

Following the definition of the turbulence kinetic energy $k = \overline{u_iu_i}/2$ the exact transport equation for k is obtained from equations (2.9) and can be written as

$$\frac{Dk}{Dt} = \underbrace{-\overline{u_iu_k}\frac{\partial U_i}{\partial x_k}}_{P_k} \underbrace{-\nu\overline{\frac{u_i}{x_k}\frac{u_i}{x_k}}}_{\varepsilon} \underbrace{-\frac{\partial}{\partial x_k}\left(\frac{\overline{pu_k}}{\rho}+\frac{1}{2}\overline{u_iu_iu_k}\right)}_{\mathcal{D}^{\mathtt{t}}_k} \underbrace{+\frac{\partial}{\partial x_k}\nu\frac{\partial k}{\partial x_k}}_{\mathcal{D}^{\mathtt{v}}_k} \tag{2.11}$$

where P_k is the production, ε is the dissipation and $\mathcal{D}^{\mathtt{t}}_k$ and $\mathcal{D}^{\mathtt{v}}_k$ are the turbulent and viscous diffusion of the turbulence kinetic energy respectively.

2.3.2 Modelling of pressure-strain correlation

The pressure-strain correlation is of decisive importance for determination of the Reynolds-stresses from their transport equations. Over the past several decades a number of studies (Chou 1945, Rotta 1951, Hanjalić and Launder 1972, Noat, Shavit, and Wolfshtein 1973, Launder, Reece, and Rodi 1975, Lumley 1978, Shih and Lumley 1985, Fu, Launder, and Tselepidakis 1987, Speziale, Sarkar, and Gatski 1991, Johansson and Hallbäck 1994, Fu and Wang 1997) have been aimed at the development of models for the pressure-strain correlation tensor. The majority of models were developed for homogeneous flows. The most important reason for it

is the simplicity of this kind of flows, especially when compared to the wall bounded flows, which are strongly non homogeneous due to the presence of a solid wall. Developed and tuned for homogeneous flows, these models usually perform rather poor when applied to wall flows, especially if the model equations are to be solved up to the wall.

In this sub-section a short review and discussion of approaches applied to modelling of wall flows with a special attention to the models integrable up to the wall with applying the exact wall boundary conditions is given.

2.3.3 Decomposition of Φ_{ij}

Taking the divergence of the transport equation for u_i (Equation 2.8) leads to the Poisson equation for the fluctuating pressure p:

$$\frac{1}{\rho}\frac{\partial^2 p}{\partial x_l\,\partial x_l} = -2\frac{\partial U_l}{\partial x_k}\frac{\partial u_k}{\partial x_l} - \frac{\partial^2\left(u_l u_k - \overline{u_l u_k}\right)}{\partial x_l\,\partial x_k}. \tag{2.12}$$

It has been shown by Chou (1945) that the solution of this equation has the following form[1]

$$\begin{aligned} p = & -\frac{1}{4\pi}\int_V \left[-2\left(\frac{\partial U_l}{\partial x_k}\frac{\partial u_k}{\partial x_l}\right)' - \frac{\partial^2\left(u_l u_k - \overline{u_l u_k}\right)'}{\partial x_l\,\partial x_k}\right]\frac{dV}{|\vec{r'}-\vec{r}|} \\ & - \int_S \frac{\mathrm{grad}p'\cdot d\vec{S}}{|\vec{r'}-\vec{r}|} + \int_S p'\,\mathrm{grad}\frac{1}{|\vec{r'}-\vec{r}|}\cdot d\vec{S}, \end{aligned} \tag{2.13}$$

where $\vec{r}$ denotes the location at which p is evaluated; V is the volume of the flow domain bounded by surface S; $\vec{r'}$ is the location on or in the flow domain over which the integration is taken and the quantities marked with a prime are evaluated at position $\vec{r'}$.

In general, for an incompressible turbulent flow under isothermal conditions, one can write

$$\begin{aligned} \overline{p\frac{\partial u_i}{\partial x_j}} = & \frac{1}{4\pi}\int_V \underbrace{\left[2\left(\frac{\partial U_l}{\partial x_k}\right)'\overline{\left(\frac{\partial u_k}{\partial x_l}\right)'\frac{\partial u_i}{\partial x_j}}\right]}_{\text{Rapid term}} + \underbrace{\overline{\left(\frac{\partial^2 u_l u_k}{\partial x_l\,\partial x_k}\right)'\frac{\partial u_i}{\partial x_j}}}_{\text{Slow term}}\Bigg]\frac{dV}{|\vec{r'}-\vec{r}|} \\ & \underbrace{-\frac{1}{4\pi}\int_S \frac{1}{|\vec{r'}-\vec{r}|}\overline{\mathrm{grad}p'\frac{\partial u_i}{\partial x_j}}\cdot d\vec{S} + \int_S \overline{p'\frac{\partial u_i}{\partial x_j}}\,\mathrm{grad}\frac{1}{|\vec{r'}-\vec{r}|}\cdot d\vec{S}}_{\text{Surface contribution}}. \end{aligned} \tag{2.14}$$

Expression (2.14) indicates that the pressure-strain correlation is dependent on two point correlations and that three basic mechanisms are present: turbulence-turbulence interaction (slow term); turbulence-mean/flow interaction (rapid term) and surface contribution (surface blockage and pressure reflection). Thus, the pressure-strain correlation is modelled in the following form

$$\Phi_{ij} = \Phi_{ij}^{1} + \Phi_{ij}^{2} + \Phi_{ij}^{w} \tag{2.15}$$

[1] In the derivation of this solution the Green's function $\frac{1}{|\vec{r'}-\vec{r}|}$ is used. Thus, the solution for p has a different form if another Green's function is used.

where Φ_{ij}^1, Φ_{ij}^2 and Φ_{ij}^w are the slow term, the rapid term and the pressure-reflection term respectively.

2.3.4 Models for homogeneous flows

Integrals in expression (2.14) have to be evaluated over the entire flow domain. However, the two-point correlations rapidly decrease as $|\vec{r'} - \vec{r}|$ increases, so that the volume integration can be performed over small space surounding the point at which the integrals are computed. Therefore, the mean velocity gradient can be taken out of the integration. For homogeneous flows away from solid walls the surface contribution can be neglected. The pressure-velocity/gradient correlation for homogeneous flows can be now written in the following form

$$-\frac{1}{\rho}\overline{p\left(\frac{\partial u_i}{\partial x_j} + \frac{\partial u_j}{\partial x_i}\right)} = A_{ij} + \frac{\partial U_l}{\partial x_k} M_{ijkl} \tag{2.16}$$

where:

$$A_{ij} = \frac{1}{4\pi}\int_V \overline{\left[\left(\frac{\partial^2 u_l u_k}{\partial x_l\, \partial x_k}\right)' \left(\frac{\partial u_i}{\partial x_j} + \frac{\partial u_j}{\partial x_i}\right)\right]} \frac{dV}{|\vec{r'} - \vec{r}|}\,, \tag{2.17}$$

$$M_{ijkl} = \frac{1}{2\pi}\int_V \overline{\left[\left(\frac{\partial u_k}{\partial x_l}\right)' \left(\frac{\partial u_i}{\partial x_j} + \frac{\partial u_j}{\partial x_i}\right)\right]} \frac{dV}{|\vec{r'} - \vec{r}|}. \tag{2.18}$$

Tensors A and M satisfy the following conditions:

- symmetry: $A_{ij} = A_{ji};\ M_{ijkl} = M_{jikl} = M_{ijlk}\,,$
- continuity: $A_{ij} = 0;\ M_{ijkk} = M_{iikl} = 0\,,$
- normalisation: $M_{ijkk} = 2\overline{u_i u_j}\,.$

The most widely spread practise of modelling the pressure-strain correlation in an algebraic manner is to express A and M tensors in terms of the Reynolds-stress anisotropy tensor

$$a_{ij} = \frac{\overline{u_i u_j}}{k} - \frac{2}{3}\delta_{ij} \tag{2.19}$$

where δ_{ij} is the Kronecker delta. The most general form of a model for the slow term obtained by using the general tensor expansion and Caley-Hamilton theorem (Lumley 1978) is:

$$\Phi_{ij}^1 = -C_1 \varepsilon a_{ij} - C_1' \varepsilon \left(a_{ik}a_{kj} - \frac{1}{3}A_2\delta_{ij}\right)\,. \tag{2.20}$$

The first term on the right hand side of equation (2.20) was proposed by Rotta (1951). A number of proposed values for coefficients C_1 and C_1' can be found in the literature.

Also based on the general tensor expansion and Caley-Hamilton theorem the most general form of a model for the rapid part can be written as (see for example Hanjalić 1994; Demuren and Sarkar 1993):

$$\begin{aligned}\Phi_{ij}^2 = & \quad \beta_1\, P_k\, a_{ij} \\ & + \beta_2\, k\, S_{ij} \\ & + \beta_3\, k \left(a_{ik}S_{jk} + a_{jk}S_{ik} - \frac{2}{3} a_{lk}S_{kl}\delta_{ij} \right) \\ & + \beta_4\, k \left(a_{ik}\Omega_{kj} + a_{jk}\Omega_{ik} \right) \\ & + \beta_5\, k \left(a_{ik}a_{kl}S_{lj} + a_{jk}a_{kl}S_{li} - 2a_{il}a_{kj}S_{lk} - 3a_{ij}a_{kl}S_{lk} \right) \\ & + \beta_6\, k \left(a_{ik}a_{kl}\Omega_{lj} + a_{jk}a_{kl}\Omega_{li} \right) \\ & + \beta_7\, k \left[a_{nn}a_{nn} \left(a_{ik}\Omega_{kj} + a_{jk}\Omega_{ki} \right) + \frac{3}{2} a_{im}a_{nj} \left(a_{mk}\Omega_{kn} + a_{nk}\Omega_{km} \right) \right] , \end{aligned} \tag{2.21}$$

where $A_2 = a_{lk}a_{kl}$ and

$$S_{ij} = \frac{1}{2} \left(\frac{\partial U_i}{\partial x_j} + \frac{\partial U_j}{\partial x_i} \right), \qquad \Omega_{ij} = \frac{1}{2} \left(\frac{\partial U_i}{\partial x_j} - \frac{\partial U_j}{\partial x_i} \right). \tag{2.22}$$

The model coefficients C_1, C_1' and β_1 to β_8 may be, in general, functions of the invariants of the anisotropy tensors of turbulence quantities and turbulence Reynolds number. A comprehensive review of models for the pressure-strain correlation with a table overview of model coefficients values were given recently by e. g. Demuren and Sarkar (1993), Hanjalić (1994) and Jakirlić (1997).

It was shown by e. g. Hanjalić and Launder (1972), Launder *et al.* (1975), Johansson and Hallbäck (1994), Fu and Wang (1997) that using the symmetry, continuity and normalisation constraints, the number of free coefficients can be reduced, i.e. the coefficients β_1 to β_8 can be expressed in terms of a smaller number of independent coefficients. In general, the values of the independent coefficients are determined either by comparing the entire model performances with available experimental and DNS data for the Reynolds-stresses, or even the mean velocity, or by direct model comparison to available DNS data in a term-by-term manner. In addition to this, some authors have used the *realisability constraints* to determine or to bound the values of the model coefficients (e. g. Shih and Lumley 1985; Fu *et al.* 1987; Speziale *et al.* 1994; Durbin and Speziale 1994). The concept of realisability requires that the model does not produce physically unrealistic solutions for the Reynolds-stresses. The basic realisability constraints require that the normal Reynolds-stresses must be positive and that the Schwarz' inequality must be satisfied:

$$\overline{u_i u_i} > 0 \qquad \text{and} \qquad \overline{u_i u_j}^2 \leq \overline{u_i u_i}\ \overline{u_j u_j}, \quad (i \neq j) \qquad \text{(no summation)} \tag{2.23}$$

2.3.5 Linear models

Although a cubic model is the most general form of the rapid term, it does not provide solution of the modelling problem. In fact, performances of cubic or, in general, non-linear models, in comparison to simpler linear ones are not always superior as shown, e.g. by Lien and Leschziner

(1993a) in a systematic comparison of some linear and non-linear models in complex flows. It has been shown by Craft and Launder (1996) that for the wall flows a cubic model with variable model coefficients still needs some corrections in order to take into account the wall effects. This increases tremendously the complexity of the pressure-strain model making it difficult for validation and implementation into more general numerical codes. There exist a number of proposals for the pressure-strain model which are linear in a_{ij} (or quasi linear) and, thus, simple and convenient for computations of complex flows, which still perform rather well when applied in a broad range of flows. Two most frequently used forms of writing the rapid part of the quasi-linear pressure-strain model are:

$$\begin{aligned}\Phi_{ij}^2 = & - C_1^{\text{A}}\left(P_{ij} - \frac{2}{3}P_k\delta_{ij}\right) \\ & - C_2^{\text{A}}\left(D_{ij} - \frac{2}{3}P_k\delta_{ij}\right) - C_3^{\text{A}}kS_{ij} - C_4^{\text{A}}P_k a_{ij}\end{aligned} \tag{2.24}$$

or

$$\begin{aligned}\Phi_{ij}^2 = & + C_1^{\text{B}}k\left(S_{ik}a_{kj} + S_{jk}a_{ki} - \frac{1}{3}S_{kl}a_{lk}\delta_{ij}\right) \\ & + C_2^{\text{B}}k\left(\Omega_{ik}a_{kj} + \Omega_{jk}a_{ki}\right) + C_3^{\text{B}}kS_{ij} - C_4^{\text{B}}P_k a_{ij}\end{aligned} \tag{2.25}$$

where:

$$D_{ij} = -\left(\overline{u_i u_l}\frac{\partial U_l}{\partial x_j} + \overline{u_j u_l}\frac{\partial U_l}{\partial x_i}\right). \tag{2.26}$$

An overview of the proposed model coefficients in forms (2.24) and (2.25) is given in Table 2.2. Two of these proposals include the quadratic term $C_4 P_k a_{ij}$, (hence "quasi-linear") (HL and SSG) whereas all others are linear. All, except SSG, keep the coefficients constants for high Re-number.

The HL model was proposed with $C_1 = 2.8$. Thus, in the logarithmic region of channel flow where $P_k/\varepsilon \approx 1$, the C_1 reduces to $C_1 = 1.9$ which is close to the most commonly used value of this coefficients ($C_1 = 1.8$). It is interesting to note that despite of two decades of time span HL and SSG arrived at the same value of the coefficient C_4 , though with the opposite sign, which, again in the HL model was due to adopting $C_1 = 2.8$.

Table 2.2: Coefficients of some linear models for Φ_{ij} as they are expressed in two forms given by formulae (2.24) and (2.25) .

Model	C_1^{A}	C_2^{A}	C_3^{A}	C_4^{A}
HL	0.6454	0.0636	0.02545	-0.9
LRR-QI	0.7636	0.1090	0.3636	0.
LRR-IP	0.6	0.	0.	0.
JM	0.67	0.125	0.260	0.
SSG	0.4125	0.2125	$0.0333 + 0.625A_2^{1/2}$	0.9
Oberlack	0.800	0.400	0.800	0.
Model	C_1^{B}	C_2^{B}	C_3^{B}	C_4^{B}
HL	0.709	0.582	0.92	-0.9
LRR-QI	0.8736	0.6536	0.8	0.
LRR-IP	0.6	0.6	0.8	0.
JM	0.795	0.545	0.8	0.
SSG	0.625	0.200	$0.8 - 0.625A_2^{1/2}$	0.9
Oberlack	1.200	0.800	0.800	0.

Note:
Abbreviations: HL - Hanjalić and Launder (1972), LRR - Launder *et al.* (1975), JM - Jones and Musonge (1988), SSG - Speziale *et al.* (1991), Oberlack - Oberlack (1997).

The correlations between coefficients of the two forms are as follows:

$$C_1^{\mathrm{B}} = C_1^{\mathrm{A}} + C_2^{\mathrm{A}}, \qquad C_2^{\mathrm{B}} = C_1^{\mathrm{A}} - C_2^{\mathrm{A}}, \qquad C_3^{\mathrm{B}} = \frac{4}{3}\left(C_1^{\mathrm{A}} + C_2^{\mathrm{A}}\right) - C_3^{\mathrm{A}}, \qquad C_4^{\mathrm{B}} = C_4^{\mathrm{A}}$$

$$C_1^{\mathrm{A}} = \frac{1}{2}\left(C_1^{\mathrm{B}} + C_2^{\mathrm{B}}\right), \qquad C_2^{\mathrm{A}} = \frac{1}{2}\left(C_1^{\mathrm{B}} - C_2^{\mathrm{B}}\right), \qquad C_3^{\mathrm{A}} = \frac{4}{3}C_1^{\mathrm{B}} - C_3^{\mathrm{B}}, \qquad C_4^{\mathrm{A}} = C_4^{\mathrm{B}}$$

Assessment of some linear models for Φ_{ij}

There have been controversial claims on the predictive ability of various models, based on partial or subjective validations, and sometimes contaminated by numerical errors. In order to verify some of the claims and to establish arguments for the choice of basic high-Re-number model to which the low Re-number modifications were implemented, we present here the results of assessment of several linear and quasi-linear models for the pressure-strain correlation in homogeneous flows and in fully developed channel flow.

Homogeneous flows

In order to assess performances of the linear models for the pressure-strain given in Table 2.2 in simple one-dimensional flows, such as, for example, the homogeneous shear flows, one can apply the stress equilibrium condition $\frac{Da_{ij}}{Dt} = 0$ (Speziale *et al.* 1991), which leads to the algebraic approximation of the transport equation for the Reynolds-stress (2.9)

$$\frac{D\overline{u_i u_j}}{Dt} - \mathcal{D}^{\mathrm{t}}_{ij} + \mathcal{D}^{\mathrm{v}}_{ij} = \frac{\overline{u_i u_j}}{k}\left(\frac{Dk}{Dt} - \mathcal{D}^{\mathrm{t}}_{k} + \mathcal{D}^{\mathrm{v}}_{k}\right). \tag{2.27}$$

If the dissipation tensor is assumed to be isotropic, equation (2.27) yields

$$P_{ij} - \frac{2}{3}P_k\,\delta_{ij} + \Phi_{ij} = \frac{\overline{u_i u_j}}{k}\left(P_k - \varepsilon\right). \tag{2.28}$$

Using the models for the slow and rapid part of the pressure-strain tensor given by (2.20) and (2.24), a system of non-linear[2] algebraic equations for unknown anisotropies of the Reynolds-stresses (a_{ij}) as function of the ratio of the production and dissipation of the turbulence kinetic energy (P_k/ε) is obtained, which can be solved to yield a_{ij}.

Table 2.3 shows the computed values of anisotropy tensor a_{ij} for two values of P_k/ε for linear models given in Table 2.2. The results are compared with experimental data for a homogeneous shear flow of Tavoularis and Corrsin (1981) for $P_k/\varepsilon = 1.7$ and with both the experiments of Laufer (1950) and DNS of (Kim *et al.* 1987) for a log-region of a plane channel for $Re_\tau = u_\tau\, h/\nu = 180$ and 395. For various models the value of coefficients in the slow-part of Φ_{ij} are also indicated in Table 2.3.

The coefficients of the Jones-Musunge model were chosen to reproduce the experimental data by Tavoularis and Corrsin (1981) and therefore this model performs very well for the case $P_k/\varepsilon = 1.7$. In general, the best results for both cases are produced by the SSG model, although it cannot capture the level of anisotropy in the logarithmic region of channel flows. The result of the SSG model for $P_k/\varepsilon = 1$ is the same as obtained by Demuren and Sarkar (1993) (also given in the data bank of *Journal of Fluids Engineering*). On the basis of the computation of a channel flow ($P_k/\varepsilon = 1$) and experimental data of Laufer (1950), Demuren and Sarkar (1993) concluded that SSG model is capable of computing the correct Reynolds-stress anisotropy in the logarithmic region without introducing any wall-reflection term. According to the results in Table 2.3 this

[2]The non-linearity of this system of equation is due to the non-linear model for the slow part and quasi-linear model for the rapid part of Φ_{ij}.

is not quite so, as the values of normal components of Reynolds-stress tensor are for about 20% underpredicted, compared to the experimental data for $P_k/\varepsilon = 1$ at high Re number. However, the agreement to DNS data, which are at lower Re-number, is much better.

Note that no model here compared includes the wall reflection term. For reference, results of the basic RSM with wall reflection Gibson and Launder (1978) (Φ_{ij}^1 Rotta model, Φ_{ij}^2 IP model, see Appendix A for full specification of the model) is given for the case with $P_k/\varepsilon = 1$ (corresponding to channel flow near the wall). According to the results, this model performs still better than any model listed here.

Table 2.3: Comparison of predicted Reynolds-stress anisotropies in 1-dimensional flow for two values of P_k/ε.

	a_{11}	a_{22}	a_{12}	$C_1,\ C_1^p$
Tavoularis and Corrsin (1981)				
Exp. $P_k/\varepsilon = 1.7$	0.403	−0.300	−0.300	
HL	0.4446	−0.2772	−0.2630	2.8
LRR-QI	0.2637	−0.2060	−0.3588	1.8
LRR-IP	0.3627	−0.1813	−0.3633	1.8
JM	0.4044	−0.2988	−0.3013	1.5
SSG	0.4334	−0.2869	−0.3188	1.7, 1.05
Oberlack	0.3358	−0.4198	−0.1746	2.0
High Re number data near wall				
Exp. $P_k/\varepsilon = 1.0$	0.51	−0.46	−0.24	
DNS $P_k/\varepsilon \approx 1.0$	(0.35...0.45)	−(0.25...0.35)	−(0.25...0.30)	
HL	0.2712	−0.1691	−0.2611	2.8
LRR-QI	0.2155	−0.1683	−0.3362	1.8
LRR-IP	0.2963	−0.1481	−0.3395	1.8
JM	0.3489	−0.2578	−0.3033	1.5
SSG	0.4007	−0.2536	−0.3137	1.7, 1.05
Oberlack	0.2667	−0.3333	−0.2160	2.0
Basic RSM	0.4313	−0.4197	−0.2550	1.8

Note:
Abbreviations: HL - Hanjalić and Launder (1972); LRR - Launder *et al.* (1975); JM - Jones and Musonge (1988); SSG - Speziale *et al.* (1991); Oberlack - Oberlack (1997); Basic RSM - Φ_{ij}^1 Rotta model, Φ_{ij}^2 IP model and Gibson and Launder (1978) model for wall reflection with $f_w = 1$, see Appendix A.

Evaluation of coefficients of Φ_{ij} model using DNS data for inhomogeneous flows

DNS data for some simple flow can be used to evaluate directly the local coefficients and their variation (if any) in the flow, instead of a qualitative estimation. DNS data for channel flows are here used to evaluate the values of the coefficients of the model for the pressure-strain correlation given by (2.20) and (2.24). A system of equations can be formed:

$$\begin{aligned}\Phi_{ij} = & - C_1\varepsilon a_{ij} - C_1'\varepsilon\left(a_{ik}a_{kj} - \frac{1}{3}A_2\delta_{ij}\right) \\ & - C_1^{\mathtt{A}}\left(P_{ij} - \frac{2}{3}P_k\delta_{ij}\right) - C_2^{\mathtt{A}}\left(D_{ij} - \frac{2}{3}P_k\delta_{ij}\right) - C_3^{\mathtt{A}}kS_{ij} - C_4^{\mathtt{A}}P_k a_{ij} \end{aligned} \tag{2.29}$$

Six coefficients are unknown in this model. Since, the channel flow is one-dimensional and homogeneous in two directions, only four components of Φ_{ij} are non-trivial. Due to redistribution, the number of independent components reduces to three. Since, commonly, coefficients in the slow part of Φ_{ij} are tuned in the shear-free flows it is justified to use those coefficient before tuning the rapid-part coefficients. Thus, these coefficients can be evaluated from the system of equations

$$\begin{aligned}-C_1^{\mathtt{A}}\left(P_{ij} - \frac{2}{3}P_k\delta_{ij}\right) - C_2^{\mathtt{A}}\left(D_{ij} - \frac{2}{3}P_k\delta_{ij}\right) - C_3^{\mathtt{A}}kS_{ij} = \\ \Phi_{ij}^{\mathtt{DNS}} + \left[-C_1\varepsilon a_{ij} - C_1'\varepsilon\left(a_{ik}a_{kj} - \frac{1}{3}A_2\delta_{ij}\right) - C_4^{\mathtt{A}}P_k a_{ij}\right] \end{aligned} \tag{2.30}$$

by feeding DNS data for $\Phi_{ij}^{\mathtt{DNS}}$. Fig 2.1 shows results for $C_1^{\mathtt{A}}$, $C_2^{\mathtt{A}}$, $C_3^{\mathtt{A}}$ as solution of system (2.30) in two channel flows ($Re_\tau = 180$ and $Re_\tau = 395$). Coefficients on the right-hand-side are those of SSG model (Table 2.2). The results show that values of the unknown coefficients are fairly constant in a large portion of the flow as presumed by most models, especially in the logarithmic region. Near wall $C_1{}^{\mathtt{A}}$ becomes negative which is corrected if C_1 is damped to zero near the wall, in which case $C_1{}^{\mathtt{A}}$ drops also to zero at the wall. It seems that there is some dependence on the Reynolds-number. Note that these values are dependent on the choice of the model for Φ_{ij}^1 and coefficient $C_4^{\mathtt{A}}$. Whether a linear model for the rapid part of Φ_{ij} can be sufficient for computation of wall flows needs to be further assessed. Possibly in a similar way as above, the value of the model coefficients need to be evaluated for some other non-homogeneous flows in order to make a final judgement.

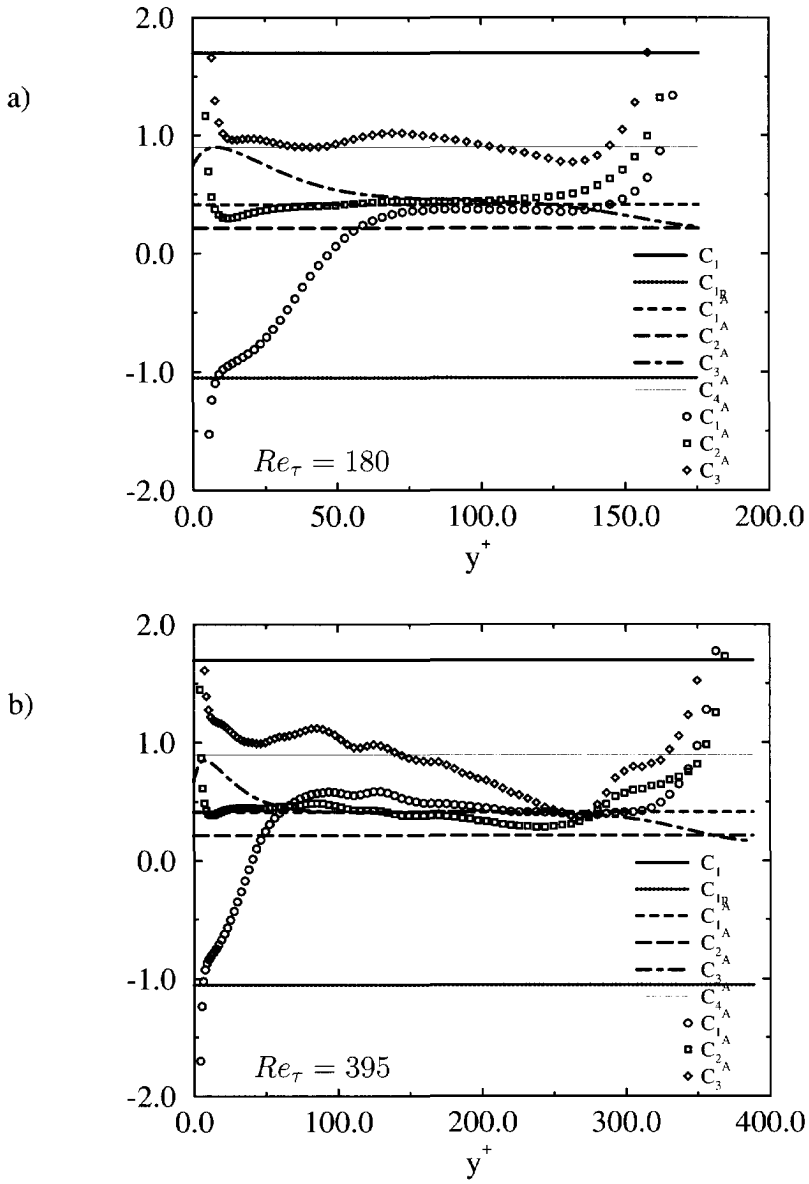

Figure 2.1: Symbols: Coefficients C_1^{A}, C_2^{A}, C_3^{A} obtained from DNS data for two channels $Re_\tau = 180$ and $Re_\tau = 395$ as solution of system of equations (2.30) with C_1, C_1' and C_4^{A} as proposed by Speziale *et al.* (1991) (SSG model coefficients are given with lines).

2.3.6 Modelling of wall-effects

Two approaches used currently for modelling wall bounded turbulent flows differ much both in requirements for the mathematical model and the numerical solver. The *high-Re-number* approach, with wall function, where some empirical laws are used to bridge a thin viscous sub-layer close to the wall requiring a mathematical model to represent turbulence only at high-Re-number (though in highly inhomogeneous conditions), so that a relatively coarse numerical mesh can be used. The *low-Re-number* approach, where the model equations are integrated to a solid boundary with the exact boundary conditions, requires more sophisticated model which needs to describe behaviour of the turbulence quantities in the wall vicinity where a multitude of effects (viscosity, high inhomogeneity, wall blockage, etc.) impose additional requirements for model modification. The model needs to satisfy the two-componentality limit which the turbulence obeys close to the wall due to a higher damping of the normal-to-the-wall fluctuations than of those in stream and spanwise directions. Therefore, a much finer numerical grid than for wall functions approach has to be used.

Since developed with assumption of the local homogeneity and equilibrium, the models for homogeneous flows described above are not capable of representing properly the behaviour of turbulent flows which are far from the equilibrium, and particularly in the near-wall flow region which is always highly inhomogeneous. Therefore, in order to compensate for difference in anisotropy of the Reynolds stress tensor in homogeneous and wall flows at comparable ratio of production/dissipation, a *wall effect* term[3] is added to model for Φ_{ij}. Although the need for such term can be justified by the existence of the surface integral in equation (2.14) the most common practice is to accommodate the need for increasing the Reynolds-stresses anisotropy in the near wall region primarily by damping the component normal to the wall in an ad-hoc manner. Thus, the complete model for Φ_{ij} is tuned to satisfy experimental and DNS data. The wall reflection term is decomposed into a slow and a rapid contribution as done with the pressure-strain model for homogeneous flows

$$\Phi_{ij}^{\mathtt{W}} = \Phi_{ij}^{\mathtt{W1}} + \Phi_{ij}^{\mathtt{W2}}. \tag{2.31}$$

Several proposals are popular and often used in computations. Shir (1973) proposed

$$\Phi_{ij}^{\mathtt{W1}} = C_1^{\mathtt{W}} \frac{\varepsilon}{k} \left(\overline{u_k u_m} n_k n_m \delta_{ij} - \frac{3}{2} \overline{u_i u_k} n_k n_j - \frac{3}{2} \overline{u_j u_k} n_k n_i \right) f_{\mathtt{W}} \tag{2.32}$$

and Gibson and Launder (1978) extended it to include the effects of the mean shear as

$$\Phi_{ij}^{\mathtt{W2}} = C_2^{\mathtt{W}} \left(\Phi_{km}^2 n_k n_m \delta_{ij} - \frac{3}{2} \Phi_{ik}^2 n_k n_j - \frac{3}{2} \Phi_{jk}^2 n_k n_i \right) f_{\mathtt{W}} \tag{2.33}$$

where $\vec{n} = (n_1, n_2, n_3)$ is the unit vector normal to the wall. For flows with arbitrarily shaped wall boundary, vector $\vec{n}$ is the unit vector that connects the position at which the model is evaluated, to the nearest position at a wall-boundary. $f_{\mathtt{W}}$ is a function which indicates proximity of a wall.

[3] Known also as "wall-echo", "wall-reflection" or "wall-blockage" effect.

The most frequently used definition of f_w was proposed by Launder *et al.* (1975) and Gibson and Launder (1978)

$$f_w = \frac{1}{C_l}\frac{L}{l_w}, \tag{2.34}$$

where $C_l = \kappa C_\mu^{-3/4} = 2.5$ is a coefficient chosen to provide unity value of f_w in the log-law region, $L = \dfrac{k^{3/2}}{\varepsilon}$ is the turbulence length scale and l_w is the distance to the nearest position at a wall-boundary. Function f_w has value of unity close to a wall and diminishes as the distance to the wall increases. As shown in Figure (2.2), the function f_w, evaluated from DNS data for channel flow at two Re-numbers, takes the value of one roughly at the beginning of the logarithmic region, but significantly exceeds that value in the buffer region and goes to zero as the wall is approached. For computations with the high-Re-number models and wall functions f_w is limited to unity. The model coefficients proposed by Gibson and Launder (1978) are: $C_1^w = 0.5$ and $C_2^w = 0.3$.

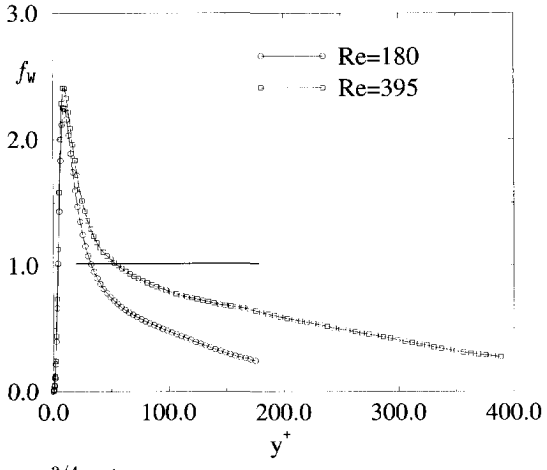

Figure 2.2: Function $f_w = \dfrac{C_\mu^{3/4}}{\kappa}\dfrac{k^{3/2}}{\varepsilon}\dfrac{1}{l_w}$ in channel flow at two Reynolds numbers ($Re_\tau = 180$ and 395) evaluated from DNS data. l_w is the wall distance and $\kappa = 0.41$ is von Karman constant.

Craft (1991) recognised that the Gibson-Launder wall reflection model (2.32) and (2.33) predicts the opposite effect in flows which are not parallel to the wall, such as in a jet impinging normally on a flat plate. The model predicts an increase in the normal-to-the-wall component of $\overline{u_i u_j}$ tensor and in reality that component is damped. Craft (1991) proposed a new model which predicts the impinging flows well and reduces to the Gibson-Launder model in the wall parallel flows such as channel or boundary layers. Craft's model is given with

$$\Phi_{ij}^{w2} = -0.044\,\frac{\partial U_l}{\partial x_m}\overline{u_l u_m}\,(n_q n_q \delta_{ij} - 3 n_i n_j)\; f_w$$

$$-0.080\ k\left(\frac{\partial U_k}{\partial x_m}n_l n_k a_{lm}\delta_{ij} - \frac{3}{2}\frac{\partial U_i}{\partial x_m}n_l n_j a_{lm} - \frac{3}{2}\frac{\partial U_i}{\partial x_m}n_l n_j a_{lm}\right)\ f_w \qquad (2.35)$$
$$+0.600\ k\frac{\partial U_k}{\partial x_m}n_l n_m\left(n_i n_j - \frac{1}{3}n_q n_q \delta_{ij}\right)\ f_w.$$

Inviscid wall effects are basically dependent on the distance to a solid wall and its orientation, as seen from the surface integral in the Poisson equation for fluctuating pressure (2.13). This term is expected to account for the wall blockage and pressure reflection. The DNS data for plane channel flow (Kim *et al.* 1987) show that this term decays fast with the wall distance and becomes insignificant outside the viscous layer. However, a notable difference in the stress anisotropy between a homogeneous shear flow and equilibrium wall boundary layer for comparable shear intensities shows that the effect of wall presence permeates much further away from the wall into the log-layer. This indicates at an indirect wall effect through a strong inhomogeneity of the mean shear rate, which is ignored by all available pressure-strain models.

The wall reflection models account predominantly for the wall effects outside the viscous layer. Despite some opposing views in literature, the wall reflection model with topology parameters was used in the present study for physical reasons as discussed above. Replacing the wall echo term by non-linear rapid pressure-strain models leads either to very complex expressions (e.g. cubic models), or insufficient effects (e.g. quasi-quadratic models of Speziale *et al.* 1991). Besides, in all flows considered, the use of wall distance and unit normal vector poses neither computational problems nor extra computing time, since both parameters are computed ones during the process of grid generation.

Durbin (1993) proposed a model integrable up to the wall which does not need any wall reflection term and predicts the near wall reasonable well. More details are given below.

Fully developed channel flow

Fig 2.3 shows results of computation of a channel flow applying wall function and using three models for the pressure-strain correlation: a) Launder, Reece, and Rodi (1975) without wall-reflection term (LRR-QI); b) The Rotta model + IP model + wall-reflection of Gibson and Launder (1978) (GL) and c) Speziale *et al.* (1991) (SSG). In all cases wall functions[4] are used for boundary conditions. Daly-Harlow model (2.75) is used for diffusion and the standard high-Re-number equation for ε (see later equation (2.98)), with $C_{\varepsilon_1} = 1.44$ and $C_{\varepsilon_2} = 1.92$ for LRR-QI and GL and $C_{\varepsilon_1} = 1.44$ and $C_{\varepsilon_2} = 1.83$ for SSG model. Model computations are performed for $Re_\tau = u_\tau h/\nu = 2000$ in order to be able to use the wall function. Symbols are DNS data for two cases: $Re_\tau = 395$ and $Re_\tau = 595$ of Kim (1990, Kim (1997). DNS data for $y^+ < 30$ are not shown in the figures.

[4]For implementation of the wall functions into the numerical code ses Section 3.6.

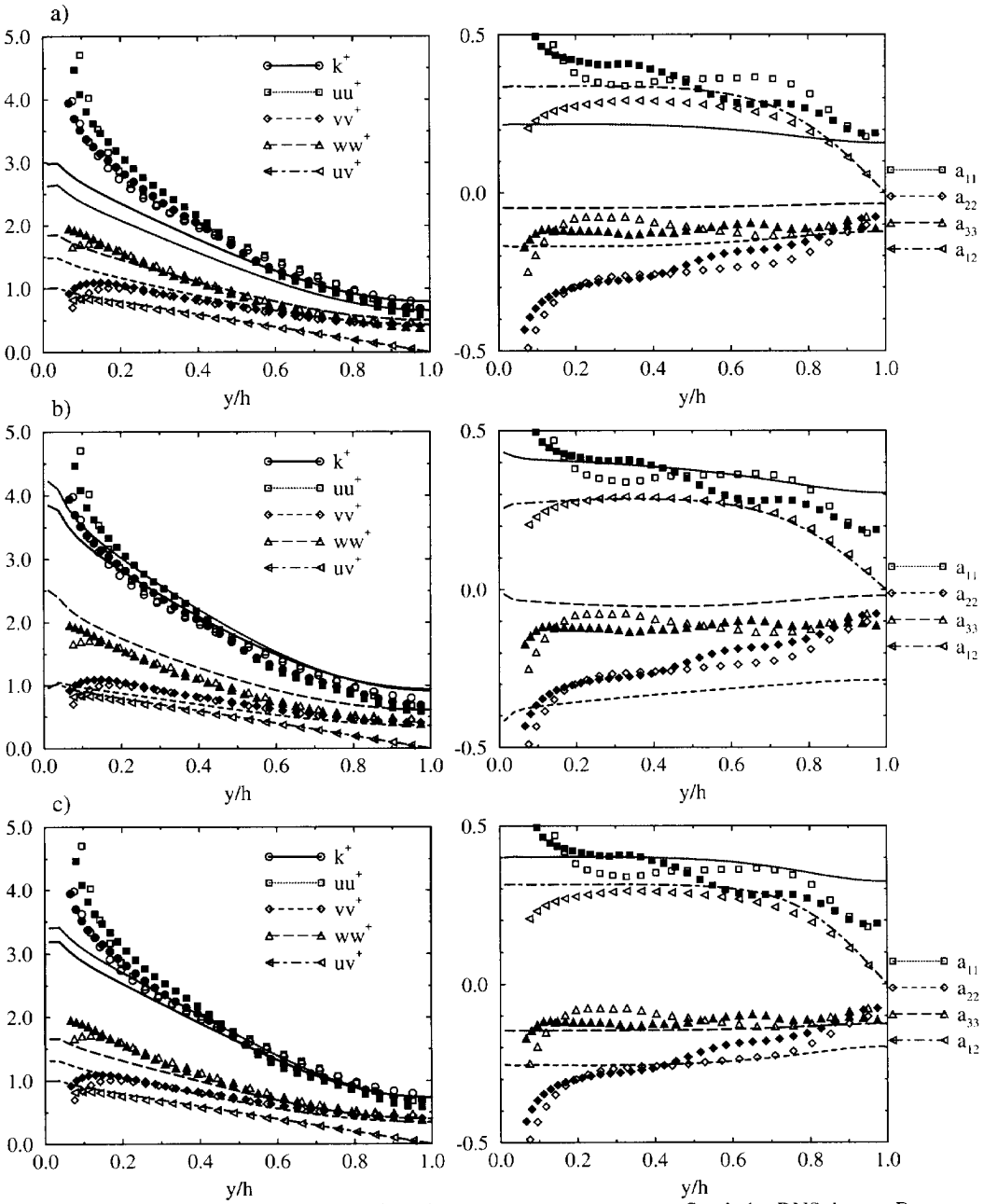

Figure 2.3: Reynolds-stress tensor and its anisotropy tensor components. Symbols: DNS data at $Re_\tau = 395$ (empty symbols, Kim (1990)) and $Re_\tau = 595$ (filled symbols, Kim (1997)). DNS data for $y^+ < 30$ are not plotted here. Lines: SMC computations at $Re_\tau \approx 2000$. a) Launder, Reece, and Rodi (1975) without wall-reflection term; b) The Rotta model + IP model + wall-reflection of Gibson and Launder (1978) and c) Speziale *et al.* (1991).

It is seen that the LRR-QI model does not predict sufficient anisotropy of Reynolds stresses, particularly close to the wall. The GL and SSG models do better but there is a difference between them. The important difference between GL model and SSG model is in the prediction of $\overline{vv}$ and $\overline{ww}$ stresses. The GL model predicts twice higher value of the difference $a_{33} - a_{22}$ than the SSG model. According to these results the SSG model predicts overall the stress anisotropy closer to DNS data. However, the major difficulty of the SSG model is predicting the near-wall stress levels, which are much too low. The GL model is obviously superior here. Whereas the anisotropy level away from the wall can be adjusted by tuning of the coefficients in GL model, it does not seem possible to improve the near-wall prediction of SSG model by simply adding the quasi-linear term as the authors claim. Fig 2.4 shows profiles of the mean velocity obtained with the three models. The model results are in good agreement with the log-law.

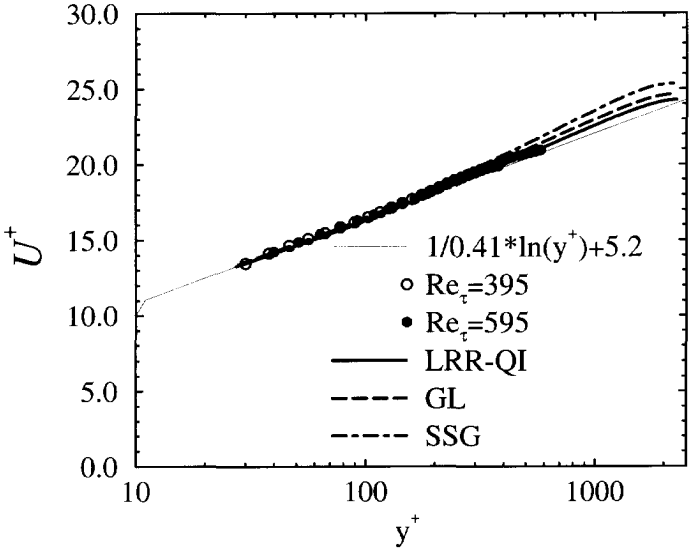

Figure 2.4: Channel flow: The mean velocity profile. Symbols and legend as in Fig 2.3.

2.3.7 A model of the pressure fluctuations

As shown above, the pressure-strain correlation models available in the literature have a diversity of forms although a general form can cover the majority of proposals. The models are developed by applying the tensor representation theory to determine the unknown tensors A and M in equation (2.16). The continuity, symmetry, normalisation and realisability constraints are used to reduce the number of unknown coefficients which are then determined from experimental and DNS data and numerical optimisations. The diversity of the models, their complexity and wide

differences of values of the model coefficients, are a consequence of the author's views on thr importance of some terms in some particular flows and the use of different data to set the model coefficients.

In this sub-section it is demonstrated that it is possible to derive the form of the most known pressure-strain models by starting from the transport equation for the velocity fluctuations and modelling the pressure-gradient fluctuations. Such practise is named by Parks *et al.* (1998) *the preclosure modelling*. In this approach the continuity and symmetry constraints are inherited from the transport equation for the velocity fluctuations. The problem of determination of the model coefficients remains the same as in the standard approach and is not addressed here.

The instantaneous pressure-gradient in an incompressible isothermal turbulent flow is given with (see equation (2.8))

$$-\frac{1}{\rho}\frac{\partial p}{\partial x_i} = \frac{Du_i}{Dt} + \frac{\partial U_i}{\partial x_k}u_k + \frac{\partial u_i}{\partial x_k}u_k - \overline{\frac{\partial u_i}{\partial x_k}u_k} - \nu\frac{\partial^2 u_i}{\partial x_k\,\partial x_k}. \tag{2.36}$$

Since, the velocity-pressure/gradient correlation is defined as

$$\Pi_{ij} = -\overline{\frac{1}{\rho}\left(u_i\frac{\partial p}{\partial x_j} + u_j\frac{\partial p}{\partial x_i}\right)} \tag{2.37}$$

a redistributive (traceless) tensor of Π_{ij} can be constructed as (Lumley 1978, see Table 2.1)

$$\Phi_{ij} = \Pi_{ij} - \frac{1}{3}\Pi_{kk}\delta_{ij}. \tag{2.38}$$

The instantaneous pressure-gradient may be expressed in terms of "known" fluctuating quantities and any mean averaged quantity, which are available as for the standard modelling purposes.

The instantaneous pressure p is the solution of equation

$$-\frac{1}{\rho}\frac{\partial^2 p}{\partial x_k x_k} = 2\frac{\partial U_k}{\partial x_l}\frac{\partial u_l}{\partial x_k} + \frac{\partial u_k}{\partial x_l}\frac{\partial u_l}{\partial x_k} - \frac{\partial^2\overline{u_k u_l}}{\partial x_l x_k}, \tag{2.39}$$

with appropriate boundary conditions. Since this equation is linear in p, the fluctuating pressure can be split into two parts: a slow part (p_S) and a rapid part (p_R) so that $p = p_S + p_R$ and

$$-\frac{1}{\rho}\frac{\partial^2 p_S}{\partial x_k x_k} = \frac{\partial u_k}{\partial x_l}\frac{\partial u_l}{\partial x_k} - \frac{\partial^2\overline{u_k u_l}}{\partial x_l x_k}, \tag{2.40}$$

$$-\frac{1}{\rho}\frac{\partial^2 p_R}{\partial x_k x_k} = 2\frac{\partial U_k}{\partial x_l}\frac{\partial u_l}{\partial x_k}. \tag{2.41}$$

The p_S and p_R contribute to the slow and rapid part of the velocity-pressure/gradient correlation (2.42)

$$\Pi_{ij} = \Pi_{ij}^S + \Pi_{ij}^R = \underbrace{-\overline{\frac{1}{\rho}\left(u_i\frac{\partial p_S}{\partial x_j} + u_j\frac{\partial p_S}{\partial x_i}\right)}}_{\text{slow part}}\underbrace{-\overline{\frac{1}{\rho}\left(u_i\frac{\partial p_R}{\partial x_j} + u_j\frac{\partial p_R}{\partial x_i}\right)}}_{\text{rapid part}} \tag{2.42}$$

Note that in this decomposition the Π_{ij}^S and Π_{ij}^R are called the slow and the rapid parts because of their physical meaning and by notation are to be distinguished from the splitting of the pressure-strain correlation given with expression (2.15).

The model for the slow term

Since the slow term represents contributions of the velocity fluctuations, a model for the pressure-gradient fluctuations may include only the velocity fluctuations. If the pressure-gradient fluctuations are approximated as

$$-\frac{1}{\rho}\frac{\partial p_S}{\partial x_i} = \frac{C_1}{2}\frac{u_i}{\tau} + \frac{C_2}{2}\frac{\overline{u_i u_k}}{k}\frac{u_k}{\tau}, \tag{2.43}$$

which is an intuitive non-linear representation of the instantaneous pressure-gradient based on the equation (2.36), the model for velocity-pressure/gradient correlation is then

$$\Pi_{ij} = C_1\frac{\overline{u_i u_j}}{\tau} + C_2\frac{\overline{u_i u_k}}{k}\frac{\overline{u_j u_k}}{\tau}. \tag{2.44}$$

The model given with (2.43) assumes proportionality between the transport of fluctuating velocity u_i and itself, and is given by

$$\frac{Du_i}{Dt} \sim \frac{u_i}{\tau}. \tag{2.45}$$

Therefore, the same assumption can be made for the averaged velocity fluctuations so that the "time scale" τ can be obtained from the transport equation for turbulence kinetic energy in homogeneous shear-free flows as follows[5]

$$\frac{Dk}{Dt} = -\varepsilon \quad \rightsquigarrow \quad \frac{k}{\tau} = -\varepsilon \quad \rightsquigarrow \quad \tau = -\frac{\varepsilon}{k}, \tag{2.46}$$

leading to a non-linear model for Π_{ij}, which expressed in terms of the anisotropy of the Reynolds-stress tensor a_{ij}, reads

$$\Pi_{ij} = -C_1\varepsilon\left(a_{ij} + \frac{2}{3}\delta_{ij}\right) - C_2\varepsilon\left(a_{ik}a_{kj} - \frac{4}{3}a_{ij} + \frac{4}{9}\delta_{ij}\right). \tag{2.47}$$

The corresponding redistribution model for the slow part is

$$\Phi_{ij} = -\left(C_1 + \frac{4}{3}C_2\right)\varepsilon a_{ij} - C_2\varepsilon\left(a_{ik}a_{kj} - \frac{1}{3}A_2\delta_{ij}\right), \tag{2.48}$$

which is equal to the model proposed by Lumley (1975), equation (2.20).

[5]The negative value of the "time scale" τ is used for convenience.

The model for the rapid term

Since the rapid term represents the influence of the mean velocity gradient and the fluctuating velocity on the pressure fluctuation, a model for the fluctuating pressure-gradient intuitively deduced from equation (2.36) may be

$$-\frac{1}{\rho}\frac{\partial p_R}{\partial x_i} = C_3 u_k \frac{\partial U_i}{\partial x_k} , \tag{2.49}$$

which leads to the model for Φ_{ij} first proposed by Noat *et al.* (1973), and known as IP-model ("isotropisation of production") given with

$$\Phi_{ij} = -C_3 \left(P_{ij} - \frac{2}{3} P_k \delta_{ij} \right) . \tag{2.50}$$

A more general model including the mean velocity strain S_{ij} is given with

$$-\frac{1}{\rho}\frac{\partial p_R}{\partial x_i} = C_3 u_k \frac{\partial U_i}{\partial x_k} + C_4 u_k \frac{\partial U_k}{\partial x_i} , \tag{2.51}$$

and leads to

$$\Phi_{ij} = -C_3 \left(P_{ij} - \frac{2}{3} P_k \delta_{ij} \right) - C_4 \left(D_{ij} - \frac{2}{3} P_k \delta_{ij} \right) . \tag{2.52}$$

which is a part of the most existing models for rapid part.

Following the same procedure it is possible to recover some forms of the non linear models for the rapid term. For example, the preclosure model given by

$$-\frac{1}{\rho}\frac{\partial p_R}{\partial x_i} = C_5 \left(u_k \overline{u_k u_l} \frac{\partial U_i}{\partial x_l} + u_k \frac{\partial U_k}{\partial x_l} \overline{u_l u_i} + u_l \frac{\partial U_l}{\partial x_k} \overline{u_k u_i} \right) \tag{2.53}$$

leads to the form which has been proposed by Fu *et al.* (1987) and more recent variants extensively used by the UMIST modelling group.

It was demonstrated above that the form of some most frequently used models for the pressure-strain correlation can be derived starting from the modelling of the pressure-gradient fluctuation. Using this approach, it might be possible to evaluate an appropriate form of the model for Φ_{ij} and, possibly, to determine the value and the form of the model coefficients.

2.3.8 Low-Re-number turbulence models

In a large number of flows application of wall functions is not possible or justified, for example in transitional flows, flows with separation and reattachment, or essentially all non-equilibrium wall flows and those where computation of the flow details in the immediate wall vicinity, such as wall friction, pressure distribution, heat and mass transfer, are of significant importance and interest.

Basically, the standard wall functions are valid only in energy equilibrium[6] fully turbulent flows such as channel and Couette flows, or a boundary-layer at zero or small pressure gradient. Thus, the first computational point near the wall is expected to be located in the region where the semi-logarithmic velocity distribution is valid, which was found experimentally to exist only in above mentioned flows. Flow details between this point and the wall are not computed. In absence of a better approach, wall functions are used widely for industrial applications of a variety of turbulent flows. Surprisingly, despite a strong departure from equilibrium and deviation from logarithmic velocity law, in many cases the predicted flow pattern is satisfactory. The problem is that there are also many situations where this is not the case, and it is difficult to know in advance what the outcome will be. Even more important is the unreliability of wall functions in predicting the wall phenomena, which, as a rule, are not well reproduced. A way to overcome the problem is in deriving more general wall functions which will be applicable to a wider class of non-equilibrium flows. While such attempts have been proposed (Chieng and Launder 1980; Kim and Choudhury 1995; Ciofalo and Collins 1989; Kiel and Vieth 1995 etc.) their success has still not been proved in a broader class of flows. The major problem is not so much in boundary conditions (wall function) for velocity, but for turbulence quantities for which the equations are solved. Integration of the equations up to the wall and using the exact boundary conditions should be, in principle, a better alternative. This requires the modification of all equations to account for multiple wall effects: viscosity (low-Re-number) as well as for non-viscous wall proximity effects.

Before such modifications are introduced it is necessary to adopt a reference high-Reynolds number model which should serve as an asymptotic model to which the modifications should reduce for sufficiently high turbulence Reynolds numbers and at a sufficient distance from a solid wall. A number of studies have been aimed at predicting turbulent flows using the low-Re-number models with exact wall boundary conditions. In the frame-work of EVM the first such model was proposed by Jones and Launder (1972). They modified the turbulent viscosity in an ad hoc manner ensuring that the turbulent viscosity is damped and becomes zero as the Re-number decreases to zero. In addition, they introduced an additional term to the transport equation for ε in order to capture the strong change of ε near the wall and its limiting value at the wall. Extensive reviews with systematic assessment and comparison of performances of some widely used low-Re-number eddy-viscosity models were given for example by Patel *et al.* (1985) and Sarkar and So (1997).

In the framework of SMC, the low-Re-number modelling requires considerable modifications of the pressure-strain model and of the dissipation rate tensor in the wall vicinity, as well as some modifications of the transport equation for ε, as done, for example, by Hanjalić and Launder (1976), Kebede *et al.* (1985), Launder and Shima (1989), Launder and Tselepidakis (1993), Shima (1993), Durbin (1993), Hanjalić *et al.* (1995), Craft and Launder (1996), Craft (1997). Essentially two rather different approaches are adopted: *i)* the coefficients of the high-Re-number model, which serve as high-Re-number asymptotes (usually constants), are modified in terms of

[6]Energy equilibrium implies that the production and dissipation of turbulence kinetic energy are in balance, i.e. that the convective and diffusive transport are small. These conditions lead to roughly constant shear stress and universal semi logarithmic mean velocity distribution in the inner-wall coordinates.

turbulent Reynolds-number Re_t, distance to the wall, or any (preferably invariant) turbulence parameters; *ii*) elliptic relaxation and scale switch (Durbin 1993) by which the pressure-strain correlation is the solution of an elliptic partial differential equation[7] which accounts for the wall effects and reduces to the high-Re-number asymptote model.

The low-Re-number models demand a fine grid near walls, which may hinder their wider application to very complex three-dimensional flows at high Re-numbers. It is argued, however, that this approach may be unavoidable if transition phenomena and accurate wall friction and heat transfer are in focus, such as, for example, in the problem of gas turbine blade cooling.

In the present work, the attention is given to the flows with transition where the dominant effect on the generation of turbulence is due to a wall bounding of the flow. Considered will be mainly flows which are, in bulk, parallel to the wall (though involving local separation), what means that flows with impingement on a solid surface, as a dominant mechanism will not be considered. For flows such as boundary layers, the basic second-moment closure[8] with a linear pressure-strain model was found to reproduce the general flow pattern reasonably well, except in the immediate vicinity of a solid wall. For this reason a version of wall-proximity modifications developed in conjunction with the basic Reynolds-stress model (Hanjalić, Jakirlić, and Hadžić 1995; Jakirlić 1997; Hanjalić and Jakirlić 1998) was explored for computation of flows which are subject of the present study. Admittedly, for the treatment of more complex flows which involve rotation or normal impingement, it may be necessary to adopt as a basis a more adequate high-Re-number SMC. However, it is believed that the low-Re-number and wall-vicinity modifications used here can equally well be adopted in conjunction with other high-Re-number models, with possibly some slight modifications of the coefficients. Another approach proposed by Durbin (1993), will also be considered as a possible alternative, though due to some noted difficulties, this model was not pursued to the same extend as the former one.

2.3.9 The adopted low-Re-number SMC

The Hanjalić-Jakirlić low-Re SMC (hereafter HJ) uses the basic high-Re-number model as its high-Re-number asymptote. The wall-proximity modifications are implemented in the pressure-strain Φ_{ij} model and in the stress dissipation ε_{ij} model. Several additional terms were also added into the ε-equation.

The model for the pressure-strain correlation is linear and has the form[9]:

$$\Phi_{ij} = \Phi_{ij,1} + \Phi_{ij,2} + \Phi^w_{ij,1} + \Phi^w_{ij,2} \tag{2.54}$$

$$\Phi_{ij,1} = -C_1 \varepsilon a_{ij} \tag{2.55}$$

$$\Phi_{ij,2} = -C_2 \left(P_{ij} - \frac{2}{3} P_k \delta_{ij} \right) \tag{2.56}$$

$$\Phi^w_{ij,1} = C^w_1 f_w \frac{\varepsilon}{k} \left(\overline{u_k u_m} n_k n_m \delta_{ij} - \frac{3}{2} \overline{u_i u_k} n_k n_j - \frac{3}{2} \overline{u_k u_j} n_k n_i \right) \tag{2.57}$$

[7] For every component of Φ_{ij} one elliptic equation is solved.

[8] See Appendix A for detailed specification of the model.

[9] Although generally the linear slow term was use in some cases the quadratic model was also explored, equation (2.20).

$$\Phi^w_{ij,2} = C^w_2 f_w \left(\Phi_{km,2} n_k n_m \delta_{ij} - \frac{3}{2} \Phi_{ik,2} n_k n_j - \frac{3}{2} \Phi_{kj,2} n_k n_i \right) \tag{2.58}$$

where $\Phi_{ij,1}$ is the return to isotropy (Rotta 1951) model for the slow part, $\Phi_{ij,2}$ is the isotropisation of production (IP) (Noat *et al.* 1973) model for the rapid part and $\Phi^w_{ij,1} + \Phi^w_{ij,2}$ is the Gibson and Launder (1978) model for the wall reflection term.

The linear model is used because of its simplicity, computational robustness and satisfactory performance in a number of wall bounded flows. Some non-linear models proposed predict some wall flows rather well, without a need to introduce variable coefficients (Craft and Launder 1996; Craft 1997), but at the expense of a large number of terms and coefficients. Hanjalić and Jakirlić (1998) argue that such a complexity in the model of just one part of a single term in the stress transport equation is disproportionate to the relative simplicity of the rest of the modelled terms both in $\overline{u_i u_j}$ and ε equation.

The adoption of the simple linear pressure-strain model requires variable coefficients to account for complex near-wall effects, if the equations are to be integrated up to the wall. The coefficients need to account for wall-vicinity and viscous effects. In addition, the model needs to satisfy the two-componentality and vanishing-Re-number limits. Wall impermeability imposes a blockage to fluid velocity and its fluctuations in the normal direction causing a strong anisotropy of the turbulence. This fact was exploited by introducing, in addition to Re_t, both the turbulent-stress and dissipation-rate anisotropy invariants A_2, A, E_2 and E as parameters in the coefficients, accounting thus far separately for the wall effect on anisotropy of stress bearing and dissipative scales (Hanjalić and Jakirlić 1998). Using these invariants, the coefficients of the pressure-strain model read

$$\begin{aligned}
&C_1 = C + \sqrt{A} E^2 && C = 2.5 A F^{1/4} f && F = \min(0.6; A_2) \\
&C_2 = 0.8 A^{1/2} && C_1^w = \max(1 - 0.7C; 0.3) && C_2^w = \min(A; 0.3) \\
&f = \min\left\{ \left(\frac{Re_t}{150} \right)^{3/2}; 1 \right\} && f_w = \min\left[\frac{k^{3/2}}{2.5 \varepsilon x_n}; 1.4 \right] && Re_t = k^2/(\nu\varepsilon),
\end{aligned} \tag{2.59}$$

where

$$\begin{aligned}
A_2 &= a_{ij} a_{ij}, \quad A_3 = a_{ij} a_{jk} a_{ki}, \quad A = 1 - 9/8(A_2 - A_3) \\
E_2 &= e_{ij} e_{ij}, \quad E_3 = e_{ij} e_{jk} e_{ki}, \quad E = 1 - 9/8(E_2 - E_3) \\
a_{ij} &= \overline{u_i u_j}/k - 2/3\delta_{ij}, \quad e_{ij} = \varepsilon_{ij}/\varepsilon - 2/3\delta_{ij}.
\end{aligned} \tag{2.60}$$

Fig 2.5 shows a comparison of the pressure-strain correlation obtained from the HJ model prediction of the channel flow at $Re_\tau = 180$ and the corresponding DNS data.

The stress dissipation rate ε_{ij} is modelled in the form proposed by Hanjalić and Jakirlić (1993), which reproduced well the components of ε_{ij} obtained by DNS in a plane channel. The

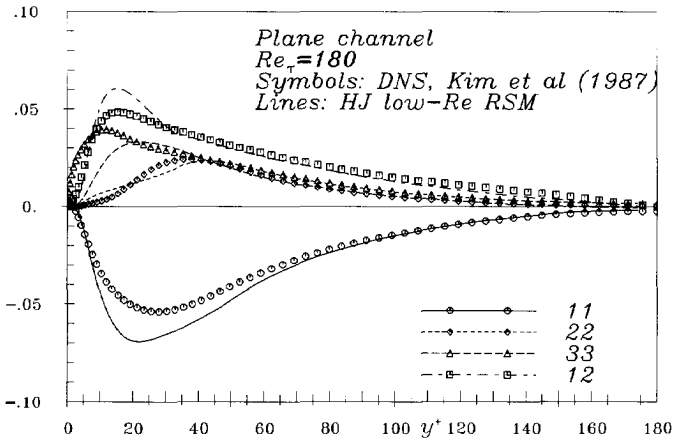

Figure 2.5: Pressure-strain correlation predicted using the HJ low-Re-number Reynolds stress model in a channel flow at $Re_\tau = 180$. Symbols are DNS data of Kim *et al.* (1987) and lines are the model results for Φ_{ij} (expressions 2.54 to 2.58) obtained in the entire computation of the flow.

model is given by the following formulae and will be discussed below

$$\varepsilon_{ij} = f_s \varepsilon^*_{ij} + (1 - f_s)\frac{2}{3}\delta_{ij}\varepsilon \tag{2.61}$$

$$\varepsilon^*_{ij} = \frac{\varepsilon}{k}\frac{[\overline{u_i u_j} + (\overline{u_i u_k} n_j n_k + \overline{u_j u_k} n_i n_k + \overline{u_k u_l} n_k n_l n_i n_j) f_d]}{1 + 1.5\,(\overline{u_p u_q}/k)\; n_p n_q\; f_d} \tag{2.62}$$

$$f_s = 1 - \sqrt{A}E^2, \qquad f_d = (1 + 0.1 Re_t)^{-1}. \tag{2.63}$$

The transport equation for ε used in conjunction with HJ model is discussed in Section 2.4.

The model had been extensively tested, as mentioned earlier, and provided good and satisfactory results in a large number of fully turbulent flows. The summary of the model, with the entire model specification and detailed results for several non-equilibrium flows are given in Appendix B.

Couette flows

As a new illustration of the HJ model performances in the non-equilibrium wall flows, relevant particularly to the present study, we show some results of computation of three cases of Couette flows at different conditions.

While the zero-pressure gradient Couette flow poses no specific challenge, some cases with imposed strong pressure gradient, and particularly the developing Couette flows, depart substantially from local equilibrium. The model results are compared to available DNS and experimental data.

The first case is the developed Couette flow with such an adverse pressure gradient $(\partial P/\partial x/\left(\rho U_w^2/\delta\right) = -1.1 \times 10^{-3})$ that the mean velocity close to the moving wall has almost uniform distribution, and, consequently, a minimum level of the mean shear rate. Here the effects of mean flow inhomogeneity, as well as of viscosity are absent, so that the wall effect is reduced to only non-viscous blockage and pressure reflection. A satisfactory reproduction of mean and turbulence quantities here is an indirect confirmation that the model distinguishes viscous effects due to wall vicinity. Fig 2.6 shows profiles of the mean velocity, turbulence kinetic energy, all components of the Reynolds-stress tensor and the dissipation rate normalised with the wall friction velocity of the fixed wall.

The next two cases considered are developing flows from a fully developed channel flow to fully developed Couette flow. The imposed speed of the moving wall determine the pressure field within the flow and the character of the flow at final stage. The Reynolds number based on the wall speed of $Re_w = U_w\delta/\nu = 3000$ produces approximately the same pressure gradient as in the previous fully developed case. The Reynolds number of $Re_w = 5000$ produces Couette flow with zero pressure gradient. In these two cases of particular interest is the model response in the developing region where the flow undergoes a transition from a plane channel flow to a fully developed Couette flow. In both cases about 40 channel widths are needed for the fully developed Couette flow to be established. Figures 2.7 and 2.8 show that the model reproduces well the evolution of the mean velocity and streamwise fluctuation after encountering the moving wall ($x = 0$).

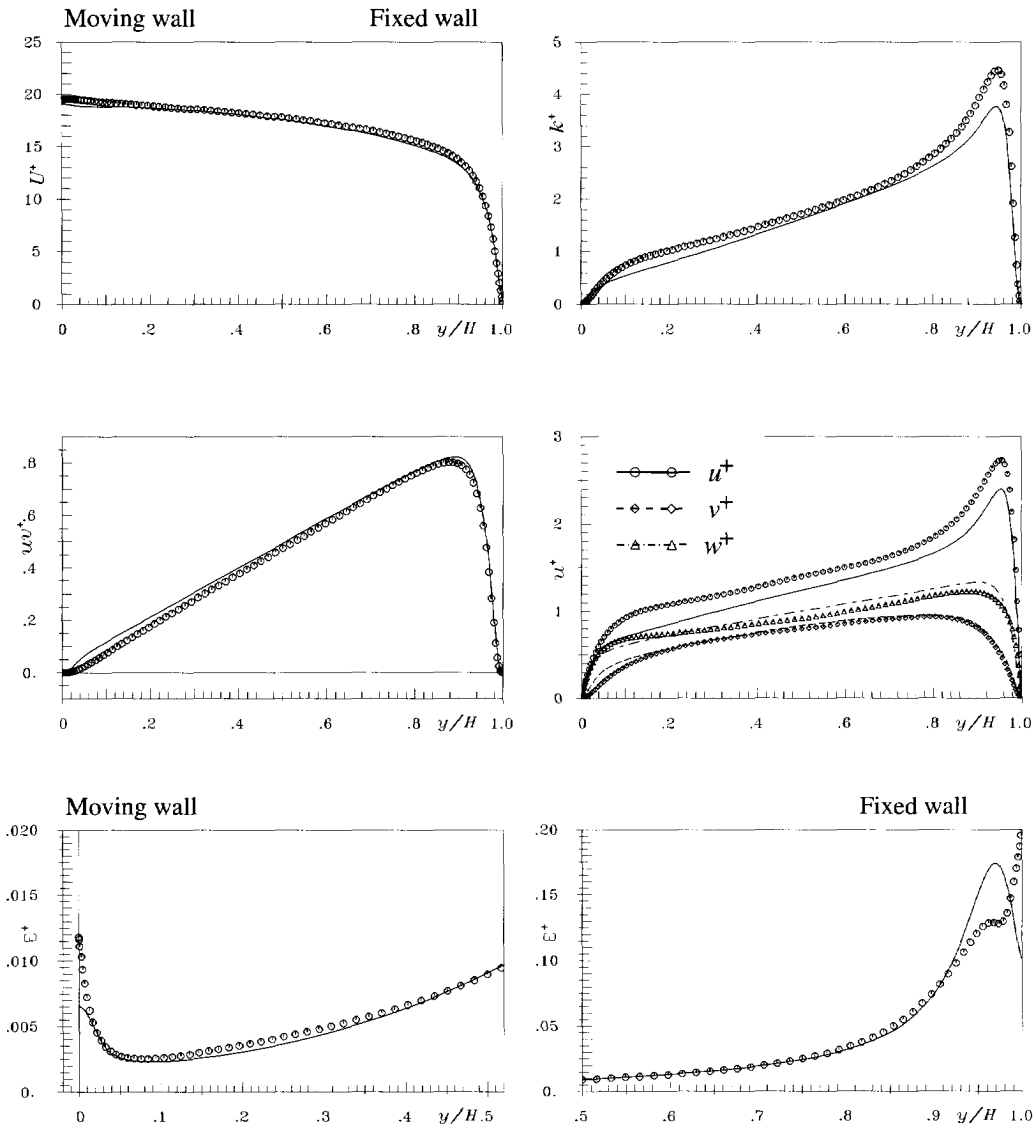

Figure 2.6: Couette flow with adverse pressure gradient: $\partial P/\partial x/\left(\rho U_w^2/\delta\right) = -1.1 \times 10^{-3}$ (which provides $\partial U/\partial y \approx 0$ near moving wall) $Re_w = U_w\delta/\nu = 3000$, Symbols: DNS of Kuroda *et al.* (1993). Lines: HJ SMC model.

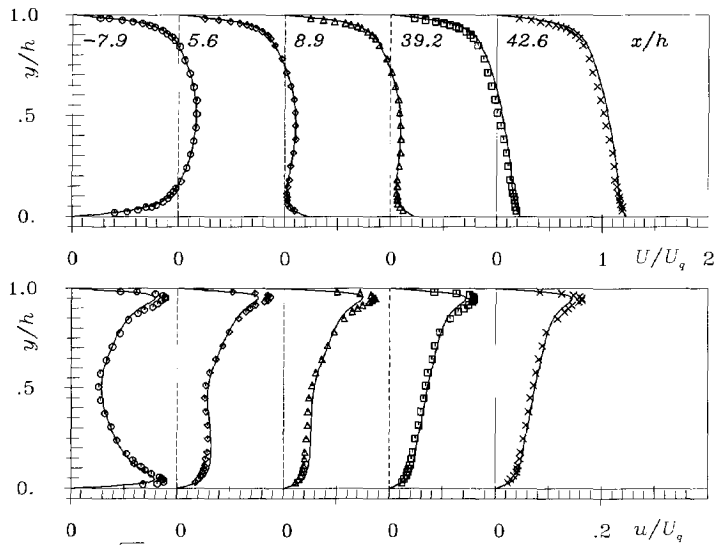

Figure 2.7: U and $\sqrt{\overline{u^2}}$ in a developing flow from pure Poiseuille to fully developed Couette flow with adverse pressure gradient as in the case shown in Fig 2.6 reached at $x/h \approx 40$. Symbols: Experiments of Corenflos *et al.* (1993). Lines: HJ SMC model. The lower wall moves from $x = 0$. U_q is the bulk mean velocity.

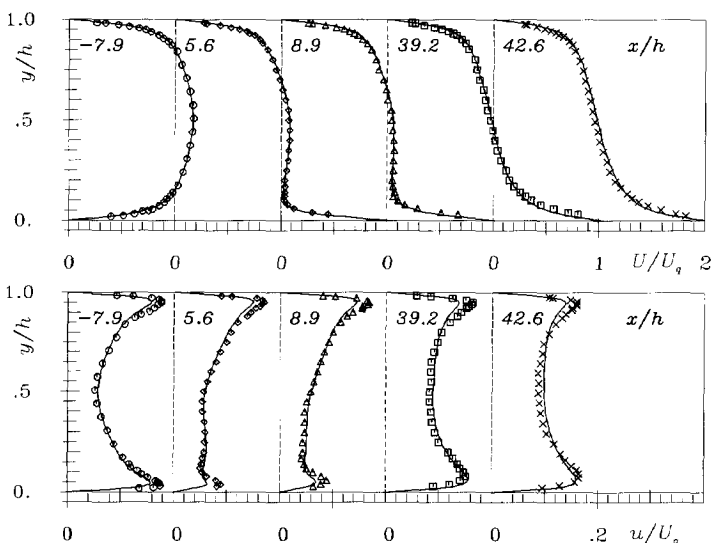

Figure 2.8: U and $\sqrt{\overline{u^2}}$ in a developing flow from pure Poiseuille flow to fully developed Couette flow with zero pressure gradient reached at $x/h \approx 40$. Symbols: Experiments of Corenflos *et al.* (1993). Lines: Low-Re-number HJ SMC. The lower wall moves from $x = 0$. U_q is the bulk mean velocity.

2.3.10 Durbin's low-Re SMC

The majority of the low-Re-number Reynolds-stress models have an algebraic form for modelling the pressures-strain correlation. The model coefficients are to adjust the values of the modelled terms, as the wall is approached and to satisfy the wall limits. The basis for this adjustment is to match the terms in the equation obtained by DNS or experiments.

Durbin (1993) proposed a different modification of the second-moment closure model based on elliptic relaxation of the pressure-strain correlation, which accounts for the wall effects. This relaxation, together with the switch from the large-eddy scale to the Kolmogorov scale when the latter becomes more dominant, allows the integration of the model equations to the wall. Durbin (1991) introduced the elliptic relaxation approach, first, in the framework of eddy-viscosity model. In addition to k and ε equations he solves a transport equation for the quantity $\overline{v^2}$ which is used to obtain the damping of the turbulent viscosity near wall. The $\overline{v^2}$ is the second-moment correlation of the velocity fluctuations normal to the wall or, in general, it can be regarded as the second-moment correlation of the velocity fluctuations normal to the streamlines. The transport equation for $\overline{v^2}$ has roots in the modelled transport equation for Reynolds-stresses but can be regarded simply as the equation for an another velocity scale used to model k and ε equations. This model is known as the $k-\varepsilon-\overline{v^2}$ model.

Durbin (1993) proposed a specific grouping of terms in the exact Reynolds-stress transport equation

$$\frac{D\overline{u_i u_j}}{Dt} = \wp_{ij} + P_{ij} - \frac{\overline{u_i u_j}}{k}\varepsilon - \frac{\partial \overline{u_l u_i u_j}}{\partial x_l} - \frac{1}{\rho}\frac{2}{3}\delta_{ij}\frac{\partial \overline{u_l p}}{\partial x_l} + \nu\frac{\partial^2 \overline{u_i u_j}}{\partial x_l} \tag{2.64}$$

where the redistribution tensor is given by

$$\wp_{ij} = -\frac{1}{\rho}\overline{u_i \frac{\partial p}{\partial x_j}} - \frac{1}{\rho}\overline{u_j \frac{\partial p}{\partial x_i}} + \frac{1}{\rho}\frac{2}{3}\delta_{ij}\frac{\partial \overline{u_l p}}{\partial x_l} - \varepsilon_{ij} + \frac{\overline{u_i u_j}}{k}\varepsilon. \tag{2.65}$$

Modelling of this redistributive tensor is done by an elliptic equation

$$-\nabla^2 f_{ij} + \frac{f_{ij}}{L^2} = \frac{f_{ij}^H}{L^2}, \tag{2.66}$$

where the redistributive tensor $\wp_{ij}$ is defined as

$$\wp_{ij} = k f_{ij}. \tag{2.67}$$

The justification of the elliptic equation for f_{ij} is given in Durbin (1993). The inviscid wall effects are accounted for by elliptic equation (2.66) where a length-scale function L ensures that function f_{ij} relaxes to the value which corresponds to a homogeneous high-Re-number model away from the wall, Φ_{ij}^H:

$$f_{ij}^H = \frac{1}{k}\left[\Phi_{ij}^H - \left(\varepsilon_{ij} - \frac{\overline{u_i u_j}}{k}\varepsilon\right)\right] \tag{2.68}$$

where Φ_{ij}^H is the homogeneous model for Φ_{ij} for which any pressure-strain model can be used. Durbin (1993) adopted a single combination: the Rotta model for the slow part (2.55) and the IP model for the rapid part (2.56) with $C_1 = 1.22$ and $C_2 = 0.6$:

$$f_{ij}^H = \frac{1 - C_1}{kT} a_{ij} - \frac{C_2}{k}\left(P_{ij} - \frac{2}{3} P_k \delta_{ij}\right). \tag{2.69}$$

Note that instead of the standard value $C_1 = 1.8$ in the Rotta model, a significantly smaller value is used, which takes into account the difference $\varepsilon_{ij} - \frac{\overline{u_i u_j}}{k}\varepsilon$ in the log-law region.

ERM wall-boundary conditions

The largest influence on the ERM behaviour in the viscous sub-layer has the wall boundary condition for f_{ij} which is derived so that the redistributive tensor $\wp_{ij}$ is in balance with diffusion and dissipation in the immediate wall vicinity. Examination of the dominant terms near the wall in the model equations for the Reynolds-stresses shows that only redistribution, dissipation and viscous diffusion are in balance in the very proximity of the wall (viscous sub-layer):

$$k f_{ij} - \frac{\overline{u_i u_j}}{k}\varepsilon + \frac{\partial}{\partial x_l}\left(\nu \delta_{lm} + \frac{\nu_{T_{lm}}}{\sigma_k}\right)\frac{\partial \overline{u_i u_j}}{\partial x_m} \approx 0 \tag{2.70}$$

$$f_{ij_w} \approx \frac{1}{k}\left[\frac{\overline{u_i u_j}}{k}\varepsilon - \frac{\partial}{\partial y}\nu \frac{\partial \overline{u_i u_j}}{\partial y}\right]_w \tag{2.71}$$

The Taylor series expansion of the velocity fluctuations near the wall ($u_i = a_i + b_i y + c_i y^2 + ...$) gives:

$$\begin{aligned}
\overline{u^2} &= \overline{b_1 b_1} y^2 + ... \\
\overline{v^2} &= \overline{c_2 c_2} y^4 + ... \\
\overline{w^2} &= \overline{b_3 b_3} y^2 + ... \\
\overline{uv} &= \overline{b_1 c_2} y^3 + ... \\
k &= \frac{1}{2}(\overline{b_1 b_1} + \overline{b_3 b_3}) y^2 + ... = \frac{\varepsilon_w}{2\nu} y^2 + ...
\end{aligned} \tag{2.72}$$

where $\overline{b_1 b_1}$, $\overline{c_2 c_2}$, $\overline{b_3 b_3}$ & $\overline{b_1 c_2}$ are functions independent of y.

Expressions (2.71) and (2.72) lead to the wall boundary conditions for f_{ij}:

$$\begin{aligned}
f_{11_w} &= 0 \\
f_{22_w} &= -20\nu^2 \left(\frac{\overline{v^2}}{y^4}\right)_p \\
f_{33_w} &= -f_{22_w} \\
f_{12_w} &= -8\nu^2 \left(\frac{\overline{uv}}{y^4}\right)_p
\end{aligned} \tag{2.73}$$

where P is the first numerical point next to the wall. Note that the arbitrary factor 20 instead of exact 8 in expression (2.73) is used in computations. This value was adopted in the course of the optimisation to reproduces the DNS data, as shown below (this is consistent with the experience of some other researcher, for example D. Laurence of EDF, *personal communication*).

Channel flow results

The following figures show the results of computation of a channel flow at $Re_\tau = u_\tau h/\nu = 395$ [10] obtained using ERM. The results are compared to DNS data of Kim (1990). Fig 2.9a shows solutions for f_{ij} and value of f_{ij}^H obtained in a channel flow. At about $y^+ = 50$, which is beginning of the logarithmic-velocity profile, function f_{ij} relaxes to f_{ij}^H. The large differences in the value and shape of $\wp_{ij}$ (Fig 2.9b) is achieved by the wall-value of function f_{ij}. Since the elliptic relaxation model accounts essentially for the near wall region, generally any other turbulence model for $\wp_{ij}$ can be used, as done, for example, by Laurence *et al.* (1995).

Figures 2.10 and 2.11 show profiles of the mean velocity and all components of the Reynolds-stress tensor in the channel flow obtained with ERM. Excellent agreement with the DNS data is achieved. Fig 2.12 shows profile of dissipation ε and $\overline{u_i u_j}/k\ \varepsilon$ compared to DNS data for ε and ε_{ij}. Excellent result for ε at wall is due to correct behaviour of k near the wall, since $\varepsilon_w = \nu \left(\partial^2 k/\partial n^2\right)_w$.

Fig 2.13 shows function $f_{ij} = \wp_{ij}/k$ evaluated from DNS data for channel at $Re_\tau = 395$. Although the above shown derivation of the value of f_{ij} (2.73) at the wall boundary seems plausible, the DNS data show that only the f_{22} component has a finite value and all other three are infinite. The reason for this is the neglect of turbulent diffusion in the derivation of the wall values.

The wall-boundary value for f_{ij} is evaluated using values of the model variables at the fist point near wall. For 22 and 12 components $f_{ij}^w \sim 1/n^4$, where n is the distance of the first point to the wall. This makes the wall boundary condition rather sensitive to the size of the numerical mesh. As the distance of the first numerical point from the wall decreases, the numerical procedure becomes more unstable. If this point is located relatively far from the wall, say at y^+-values between 1 and 5, the convergence of the numerical code is good. Because of this one may employ a smaller number of computational points in the viscous sub-layer than it is usually the case if an algebraic model for Φ_{ij} is used. On the other hand, a fine mesh close to the wall is required if the viscous sublayer is to be resolved, what is particularly important when treating the laminar to turbulent transition. This is, however, rather difficult and often not possible to achieve in complex flow simulations. This was the main reason that the present author did not achieve good convergence using the elliptic relaxation model for computation of several flow-cases with by-pass transition and with separation induced transition. Despite appealing advantages, it seems that modifications of Durbin model are needed to make it applicable to transitional flows and, therefore, this model was not further pursued here.

[10] This is equal to $Re_m = \dfrac{U_m\, 2h}{\nu} = 13500$ where h is the half of the channel width.

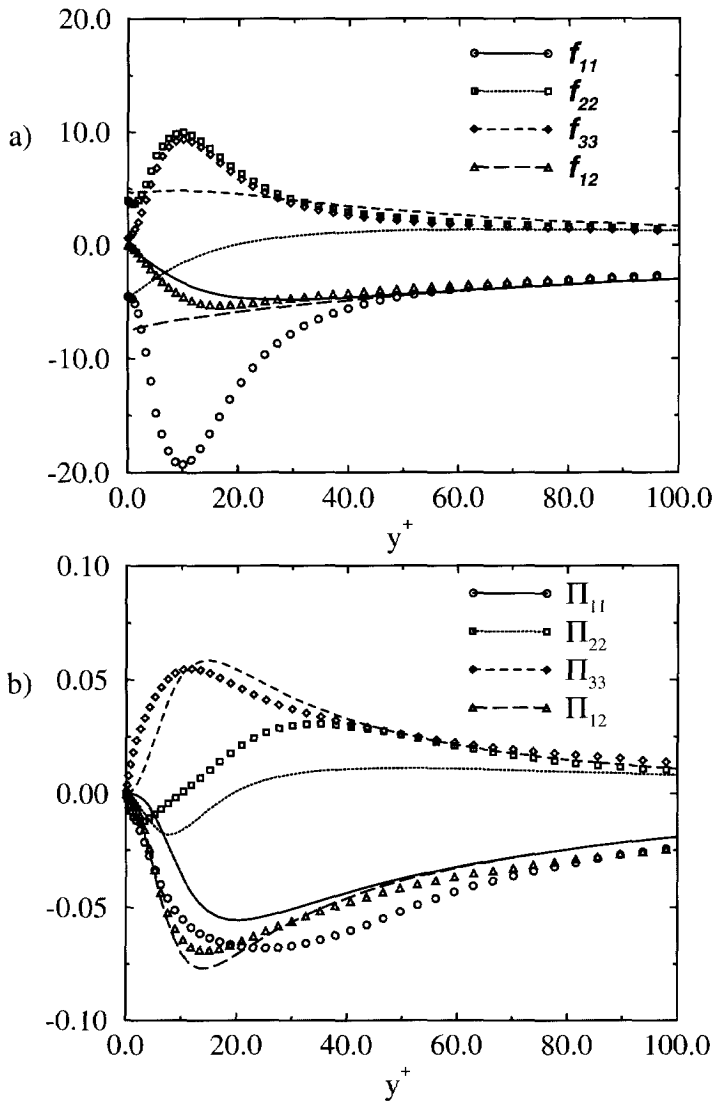

Figure 2.9: Elliptic relaxation model computation of channel flow at $Re_\tau = 395$. a) Symbols: Functions f_{ij}^H as given with equation (2.69); Lines: f_{ij}, solution of equation (2.66). b) Symbols: Velocity-pressure/gradient correlation (Π_{ij}) from DNS data of Kim (1990); Lines: ERM for $\wp_{ij} = k\, f_{ij}$.

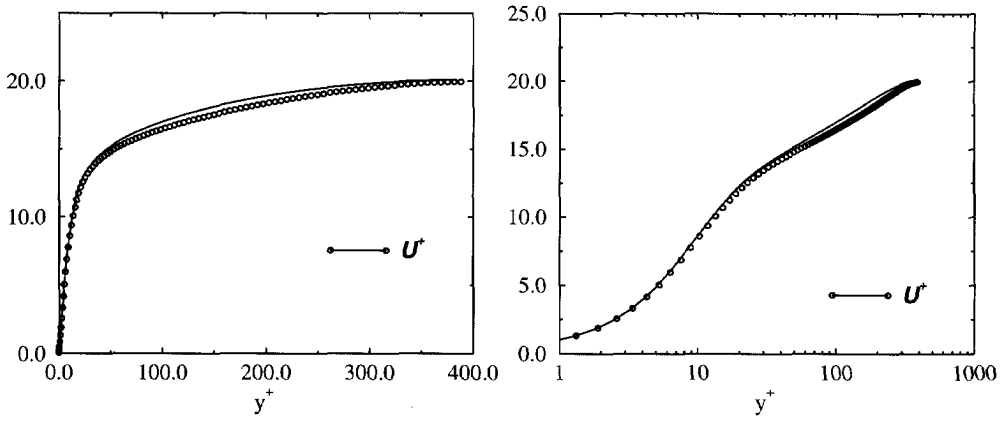

Figure 2.10: Mean velocity in linear and logarithmic scale (Symbols: DNS data of Kim (1990); Lines: ERM).

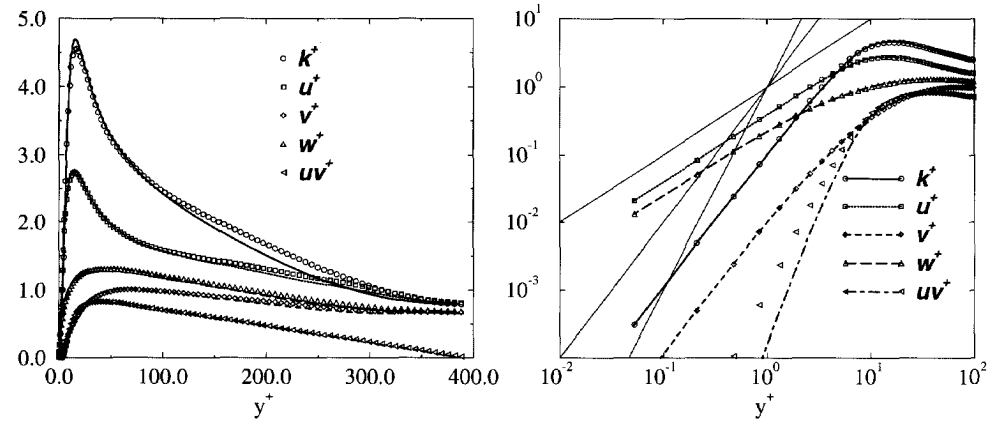

Figure 2.11: Turbulence kinetic energy and Reynolds-stresses (Symbols: DNS data Kim (1990); Lines: ERM).

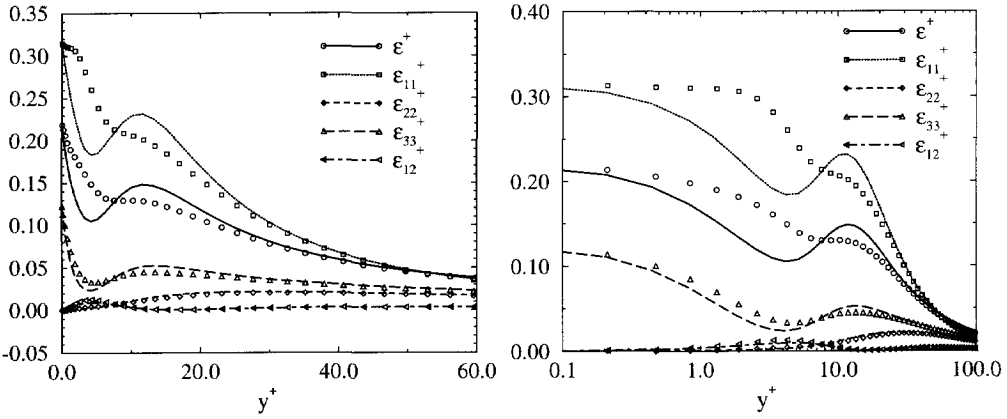

Figure 2.12: Dissipation rate tensor components (Symbols: DNS data Kim (1990); Lines: ERM).

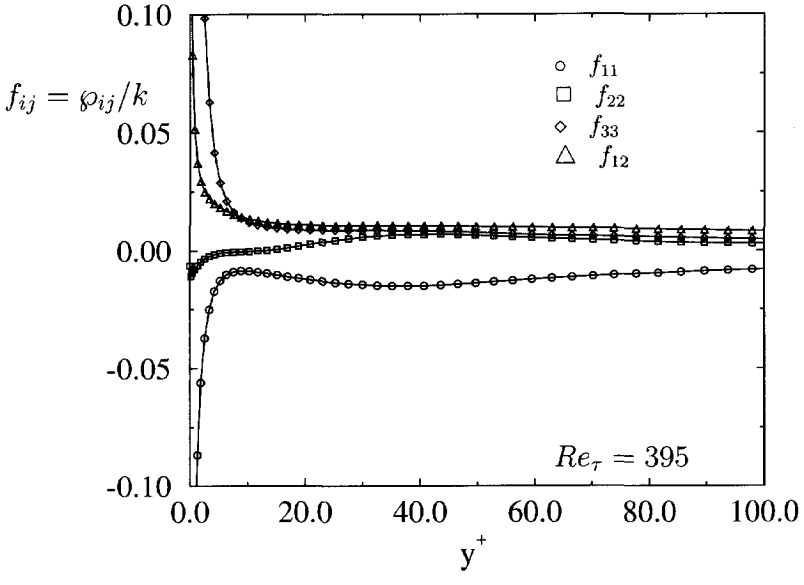

Figure 2.13: Function $f_{ij} = \wp_{ij}/k$ evaluated from DNS data.

2.3.11 Turbulent diffusion and pressure transport

The turbulent diffusion $\mathcal{D}_{ij}^{\mathrm{t}}$, as defined in equation (2.9), is usually modelled jointly with the deviatoric tensor obtained after splitting of the velocity-pressure/gradient fluctuation (equation (2.10)). If the pressure-strain decomposition (Table 2.1) is used, this is given by

$$\mathcal{D}_{ij}^{\mathrm{t}} + D_{ij}^{\mathrm{p}} = -\frac{\partial \overline{u_i u_j u_k}}{\partial x_k} - \frac{1}{\rho}\left(\frac{\partial \overline{p u_i}}{\partial x_j} + \frac{\partial \overline{p u_j}}{\partial x_i}\right). \tag{2.74}$$

Models for $\mathcal{D}_{ij}^{\mathrm{t}}$ have roots in the transport equation for the triple moments of the fluctuating velocity $\overline{u_i u_j u_k}$ which is derived from equation (2.8). Thus, the model coefficients are set to obtain optimal overall prediction of the Reynolds-stresses or the mean velocity. In that way the pressure diffusion is modelled implicitly, or can be regarded as neglected.

The most frequently used model for the turbulent diffusion is that proposed by Daly and Harlow (1970) (also called, the generalised gradient diffusion hypothesis, GGDH) and reads

$$\overline{u_i u_j u_k} = -C_s \tau \overline{u_l u_k} \frac{\partial \overline{u_i u_j}}{\partial x_l}. \tag{2.75}$$

The value of C_s is obtained by the numerical optimisation of the model results and has a value of about 0.20. A weakness of this model is that it is not tensorially invariant, although it is symmetric in i and j, but the triple correlation $\overline{u_i u_j u_k}$ is symmetric in all three indexes. Hanjalić and Launder (1972) neglected the transport terms in the exact transport equation for triple correlation $\overline{u_i u_j u_k}$ and assumed the quasi-Gaußian property of the fourth order correlations of the fluctuating velocities, and proposed a model which is tensorially invariant:

$$\overline{u_i u_j u_k} = -C_s \tau \overline{u_l u_k}\left(\overline{u_i u_l}\frac{\partial \overline{u_j u_l}}{\partial x_k} + \overline{u_j u_l}\frac{\partial \overline{u_k u_l}}{\partial x_i} + \overline{u_k u_l}\frac{\partial \overline{u_i u_l}}{\partial x_j}\right) \tag{2.76}$$

where $C_s = 0.11$.

The required timescale in models (2.75) and (2.76) is computed commonly as $\tau = k/\varepsilon$. Durbin (1993) argued that the time scale cannot be smaller than the Kolmogorov timescale $\tau_k = (\nu/\varepsilon)^{1/2}$ and proposed

$$\tau = \frac{k}{\varepsilon}\ \max\left(1, \frac{C_T}{Re_t^{1/2}}\right), \qquad \text{where} \qquad C_T = 6, \tag{2.77}$$

which is different from the large-eddy time scale only when turbulence Reynolds-numbers $Re_t = k^2/\nu\varepsilon < 36$ which occurs in the final stage of the decay of grid turbulence and in the immediate wall vicinity. The author's experience is that the use of the time-scale switch in the turbulent diffusion of $\overline{u_i u_j}$ is not so rewarding as it is e.g. in ε equation, where it is used to prevent the singularity of ε equation at the wall and contributes to relatively correct behaviour of ε in the viscous sublayer, as obtained by ERM.

Other more complex models for the triple-moments have been proposed e. g. by Lumley (1978), Reynolds (1984), Obi and Hara (1995) and Craft (1997). Most of these models have not

yet been extensively tested. In this thesis the turbulent diffusion is modelled by equation (2.75) which was also used during development and testing of the HJ low-Re-number model. Although inconsistent with the general modelling principles adopted in this thesis (lack of tensorial invariance), the model was used because more complex models yield little benefit but at the expense of higher computational demands, and, in some cases, of computational robustness. Most of all, the use of a different model for diffusion will require significant additional adjustment of the other model coefficients.

2.3.12 Dissipation Rate Tensor

The second most important term to be modelled in the Reynolds-stress transport equation (2.9) is the dissipation-rate tensor defined as

$$\varepsilon_{ij} = 2\nu\overline{\frac{\partial u_i}{\partial x_k}\frac{\partial u_j}{\partial x_k}}. \tag{2.78}$$

For high Re-number flows this term is usually modelled assuming that the smallest scale dissipative eddies are isotropic (Rotta 1951)

$$\varepsilon_{ij} = \frac{2}{3}\varepsilon\delta_{ij}, \tag{2.79}$$

where ε is the isotropic dissipation which is discussed in Section 2.4 below. According to the DNS of homogeneous flows at low to moderate turbulence Reynolds number (e. g. Matsumoto *et al.* 1991) as well as DNS of channel flows, the dissipation rate tensor does not comply with the notion of isotropic condition assumed by the model (2.79).

Rotta (1951) argued that ε_{ij} in the limit of zero turbulence Reynolds number $Re_t = k^2/(\nu\varepsilon)$ is

$$\varepsilon_{ij} = \frac{\overline{u_i u_j}}{k}\varepsilon. \tag{2.80}$$

This model produces the correct wall values (for $Re_t = 0$), but as it follows fully the anisotropy of Reynolds-stresses, i.e. $e_{ij} = a_{ij}$, it cannot reach the isotropic state as fast as the DNS data show that happens. Fig 2.14 shows the distribution of the flatness factors of the Reynolds-stress anisotropy tensor $a_{ij} = \overline{u_i u_j}/k - 2/3\delta_{ij}$ and the dissipation-rate anisotropy tensor $e_{ij} = \varepsilon_{ij}/\varepsilon - 2/3\delta_{ij}$, A and E respectively, in a Couette flow with adverse pressure gradient obtained from DNS data. The dissipation anisotropy tensor e_{ij} reaches the isotropic state (which is given by $E = 1$) much closer to the walls than the stress anisotropy tensor disapproving, thus, far the model (2.80) for near wall-flows.

Hanjalić and Launder (1976) introduced a form which covers the high Re-number flows as well as the near-wall region

$$\varepsilon_{ij} = (1 - f_s)\frac{2}{3}\varepsilon\delta_{ij} + f_s\varepsilon^*_{ij}, \tag{2.81}$$

where ε_{ij}^* is a model for the dissipation rate valid near the wall, and in this model is given by (2.80). The blending function $f_s = e_{ij}/a_{ij}$ expresses the proportionality between the small-scale (dissipation rate) and the large-scale (Reynolds stress) anisotropies. It takes the value of unity at the wall and tends to zero at appropriate distance from the wall, or at the appropriate Re-number, ensuring the transition between the low Re-number region near the wall and the high Re-number region far from the wall. This function is usually modelled in terms of Re_t (Hanjalić and Launder 1976) and more recently in terms of A and E (Hanjalić and Jakirlić 1993). According to DNS results of wall flows the function f_s is not universal, but rather different for each component of the stress and dissipation tensor.

Launder and Reynolds (1983) demonstrated that expression (2.80) of the model for ε_{ij} is asymptotically incorrect in the wall limit for the components which contain the index of the direction normal to the wall (e. g. 2). Applying the Taylor series expansion to the velocity fluctuation in the vicinity of a wall they obtained

$$\frac{\varepsilon}{k} = \frac{\varepsilon_{11}}{\overline{u_1u_1}} = \frac{1}{4}\frac{\varepsilon_{22}}{\overline{u_2u_2}} = \frac{\varepsilon_{33}}{\overline{u_3u_3}} = \frac{1}{2}\frac{\varepsilon_{12}}{\overline{u_1u_2}} = \frac{1}{2}\frac{\varepsilon_{23}}{\overline{u_2u_3}} = \frac{\varepsilon_{13}}{\overline{u_1u_3}}. \tag{2.82}$$

In order to obtain a correct behaviour in the wall limit, Launder and Reynolds (1983) proposed a correction in terms of the wall unit vector

$$\varepsilon_{ij}^* = \varepsilon\left[\frac{\overline{u_iu_j}}{k} + \left(\frac{\overline{u_iu_k}}{k}n_kn_j + \frac{\overline{u_ju_k}}{k}n_kn_i\right) + \frac{\overline{u_ku_l}}{k}n_kn_l\,\delta_{ij}\right], \tag{2.83}$$

where the n_i is the unit vector of the direction normal to the wall.

Kebede *et al.* (1985) extended further this expression as follows, in order to provide that ε_{ij}^* contracts to ε:

$$\varepsilon_{ij}^* = \frac{\varepsilon}{F}\left[\frac{\overline{u_iu_j}}{k} + \left(\frac{\overline{u_iu_k}}{k}n_kn_j + \frac{\overline{u_ju_k}}{k}n_kn_i\right) + \frac{\overline{u_ku_l}}{k}n_kn_l\,\delta_{ij}\right] \tag{2.84}$$

where $F = 1 + \frac{5}{2}\frac{\overline{u_pu_q}}{k}n_pn_q$.

In order to reduce an unrealistically prolonged effect of the wall correction, Hanjalić and Jakirlić (1993) proposed the model in the form

$$\varepsilon_{ij}^* = \frac{\varepsilon}{F}\left[\frac{\overline{u_iu_j}}{k} + \left(\frac{\overline{u_iu_k}}{k}n_kn_j + \frac{\overline{u_ju_k}}{k}n_kn_i + \frac{\overline{u_ku_l}}{k}n_kn_ln_in_j\right)f_d\right], \tag{2.85}$$

where $F = 1 + \frac{3}{2}\frac{\overline{u_pu_q}}{k}n_pn_qf_d$, $f_d = \dfrac{1}{1+0.1Re_t}$. Of several forms for f_s tested by them, the DNS results of ε_{ij} are best reproduced by the function

$$f_s = 1 - \sqrt{A}E^2. \tag{2.86}$$

Fig 2.14 shows the shape of function (2.86) in a Couette flow evaluated from the DNS data.

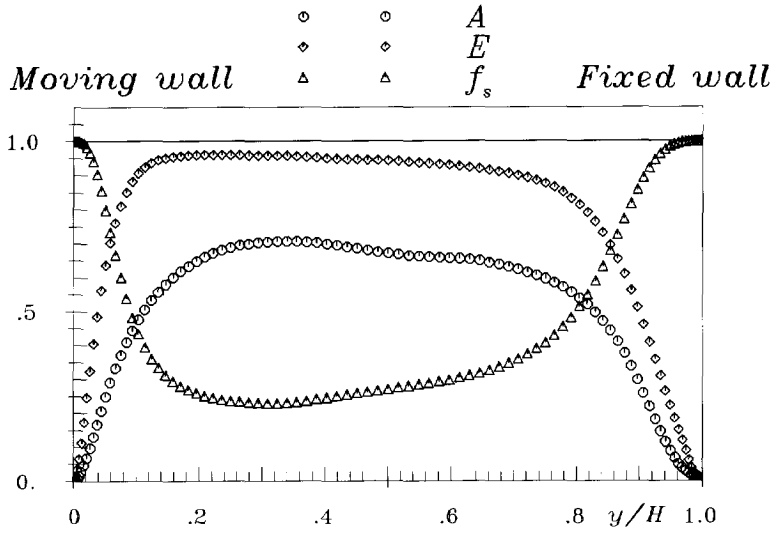

Figure 2.14: A, E and f_s evaluated from DNS data of Kuroda *et al.* (1993) for a Couette flow with adverse pressure gradient $\partial P/\partial x/\left(\rho U_w^2/\delta\right) = -1.1 \times 10^{-3}$ (which provides $\partial U/\partial y \approx 0$ near the moving wall) at $Re_w = U_w\delta/\nu = 3000$.

A comprehensive review of the algebraic models for the dissipation rate tensor, which include the wall correction in terms of the wall orientation vector was recently given by Jakirlić (1997). The wall-normal vector cannot be uniquely defined for complex wall flows, and in the numerical sense, such models are not convenient for applications to the wall-flows in arbitrary geometries. Attempts have been made recently to design the models for the dissipation rate tensor which satisfy the near wall behaviour without using the wall topology information (e. g. Shima 1995, Perot and Moin 1995b and Craft and Launder 1996).

Shima (1995) and Hanjalić *et al.* (1996) proposed a dissipation rate model which does not use the wall orientation vector. Model (2.81) was extended by including the viscous diffusion of Reynolds-stresses and turbulence kinetic energy to satisfy the wall limit and was inspired by the analysis of the near-wall values of every single term in the transport equation for $\overline{u_i u_j}$. The model of Shima is given by

$$\varepsilon_{ij} = (1-f_s)\frac{2}{3}\varepsilon\delta_{ij} + f_s\frac{\overline{u_iu_j}}{k}\varepsilon + \frac{1}{2}\left(\nu\frac{\partial^2\overline{u_iu_j}}{\partial x_l^2} - \nu\frac{\overline{u_iu_j}}{k}\frac{\partial^2 k}{\partial x_l^2}\right). \tag{2.87}$$

where the blending function f_s has form (2.86).

A disadvantage of this model is the use of the second derivatives of $\overline{u_iu_j}$ and k, since their evaluation is always accompanied by a relatively large numerical error, which can contaminate the solution.

Perot and Moin (1995b) proposed a model for ε_{ij} which does not use any damping function and has a very simple form

$$\varepsilon_{ij} = \frac{2}{3}\tilde{\varepsilon}\frac{\overline{u_i u_j}}{k} + 2\nu\frac{\partial Q_{ik}}{\partial x_l}\frac{\partial Q_{jk}}{\partial x_l}, \tag{2.88}$$

where the tensor Q_{ij} is the solution of equation $Q_{ik}Q_{kj} = \overline{u_i u_j}$. This makes Q_{ij} a generalised square root of Reynolds-stress tensor and, for that reason it does not have a unique solution. However, this does not seem to be important in the model because Q appears in pairs cancelling any dependence of sign (Perot and Moin 1995b). The model reproduce well DNS data for channel flows, shear-free wall boundary layers as well as shear-free free-surface boundary layers. However, calculation of Q_{ij} was found by Craft and Launder (1996) to be unsuitable for computation of complex flows.

A new near wall correction model

In the remaining part of this sub-section a new form of the wall-correction part of the model for the dissipation rate tensor (equation 2.81) is derived. This model does not involve the wall-orientation vectors and uses only the first derivatives of the Reynolds-stress. It is therefore simpler than Shima's model as well as any other model with the wall-orientation vector, and, as such, it is more convenient to be applied to computation of complex flows.

The starting point of the derivation is the fluctuating velocity which can be expressed as

$$u_i = a_i k^{1/2}, \tag{2.89}$$

where k is turbulence kinetic energy and a_i is a dimensionless fluctuating variable. By differentiating expression (2.89) and averaging, the dissipation rate tensor is

$$\varepsilon_{ij} = 2\nu\overline{\frac{\partial u_i}{\partial x_k}\frac{\partial u_j}{\partial x_k}} = 2\nu\left[\overline{\frac{\partial a_i}{\partial x_k}\frac{\partial a_j}{\partial x_k}}k + \frac{1}{2}\frac{\partial\overline{a_i a_j}}{\partial x_k}\frac{\partial k}{\partial x_k} + \overline{a_i a_j}\frac{\partial k^{1/2}}{\partial x_k}\frac{\partial k^{1/2}}{\partial x_k}\right], \tag{2.90}$$

and the dissipation of turbulence kinetic energy is

$$\varepsilon = \nu\left[\overline{\frac{\partial a_i}{\partial x_k}\frac{\partial a_i}{\partial x_k}}k + \overline{a_i a_i}\frac{\partial k^{1/2}}{\partial x_k}\frac{\partial k^{1/2}}{\partial x_k}\right] \tag{2.91}$$

where $\overline{a_i a_j} = \dfrac{\overline{u_i u_j}}{k}$ and $\overline{a_i a_i} = 2$. The only terms to be modelled in equations (2.90) and (2.91) are the correlations of gradients of a_i. Here we model this terms as

$$\overline{\frac{\partial a_i}{\partial x_k}\frac{\partial a_j}{\partial x_k}} = \frac{\overline{a_i a_j}}{L^2}. \tag{2.92}$$

From equations (2.90) and (2.91) the length scale L is obtained as

$$L = \left(\frac{2\nu k}{\tilde{\varepsilon}}\right)^{\frac{1}{2}} \tag{2.93}$$

where

$$\tilde{\varepsilon} = \varepsilon - 2\nu \frac{\partial k^{1/2}}{\partial x_k} \frac{\partial k^{1/2}}{\partial x_k}. \tag{2.94}$$

Finally the model for ε_{ij} is given by

$$\varepsilon_{ij} = \overline{a_i a_j}\varepsilon + \nu \frac{\partial \overline{a_i a_j}}{\partial x_k} \frac{\partial k}{\partial x_k}, \tag{2.95}$$

where $\overline{a_i a_j} = \dfrac{\overline{u_i u_j}}{k}$. The first term on the right-hand-side of equation (2.95) is Rotta's model and the examination of the second term shows that this term has the zero value at a wall and becomes again zero at $y^+ \approx 10$. Therefore, this model can be regarded as a correction to the Rotta model in the wall vicinity, and a correction for the transition from the wall region to the core, or high-Re-number region, is still needed. For that purpose we adopted the function used in the model of Hanjalić and Jakirlić (1993). The author's experience shows that this function provides the best convergence[11] among several different forms examined. The new model is given finally as

$$\varepsilon_{ij} = (1 - f_s)\frac{2}{3}\varepsilon\delta_{ij} + f_s \left[\frac{\overline{u_i u_j}}{k}\varepsilon + \nu \frac{\partial}{\partial x_k} \left(\frac{\overline{u_i u_j}}{k} \right) \frac{\partial k}{\partial x_k} \right] \tag{2.96}$$

Fig 2.15 shows *a priory* testing of three models: the HJ model (equations 2.81 and 2.85), the Shima model (equation 2.87) and the new model given with (equation 2.96) in the channel flow at two Re-numbers using DNS data. Fig 2.16 shows the near-wall limit value $\dfrac{\varepsilon_{ij}}{\varepsilon}\dfrac{k}{\overline{u_i u_j}}$ for the three models compared to DNS data. Fig 2.17 and Fig 2.18 show the *a priory* model testing in two flows for which the DNS data of Perot and Moin (1995a) are available: the wall shear-free flow and the free-surface shear-free flow. These results show that the new model performs reasonably well in the wall flows and provides results closer to DNS than the other two models compared here. The new model predicts the wall-limiting values of components of ε_{ij} tensor correctly. For the ε_{11} component a larger deviation from DNS data is observed although the model predicts the ε_{11} component in good agreement with DNS data, as shown in Fig 2.15 and Fig 2.17. Because they were developed for wall flows, these models predict incorrect wall boundary behaviour in the free-surface shear-free flow.

[11] System of equations given with (2.81) is non-linear when the function f_s (2.86) is used.

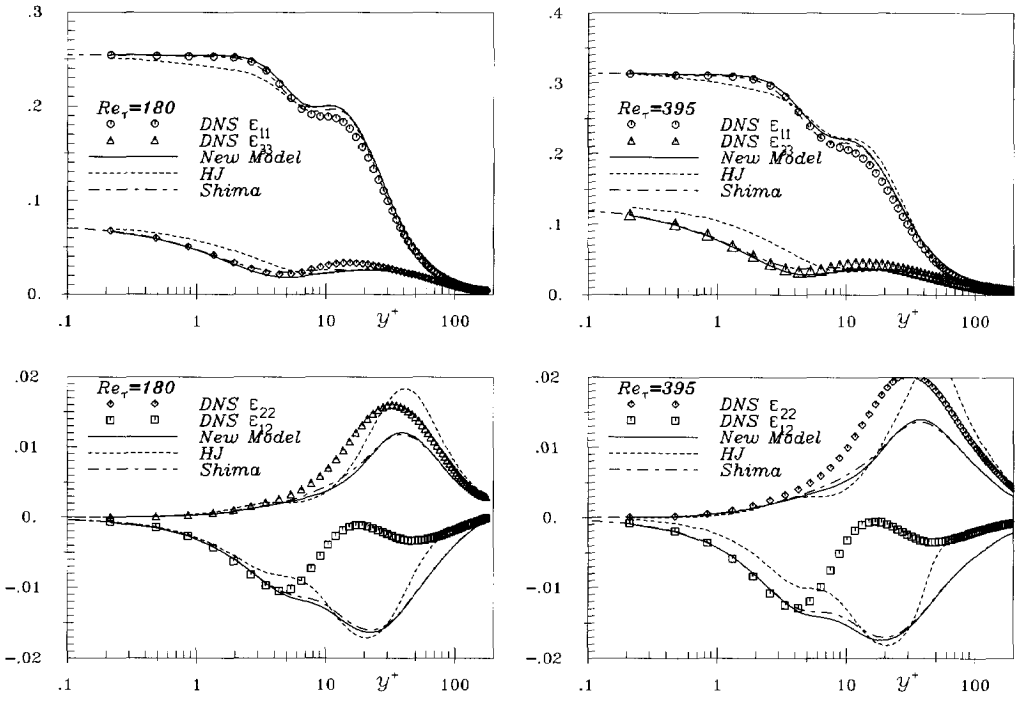

Figure 2.15: A priory testing of three models for ε_{ij} and comparison with DNS data for two channel flows: $Re_\tau = 180$ Kim *et al.* (1987) and $Re_\tau = 395$ Kim (1990)

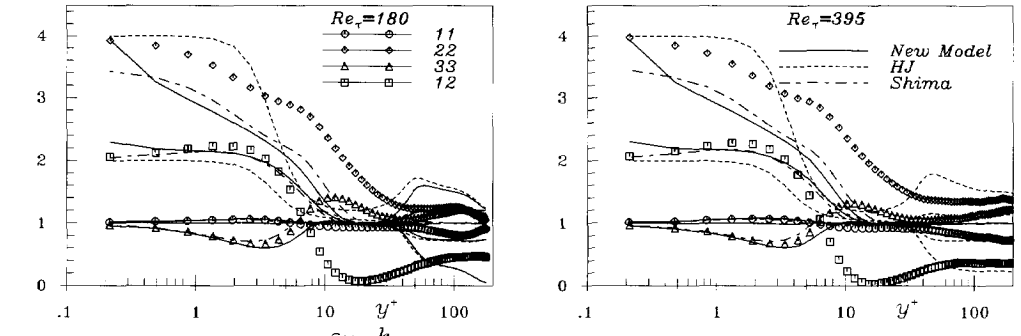

Figure 2.16: Model results for $\dfrac{\varepsilon_{ij}}{\varepsilon}\dfrac{k}{\overline{u_i u_j}}$ evaluated from DNS (lines, as given on the right) and compared with corresponding DNS data (symbols).

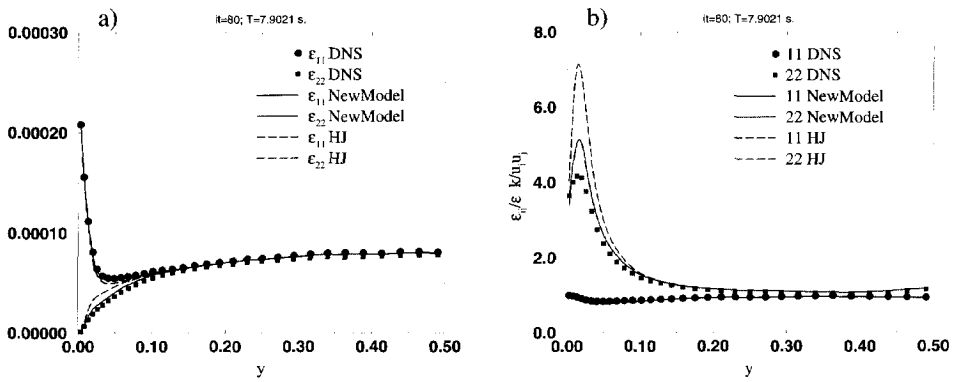

Figure 2.17: Components of the dissipation tensor (a) and its near-boundary-limit value (b) in a wall shear-free flow. Symbols are the DNS data of Perot and Moin (1995a) and lines are the *a priory* tests of models given by (2.85) and (2.95).

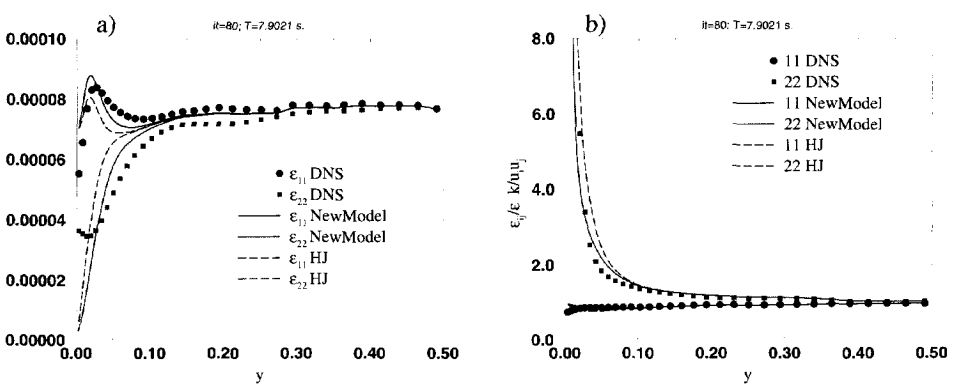

Figure 2.18: Components of the dissipation tensor (a) and its near-boundary-limit value (b) in a free-surface flow. Symbols are the DNS data of Perot and Moin (1995a) and lines are the *a priory* tests of models given by (2.85) and (2.95).

2.4 Modelling the dissipation of turbulence kinetic energy

2.4.1 The standard model

The EVMs directly and the SMC models indirectly solve the transport equation for the turbulence kinetic energy k which can be regarded as the velocity scale of the turbulent motion. For modelling purposes, almost all single-point closure models require a timescale and a lengthscale. In most proposals these scales are computed using k and the dissipation rate of turbulence kinetic energy ε for which a scalar transport equation is solved. Dissipation rate ε appears in the transport equation for k and can be regarded as a destruction of turbulence kinetic energy by small scale motions of fluid and, ultimately, by viscosity.

The exact transport equation for ε is derived from the transport equation for the velocity fluctuation following the definition of ε (equation 2.11) and can be written as[12]

$$\frac{D\varepsilon}{Dt} = P_\varepsilon^1 + P_\varepsilon^2 + P_\varepsilon^3 + P_\varepsilon^4 - Y + T_\varepsilon + \Pi_\varepsilon + \mathcal{D}_\varepsilon, \tag{2.97}$$

where

$$P_\varepsilon^1 = -2\nu \overline{\frac{\partial u_i}{\partial x_k}\frac{\partial u_j}{\partial x_k}} S_{ij} = -\varepsilon_{ij} S_{ij} = -\varepsilon_{ij}\frac{\partial U_i}{\partial x_j} \quad \text{- Mixed production,}$$

$$P_\varepsilon^2 = -2\nu \overline{\frac{\partial u_k}{\partial x_i}\frac{\partial u_k}{\partial x_j}} S_{ij} = -2\nu \overline{\frac{\partial u_k}{\partial x_i}\frac{\partial u_k}{\partial x_j}}\frac{\partial U_i}{\partial x_j} \quad \text{- Production by mean rate of strain,}$$

$$P_\varepsilon^3 = -2\nu \overline{u_j \frac{\partial u_i}{\partial x_k}}\frac{\partial^2 U_i}{\partial x_j \partial x_k} \quad \text{- Gradient production,}$$

$$P_\varepsilon^4 = -2\nu \overline{\frac{\partial u_i}{\partial x_j}\frac{\partial u_i}{\partial x_k}\frac{\partial u_j}{\partial x_k}} \quad \text{- Turbulent production,}$$

$$Y = 2\nu^2 \overline{\frac{\partial^2 u_i}{\partial x_j \partial x_k}\frac{\partial^2 u_i}{\partial x_j \partial x_k}} \quad \text{- Dissipation,}$$

$$T_\varepsilon = -\nu \frac{\partial}{\partial x_k}\left(\overline{u_m \frac{\partial u_i}{\partial x_j}\frac{\partial u_i}{\partial x_j}}\right) \quad \text{- Turbulent transport,}$$

$$\Pi_\varepsilon = -\frac{2}{\rho}\nu \overline{\frac{\partial}{\partial x_k}\left(\frac{\partial p}{\partial x_i}\frac{\partial u_k}{\partial x_i}\right)} \quad \text{- Pressure transport,}$$

$$D_\varepsilon = \nu \frac{\partial^2 \varepsilon}{\partial x_k \partial x_k} \quad \text{- Viscous diffusion.}$$

[12]Notation as given by Mansour *et al.* (1988) and used in Fig 2.19.

All terms on the right hand side of equation (2.97), excluding the viscous diffusion, have to be modelled. Distribution of all terms in equation (2.97) obtained with DNS by Kim (1990) in a fully developed channel flow at $Re_\tau = 395$ is displayed in Fig 2.19. It shows that P_ε^4 and Y are the dominant terms in the core region ($y^+ > 50$) but near the wall they are of the same order as other production terms. At the wall the dissipation Y is in balance with the viscous diffusion D_ε.

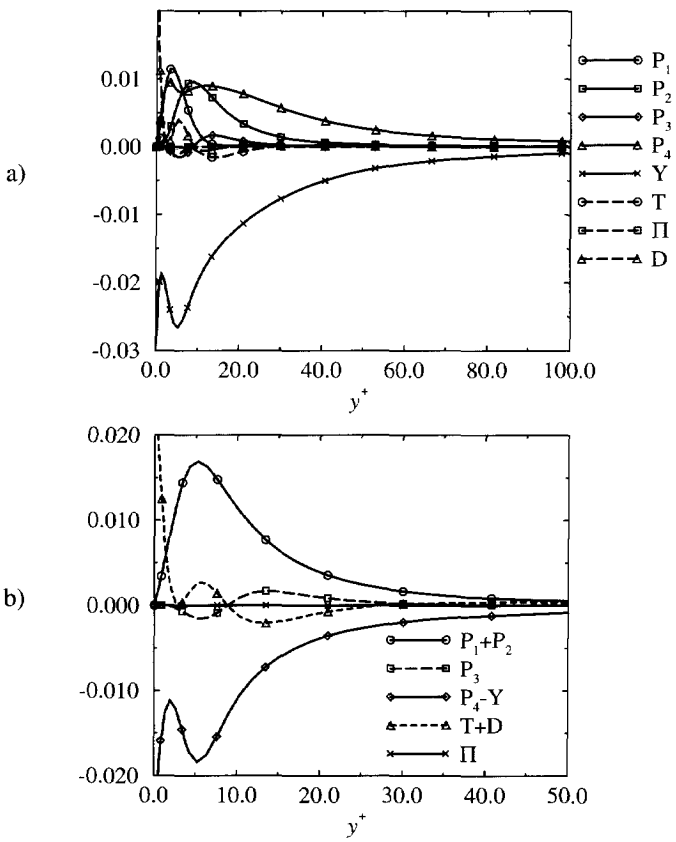

Figure 2.19: Budget of ε equation obtained with DNS of a channel flow at $Re_\tau = 395$ (Kim 1990). a) Notation as given in equation (2.97). b) Terms arranged accordingly to equations (2.99) and (2.100). All terms are made dimensionless with u_τ^6/ν^2.

The most frequently used form of the modelled transport equation for ε is that proposed by Davydov (1960) and later reformulated by Hanjalić and Launder (1972)

$$\frac{D\varepsilon}{Dt} = C_{\varepsilon_1}\frac{P_k}{\tau} - C_{\varepsilon_2}\frac{\varepsilon}{\tau} + \frac{\partial}{\partial x_l}\left(\nu\delta_{lm} + C_\varepsilon\tau\overline{u_l u_m}\right)\frac{\partial\varepsilon}{\partial x_m}. \tag{2.98}$$

The first two terms on the right-hand-side of equation (2.98), the source and the sink term,

which are supposed to model the production and the destruction (dissipation) of ε respectively, are given by

$$P_\varepsilon^1 + P_\varepsilon^2 + P_\varepsilon^3 = C_{\varepsilon_1} \frac{P_k}{\tau}, \tag{2.99}$$

$$P_\varepsilon^4 - Y = -C_{\varepsilon_2} \frac{\varepsilon}{\tau}, \tag{2.100}$$

where the model coefficients were chosen to satisfy some simple flows such as decay of isotropic turbulence and shear homogeneous flows. A range of values for these two coefficients can be found in literature. The coefficients C_{ε_2} was determined using experimental data for isotropic decaying turbulence ($P_k = 0$). According to most experimental data C_{ε_2} must take a value of around 1.9 in order to give the correct decay rate of the turbulence kinetic energy in the inertial range. C_{ε_1} can be obtained by optimisation in a local equilibrium shear flow. In this way the standard model values are obtained: $C_{\varepsilon_1} = 1.44$ and $C_{\varepsilon_2} = 1.92$. The UMIST turbulence modelling group proposed (Fu *et al.* 1987, Craft 1991, Launder and Tselepidakis 1991) $C_{\varepsilon_1} = 1$ and $C_{\varepsilon_2} = 1.92/(1 + 0.63\,(AA_2)^{1/2})$ which were used in free flows as well as in wall flows.

2.4.2 A critical analysis of the model and possible improvements

We now turn to a critical analysis of modelling the transport equation for ε based on recent DNS data. Fig 2.20 shows the ratio of the production and the dissipation terms $(P_\varepsilon^1 + P_\varepsilon^2 + P_\varepsilon^3)/(P_\varepsilon^4 - Y)$ in the ε equation obtained with DNS in a channel flow. Apparently this function has a very similar shape to that of the ratio P_k/ε, shown in Fig 2.21. Using expressions (2.99) and (2.100) a model for the ratio of the production and the dissipation in ε equation is given by

$$\frac{P_\varepsilon^1 + P_\varepsilon^2 + P_\varepsilon^3}{P_\varepsilon^4 - Y} = -\frac{C_{\varepsilon_1}}{C_{\varepsilon_2}} \cdot \frac{P_k}{\varepsilon}. \tag{2.101}$$

The *a priory* tests using expression (2.101) and three sets of model coefficients: the standard model, the UMIST model and the SSG model (Speziale *et al.* 1991) ($C_{\varepsilon_1} = 1.44$ and $C_{\varepsilon_2} = 1.83$), are shown in Fig 2.20. All three models perform fairly well in the log-law region ($P_k/\varepsilon \approx 1$) although it may be said that the standard model (with $C_{\varepsilon_1} = 1.44$ and $C_{\varepsilon_2} = 1.92$) gives the closest results to DNS data. It is also shown here that the models with constant coefficients capture also the peak at $y^+ \approx 15$ almost correctly but the more complex model, with variable model coefficients (the UMIST model), is not so good. Note that the production P_ε^3, which is important only in the near wall region, is included in the evaluation of DNS data. None of the models follow the DNS data in the viscous sub-layer $y^+ < 5$ (Fig 2.20a).

The most important conclusion from these DNS data is that the ratio $(P_\varepsilon^1+P_\varepsilon^2+P_\varepsilon^3)/(P_\varepsilon^4-Y)$ is a function proportional to the ratio P_k/ε. This is observed here in a case of equilibrium flow. Nevertheless, it has to be mentioned that the form of the model and the values of coefficients were proposed two decades before DNS data were available.

Since ε is used in obtaining of the time- and length-scale of turbulence, which are crucial in the closure problem, ε equation is often blamed for some unsatisfactory results of RANS

models, especially in complex flows. The above shown analysis of DNS data may justify particularly good results of RANS models in the equilibrium flows. A similar investigation of non-equilibrium flows would be particularly challenging and might provide insight into modelling of ε equation as well as to cure some deficiencies observed in computing relatively complex flows.

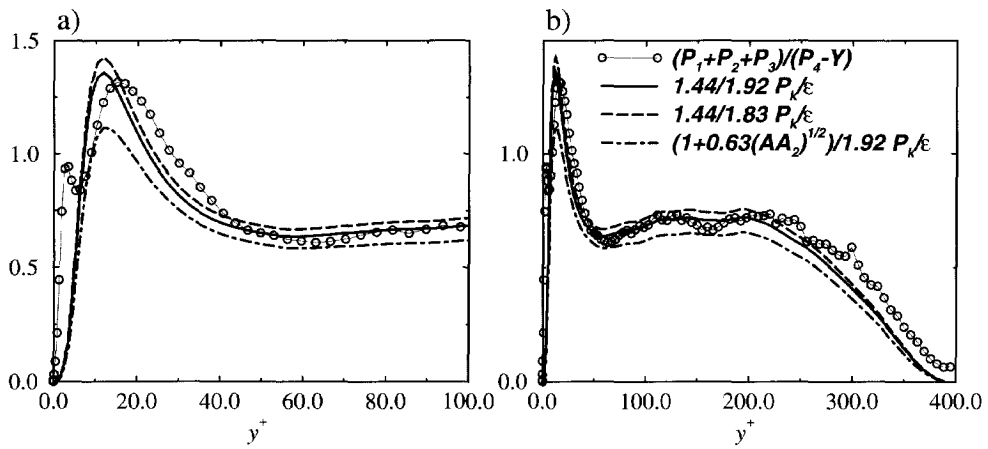

Figure 2.20: Ratio of the dissipation and the production in the ε equation $(P_\varepsilon^1 + P_\varepsilon^2 + P_\varepsilon^3)/(P_\varepsilon^4 - Y)$ obtained from DNS data in channel flow at $Re_\tau = 395$ and compared to model results for $C_{\varepsilon_1}/C_{\varepsilon_2} \cdot P_k/\varepsilon$ with: $C_{\varepsilon_1} = 1.44$ and $C_{\varepsilon_2} = 1.92$; $C_{\varepsilon_1} = 1.44$ and $C_{\varepsilon_2} = 1.83$; $C_{\varepsilon_1} = 1$ and $C_{\varepsilon_2} = 1.92/(1 + 0.63\,(AA_2)^{1/2})$. a) magification near the wall.

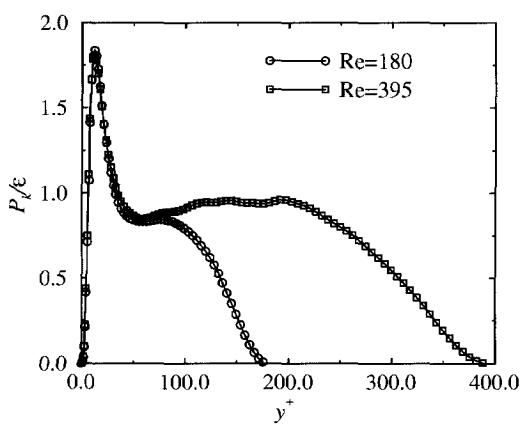

Figure 2.21: Ratio of production P_k and dissipation ε of the turbulence kinetic energy k in a channel flow at $Re_\tau = 180$ and 395 obtained with DNS (Kim *et al.* 1987, Kim 1990).

The DNS data show that in the log-region of the fully developed channel flow the production $P_\varepsilon^1 + P_\varepsilon^2 + P_\varepsilon^3$, the dissipation $P_\varepsilon^4 - Y$ and the turbulent transport T_ε close the balance of the equation. Since the ratio production/dissipation in this flow is about 0.7 (Fig 2.20), the turbulent transport participates with remaining 30% in the budget of this equation. Therefore, the modelling of diffusion is as important as modelling of the production and the dissipation. In the framework of SMC the Daly-Harlow model is commonly used (expression (2.75)) with $C_\varepsilon = 0.18$.

2.4.3 The low-Re-number models

Equation (2.98) is used only in high-Re-number models, which, in the case of wall flows, use the wall functions. This means that for the low-Re-number flow and near wall layer, the equation needs to be extended to account for the viscosity and near wall effects. The above neglected terms, such as the gradient production Y (2.97), have to be modelled.

The first low-Re number modification of equation (2.98) was proposed by Jones and Launder (1972) (JL) in the framework of EVM. This model was subsequently modified by Launder and Sharma (1974) (LS) and this form is still the most frequently used low-Re number model. JL and LS models have a modified turbulent viscosity which, following its definition, accommodate for the change of the shear stress near the wall, which is given as (LS model):

$$\nu_t = \exp\left(\frac{-30}{(1+Re_t/50)^2}\right)\cdot C_\mu \frac{k^2}{\tilde{\varepsilon}}, \qquad \text{where} \qquad \tilde{\varepsilon} = \varepsilon - 2\nu\left(\frac{\partial k^{1/2}}{\partial x_l}\right)^2 \tag{2.102}$$

Analysing the DNS data of Mansour *et al.* (1988), Rodi and Mansour (1993) found that none of the popular proposals for ν_t is in satisfactory agreement with DNS data.

The LS model solves the transport equation for $\tilde{\varepsilon}$ which is numerically more convenient because $\tilde{\varepsilon}$ at wall is zero. Further, the turbulent production term P_ε^3 in equation (2.97) is modelled as

$$P_\varepsilon^3 = 2\nu\nu_t \frac{\partial^2 U_i}{\partial x_k \partial x_m}\frac{\partial^2 U_i}{\partial x_k \partial x_m}, \tag{2.103}$$

and a damping of the dissipation term is done so that

$$P_\varepsilon^4 - Y = -f_\varepsilon\, C_{\varepsilon 2}\, \frac{\varepsilon}{\tau}, \tag{2.104}$$

where $f_\varepsilon = 1 - 0.3\exp\left(-Re_t{}^2\right)$. Entire specification of the Launder-Sharma model is given in Appendix D.

The low-Re number transport equation for the dissipation rate ε in connection with SMC proposed by Hanjalić and Launder (1976) is a modification of equation (2.98) and expression (2.103) and can be written as

$$\frac{D\varepsilon}{Dt} = C_{\varepsilon_1}\frac{P_k}{\tau} - f_\varepsilon C_{\varepsilon_2}\frac{\varepsilon}{\tau} + \frac{\partial}{\partial x_l}\left(\nu\delta_{lm} + C_\varepsilon \tau \overline{u_l u_m}\right)\frac{\partial \varepsilon}{\partial x_m}$$
$$+C_{\varepsilon_3}\,\nu\,\frac{k}{\varepsilon}\overline{u_k u_l}\frac{\partial^2 U_i}{\partial x_k \partial x_m}\,\frac{\partial^2 U_i}{\partial x_k \partial x_m}, \tag{2.105}$$

where

$$f_\varepsilon = 1 - \frac{C_{\varepsilon_2} - 1.4}{C_{\varepsilon_2}}\exp\left[-\left(\frac{Re_t}{6}\right)^2\right] \tag{2.106}$$

was chosen to satisfy a change from inertial to the final period of decay of isotropic turbulence.

In order to compensate for excessive growth of the length scale L, Hanjalić and Jakirlić (1998) introduced an additional source term into the transport equation for ε, which reads

$$S_l = \max\left\{\left[\left(\frac{1}{C_l}\frac{\partial L}{\partial x_j}\right)^2 - 1\right]\left(\frac{1}{C_l}\frac{\partial L}{\partial x_j}\right)^2 ; 0\right\}\frac{\tilde{\varepsilon}\varepsilon}{k}\,A, \qquad L = k^{3/2}/\varepsilon. \tag{2.107}$$

This term has its origin in the correction introduced first by Yap (1987), but has been reformulated in an invariant form. It uses the gradient of the length scale, and was proved particularly beneficial to the improvement of the predictions of reattaching separated flows. Fig 2.22 demonstrates the effect of inclusion of this term on the prediction of the streamlines in a fully periodic flow over ribs. It shows the computed streamline pattern obtained with the basic high-Re-number Reynolds-stress model, with two sets of coefficients in ε equation, the standard values and the UMIST model. The shape and the size of the bubble remained almost the same, but the anomaly in the streamline pattern in the reattachment region, predicted with most Reynolds-stress models, disappeared. This also had a favourable effect on the predictions of the flow properties in the reattachment region and downstream, as obtained in this case and shown by Hanjalić and Jakirlić (1998) in computations of the back-step flows. For the particular flow shown in Fig 2.22, due to the periodicity of the flow, the S_l term has a more pronounced influence than in some other flows (e.g. back-step). By producing a realistic shape of the streamlines in the reattachment region the recirculation bubble is extended. Due to presence of the subsequent rib and a bubble in front of it, the use of S_l results in connecting of these two bubbles. Since there is not sufficient experimental evidence (experiments performed by Drain and Martin 1985) about the length of these two bubbles, it is difficult to judge the model performances. Nevertheless, available experimental data indicate that the standard model with the new term, predicts velocity profiles closer to experiments than without this term (not shown here). Note that the UMIST model predicts a somewhat shorter recirculation, and similar underprediction of the recirculation in some back-step flows is also obtained (not shown here).

The transport equation for the dissipation rate ε used by Durbin (1993) with ERM is given with

$$\frac{D\varepsilon}{Dt} = \frac{C^*_{\varepsilon_1} P_k - C_{\varepsilon_2}\varepsilon}{\tau} + \frac{\partial}{\partial x_l}\left(\nu\delta_{lm} + C_\varepsilon\, \tau\, \overline{u_l u_m}\right)\frac{\partial \varepsilon}{\partial x_m} \tag{2.108}$$

where $C^*_{\varepsilon_1} = 1.44\left(1 + 0.1\dfrac{P_k}{\varepsilon}\right)$, $C_{\varepsilon_2} = 1.9$ and $C_\varepsilon = 0.14$. The timescale τ is given with (2.77) which switches from the large-eddy time scale k/ε to the Kolmogorov time scale at $Re_t = 36$. The "scale-switch" can be also seen as a damping function f_ε (expression (2.106)). As mentioned above, the use of a scale-switch removes the singularity of ε equation. In addition, it plays an important role in obtaining a good shape of ε near wall and correct wall value of ε (see Fig 2.12). Note that equation (2.108) does not involve the second derivatives of the mean velocity making this equation simple and numerically convenient.

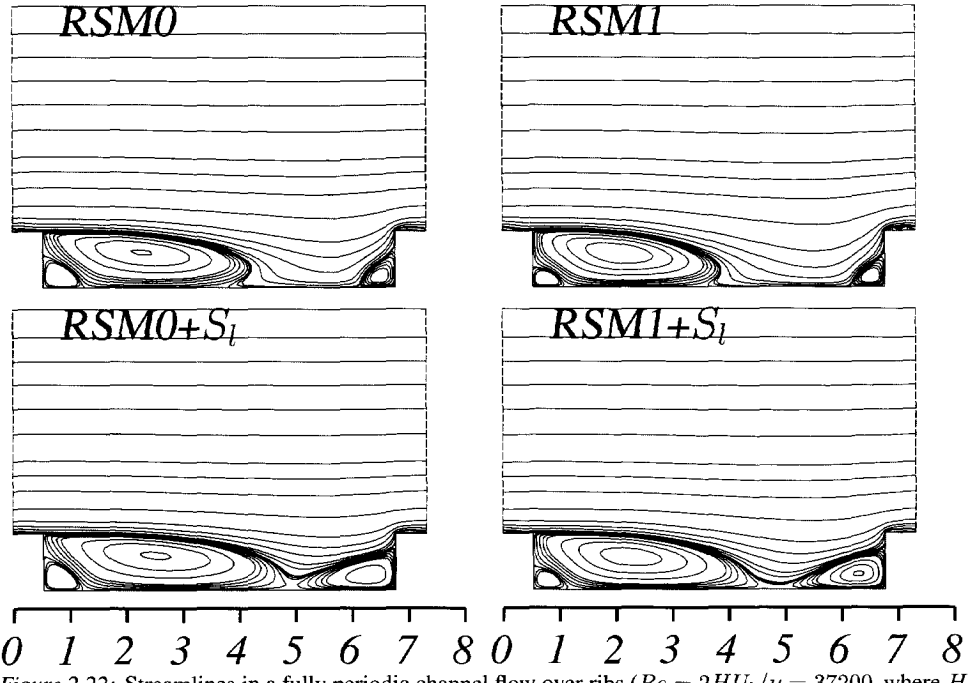

Figure 2.22: Streamlines in a fully periodic channel flow over ribs ($Re = 2HU_b/\nu = 37200$, where H is the channel width) obtained with the basic high-Re-number RSM and four variations in transport equation for ε (2.98). RSM0: $C_{\varepsilon_1} = 1.44$ and $C_{\varepsilon_2} = 1.92$; RSM1: $C_{\varepsilon_1} = 1$ and $C_{\varepsilon_2} = 1.92/(1 + 0.63\,(AA_2)^{1/2})$.

CHAPTER 3

Adopted Numerical Method

In this chapter the numerical method used in the present study is briefly described. Further, the main features of the implementation of the turbulence models used into the numerical code are outlined. Some examples of validation of the implementation of the models and the numerical schemes for convection are presented. Attention is especially given to: discretisation for non-orthogonal mesh, block-wise local mesh refinement, approximation of convection, numerical aspects of second-moment closure (SMC) modelling, applying both the wall functions and the exact wall boundary conditions.

The basis for implementation of the turbulence models is a widely used method for computation of fluid flows in arbitrary geometries developed by Perić (1993)[1]. A numerical code for laminar flows in two-dimensional arbitrary geometries, provided by courtesy of Prof. M. Perić of University of Hamburg, has been extensively modified for the purposes of the present study. *The goal was to establish a reliable, accurate and efficient solver for turbulent flows when SMC models are used.*

3.1 Introduction

Computational fluid dynamics (CFD) is nowadays often used to gain insight into fluid flows. Reliability is a basic requirement which CFD techniques have to fulfill in order to be used for engineering design purposes. Two basic ingredients of CFD, the *numerical technique* and the *mathematical model* of physical processes, are the crucial factors which influence the quality of CFD-code results. The optimal results in geometrically and physically complex turbulent flows can be achieved only by combining the latest accomplishments which have been made in the areas of both principal ingredients of CFD. Therefore, combining the SMC models and numerical solution algorithms for non-orthogonal meshes with collocated variable arrangement is a particularly challenging task, especially if the model equations are to be integrated up to the wall. The design of an efficient and robust numerical algorithm for solving SMC model equations for an arbitrary numerical mesh is an essential prerequisite for taking advantage of better physical foundation and performances of SMC models over simpler models such as eddy-viscosity or algebraic models.

[1] Details can be also found in Ferziger and Perić (1996).

Numerical solution algorithm for turbulent flows using RANS approach is usually an extension of the solution procedure for laminar flows. In the case of the eddy-viscosity type of models the model implementation is straightforward, primarily due to the way in which these models couple to the momentum equations that is essentially a contribution to the diffusion. Only two additional scalar equations (for turbulence kinetic energy k and its dissipation rate ε) are to be solved. In the case of SMC models a number of numerical difficulties arise. First, a larger number of transport equations (up to 6 equations for the Reynolds-stresses $\overline{u_i u_j}$ and one equation for the dissipation rate ε) have to be solved. Depending on the complexity of the SMC model used, these equations contain a relatively large number of terms (especially redistribution and diffusion process models, leading often up to more than one hundred terms) weakening the coupling between the model variables themselves and the velocity field as well. Second, the coupling between the Reynolds stresses and velocity in the momentum equation is rather weak and it is widely recognised as a main cause of lower stability that the SMC models have in comparison to EVMs (Huang and Leschziner 1985, Obi *et al.* 1989, Lien and Leschziner 1993b).

The majority of the SMC model computations (including some major commercial CFD software such as `Fluent, Star-CD, Fire`) employ the wall functions (WF) for the mean velocity and the model variables utilising some empirical lows. By doing this, the first numerical point is located in the logarithmic-law region relatively far from the wall (in wall units it is at $y^+ > 30$). In contrast to this approach, it is possible to solve the turbulence model equations by integrating them up to the wall and imposing exact wall boundary conditions. In this approach all sources of the numerical instabilities and difficulties present in the WF approach are significantly more pronounced. This is primarily due to the fact that the changes of all model variables are most dramatic in the region which is covered by only one control volume (CV) in the WF approach. In that region the Reynolds-stress components change from zero at the wall, reaching maximum value at the edge of the viscous sub-layer which is located around the midway between the wall and the first numerical point of WF approach, and then falling down for about 10 to 20 % of their peak value by the end of first CV of WF approach. Further, the wall region has to be covered by a dense numerical mesh in the direction normal to the wall employing at least 10 points in the space where only one control-volume is placed in WF approach. In order to obtain a more stable procedure, the numerical mesh in the wall directions has to be much finer than that of WF approach.

A very important factor which has a strong influence on the stability and even ability of the numerical procedure to converge to the solution (*if it exists*) is the model capability to describe the variable behaviour physically correctly. This is more pronounced in the low-Re-number approach when it is possible that the model tends to a laminar or even a non-physical solution, leading to divergence. Therefore, the quality of a turbulence model is a very important factor which may strongly determine the numerical stability of the solution algorithm. This is especially important for the low-Re-number models.

The objective of the present study is the computation of the wall flows in arbitrary geometries with integration of the model equations up to the wall and imposing exact wall boundary conditions (so called low-Re-number modelling). The following text presents the practise adopted in the present study directed to solve the SMC model equations together with the Reynolds-averaged Navier-Stokes equations in the framework of low-Re-number modelling of turbulent

flows in arbitrary geometries. The above addressed problems and their solution towards a reliable and efficient solution algorithm are described.

3.1.1 Numerical solution procedure

In the framework of this study a computational procedure for solving the Navier-Stokes equations in arbitrary two-dimensional geometries, developed by Perić (1993), has been extended to computation of turbulent flows using SMC models. This is not a straightforward and easy task, as the use of SMC model changes the character of the momentum equations (now Reynolds equations) in which the molecular diffusion is negligible except within the viscosity affected regions, whereas the dominating turbulent stresses, supplied from separate transport equation, appear as source terms. This change has serious implications on the equations' character and therefore on their solution. The procedure is based on a fully conservative finite volume method for non-orthogonal meshes. A block-structured body-fitted mesh with block-wise local grid refinement is employed for the discretisation of the transport equations. This preserves the simplicity of the method and achieves the flexibility needed to handle geometrically complex flow situations. Block interfaces are treated in a conservative manner, consistent with the treatment of inner cell-faces. Cell centred (collocated) variable arrangement and Cartesian vector and tensor components are used. No transformation of vector or tensor variables in the discretisation procedure is needed. In order to account for non-linearity and coupling between transport equations, an iterative solution algorithm with under-relaxation of the variables is used to approach the steady or the instantaneous solution. A pressure-correction method based on SIMPLE algorithm (Patankar 1980) is used for pressure-velocity coupling.

The starting point of the procedure are the transport equations in their integral form. The surface and volume integrals are approximated using second-order approximations based on mean value approach (mid-point rule). The cell-face values of variables and gradients featuring in surface integrals are approximated using linear interpolation and central differences, respectively. The equations are linearised and solved sequentially. The ILU solver (Stone 1968) has been adopted for solving systems of linear equations.

In order to minimise numerical error and retain/preserve the stability of the procedure when the SMC models are used, the higher order upstream-weighted approximation schemes (linear upwind scheme - LUDS and quadratic upwind scheme - QUICK) as well as total variation diminishing (TVD) - type schemes have been employed to approximate convection.

In order to prevent the appearance of oscillatory pressure field, a selective interpolation procedure for the cell-face velocity entering the continuity equation is applied.

Turbulence has been predicted using two-equation eddy-viscosity models and second-moment closure models. Both the high and low Reynolds-number variants of these models have been used by applying the wall functions or exact boundary conditions respectively.

The stability of the numerical procedure when SMC models are used is achieved with the artificial turbulent viscosity introduced into the momentum equations.

3.2 Discretisation of transport equations

In this section the discretisation of the transport equation is outlined. The numerical method used in this work allows division of the solution domain into a finite number of blocks which can have irregular structure and which are further divided in a finite number of control volumes of quadrilateral form with the straight line connection between corner-points. A typical numerical cell with definition and notation is shown in Fig 3.1.

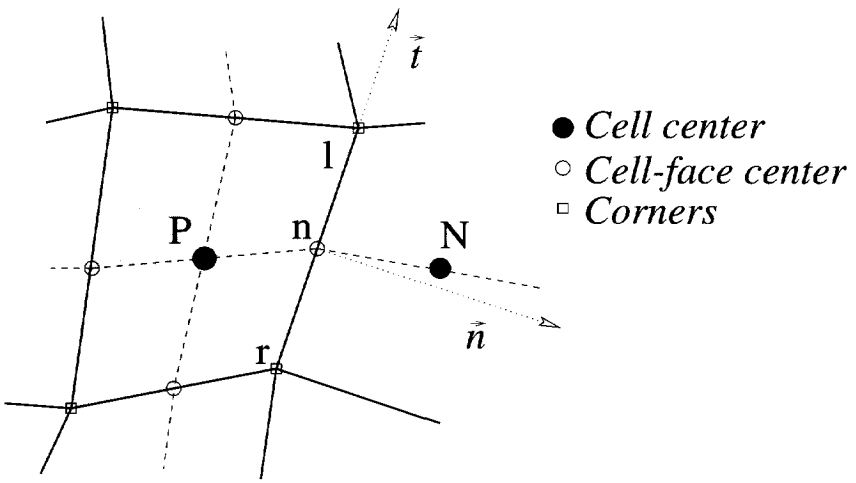

Figure 3.1: A generic numerical cell with definition and notation.

The connection between blocks is obtained by matching grid lines at block-interfaces. One example of possible block organisation is given in Fig 3.6 on page 68 and some others can be found in Chapter 5. More flexibility has been achieved for the block structured grids using the block-wise refinement doubling the number of control volumes in each direction. In this case the matching of the grid lines is required for each even grid line. This allows the use of finer grids in regions where needed (for example near walls if low-Re number models are used) which results in a cost-effective meshing of the domain. In both variants the interface is treated in a fully conservative manner consistent with the treatment of inner cell-faces.

A turbulence model in the framework of RANS modelling approach is usually a system of partial differential equations where each of them can be written in a general form. Thus, the differential transport equation for a generic quantity ϕ can be written in the coordinate-free form as

$$\underbrace{\frac{\partial \rho\, \phi}{\partial t}}_{\substack{\text{Transient}\\ \text{term}}} + \underbrace{\operatorname{div}(\rho \vec{v} \phi)}_{\text{Convection}} - \underbrace{\operatorname{div}(\Gamma\, \operatorname{grad}\phi)}_{\text{Diffusion}} = \underbrace{q}_{\text{Source}} , \tag{3.1}$$

where ϕ stands for the mean velocity vector components U_i, Reynolds-stress tensor components $\overline{u_i u_j}$, turbulence kinetic energy k, its dissipation rate ε, or, generally, for any transported variable.

In order to solve the differential equation (3.1) this equation is integrated over each control volume Ω. Using Gauß' divergence theorem the volume integrals of convection and diffusion in equation (3.1) are converted into the surface integrals and this equation in the integral form can be written as

$$\underbrace{\frac{\partial}{\partial t}\int_{\Omega} \rho\,\phi\,d\Omega}_{\text{Transient term}} + \int_{S} \underbrace{(\rho\vec{v}\phi}_{\text{Convection}} \underbrace{-\Gamma\,\text{grad}\phi)}_{\text{Diffusion}} \cdot d\vec{S} = \underbrace{\int_{\Omega} q\,d\Omega}_{\text{Source term}} \quad . \tag{3.2}$$

Two integral types are present in equation (3.2): integrals over the control volume Ω (unsteady and source terms) and integrals over the closed surface S surrounding the control volume (convection and diffusion).

3.2.1 Volume integrals

The volume integrals here are approximated by the mid-point rule, which is second-order accurate, where the mean value of the integrated variable is approximated by the value of the function at the control volume center P

$$\int_{\Omega} q\,d\Omega = \overline{q}\,\Delta\Omega_P \approx q_P\,\Delta\Omega_P. \tag{3.3}$$

For the unsteady flow cases the integration of transport equations needs to be performed in time. Since the surface and volume integrals are evaluated in an implicit scheme at the new time level, the flow history is then taken into account through the unsteady (transient) term only. The simplest implicit scheme for discretisation of the unsteady term is the first-order Euler scheme

$$\int_{\Omega} \frac{\partial \rho\,\phi}{\partial t}\,d\Omega \approx \frac{\Delta\Omega_P}{\Delta t}\,(\rho_P\,\phi_P - \rho_P\,\phi_P^o) \quad , \tag{3.4}$$

where the superscript 'o' denotes the previous time level ($t - \Delta t$, Δt is time step), and the variable value is evaluated at CV-center P. This scheme is unconditionally stable but suffers of low accuracy and in this work it has been used only when a steady state was computed by marching in time toward solution. This false time stepping sometimes improves convergence of entire solution procedure and was applied in some cases with SMC models, especially for transitional flows with coexistence of laminar and turbulent regions.

An implicit second-order approximation of the unsteady term at time level (t) for which we seek solution is achieved by fitting a parabola through the solution at three time levels and then taking the derivative at time level t

$$\int_{\Omega} \frac{\partial \rho\, \phi}{\partial t}\, d\Omega \approx \frac{\Delta\Omega_P}{\Delta t} \frac{3\, \rho_P\, \phi_P - 4\, \rho_P\, \phi_P^o - \rho_P\, \phi_P^{oo}}{2}\,, \tag{3.5}$$

where the superscript 'oo' denotes time $t - 2\Delta t$. This scheme is marginally more complex than the Euler scheme (only solutions of one more level have to be stored) but is second-order accurate and is also less prone to oscillations than the Crank-Nicolson scheme with almost the same accuracy (Lilek *et al.* 1997).

3.2.2 Surface integrals

The surface integral in the equation (3.2) is the sum of integrals over all CV faces:

$$\int_S \vec{f} \cdot d\vec{S} = \sum_n \int_{S_n} \vec{f} \cdot d\vec{S} = \sum_n F_n\,, \tag{3.6}$$

where $\vec{f}$ is the convective ($\rho\vec{v}\phi$) or diffusive (Γ gradϕ) vector.

Diffusion

The diffusive flux applying the midpoint rule is approximated as

$$F_n^d = \int_{S_n} \Gamma\, \text{grad}\phi \cdot d\vec{S} \approx (\Gamma\, \text{grad}\phi \cdot \vec{S})_n\,. \tag{3.7}$$

The gradient of ϕ in the Cartesian coordinates is

$$\text{grad}\phi = \frac{\partial \phi}{\partial x_l}\, \vec{l}\,, \tag{3.8}$$

and the diffusive flux becomes

$$F_n^d \approx (\Gamma\, \frac{\partial \phi}{\partial x_l} S_l)_n\,. \tag{3.9}$$

It is assumed here that mass fluxes, fluid density ρ and diffusivity Γ are known at the center of each CV face n. In order to calculate the convective and diffusive fluxes the value of ϕ and its gradients on the CV faces are expressed as a function of the nodal values by means of interpolation. The value of derivatives of any variable in any direction i in the Cartesian coordinates at CV centre is evaluated from the Gauß' theorem, (Perić 1993)

$$\left(\frac{\partial \phi}{\partial x_i}\right)_P \approx \frac{\sum_n \phi_n S_n^i}{\Delta\Omega_P}\,, \tag{3.10}$$

where ϕ_n is the value of generic variable ϕ at center of the cell face calculated by linear interpolation from two neighbouring nodal values. This formula is valid for CVs of arbitrary shape. It is of decisive importance for implementation of the block-wise grid refinement where some control volumes at block interface can have 5 or even 7 cell-faces.

In order to calculate diffusion, the gradients at cell-face are required. In the framework of a structured grid approach it is possible to evaluate gradients using the co-ordinate transformation as follows:

$$\begin{aligned} \left(\frac{\partial\phi}{\partial x}\right)_n &= \frac{1}{\Delta\Omega_n}\left[(\phi_N-\phi_P)(y_l-y_r)-(\phi_l-\phi_r)(y_N-y_P)\right] \\ \left(\frac{\partial\phi}{\partial y}\right)_n &= \frac{1}{\Delta\Omega_n}\left[(x_N-x_P)(\phi_l-\phi_r)-(x_l-x_r)(\phi_N-\phi_P)\right] \end{aligned} \tag{3.11}$$

where $\Delta\Omega_n$ is the volume with centre at point n and bounded by the central and corner points P, N, l and r (for notation see Fig 3.1)

$$\Delta\Omega_n = (x_N-x_P)(y_l-y_r)-(x_l-x_r)(y_N-y_P)\ . \tag{3.12}$$

The cell-corner values involved in equation (3.11) are evaluated by interpolation from four neighbouring central points and the nodal values are considered as unknown. Other possibilities to express the derivatives at cell-face are proposed by for example Muzaferija (1994) and Lilek *et al.* (1997). It does not require transformation at cell-face but has a simpler form than adopted here.

Convection

The convective flux through the cell face n is approximated as

$$F_n^c = \int_{S_n} \rho\phi\vec{v}\cdot d\vec{S} \approx \dot{m}_n\phi_n\ , \tag{3.13}$$

where $\dot{m}_n$ is the mass flux through the cell face n approximated with midpoint rule

$$\dot{m}_n = \int_{S_n} \rho\vec{v}\cdot d\vec{S} \approx (\rho U_i S_i)_n \approx (\rho U\delta y - \rho V\delta x)_n\ , \tag{3.14}$$

where $\vec{v} = U\ \vec{i} + V\ \vec{j}$ is velocity and $\vec{S}_n = \delta x\ \vec{i} + \delta y\ \vec{j}$ is the volume surface vector parallel to the unit normal vector $\vec{n}$ at the call face n.

Differencing Scheme (CDS): The large majority of the numerical procedures for solving laminar and turbulent flows nowadays are based on second-order central differencing for the spatial derivatives. While the central differencing is regarded as the most natural representation of diffusive terms in equation (3.2) it has been found that CDS applied to convection may, in certain

circumstances (e. g. when the local cell Peclet number $Pe = \rho U_x \Delta_x / \Gamma$ exceeds value of 2 and especially in computations of turbulent flows), produces a non-physical oscillatory solution (wiggles) or even causes divergence of the solution procedure. Therefore, the numerical approximation of the convection in transport equation (3.2) has been recognised as the weakest point of the discretisation procedure and crucial for numerical accuracy and stability.

Upstream Differencing Schemes: The simplest and widely used technique to cure the deficiency of the CDS is the upstream extrapolation from the neighbouring nodes which is usually called *upwind differencing scheme* (UDS). This scheme is only first order accurate but bounded and very stable. The good stability of UDS is due to its *large numerical error* which has the form of diffusive terms (also called artificial numerical diffusion) acting stabilizingly to solution procedure. Linear upwind differencing scheme (LUDS) and quadratic upwind scheme (QUICK) (Leonard 1979) are the natural straightforward higher-order extensions of the UDS. They were shown to be relatively stable and, because of this, they have been widely used. In the same way as CDS, the LUDS and QUICK are not bounded and therefore may lead to oscillatory non-physical solutions (wiggles). This becomes especially dangerous when such schemes are applied to transport equations for the turbulence quantities used in models. An unrealistic solution, as for example negative turbulence kinetic energy or its dissipation rate, might lead the entire numerical procedure to be unstable or to diverge.

Figure (3.2) is a schematic representation of evaluation of cell-face value ϕ_n by CDS and three upstream-weighted approximations for convection (UDS, LUDS and QUICK) which were also adopted for the purposes of the present studies. Because of its good stability and efficiency, UDS was, in the present study, usually used to approach solution, but final results were *always* obtained with more accurate higher order schemes.

Total Variation Diminishing (TVD) Schemes: The QUICK scheme is often seen as the best compromise in terms of accuracy and stability (e. g. Lien and Leschziner 1994) and therefore used in many research and commercial CFD codes. However this scheme is not bounded and as such it is not convenient for computation of variables for which an unbounded scheme may cause serious difficulties in obtaining solution as mentioned above. A number of studies have been published concerning the reliability of the turbulence models in the frame-work of the second-moment closure modelling (e. g. Speziale *et al.* 1994; Durbin and Speziale 1994). It was reported that some models for the pressure-strain Φ_{ij} can lead to unrealistic solution of Reynolds-stresses especially in the case of the two-dimensional turbulence limit of which the wall flows are one example. Therefore, it is important to have a solution procedure which does not tend to produce an unrealistic solution due to numerical discretisation.

The concept of the TVD class of differencing schemes for convection is based on controlling the numerical solution in a non-linear way such as to prevent the appearance of any new extreme (Hirsch 1990). This provides a monotone and bounded solution and prevents numerical oscillations by controlling the flux of computed quantity within the control volume. This is achieved by not allowing the quantity called *Total Variation* (TV) defined as

$$TV_{(\phi)} = \sum_k |\phi_{k+1} - \phi_k| \,, \tag{3.15}$$

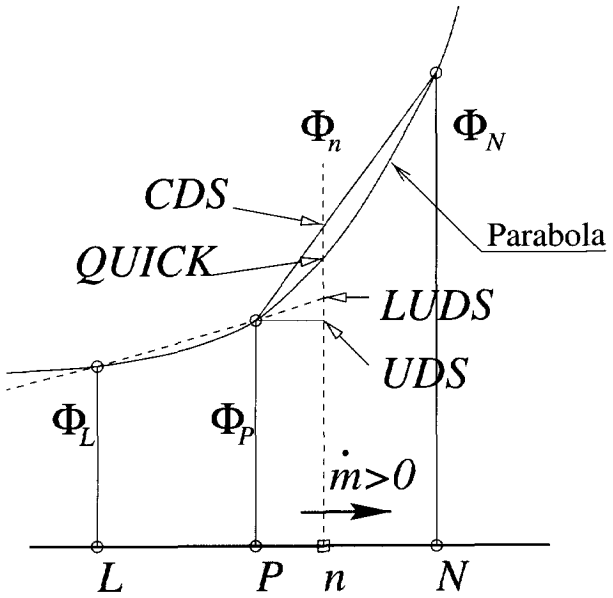

Figure 3.2: Schematic presentation of the upstream numerical schemes for convection. UDS – Upwind; CDS – Central; LUDS – Linear Upwind; QUICK – Quadratic Upwind Differencing Scheme.

to increase. If on a uniform collocated one-dimensional mesh (Fig 3.3) the flux-limiter is defined as

$$r_{i+1/2} = \frac{\phi_{i+1} - \phi_i}{\phi_i - \phi_{i-1}} , \tag{3.16}$$

and the flux-limiter function $\psi_{(r)}$ is used as

$$\phi_{i+1/2} = \phi_i + \frac{1}{2}\psi_{(r_{i+1/2})} \left(\phi_i - \phi_{i-1}\right) , \tag{3.17}$$

the flux-limiter functions used in present study are listed in Table 3.1. The graphical representation of several flux-limiter functions of the TVD scheme is given in Fig 3.4.

In order to make the implementation of the higher-order schemes for convection into the computer code simpler, we use the so called deferred correction approach: the UDS scheme is implemented in an implicit manner and the difference between a particular higher-order scheme and the UDS is treated explicitly.

The importance of accurate discretisation of convection has been recognised over about two decades of experience of application of CFD technique to engineering flows. In a review paper on application of numerical methods to computation of fluid flows Leonard (1997) summarised

Table 3.1: Flux-limiters in the TVD scheme.

Flux-limiter function	$\psi_{(r)}$
SMART, Gaskell and Lau (1988)	$max\left[0, min\left(4, \frac{3}{4}r + \frac{1}{4}, 2r\right)\right]$
MUSCL, van Leer (1974)	$max\left[0, min\left(2, \frac{3}{4}r + \frac{1}{4}, 2r\right)\right]$
UMIST, Lien and Leschziner (1993b)	$max\left[0, min\left(2, \frac{3}{4}r + \frac{1}{4}, \frac{1}{4}r + \frac{3}{4}, 2r\right)\right]$

this in the following conclusion: *the first-order schemes should not be used for practical calculations*. Also, the policy of some journals is to publish only the numerical solution proven to be free of numerical error (e.g. *Journal of Fluids Engineering*). Nevertheless, solutions obtained by UDS or by blending of UDS and CDS, where the portion of UDS has to be relatively high in order to promote stability, are still often used especially for computation of industrial turbulent flows.

Fig 3.5 demonstrates the importance of the use of non-diffusive high-accurate discretisation of convection in computation of a turbulent flow. It shows profiles of mean velocity and streamwise normal component of Reynolds-stress tensor in a by-pass transition on a flat-plate with circular leading edge (for details for this flow-case see Chapter 5). Results are obtained using the HJ low-Re-number SMC with two schemes: UDS scheme and TVD scheme with UMIST limiter applied to convection in momentum and model equations. Under the same conditions the UDS approximation fails to capture the separation-bubble (as seen from profiles of the mean velocity at $x = 0.015\ m$). The more accurate approximation of convection done with TVD scheme leads to excellent representation both of mean flow and the turbulence. Basically, it is the model's capability to predict the separation and transition, but it is shown here that some numerical diffusion can strongly influence the solution.

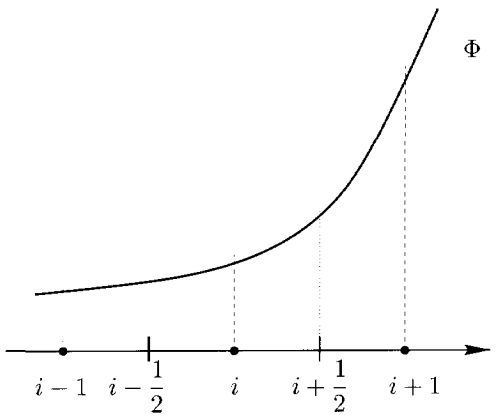

Figure 3.3: One-dimensional collocated mesh showing computational nodes as defined in equation (3.17)

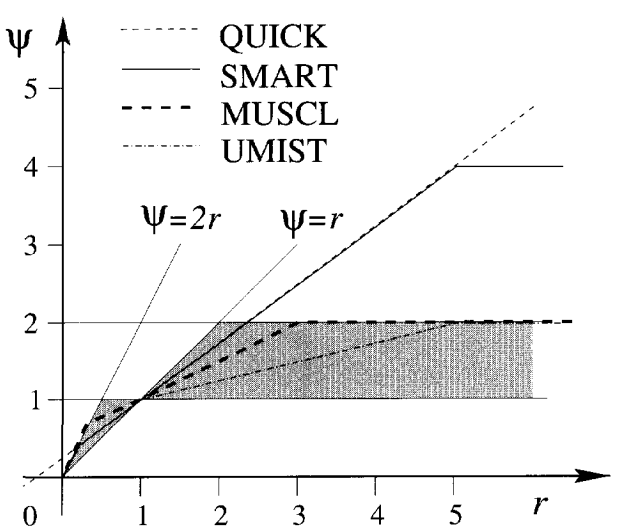

Figure 3.4: SMART, MUSCL and UMIST flux-limiter functions for TVD schemes as given in Table 3.1. The shaded area indicates region of second order accuracy for TVD flux-limiter functions.

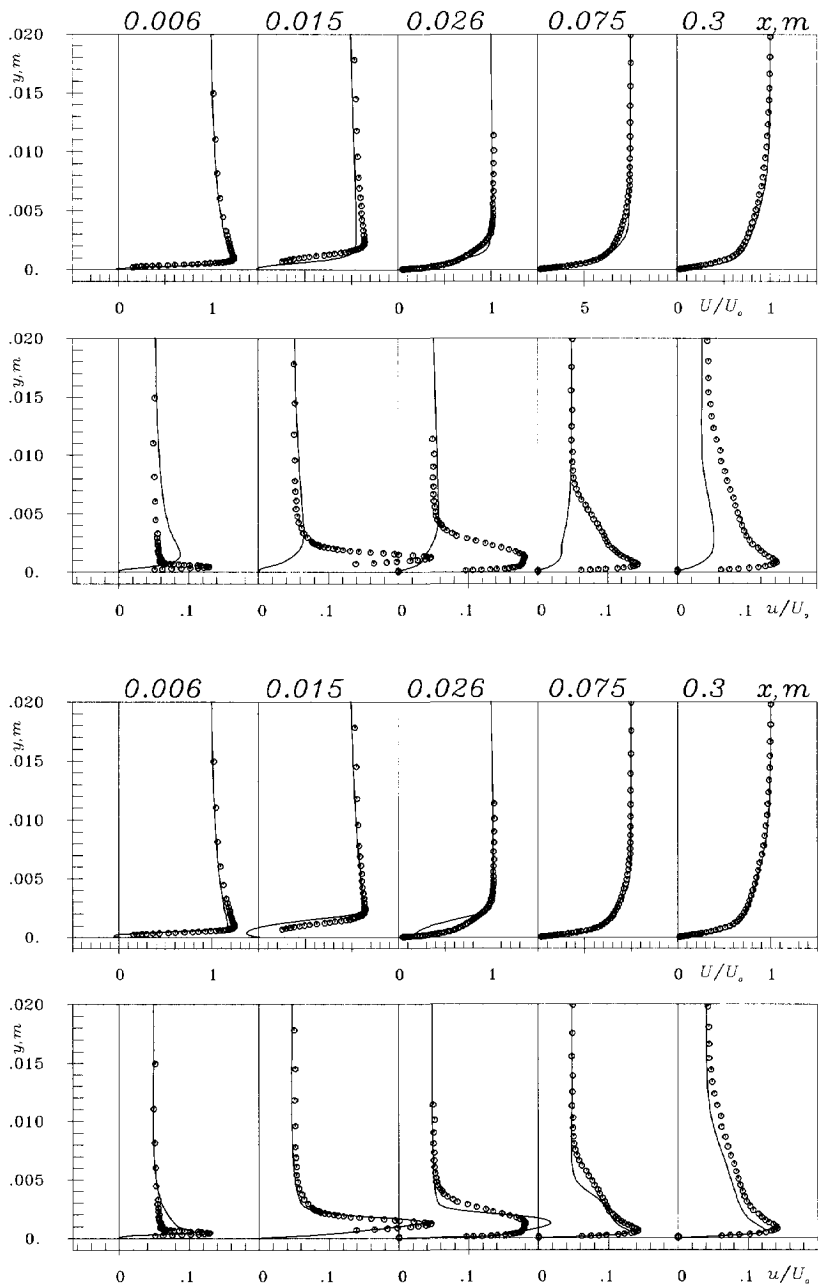

Figure 3.5: By-pass transition on a flat plate with circular leading edge (for more details about this flow see Chapter 5). Profiles of mean velocity and stream-wise fluctuation obtained with the HJ low-Re SMC model and two schemes for convection: UDS and TVD with UMIST limiter (lines) compared to experiments by Coupland (1995) (symbols).

3.3 Local grid refinement

The numerical procedure allows division of the solution domain into a number of non-overlapping blocks and each block is subdivided into a finite number of control volumes by a structured mesh. The grid lines have to match at block interfaces. In order to achieve more flexibility, block-wise grid refinement has been implemented in the present work. A refined block is made by doubling the number of control volumes in both directions so that each even grid line of refined block has to match the corresponding grid line of non-refined block at the block-interfaces. This is illustrated in Fig 3.6, which shows a numerical mesh used to study the lid- and buoyancy-driven cavity flows. These cases were used to assess implementation of grid-refinement algorithm into the numerical code. Results are compared with the benchmark solutions of Demirdžić *et al.* (1992) showing that it is possible to obtain essentially the same results as on the mesh which corresponds to the most refined blocks of refined mesh, but with a significant reduction (50%) of the number of computational points and the computing time. In the case of buoyancy-driven cavity the mesh is kept coarser in the core region where the computed variables do not vary significantly while the mesh is refined in the wall vicinity, especially near inclined walls which are in this case heated/cooled and where the gradients of temperature and velocity are the largest. The result shown in Fig 3.6 is obtained on a mesh made of seven blocks containing in total 36992 CVs. A corresponding 'non-refined' mesh with the same density near walls has 69632 CVs. The results obtained on these two meshes (the latter type computed with only one block and also seven blocks) are practically identical. This proves that local mesh refinement is a useful and worthwhile technique for computation of complex fluid flows.

The criteria for the grid generation and refinement is the user's estimation of possibilities and needs to cover some flow regions with either coarser or finer mesh. One possible basis for making decision (besides the user's experience) can be, for example, the steepness of the variable gradients. For example, in a back-step flow all variables undergo the strongest changes in the recirculation and recovery region which can, therefore, be covered with a refined block. Another important characteristic of the refinement is that it preserves the ratio of CV dimensions which acts favourably on the numerical stability.

In the method used here the computational nodes are placed in the center of each control volume (see Fig 3.7) and all unknowns at these positions are found by solving a system of linear equations obtained by discretising the physical equations. Although the structured four-neighbours computational cell is employed within a block, equation (3.10) enables evaluation the gradients irrespective of the number of cell-faces of a CV. The fluxes at block interfaces are evaluated using the neighbouring cell-center and cell-vertex values.

3.4 Modified pressure-correction algorithm

In the case of incompressible flows, continuity equation is often used to derive a method for calculation of the pressure field. The so-called pressure-correction algorithms are perhaps the most widely used and possibly the most successful approaches to determine the pressure in implicit incompressible flow solvers. The approach adopted here is an iterative method in which velocity

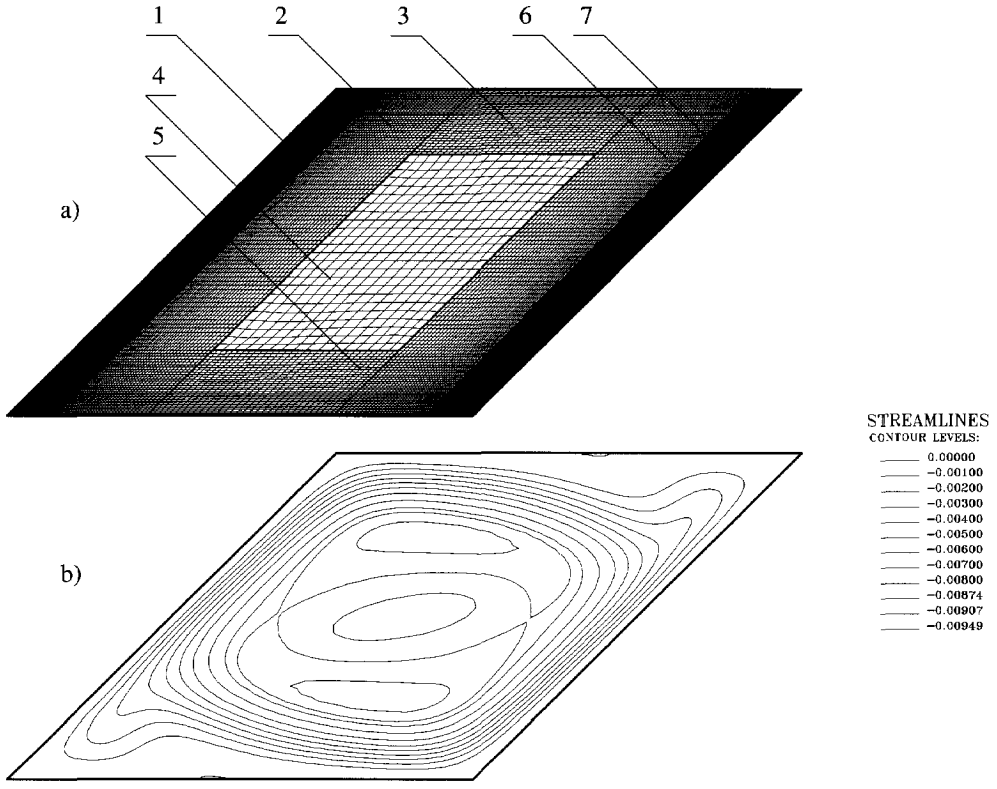

Figure 3.6: a) Numerical mesh for study flows in buoyancy-driven cavity. The mesh is made of 7 blocks containing in total 36992 CVs. b) Stream lines obtained on this mesh for the benchmark conditions of Demirdžić *et al.* (1992) ($Pr = 0.71$ and $Ra = g\beta\Delta TL^3Pr/\nu^2 = 10^6$. Top and bottom boundaries are adiabatic walls and the inclined boundaries (angle 45^o) are heated and cooled walls with constant flux.)

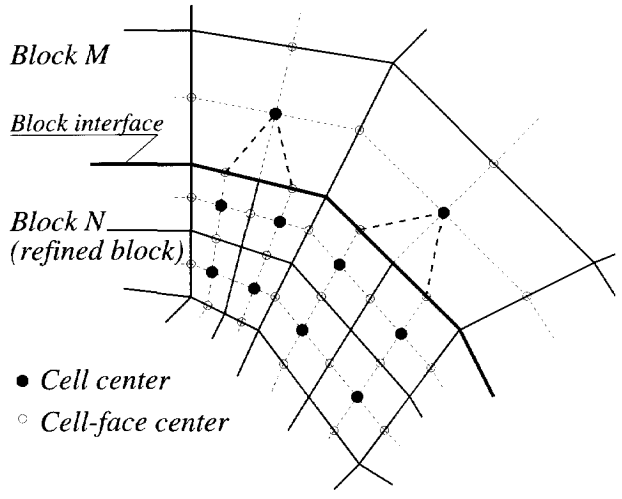

Figure 3.7: Block-interface between non-refined (M) and refined (N) block. The even mesh-lines of the refined block have to match grid lines of the neighbouring block. Interpolation for cell-face values at interface is done using the nearest nodal values.

components are obtained with an estimated pressure field, which was obtained from the previous non-linear iteration or time step. The obtained velocity field does not satisfy the continuity equation. In order to enforce the continuity condition, the velocity is corrected. This is done by using pressure-velocity coupling method based on SIMPLE-algorithm (Patankar 1980) where the mass imbalance is used to calculate the pressure-correction field which forces the velocity to satisfy continuity. A detailed description of the algorithm for laminar flows is given in Perić (1993), and Ferziger and Perić (1996).

The same procedure as for laminar flows is applied for turbulent flows when linear eddy-viscosity models are used. Since the Reynolds-stress is then modelled as

$$\overline{u_i u_j} = \frac{2}{3} k \delta_{ij} - \nu_t \left(\frac{\partial U_i}{\partial x_j} + \frac{\partial U_j}{\partial x_i} \right) ,$$

the momentum equation can be rewritten as follows

$$\frac{DU_i}{Dt} = -\frac{1}{\rho} \frac{\partial \mathcal{P}}{\partial x_i} + \frac{\partial}{\partial x_i} (\nu + \nu_t) \left(\frac{\partial U_i}{\partial x_j} + \frac{\partial U_j}{\partial x_i} \right) , \tag{3.18}$$

where $\mathcal{P} = P + \frac{2}{3} k$ is then computed, and the real pressure predicted by eddy-viscosity model should be evaluated from this.

Since the SMC models predict the anisotropy of the normal components of the Reynolds-stress tensor, the contributions of the stresses to the momentum equations which can be associated with

pressure are, in general, different in each direction, unlike that of linear eddy-viscosity models. Modification of the pressure algorithm is therefore necessary and this was done here as described below.

The discretised momentum equation may be written as

$$A_P^{U_i} U_{i,P}^{m*} + \sum_N A_N^{U_i} U_{i,N}^{m*} = Q_{i,P}^{m-1} - \left(\frac{\partial (P + \rho \overline{u_i^2})}{\partial x_i} \right)_P^{m-1} \Delta\Omega_P \,, \tag{3.19}$$

and then the velocities calculated at the CV center can be expressed explicitly as functions of gradients of the pressure associated with the corresponding normal components of the Reynolds-stress tensor:

$$U_{i,P}^{m*} = \tilde{U}_{i,P}^{m*} - \frac{\Delta\Omega_P}{A_P^{U_i}} \left(\frac{\partial \left(P + \rho \overline{u_i^2} \right)^{m-1}}{\partial x_i} \right)_P \,, \tag{3.20}$$

where the pseudo-velocity $\tilde{U}_{i,P}^{m*}$ is defined as

$$\tilde{U}_{i,P}^{m*} = \frac{\sum_N A_N^{U_i} U_{i,N}^{m*} + Q_{i,P}^*}{A_P^{U_i}} \,, \tag{3.21}$$

and the superscript m denotes the non-linear iteration and the $*$ indicates the non-corrected velocity.

For the calculation of mass-fluxes we need the velocities at cell-faces, which are calculated by using equation (3.20). Pseudo-velocity is interpolated from CV centers, and the pressure contribution is calculated directly at the cell-face. The velocity at cell-face n is

$$U_{i,n}^{m*} = \left\langle \tilde{U}_i^{m*} \right\rangle_n - \Delta\Omega_n \left\langle \frac{1}{A_P^{U_i}} \right\rangle_n \left(\frac{\partial \left(P + \rho \overline{u_i^2} \right)^{m-1}}{\partial x_i} \right)_n \,, \tag{3.22}$$

where $\Delta\Omega_n$ is the control volume bounded by points P and N and corners l and r (see Figure 3.1). Instead equation (3.21), which would lead to a complicated calculation, the interpolation of the pseudo-velocity at cell-face is done by using equation (3.22). This leads to the following expression for non-corrected velocities at cell-face

$$U_{i,n}^{m*} = \left\langle U_{i,P}^{m*} \right\rangle_n - \Delta\Omega_n \left\langle \frac{1}{A_P^{U_i}} \right\rangle_n \left[\left(\frac{\partial (P + \rho \overline{u_i^2})}{\partial x_i} \right)_n - \left\langle \frac{\partial (P + \rho \overline{u_i^2})}{\partial x_i} \right\rangle_n \right] \,, \tag{3.23}$$

where $\langle \cdot \rangle$ denotes linear interpolation from the neighbour nodal values and no summation over i is applied. The second term on the right hand side can be seen as a correction to the linear interpolation using the nodal values. It vanishes when the function $(P + \rho \overline{u_i^2})$ is linear or quadratic, and is proportional to the square of mesh spacing and the third derivative of the function (Ferziger and Perić 1996). Thus, this term is a second order correction which goes consistently

towards zero as the grid is refined. It is large only when the variation of this function is not smooth (Lilek *et al.* 1997).

The mass fluxes through the cell face n calculated using Equations (3.23) do not satisfy the continuity equation

$$\sum_n \dot{m}_n^* = \Delta\dot{m} \,, \tag{3.24}$$

and need to be corrected so that

$$\sum_n \left(\dot{m}_n^* + \dot{m}_n^{'}\right) = 0 \,, \tag{3.25}$$

where $\dot{m}_n^{'}$ is the mass-flux correction. By truncating equation (3.23) when approaching continuity the velocity correction can be expressed in terms of the pressure correction as

$$U_{i,n}^{'} = -\left\langle \frac{\Delta\Omega_P}{A_P^{U_i}} \right\rangle_n \left(\frac{\partial P^{'}}{\partial x_i}\right)_n \,. \tag{3.26}$$

The gradients of P' can be evaluated by using expressions (3.10). Since in an implicit iterative method the mass conservation does not have to be satisfied exactly at the end of each outer iteration, the gradient of pressure-correction can be calculated as (Perić 1993; Demirdžić *et al.* 1992)

$$\left(\frac{\partial P^{'}}{\partial x_i}\right)_n \approx \frac{P_N^{'} - P_C^{'}}{\overline{NP}} \tag{3.27}$$

where $\overline{NP}$ is the distance between central point P and the neighbouring central point N. The equation for the pressure correction $P^{'}$ follows from Equations (3.27), (3.25) and (3.26).
By the wall-, inlet-, outlet- and symmetry-boundary conditions the velocity is prescribed and therefore does not need to be corrected. Thus the zero-gradient boundary condition is applied on the pressure-correction equation. If the pressure is prescribed at a boundary (so called pressure boundary condition) the velocity is computed to satisfy that pressure.

3.5 Stability treatment of SMC modelling

While the implementation of the eddy-viscosity models into a numerical code for laminar flows is straightforward, the experience of researchers working on numerical aspects of SMC modelling show that the implementation of such models into the numerical code is a non-trivial task (Lien and Leschziner 1994). It has been experienced that the solvers for turbulent flows which use eddy-viscosity models are more stable than those that employ Reynolds-stress models. The main reason is that these two models contribute to the momentum equations in a rather different manner. The contribution of the linear EVM does not change the form and character of the

Navier-Stokes equations. On the other hand, the contribution of the SMC models to the momentum equations is non-diffusive and for the high-Re number flows it is much larger than the viscous diffusion.

Since the Reynolds-stresses in the linear EVM approach are expressed in terms of the velocity gradients associated with the eddy-viscosity, the contribution of the stresses to the momentum equation in this case is in essence diffusive to that equation and, basically, the same as in laminar flow. This is of decisive importance to stability, because the diffusive terms in substance stabilise the numerical procedure. The viscosity coefficient in momentum equation is now the sum of the laminar and turbulent viscosity. In the case of the SMC modelling the contribution of Reynolds-stresses is through their gradients that can cause or reinforce the oscillations in a similar manner as the pressure does. These contributions are dominant part of the momentum equation because the only diffusion here is molecular one, which is rather small, especially if the Reynolds-number is high. All this becomes more pronounced when non-orthogonal grid is applied.

Several, in essence similar techniques, to promote stability in framework of SMC modelling have been proposed in last few years. It was recognised that low stability of SMC model is basically due to absence of diffusive terms in the momentum equation and that the stability can be restored by increasing diffusive coefficients in discretised momentum equations. In the framework of a staggered finite-volume approach with orthogonal grid Huang and Leschziner (1985) introduced a technique by which the velocity-gradient type diffusion terms are extracted from the discretised Reynolds-stress transport equations. An apparent viscosity appears and enlarges the diffusion coefficients in discretised momentum equations. This technique was adopted by Obi *et al.* (1989) in the framework of a finite-volume approach with collocated variable arrangement for orthogonal grid and extended later by Obi (1991) to non-orthogonal grids. The Reynolds-stresses extracted from its discretised transport equation can be expressed in this form

$$\overline{u_i u_j}_P = -\Gamma_P^{ij} \left(\frac{U_i}{\partial x_j} \right)_P \frac{\Delta\Omega_P}{A_P^{\overline{u_i u_j}}} + S_P^{\overline{u_i u_j}} , \tag{3.28}$$

where Γ_{ij} is an apparent diffusivity, which is a function of the SMC model used, and which, for a stable procedure, must be unconditionally positive. Stresses expressed by equation (3.28) are then used in the discretisation of the momentum equation. In this way the first terms on the right hand side of the equation (3.28) are associated with viscous diffusive terms in momentum equation and contribute significantly to diffusive coefficients. Because of this, new source terms appear in the momentum equations.

For the same purpose Lien (1992) (see also Lien and Leschziner (1994)) have extracted an expression for $\overline{u_i u_j}$ from the algebraic truncation of the modelled Reynolds-stress transport equation so that

$$\overline{u_i u_j} = -\nu_{ij}^t \frac{\partial U_i}{\partial x_j} , \tag{3.29}$$

and then expressed the Reynolds-stress computed in the m-th non-linear iteration as

$$(\overline{u_i u_j})^m = -\left(\nu_{ij}^t \frac{\partial U_i}{\partial x_j} \right)^m + \left(\overline{u_i u_j} + \nu_{ij}^t \frac{\partial U_i}{\partial x_j} \right)^{m-1} , \tag{3.30}$$

Table 3.2: Apparent viscosity tensor in Obi's and Lien's approach.

Interpolation of equations Obi (1991)	Anisotropic turbulent viscosity Lien and Leschziner (1994)
$\Gamma_{11} = \left[2 - \frac{4}{3}C_2 + \frac{2}{3}C_2^w C_2(4f_x + f_y)\right] \frac{\overline{u^2}\,\Omega_P}{A_P^{\overline{uu}}}$	$\nu_{11} = \frac{2 - \frac{4}{3}C_2 + \frac{2}{3}C_2^w C_2(4f_x + f_y)}{C_1 + 2C_1^w f_x} \frac{\overline{u^2}}{k} \frac{k^2}{\varepsilon}$
$\Gamma_{22} = \left[2 - \frac{4}{3}C_2 + \frac{2}{3}C_2^w C_2(f_x + 4f_y)\right] \frac{\overline{v^2}\,\Omega_P}{A_P^{\overline{vv}}}$	$\nu_{22} = \frac{2 - \frac{4}{3}C_2 + \frac{2}{3}C_2^w C_2(f_x + 4f_y)}{C_1 + 2C_1^w f_y} \frac{\overline{v^2}}{k} \frac{k^2}{\varepsilon}$
$\Gamma_{12} = \left[1 - C_2 + \frac{3}{2}C_2^w C_2(f_x + f_y)\right] \frac{\overline{v^2}\,\Omega_P}{A_P^{\overline{uv}}}$	$\nu_{12} = \frac{1 - C_2 + \frac{3}{2}C_2^w C_2(f_x + f_y)}{C_1 + \frac{3}{2}C_1^w (f_x + f_y)} \frac{\overline{v^2}}{k} \frac{k^2}{\varepsilon}$
$\Gamma_{21} = \left[1 - C_2 + \frac{3}{2}C_2^w C_2(f_x + f_y)\right] \frac{\overline{u^2}\,\Omega_P}{A_P^{\overline{uv}}}$	$\nu_{21} = \frac{1 - C_2 + \frac{3}{2}C_2^w C_2(f_x + f_y)}{C_1 + \frac{3}{2}C_1^w (f_x + f_y)} \frac{\overline{u^2}}{k} \frac{k^2}{\varepsilon}$

and introduced it into the momentum equation. This is usually called *artificial viscosity approach* meaning that some diffusion is added to and subtracted from the momentum equation while they are then discretised as source and diffusion respectively. When the numerical procedure converges to the solution, expression (3.30) reduces to the Reynolds-stress. By this an amount of numerical diffusion, equal to the difference of discretisation of introduced terms, is inserted into momentum equation.

The coefficients Γ_{ij} and ν_{ij}^t in equations (3.28) and (3.29) are given in Table 3.2. They have slightly different form due to the manner of extraction of apparent viscosity. In both cases the same pressure-strain model of Gibson and Launder (1978) was used.

The apparent viscosity in the Lien and Leschziner approach can be expressed as $\nu_{ij} = C_\mu^{ij} \frac{k^2}{\varepsilon}$ where the coefficients C_μ^{ij} are functions of the turbulence model used. The value of coefficient C_μ^{ij} in Table 3.2 vary between 0.065 – 0.951 in the near wall region and 0.175 – 0.577 in the free flows[2]. The above described techniques for stabilisation of the numerical method are strongly dependent on the SMC model used. The Lien-Leschziner approach introduces a non-invariant viscosity in momentum equation that may lead to a non-invariant solution.

Since the present work was aimed primarily at low-Re-number SMC modelling, and for the sake of general applicability and simplicity, we adopted here the approach with invariant apparent viscosity equal to that of the eddy-viscosity approach i.e. $\nu_t = C_\mu \frac{k^2}{\varepsilon}$ instead of tensorial expression

[2]These values correspond to four components of Reynolds-stress tensor in 2D flows.

proposed by Lien-Leschziner. The Reynolds-stress is now expressed as

$$(\overline{u_i u_j})^m = -\left[\nu_t \left(\frac{\partial U_i}{\partial x_j} + \frac{\partial U_j}{\partial x_i}\right)\right]^m + \left[\overline{u_i u_j} + \nu_t \left(\frac{\partial U_i}{\partial x_j} + \frac{\partial U_j}{\partial x_i}\right)\right]^{m-1} \tag{3.31}$$

where m indicates the current outer iteration. The momentum equation becomes

$$\begin{aligned} \frac{\partial \rho U_i}{\partial t} + \frac{\partial \rho U_j U_i}{\partial x_j} &- \frac{\partial}{\partial x_j}\left[(\mu + \mu_t)\left(\frac{\partial U_i}{\partial x_j} + \frac{\partial U_j}{\partial x_i}\right)\right] = \frac{\partial P}{\partial x_i} \\ &- \frac{\partial}{\partial x_j}\left[\overline{u_i u_j} + \mu_t \left(\frac{\partial U_i}{\partial x_j} + \frac{\partial U_j}{\partial x_i}\right)\right] \end{aligned} \tag{3.32}$$

All terms on the right-hand side of equation (3.32) are treated explicitly using values from the previous iteration. In this way the diffusive coefficients of the discretised momentum equations become identical to these of eddy-viscosity model, and the stability of the SMC computations is considerably retained. From the author's experience, the stability of SMC models is still lower than that of EVMs, which is primarily due to the complexity of these models.

The contribution of the artificial diffusion to the discretised momentum equation is due to a different treatment of the diffusive terms. Since the central discretisation is used for diffusion and linear interpolation for the evaluation of cell-face values, this contribution is zero when the variation of velocity is linear or quadratic on uniform mesh. This contribution is large only in regions where the velocity varies strongly, and goes consistently towards zero as the mesh is refined.

The author's experience is that the same treatment is needed when the SMC modelling is applied to heat transfer and cures apparently the same problem which appears in the transport equation for the mean temperature.

3.6 Wall boundary conditions

In the present studies two classes of the turbulence models to account for the presence of the permeable wall are used: *i*) high-Re number models where the near wall region is bridged by so called *wall function*, and *ii*) low-Re number models when the transport equations are integrated up to the wall, imposing *exact boundary conditions* to each equation. If the wall-function approach is used, the near-wall computational point should be located in the logarithmic-law region. In contrast to this, if low-Re-number models are used, a large number of computational points have to be placed in the region between the wall and the position were the first near-wall point of WF approach would be located[3].

3.6.1 Wall functions

The wall function for SMC models is essentially the same as for EVM. The only difference is that it needs to take into account anisotropy of the Reynolds-stress tensor at the first near-wall

[3]Usually more then 20 control volumes; this number depends also on the bulk Reynolds number.

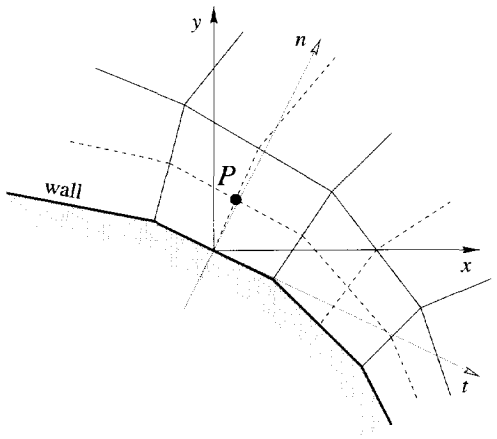

Figure 3.8: First control volume near wall and definition of the global Descartes (x, y) and the local wall-oriented co-ordinate system (t, n) with notation.

point. A possibility is, as used earlier by several authors (g.g. Lien 1992), to prescribe the values of all Reynolds-stresses in the near-wall node as functions of turbulence kinetic energy k. For a particular turbulence closure model the values of the Reynolds-stresses in the log-law region can be derived by imposing 'local equilibrium condition', $P_k = \varepsilon$, and neglecting convection and diffusion (that may be seen as a good approximation for near equilibrium flows). In the wall-oriented co-ordinates the Reynolds-stresses obtained with GL and SSG model are

	$\frac{\overline{u_t^2}}{k}$	$\frac{\overline{u_n^2}}{k}$	$\frac{\overline{w^2}}{k}$	$\frac{\overline{u_t u_n}}{k}$
GL	1.098	0.247	0.655	0.255
SSG	1.067	0.413	0.520	0.314

The wall-damping function f_w of GL model is set to unity. The transformation of the Reynolds-stresses from the Cartesian to the wall-oriented co-ordinates and vice versa is given in Appendix E.1.

In order to explicitly impose the values of Reynolds-stresses, one first has to determine these values which is only a simple problem for linear models and 2D flows.

A general way to provide correct values of the Reynolds-stresses independent of the model used is to impose the value of the production of each particular stress in accordance with the wall function. The production of turbulent kinetic energy in the log-low region is in balance with the dissipation rate, and in wall-oriented co-ordinate system, it can be written as

$$P_k = -\overline{u_t u_n}\frac{\partial U_t}{\partial n} \approx \varepsilon. \tag{3.33}$$

The mean velocity parallel to the wall in the log-low region is given with

$$\frac{U_t}{u_\tau} = \frac{1}{\kappa}\, ln\left(En^+\right), \tag{3.34}$$

where $n^+ = \dfrac{nu_\tau}{\nu}$ is normalised distance from the wall, $\kappa = 0.41$ is von Karman constant and $E = 8.41$ is an experimental constant. The wall velocity u_τ computed from equation (3.34) is

$$u_\tau^* = \frac{U_t \kappa}{ln\left(En^+\right)}. \tag{3.35}$$

Following the definition of C_μ in the eddy-viscosity approach the wall velocity can be calculated as

$$u_\tau^\star = C_\mu^{1/4}\, k^{1/2} \tag{3.36}$$

The wall velocity expressed in two different ways, Equations (3.35) and (3.36) are used to calculate the wall-shear stress as follows

$$\tau_w = -\frac{U_t}{\mid U_t \mid}\, \rho\, u_\tau^* u_\tau^\star. \tag{3.37}$$

The turbulent shear-stress in the wall-oriented co-ordinates in log-low region is

$$\overline{u_t u_n} \approx \frac{\tau_w}{\rho}. \tag{3.38}$$

From the logarithmic law the gradient of the velocity parallel to the wall in the direction normal to the wall can be expressed as

$$\frac{\partial U_t}{\partial n} = \frac{u_\tau}{\kappa n} \tag{3.39}$$

where n is distance the first computational point from the wall. The remaining gradients of the velocity components can be neglected $\partial U_t/\partial t = \partial U_n/\partial n = \partial U_n/\partial t = 0$. These velocity gradients obtained in the wall-oriented co-ordinates are transformed to Cartesian co-ordinates and together with stresses used to calculate the production terms in the $\overline{u_i u_j}$ transport equation. In this way the logarithmic-law for the equilibrium wall flows and non-orthogonal grids is imposed. The expressions for the transformation from the Cartesian co-ordinates to the arbitrary coordinates and vice versa are given in Appendix E.1.

In an equilibrium flow the results obtained with both methods described above are identical. The later approach takes into account deviation of the ratio P_k/ε from unity which might be significant in non-equilibrium flows such as those with separation, recirculation, reattachment, recovery and impingement. Although, in the author's experience the former approach is numerically more stable, we applied the latter because of its obvious advantages in computing complex flows and implementation into the computer code.

Dissipation of turbulence kinetic energy ε in the log-law region follows directly from the equilibrium assumption $\varepsilon = P_k$. Using equations (3.33), (3.39) and (3.38) dissipation is

$$\varepsilon = \frac{u_\tau^{\star 3}}{\kappa n}. \tag{3.40}$$

The zero gradient (Neumann) boundary condition is specified to each Reynolds-stress component and turbulence kinetic energy. The dissipation ε given with equation (3.40) is prescribed explicitly. Although consistent with the treatment of production of the mean-equilibrium flows, this is the weak point in the conventional wall function approach. Several more sophisticated proposals were published (e.g. Chieng and Launder 1980; Kim and Choudhury 1995; Ciofalo and Collins 1989; Kiel and Vieth 1995) but which only marginally gain in prediction quality.

3.6.2 The exact wall boundary conditions

In order to apply the exact wall boundary condition to the velocity and turbulence model equations, one has to use a turbulence model suitable to account for strong variation of model variables through the viscous sub-layer and the buffer region. The exact wall boundary conditions are determined by the physical behaviour of moving fluid approaching a solid wall and the definition of turbulence model variables.

For the mean velocity and the Reynolds-stresses the Dirichlet boundary condition $U_i = 0$, $\overline{u_i u_j} = 0$ are applied. For the pressure the Neumann boundary condition is used $dP/dn = 0$. For the dissipation rate ε the Dirichlet boundary condition is applied. The value of ε at the wall is derived from the balance of transport equation for k at the wall:

$$\varepsilon_w = \nu \left(\frac{\partial^2 k}{\partial n^2} \right)_w. \tag{3.41}$$

Since the evaluation of second derivatives of k at the wall is connected with the numerical uncertainty and a need for a very fine numerical mesh, a simplification of expression (3.41) can be applied. Using the asymptotic expansion of fluctuating velocity near the wall it can be shown that turbulence kinetic energy k behaves as

$$k = a_k n^2 + b_k n^3 + ... \tag{3.42}$$

where n is distance from the wall. Keeping only the first term of (3.42) the dissipation at the wall can be computed as

$$\varepsilon_w = \nu \left(\frac{\partial k^{1/2}}{\partial n} \right)_w^2 \tag{3.43}$$

Expression (3.43) is equivalent to expression (3.42) if the first numerical point to the wall is at $n^+ < 5$. This allows the numerical mesh to be distributed so that the first point can be located at $n^+ \approx 1 - 2$ without serious numerical difficulties. For larger n^+ the numerical results are contaminated and it causes other numerical problems such as slow convergence.

3.7 Treatment of the source terms

The numerical treatment of source terms of the turbulence model equations is often of decisive importance for the numerical stability of the entire numerical scheme. For these turbulence quantities which are physically always positive (e. g. ε and normal components of the Reynolds stress tensor) we treat implicitly all negative contributions and explicitly all positive ones. This leads to an increase in the diagonal dominance of the implicit portion of the scheme and thereby, enhances its stability. The source contribution to these equation can be written as

$$q_P^{\phi}\,\Delta\Omega_P \;=\; q_P^{+\,\phi}\,\Delta\Omega_P \;+\; \frac{q_P^{-\,\phi}\,\Delta\Omega_P}{\phi_P}\,\phi_P, \tag{3.44}$$

where q_P^+ includes all the positive contributions and q_P^- all the negative ones, whereas $\dfrac{q_P^{-\,\phi}\,\Delta\Omega_P}{\phi_P}$ is the contribution to the A_P coefficients.

CHAPTER 4

Oscillating and Pulsating Flows

This section describes the application of the second-moment closure model to computations of oscillating and pulsating boundary layer, channel- and pipe-flows at transitional and higher Reynolds numbers. The particular emphasis is on prediction of the reciprocating flows with the laminar-to-turbulent and turbulent-to-laminar transition which occurs within an oscillation cycle. Two of the considered cases for which DNS data are available (oscillating boundary layers with sinusoidal free-stream velocity by Spalart and Baldwin (1989) and with steep but not sinusoidal free-stream velocity variation by Justesen and Spalart (1990), both at $Re_{\delta_S} = 1000$) were used to tune some of the model coefficients. The model reproduces well the "conditional turbulence", with sudden turbulence bursts and subsequent relaminarization, in the oscillating boundary layers and pipes in the whole range of transitional Reynolds numbers in accord with results of DNS and experiments. Predictions of turbulence dynamics in the outer region of a channel or pipe show also good qualitative agreement with experimental records.

4.1 Introduction

From the variety of unsteady turbulent flows our interest in the present study lies at the ones that are bounded by smooth plane walls and forced by a periodic time-varying *flow-rate* or *pressure gradient*. These flows can be classified into two groups: *i*) reciprocating flows with zero time-mean flow-rate and velocities (oscillating or "oscillatory" flows); and *ii*) the flows with non-zero mean flow-rate and velocities (pulsating or "pulsatile" flows). Oscillating and pulsating wall-bounded flows are often encountered in engineering (aerodynamics and thermodynamics, e.g. rotating airfoils and turbomachinery blades, heat exchangers attached to reciprocating engines), in environment (e.g. coastal waters), and in bio-engineering and biomedical sciences (e.g. blood flow in major mammalian arteries and air in lungs). These flows have been the subject of extensive experimental and, more recently, numerical investigations. Because of their importance, the understanding and accurate prediction capability of these flows is of great practical interest.

Such unsteady flows are the next in complexity, compared to the steady wall flows, such as channel- and pipe-flows, which are the basic test cases for the development of turbulence models. From the numerical point of view, these unsteady flows are as simple as the steady channel and pipe flow and are, therefore, very suitable for the validation of turbulence models. Since

these flows are periodic, they are independent of the initial conditions and the uncertainty of the inflow conditions is eliminated, which is also of significant importance for the turbulence model development. These flows are one-dimensional in space (homogeneous in the two directions parallel to the wall) requiring small computational resources. At the same time, these flows are physically rather complex, being significantly different from the steady equilibrium flows and are, therefore, a severe test for turbulence models. Any turbulence model intended for unsteady wall flows (e.g. internal combustion engine, Sterling engine, vortex shedding flows, etc.) should be first tested in oscillating and pulsating wall flows.

Oscillating and pulsating turbulent flows exhibit a number of features, seldom encountered jointly in other flows. Such are the periodic interchange of favourable and adverse pressure gradients, reversal of the mean flow and the shear stress, inflection of the mean velocity profiles, laminar to turbulent and reverse transition. Reciprocating flows are more complicated than pulsating flows, because the flow may go through laminar and turbulent stages and transitions in between. In pulsating pipe or channel flows, the time-mean properties are largely unaffected by the forced oscillations.

In general, the oscillating pipe or channel flows with zero time mean can be characterised by the Reynolds number $Re_{\delta_S} = U_0\ \delta_S/\nu$ (U_0 is the amplitude of mean velocity, $\delta_S = \sqrt{2\nu/\omega}$ is the Stokes layer thickness[1], ω is oscillation frequency) and the Stokes parameter $\lambda = R/\delta_S$ (R is the pipe radius or the half of channel width). These flows can be classified into four broad types (Hino *et al.* 1989): *i*) laminar flow; *ii*) disturbed laminar or weakly turbulent flow, where 'small-amplitude' perturbations appear superimposed on the velocity traces towards the end of the acceleration phase of the cycle but where otherwise the velocity traces agree with laminar theory; *iii*) intermittently (conditionally) turbulent flow; where turbulent bursts appear violently and explosively during the decelerating phase of the cycle while during the acceleration phase the flow reverse to laminar; and possibly *iv*) fully turbulent flow, where the flow remains turbulent throughout the cycle. The weakly turbulent regime (hereafter denoted as "turbulescence", Hanjalić, Jakirlić, and Hadžić 1995) is characterised by a visible but small amplitude perturbations in the mean velocity oscillogram over the whole cycle, which only marginally affects the laminar-like mean flow properties. The conditional turbulence denotes the pattern with pronounced turbulence bursts sustained only over a part of the cycle. It seems more appropriate to call this regime periodically turbulent or simply 'bursting' regime. Hino *et al.* (1989) argued that this regime will prevail always if $Re_{\delta_S} > 550$, (close to the stability criterion for the oscillating boundary layer) provided that Stokes parameter is $\lambda > 1.6$. Hino *et al.* (1989) plotted a demarcation line separating the weakly and conditionally turbulent regimes, which follows the relation $Re_m \approx 1100\lambda$. Seume (1988) identified a similar relationship expressed in terms of the Valensi number, $Va = \omega d^2/4\nu = 2\lambda^2$ for the transition Reynolds number above which a rapid increase in the measured velocity fluctuations was detected. Hino *et al.* (1989) concluded that oscillating pipe flows are more 'stable' than unidirectional steady flows and can be turbulent only during a part of each cycle, decaying suddenly when the direction of flow is reversed. This conclusion can be extended by saying that the bursting regime in an oscillating pipe or channel flow can exist over a wide range of Reynolds numbers, its span increases progressively as the Stokes para-

[1] Stokes layer thickness is a measure of the "penetration depth" in oscillating flows.

meter λ increases. In the experiments of Jensen *et al.* (1989) on oscillating boundary layers the bursting turbulence was detected over a range in which Re-number varied almost by one order of magnitude. Hino *et al.* (1989) constructed the stability diagram, summarising their experimental results. The transition from laminar to weakly turbulent flow of type (iii) and turbulent flow of type (iv), as well as the transition from type (iii) to (iv) were determined.

Oscillating boundary layers are characterised only by the Reynolds number Re_{δ_S}. Stability analysis (Davis 1972) suggests $Re_{\delta_S} \approx 600$ to be the laminar stability threshold. The direct numerical simulation (DNS) by Spalart and Baldwin (1989) for this Re_{δ_S} showed flow features which differ from typical laminar flows. But, it was only for $Re_{\delta_S} = 800$ and 1000 that DNS showed a marked transition to turbulence around the start of the deceleration phase to be followed by laminarization during the acceleration phase. Very similar shapes of the wall-shear stress distribution over a cycle were found experimentally by Jensen *et al.* (1989) for Re_{δ_S} =760 and 1140 in oscillating boundary layer flows and Akhavan *et al.* (1991) for $Re_\delta = 1080$ and $\lambda = 10.6$ in oscillating pipe flows. Hino *et al.* (1983) recorded a similar profile in a rectangular duct for $Re_{\delta_S} = 876$. Neither Hino *et al.* (1989) nor other authors defined the criterion above which no relaminarization will occur and the flow will remain fully turbulent over the whole cycle.

4.1.1 Relevant experimental and DNS studies

Due to relatively simple configurations of the oscillating flows and their possible control through imposed force, these flows have recently received special attention in experimental studies as well as in numerical ones particularly as test cases for turbulence models. The flows are periodic in time, homogeneous in the directions parallel to wall and all flow quantities are functions only of the wall normal coordinate and the time.

Oscillating wall-bounded flows with imposed periodical unsteadiness have been the subject of great interest for a long time. Several valuable experimental studies of these flows have been conducted over past few years. In the present study we turn our attention to experimental and numerical (DNS) studies which provide data bases suited for model validation. Jensen *et al.* (1989) studied experimentally oscillating boundary layer flows over both smooth and rough walls with purely sinusoidal variation of free-stream velocity. This work provided detailed measurement results of mean velocity, wall shear stress and turbulence properties in the streamwise direction and in the direction perpendicular to the wall, for the flows at Re_{δ_S} from 120 up to 3460. Since the transition to turbulence in these flows occurs at $Re_{\delta_S} \approx 800$ the measurements were carried out for the laminar, transitional and turbulent flows. All experiments were performed in a channel with the cross-section aspect ratio of $1 : 1.4$ but the Stokes parameter is sufficiently large ($\lambda \approx 75$) to consider these flows as boundary layers. Akhavan *et al.* (1991) reported detailed measurements of oscillating pipe flows for three different flow conditions, all in the transitional flow regime. The Stokes parameter λ and Reynolds number Re_{δ_S} were varied. Experimental results include the mean streamwise velocity, the streamwise and radial as well as shear component of the Reynolds stress tensor and the wall shear stress. Spalart and Baldwin (1989) conducted direct numerical simulation of the oscillating boundary layers with sinusoidal variation of free-stream velocity for four Reynolds numbers Re_{δ_S} = 600, 800, 1000 and 1200. Justesen and Spalart (1990) carried out a DNS of an oscillating boundary layer with a steep variation of

pressure-gradient and a resting period between acceleration and deceleration at Re_{δ_S} = 1000. The DNS databases provide the mean velocity and the Reynolds-stress tensor components.

4.1.2 Relevant modelling studies

Numerical simulations by the Reynolds averaged Navier-Stokes modelling cannot predict all the phenomena observed in experiments such as the subtle details of the turbulence initiation at the very edge of laminar regime. Since the assumptions on which the wall functions are based are not valid in the most of the oscillating flows, the basic requirement concerning a turbulence model to be employed for computation of these flows is the integration of model equations up to the wall. HaMinh, Viegas, Rubesin, Vandromme, and Spalart (1989) reported reasonable agreement between computations with a low-Re-number SMC model and DNS results of Spalart and Baldwin (1989) for an oscillating boundary layer at Re_{δ_S} = 1000. The model could not describe the behaviour of turbulent quantities in the near wall region nor it could maintain the turbulence at $Re_{\delta_S} = 600$. Justesen and Spalart (1990) applied three low-Reynolds-number eddy-viscosity models to compute the oscillating boundary layers. The results were compared with DNS data of Spalart and Baldwin (1989), experiments of Jensen *et al.* (1989) for purely sinusoidal oscillating boundary layers, and with DNS of an oscillating boundary layer with 'steep' variation of free-stream velocity at $Re_{\delta_S} = 1000$ for which they performed also a DNS. It was shown that these models provide relatively good results for the wall shear stress as well as velocity profiles, turbulent kinetic energy and dissipation. The major deficiencies of Jones and Launder (1972) and Chien (1982) $k-\varepsilon$ models are in the computation of flows at transitional Reynolds-numbers. Both models predict the transition to early. Shima (1993) computed the oscillating boundary layer for $Re_{\delta_S} = 1000$ with his version of a low-Reynolds-number SMC. The results are in good overall agreement with corresponding DNS results. This model does not produce correctly the peak of the wall shear stress, its value and position. Dafa'Alla, Juntasaro, and Gibson (1996) compared their $q-\zeta$ model with DNS data of Spalart and Baldwin (1989) for $Re_{\delta_S} = 1000$ and with experiments of Jensen *et al.* (1989) at $Re_{\delta_S} = 3460$. This model gives very similar level of accuracy as the Launder–Sharma $k-\varepsilon$ model.

4.1.3 Decompositions of unsteady turbulent flows

The most convenient way to isolate the turbulence from organised unsteadiness is to employ the *phase* or the *ensemble averaging*. Most of the experimental studies provide such results. From the computational point of view, it becomes easy to employ the single-point closure models to predict these flows if any of these approaches are used, which, in contrast to the time averaging, provide detailed information about the time history during a cycle that can be very important in flows with reverse velocity.

According to the *phase averaging* any periodic flow variable $\mathcal{G}_{(\mathbf{x},\,t)}$ can be decomposed into 3 components (Hussain and Reynolds 1970)

$$\mathcal{G}_{(\mathbf{x},t)} = \overline{G}_{(\mathbf{x})} + \tilde{G}_{(\mathbf{x},\phi)} + g_{(\mathbf{x},t)} \,, \tag{4.1}$$

where $\overline{G}_{(\mathbf{x})}$ is the time-mean value of the variable $\mathcal{G}$ at location $\mathbf{x}$, $\tilde{G}_{(\mathbf{x},\,\phi)}$ is the periodic component at a phase angle ϕ at the same position $\mathbf{x}$ and $g_{(\mathbf{x},\,t)}$ is the fluctuating part. In the case of the *ensemble averaging* any considered quantity is decomposed into two components

$$\mathcal{G}_{(\mathbf{x},\,t)} = G_{(\mathbf{x},\,\phi)} + g_{(\mathbf{x},\,t)} \,, \tag{4.2}$$

where $G_{(\mathbf{x},\,\phi)} = \overline{G}_{(\mathbf{x})} + \tilde{G}_{(\mathbf{x},\,\phi)}$ and t is the time. Ensemble averaging leads to the same transport equation as for the steady flow, but with only one additional term which accounts for the variable change in time. In all unsteady computations in this study the ensemble averaging approach is used.

4.1.4 Flow definition

The laminar boundary layer with a free-stream velocity that varies sinusoidally in time around a zero mean in a semi-infinite domain, bounded by a flat wall, is the simplest example of the oscillating flows and has the well-known analytical solution (see for example Schlichting (1969)).

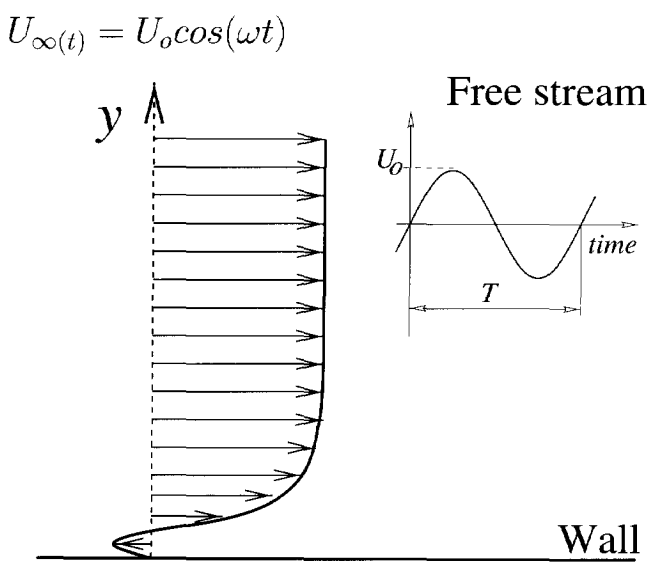

Figure 4.1: The definition sketch of oscillating boundary layers.

The free-stream velocity is given by

$$U_{\infty(t)} = U_o cos(\omega t) \tag{4.3}$$

where U_o is the peak of free-stream velocity, $\omega = 2\pi/T$ is angular frequency, T is the period of the oscillations, and t is time. The pressure gradient calculated from the free-stream velocity is

$$\frac{\partial P}{\partial x} = -\rho \frac{\partial U_\infty}{\partial t} = \rho \omega U_o sin(\omega t) \tag{4.4}$$

The solution of Navier-Stokes equations that describes the flow is

$$U_{(y,t)} = U_{\infty(t)} - U_o e^{-y/\delta_S} cos(\omega t - y/\delta_S), \tag{4.5}$$

where $\delta_S = (2\nu/\omega)^{\frac{1}{2}}$ is the Stokes-layer thickness, and y is distance from the wall. The wall-shear stress is calculated from the mean velocity:

$$\tau_w = \left(-\mu \frac{\partial U}{\partial y}\right)_w = \mu \frac{\sqrt{2} U_o}{\delta_S} cos(\omega t + \frac{\pi}{4}). \tag{4.6}$$

The friction coefficient is

$$C_f = \frac{\tau_w}{\rho {U_o}^2/2} = \frac{2}{Re_{\delta_S}} cos\left(\omega t + \frac{\pi}{4}\right) \tag{4.7}$$

and is a periodic function similar to the free-stream velocity with the phase lead of $\phi = \pi/4$ with the maximum which can be expressed as a function of a nondimensional parameter the Reynolds number based on Stokes-layer thickness and maximum free-stream velocity $Re_{\delta_S} = U_o \delta_S/\nu$, ($\nu$ is the kinematic viscosity). The amplitude of the wall shear stress in the laminar flows is universal function of Reynolds number $C_{fo} = 2/Re_{\delta_S}$. The peak of the wall-shear stress and the phase lead ϕ (for laminar flow $\phi = 45^o$) are often used to show the departure of a turbulent flow from the laminar state (see Jensen *et al.* 1989). Jensen *et al.* (1989) used the Reynolds number based on the amplitude of the free-stream motion $a = U_o/\omega$ and the maximum of the free-stream velocity, $Re_a = U_o a/\nu = Re_{\delta_S}^2/2$. The above given analytical solutions are commonly used to asses the accuracy of the numerical method. The numerical method adopted here provides fairly good agreement with the theoretical solutions.

4.2 Oscillating flows

In this section the predictions of oscillating (reciprocating) boundary layers, channel and pipe flows in a range from laminar to fully turbulent flow regime with sinusoidal and 'steep' variation of pressure gradient are considered.

4.2.1 Mathematical model

Oscillating flows were studied using the low-Re-number eddy-viscosity model of Launder and Sharma (1974) and the low-Re-number SMC model of Hanjalić and Jakirlić (HJ) (Hanjalić, Jakirlić, and Hadžić 1995; Jakirlić 1997; Hanjalić and Jakirlić 1998) which is described in details in Section 2.3.9. Most of the results are given for SMC model, because the eddy-viscosity model

results were published earlier by some researchers (see for example Sana and Tanaka 1995, Dafa'Alla *et al.* 1996, Justesen and Spalart 1990). Since, the flow is fully developed in the space, the only Reynolds stress component appearing in the U mean velocity transport equation is the shear stress $\overline{uv}$. The normal components of the Reynolds stress tensor appear in the turbulence model closure. In the SMC model employed here the pressure-strain correlation is modelled conventionally as the sum of the linear return-to-isotropy model for the slow part and the linear isotropisation-of-production model for the rapid part. A wall reflection term is employed to account for the wall effects on the wall-bounded flows. By adopting the linear models of Φ_{ij}, we followed initially the approach of Launder and Shima (1989), but modified first the coefficients C_1, C_2, C_1^w and C_2^w to achieve best overall performances in testing several non-equilibrium flows with pronounced low-Re-number and wall proximity effects (see Jakirlić 1997). This model is given with:

$$\begin{aligned}
\Phi_{ij,1} &= -C_1\varepsilon a_{ij} \\
\Phi_{ij,2} &= -C_2\left(P_{ij} - \frac{2}{3}P_k\delta_{ij}\right) \\
\Phi^w_{ij,1} &= C_1^w f_w \frac{\varepsilon}{k}\left(\overline{u_k u_m}n_k n_m\delta_{ij} - \frac{3}{2}\overline{u_i u_k}n_k n_j - \frac{3}{2}\overline{u_k u_j}n_k n_i\right) \\
\Phi^w_{ij,2} &= C_2^w f_w\left(\Phi_{km,2}n_k n_m\delta_{ij} - \frac{3}{2}\Phi_{ik,2}n_k n_j - \frac{3}{2}\Phi_{kj,2}n_k n_i\right).
\end{aligned} \tag{4.8}$$

The coefficients of the pressure strain correlation, originally proposed as constants by Gibson and Launder (1978), are extended to take into account the strong change of the Reynolds stresses from the peak value in logarithmic region to zero at the wall. Various forms of the functional expression for the coefficients have been tested in a number of wall-parallel test flows, Jakirlić (1997). Here two variants of the model that differ only slightly, both relevant to the simple linear model as given by expressions (4.8) are presented.

The coefficients adopted in both models of Φ_{ij} are summarised in Table 4.1. Some of the model coefficients were chosen to have this particular form and value as a result of the *a priory* testing and optimisation of the pressure strain model in channel flows using available DNS data. Optimisation of these coefficients was subsequently performed for the very basic wall flows such as channel and zero-pressure gradient boundary layer flows as well as the oscillating boundary layer at $Re_{\delta_S} = 1000$, comparing overall model performances with DNS and experimental data.

The first model, denoted as M1, reproduced very well the appearance of turbulent burst over the whole considered range of transitional Re-numbers, but produced an increase in the friction factor in wall flows at high Re-numbers, where the employed modifications were expected to fade out completely. The second, slightly different model, denoted as M2, is void from this deficiency, as discussed later.

4.2.2 Numerical details

A numerical code based on the control volume approach, as described in Chapter 3, is applied to all cases under consideration. For the oscillating boundary layer flows a parabolised version of this code is used. The time dependent pressure gradient given with (4.4) is imposed explicitly

Table 4.1: Specification of model coefficients

	Model M1	Model M2
C	$2.6AA_2^{1/4}f$	$2.5AF^{1/4}f$
F	-	$\min\{0.6; A_2\}$
f	$1-\exp[-(Re_t/150)]$	$\min\{(Re_t/150)^{3/2}; 1\}$
C_1	$C+\sqrt{A}E^2$	
C_2	$0.75A^{1/2}$	$0.80A^{1/2}$
C_1^w	$1-0.67C$	$1-0.70C$
C_2^w	$\max\{2/3-1/(6C_2); 0\}$	$\min(A; 0.3)$
C_{ε_3}	0.35	0.25
f_w	$\max\{k^{3/2}/(2.5\varepsilon x_n); 1\}$	$\max\{k^{3/2}/(2.5\varepsilon x_n); 1.4\}$

in equation for the streamwise mean velocity U which is the only mean quantity computed. The mean velocity normal to the wall is set to zero. Zero gradients in flow direction are applied to all variables. The typical time step used in the computations was 1 degree. Tests performed with time steps of 5, 2.5, 1, 0.5 and 0.20 degrees showed that the time step of $\Delta t = 1^o = 1/360T$ provides the grid independent solution. In these computations the implicit three-level second order scheme (see Section 3.2) for discretisation of unsteady terms is used. For oscillating boundary layer flows a Cartesian one-dimensional numerical mesh (with only one control volume in streamwise direction) with 100 control volumes in y direction is employed. The size of CVs is increased exponentially starting from the wall where it was ensured that the first numerical point is placed within $y^+ < 0.5$ and providing about 20 points in the viscous sub-layer and buffer region. Tests with coarser (80 CVs) and finer (120 CVs) mesh showed that the solution on 100 CVs is grid independent. Diffusion and source terms are discretised with second order schemes. For computation of oscillating and pulsating pipe and channel flows an appropriate flow rate is imposed. Thus, the pressure is solved using SIMPLE algorithm. The computational domain had the length of usually $0.5R$ and grid of 5 to 10 CVs in the flow direction. The periodic boundary conditions are applied to set fully developed flow in space. The initial conditions are not relevant, but their choice influences the duration of computations. The periodical solution is usually obtained in about 4 to 6 periods.

4.2.3 OBL with sinusoidal free-stream velocity

The first group of flows considered are boundary layers on a flat wall subjected to the sinusoidal free stream variation $U_\infty = U_0 \cos(\omega t)$, at several Re_{δ_S} ranging from the fully laminar flow at $Re_{\delta_S} = 120$ to the fully turbulent flow at 3460. The evolution of the wall shear stress over the cycle provides a good illustration of the flow dynamics in the near-wall area, where the instabilities are generated first. Fig 4.2 compares SMC computations with the measurements of Jensen *et al.* (1989) and with the results of DNS by Spalart and Baldwin (1989) for a range of

Re-numbers. Since the flow is symmetric with regard to phase angle the results could be given only for one half of the cycle, but because of some asymmetry in the experimental results, the results are given for the entire cycle. The absolute value of the wall shear stress is given in the figure.

At the lowest $Re_{\delta_S} = 560$ shown here, which corresponds to the Hino *et al.* demarcation between the 'deformed laminar' and 'weakly turbulent' (turbulescent) regimes, the experimental profile looks like laminar, though shifted by a small phase angle and slightly perturbed over the whole cycle in the same sense as seen in velocity oscillogram of Hino *et al.* (1989). The SMC model could not reproduce these small perturbations and yielded laminar solutions irrespective of the initial turbulence field. Similar features have been reproduced by the DNS of Spalart and Baldwin (1989) at $Re_{\delta_S} = 600$. Although, this Re-number is marginally higher than the previously considered and the flow is still in the turbulescent regime, which is far from real turbulence, both models considered agreed very well with the DNS data, as shown in Fig 4.2. Already at $Re_{\delta_S} = 760$, which falls in the range of bursting ('conditionally turbulent regime') the models reproduce very well the experimentally detected sudden jump in the wall shear stress corresponding to the turbulent bursts after the onset of the deceleration phase, as well as a subsequent relaminarization during the acceleration. As the Re-number increases, the transition appears earlier and this behaviour is well predicted by the models, as indicated by a sharp bend in the curves. There is, however, a distinct difference between the performances of the two models at this and slightly higher Re-numbers. The earlier model M1 produces a sharp turbulent burst very similar to that recorded by experiments in the second half of the cycle, but its peak appears about 12 to 15 degrees earlier than recorded by experiments. The second model M2 yields a more gradual development of the turbulent burst and agrees very well with the experimental data in the first half of the cycle. The experimental scatter and the difference between the two halves of the cycle makes it difficult to judge which of the model reproduces the experiments better. However, at a still slightly higher Re-number of 800, for which Spalart and Baldwin performed direct numerical simulations, the model M1 gave excellent agreement with the DNS data. At higher Re-numbers the difference between the performances of the two models fades away, but becomes noticeable again at the two highest Re-numbers, where the flow becomes fully turbulent over the whole cycle. Although both models yield a too high (about 20%) maximum wall shear stress, it is believed that the model M2 gives the realistic value and that the experimental data might be somewhat too low. This is partly substantiated by the fact that the model M2 gave a very good reproduction of the channel flow and of boundary layers at various pressure gradients at high Re-numbers (Jakirlić 1997). Also, the log-plot of the mean velocity profiles, shown in Fig 4.3 for a range of phase angles φ at $Re_{\delta_S} = 3460$ seems to confirm the above conclusion. Excellent agreement is obtained during the acceleration, whereas a disagreement appears around the peak velocity, but only in the outer layer, while the inner wall layer follows closely the universal logarithmic law. Similar level of over-prediction of the wall shear stress (between 15 and 25%) for the case of $Re_{\delta_S} = 3460$ was reported by Justesen and Spalart (1990) and Dafa'Alla *et al.* (1996) who used eddy-viscosity type of models. The broken line in Fig 4.2 indicates the beginning of transition to fully turbulent regime. Both models, M1 and M2 predict this position very well.

A summary of the comparison of the wall shear stress is given in Fig 4.4 in form of the

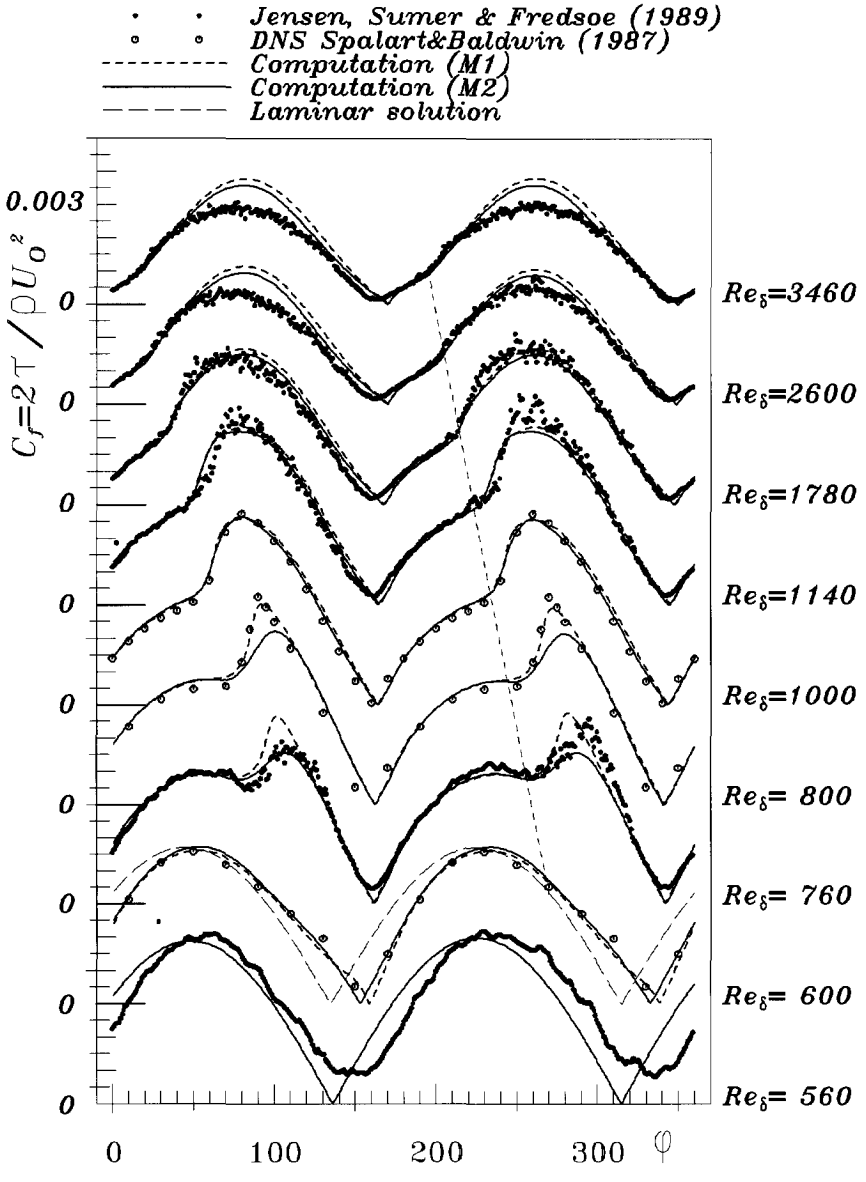

Figure 4.2: Evolution of the wall shear stress in an oscillating boundary layer over a cycle for different Re-numbers; the dotted line denotes the incipience of turbulent bursts.

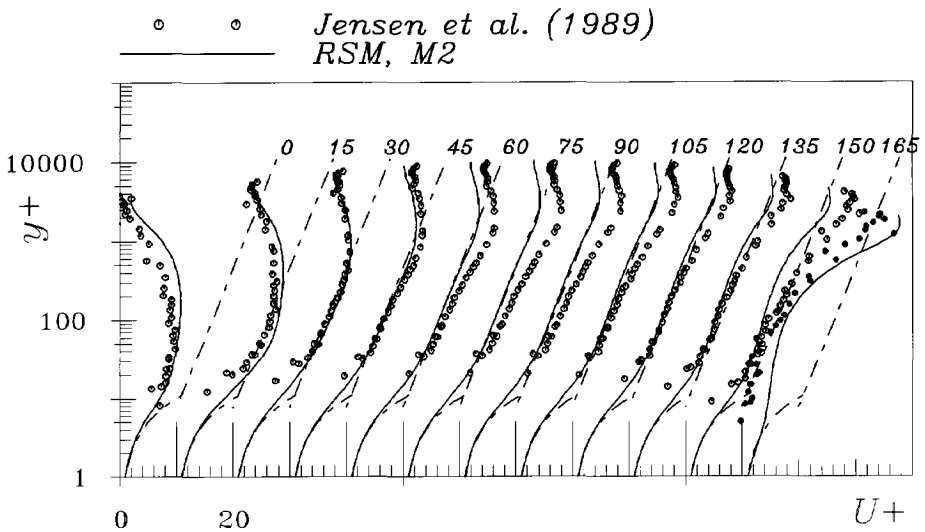

Figure 4.3: Semi-logarithmic plot of the mean velocity at different phase angles for $Re_{\delta_S} = 3460$.

peak τ_w, normalised with $\rho U_0^2/2$. The diagram confirms a very good agreement, apart from the highest Re-numbers, as discussed earlier. It should be noted, however, that a line drawn through the experimental points in the Re-number region after the transition, would exhibit a convex form mainly due to a low friction factor at the highest Re-number, whereas typical experimental friction factor curves in a channel or for boundary layer are concave. Such feature show also the predicted results.

Fig 4.5 compares the phase lead of the maximum wall shear stress over the peak free-stream velocity, showing a change-over from 45 degrees for laminar to about 8 degrees for turbulent flow at $Re_{\delta_S} = 3460$. In a range of Re-numbers where the transition occurs *after* the start of the deceleration phase, τ_w exhibits two peaks: the first corresponding to almost laminar regime and the second, which lags behind the velocity maximum, corresponding to the turbulent burst (negative φ).

A more detailed comparison was made with the DNS data of Spalart and Baldwin, showing a very good agreement of the mean velocity and all stress components at different phase angles for $Re_{\delta_S} = 1000$. The comparison of the wall shear stress for this case is shown in Fig 4.6. This figure shows the free-stream velocity and the pressure gradient $\partial P/\partial x$ as functions of phase angle ϕ. Both variants of SMC models follow closely the DNS points, better than any earlier reported model, though they do not reproduce in full the asymmetric sharp peak. For the reference the result obtained using low-Re-number linear eddy-viscosity model of Launder and Sharma (1974) is given. A sharper transition can be generated e.g. by replacing the f-function in the model M1 by $1 - exp[-(Re/150)^2]$ (not shown here), but this function delays the transition and already at $Re_{\delta_S} = 760$ the model could not maintain the turbulence. The sharp increase of the wall shear stress beginning at $\phi \approx 135°$ is a direct consequence of the deceleration of the mean flow. In a laminar flow the wall shear stress reaches the maximum at $\phi = 135°$. Therefore, this is the crit-

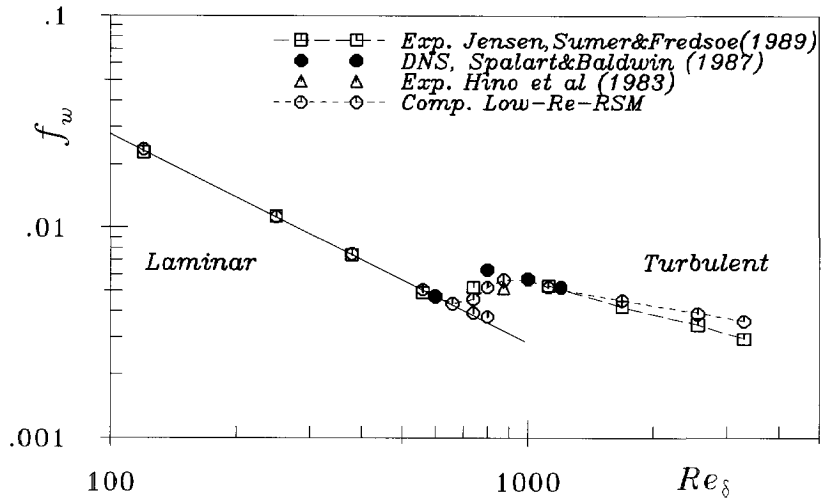

Figure 4.4: Non-dimensional maximum wall shear stress (wave friction factor) versus Re_δ.

ical moment when the present back-ground small level turbulence acts favourable in generation of the Reynolds-stresses $\overline{u^2}$ and $\overline{uv}$ via their production.

Fig 4.7 shows the mean velocity profiles in the wall coordinates. The model predicts the existence of the logarithmic law, but also the large deviation of this law at ϕ between 60 and 110 degrees closely following the DNS data. We need to note here, that the large deviation of the model results from DNS at $\phi = 70^o$ is because the wall shear stress τ_w used for velocity and the length scaling is here rather close to zero and any small difference in τ_w between model computation and DNS produce a large difference. Linear plots of the mean velocity show that the predicted velocity at this phase angle is very close to DNS data, and Fig 4.6 shows that the wall shear stress predicted with the model does not match DNS data exactly.

Fig 4.8 shows profiles of the shear-stress $\overline{uv}$ as function of the wall distance at various phase angles. Because of the logarithmic scale used for the wall distance this figure shows comparison very close to the wall. Agreement between the model computation and DNS data is very good. It indicates a very low value of $\overline{uv}$ near the wall between $\phi = 50^o$ and $\phi = 150^o$ which occurs during acceleration towards the beginning of deceleration phase, which is at $\phi \approx 135^o$. This laminarization is due to acceleration of the mean flow. In this phase the wall shear stress behaves closely to laminar solution which is due to absence of the shear stress in the wall vicinity. Also, other Reynolds-stresses are rather small in this phase, as show shown in Fig 4.9. The model predicts well the dynamics of all stresses. Some difference to DNS data is observed at $\phi = 140^o$ and 150^o, which are at the beginning of the steep increase in the wall shear stress (see Fig 4.6), which indicates transition to fully turbulent flow near the wall.

The variation of maxima of all non-zero turbulent stresses during the half of the cycle is shown in Fig 4.10. The $\overline{u^2}$ stress increases first. The $\overline{uv}$ stress, which is negative near the wall, contributes first to the generation of $\overline{u^2}$ stress, which starts just after $\phi = 100^o$ The major

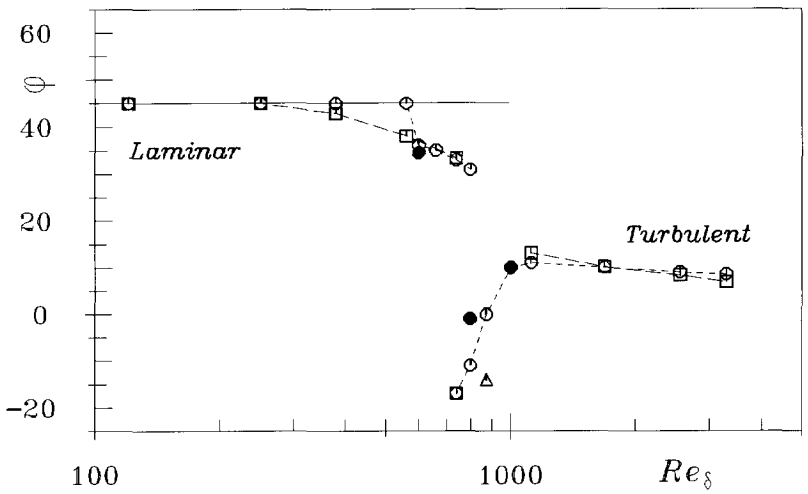

Figure 4.5: Phase lead of the maximum wall shear stress with respect to the maximum free-stream velocity. Legend as in Fig 4.4.

increase in $\overline{u^2}$ and $\overline{uv}$ stresses occurs between this point and 160 degrees. Since $\overline{v^2}$ stress is still decreasing in time a rapid growth of the $\overline{uv}$ stress is due to turbulent diffusion and pressure fluctuations. This diagram shows that despite small value of the shear stress $\overline{uv}$ (it is only 10% of $\overline{u^2}$ stress) a substantial variation of $\overline{uv}$ is important for prediction of the dynamics of turbulence. It should be noted that the distance of the position of the stress maxima from the wall varies along the flow and that it increases during acceleration, thickening the viscous boundary layer and producing the laminarizing effects on the mean flow.

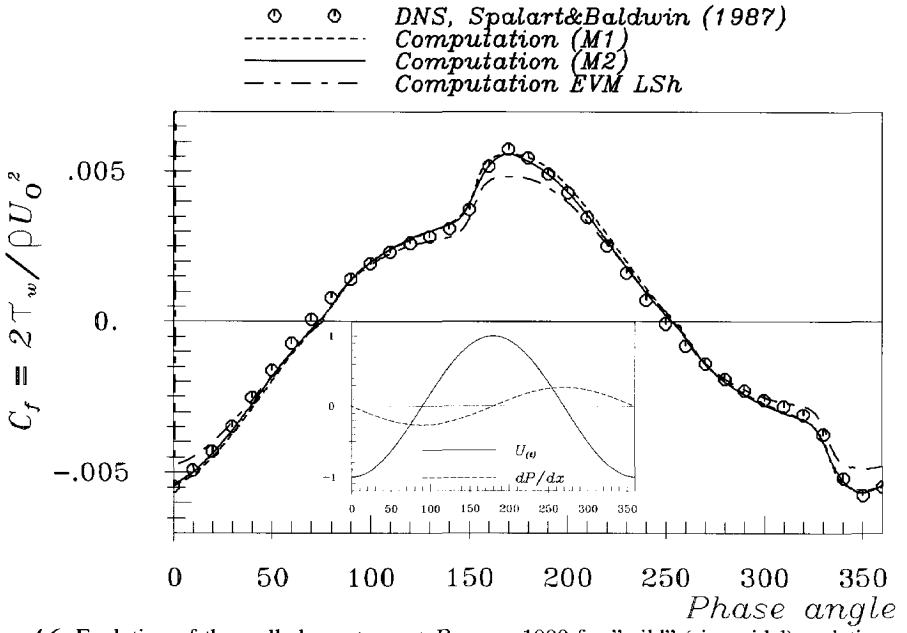

Figure 4.6: Evolution of the wall shear stress at $Re_{\delta_S} = 1000$ for "mild" (sinusoidal) variation of the free-stream velocity. Lines are computations obtained with two sets of the model coefficient as given in Table 4.1 and the eddy-viscosity model of Launder and Sharma (1974).

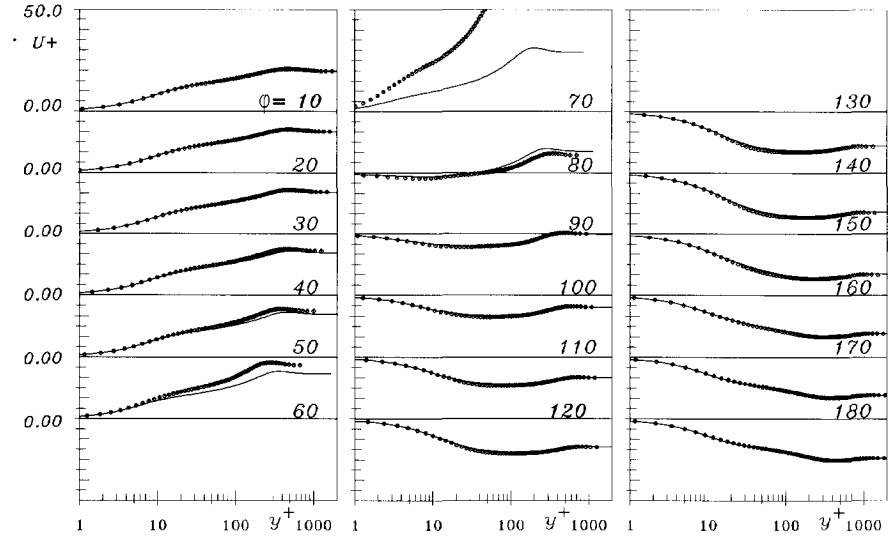

Figure 4.7: Comparison of computed profiles of mean velocity with DNS data results for the sinusoidal case at different phase angles. Symbols: DNS (Spalart and Baldwin 1989), Lines: SMC M2.

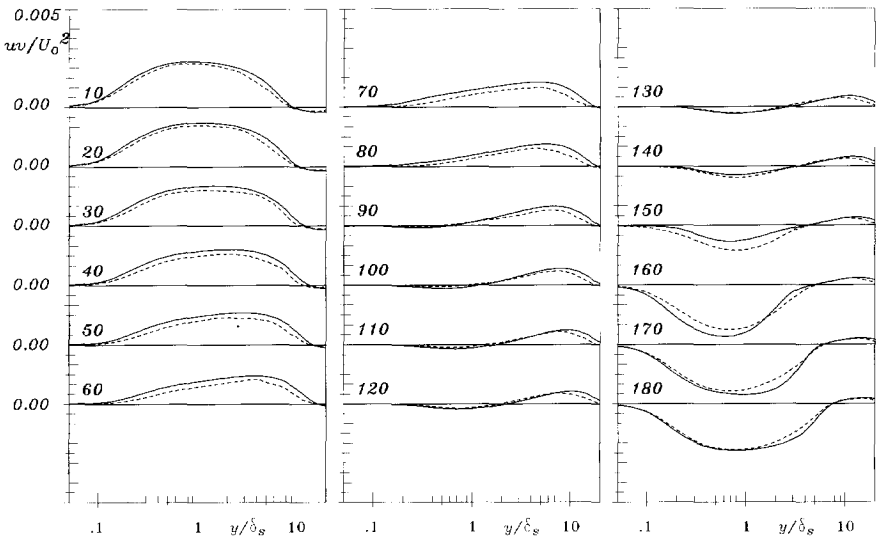

Figure 4.8: Comparison of computed profiles of turbulent shear stress with DNS results at different phase angle. Oscillating boundary layer with sinusoidal variation of free stream velocity. - - - DNS (Spalart and Baldwin 1989), —— SMC M2.

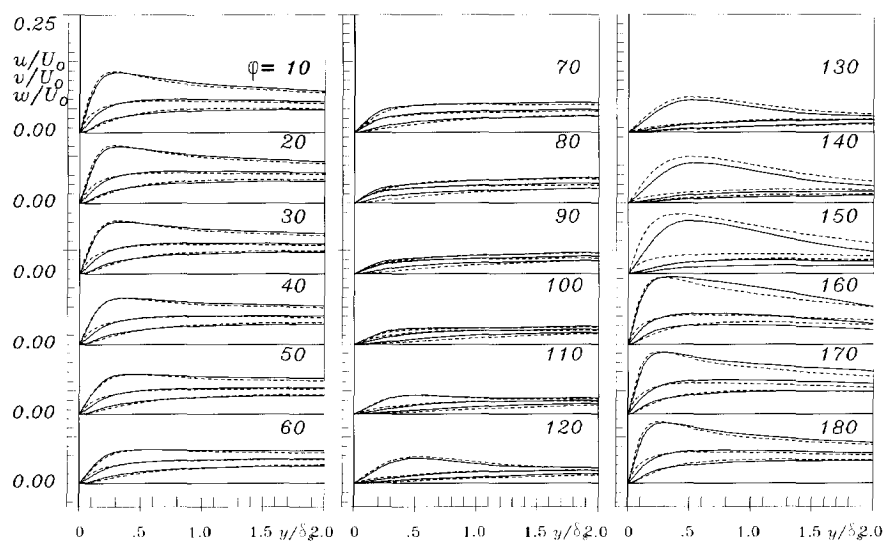

Figure 4.9: Near-wall profiles of normal components of the Reynolds-stress tensor over a cycle in oscillating boundary layer with sinusoidal variation or free stream velocity at $Re_{\delta_S} = 1000$. - - - DNS (Spalart and Baldwin 1989), —— SMC M2. $u = \sqrt{\overline{u^2}}$, $v = \sqrt{\overline{v^2}}$, $w = \sqrt{\overline{w^2}}$; at all phase angles the largest value has the u component and the smallest one is the v component.

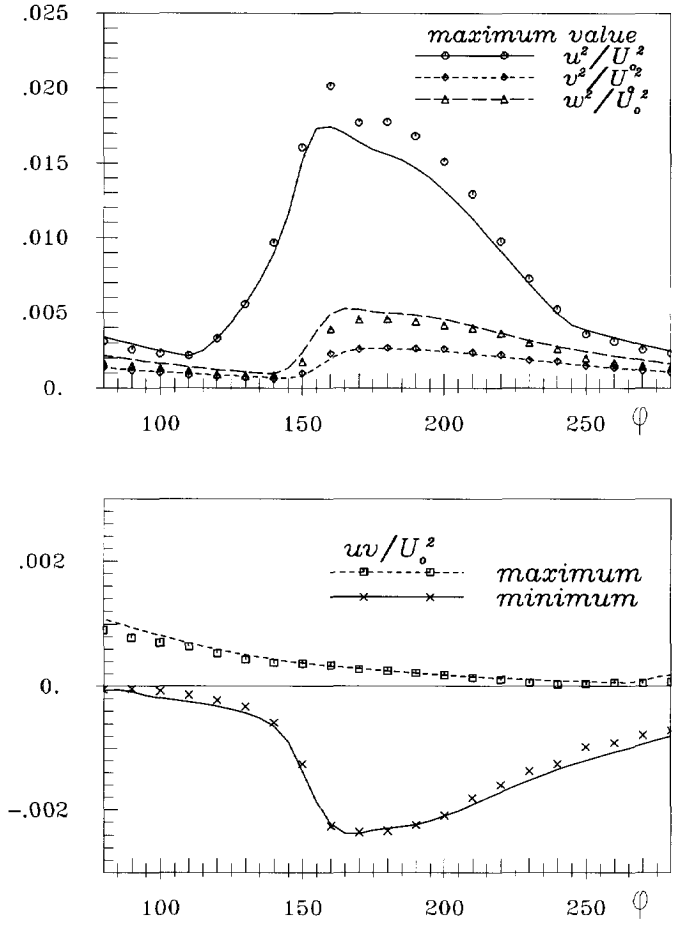

Figure 4.10: Evolution of peak values of all components of Reynolds-stress tensor over a half of the cycle. Sinusoidal variation of free stream velocity, $Re_{\delta_S} = 1000$. Symbols DNS (Spalart and Baldwin 1989), Lines SMC M2.

4.2.4 OBL with 'steep' pressure gradient

The next case considered is a more rigourous test than the previous one. This flow, simulated by Justesen and Spalart (1990), was subjected to much steeper acceleration and deceleration, with quasi-steady intervals in between. The mean free-stream velocity is given by Fig 4.11.

$$U_{o_{(t)}} = U_0 \left[320166\cos(\omega t) - 76230\cos(3\omega t) + 22869\cos(5\omega t) \right. \\ \left. -5445\cos(7\omega t) + 847\cos(9\omega t) - 63\cos(11\omega t)\right]. \tag{4.9}$$

The pressure gradient is computed from (4.9) and imposed into the momentum equation. The pressure-gradient peak is about three times larger than that of the previous sinusoidal case.

Predicted and DNS results for the wall shear stress, are compared in Fig 4.11 showing an excellent agreement with both models.

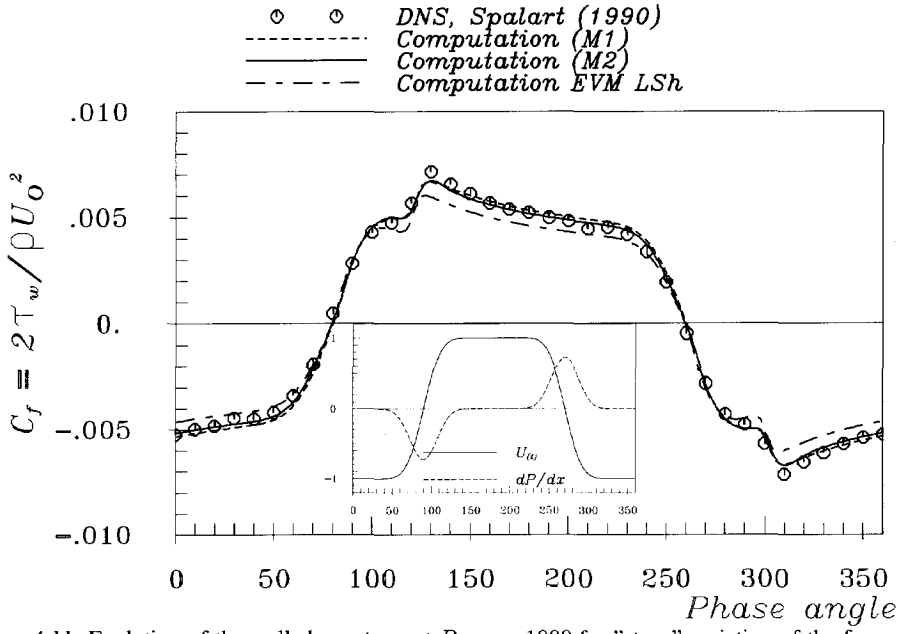

Figure 4.11: Evolution of the wall shear stress at $Re_{\delta_S} = 1000$ for "steep" variation of the free-stream velocity. Lines are computations obtained with two sets of the model coefficient as given in Table 4.1 and the eddy-viscosity model of Launder and Sharma (1974).

More details for this case are shown in Fig 4.12 and 4.13 where the normal- and shear stress components are plotted in parallel. Turbulent stresses are also well predicted apart from some curious bumps, exhibited by the DNS results in the outer region at φ of 10 and 20 degrees.

Some further illustration of the ability of the models to reproduce the dynamics of the turbulence field can be obtained from Fig 4.14 where the computed time contours of all Reynolds-stress components are compared with those obtained from DNS. Note that the covered boundary

layer thickness on the ordinate is $20\delta_s$, corresponding to the thickness over which the data in Fig 4.12 and 4.13 are plotted. For comparison, the DNS by Justesen and Spalart (1990) covered $\delta_S = 35$, whereas the half channel width of the experimental flow of Jensen *et al.* was $\approx 73\delta_s$. The time co-ordinate on the abscissa covers one cycle. Both, the qualitative and quantitative comparison show excellent agreement with the DNS results. These plots give the possibility of comparing the time response and the evolution of different stress components. In wall-parallel flows the energy from the mean motion is being transferred directly into the $\overline{u^2}$ component due to the shear deformation, so that $\overline{u^2}$ reaches the maximum value earlier than any other stress component. The computations give the maximum $\overline{u^2}$ at $\varphi \approx 135^o$, in good agreement with DNS, as indicated also in Fig 4.15. Other normal stresses, $\overline{v^2}$ and $\overline{w^2}$ lag behind, since they receive energy solely through the redistributive action of the fluctuating pressure. The model computations yield the maximum $\overline{v^2}$ and $\overline{w^2}$ in excellent agreement with DNS (Fig 4.15). Evolution of the peak shear-stress across the flow in time is computed satisfactorily. As in the case with sinusoidal pressure-gradient, this is of decisive importance for the generation of turbulence, primarily $\overline{u^2}$ component. We observe also that the time and space development of Reynolds-stresses is very well captured by the model. Although the agreement for $\overline{u^2}$ is not ideal, it can be concluded that the model of the pressure redistribution process (Φ_{ij}) responds well to the imposed steep variation of the free stream velocity.

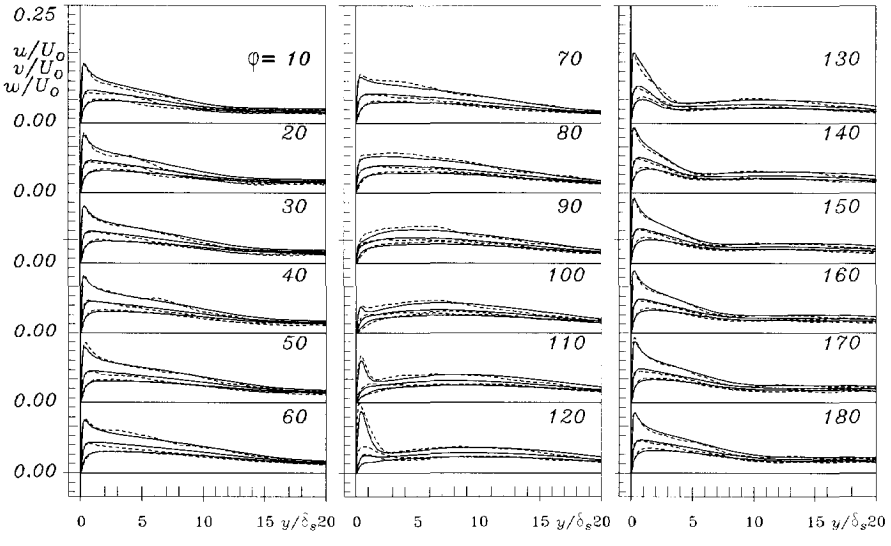

Figure 4.12: Profiles of normal components of the Reynolds-stress tensor over a cycle in oscillating boundary layer with 'steep' variation or free stream velocity at $Re_{\delta_S} = 1000$. - - - DNS (Justesen and Spalart 1990), —— SMC M2.

Fig 4.16 shows the mean velocity and the turbulent shear stress for both cases of an oscillating boundary layer considered above. Both cases show an abrupt amplification of turbulence at the

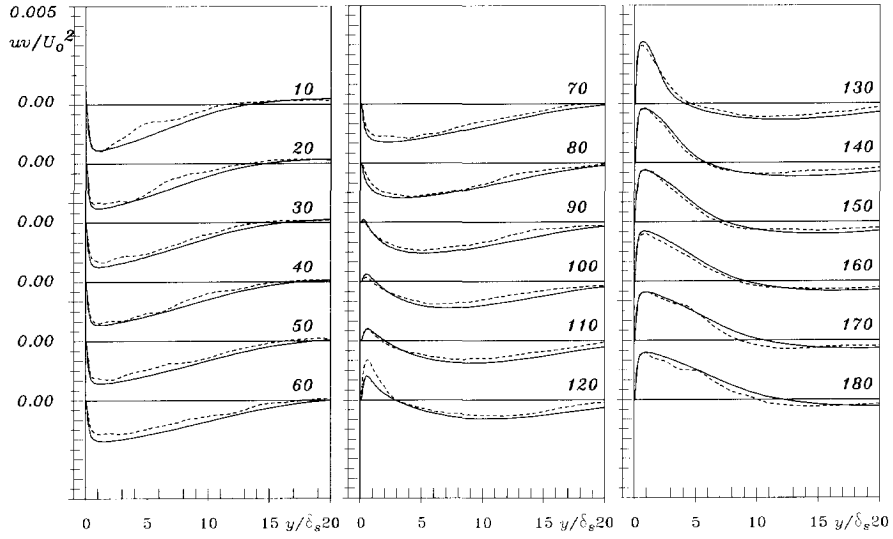

Figure 4.13: Comparison of computed profiles of turbulent shear stress with DNS results at different phase angle. Oscillating boundary layer with 'steep' variation of free stream velocity. - - - DNS (Justesen and Spalart 1990), —— SMC M2.

onset of flow deceleration, followed by its gradual damping during acceleration to the level at which the turbulent fluctuations exert negligible influence upon the mean flow. The results are plotted in form of closed loops over the abscissa which is folded around the free stream reversal point (180 deg) to exhibit the hysteresis of the flow properties at different flow depths. In addition to the illustration of excellent agreement between the model computations (lines) and direct numerical simulations (symbols), Fig 4.16 indicates clearly the ability of the model to reproduce well the dynamics of the response and different modulations of mean and turbulence properties at different distance from the wall, with variable phase shifts.

4.2.5 Oscillating channel and pipe flows

If $\lambda \gg 1$ the boundary layer in a pipe or channel flow remains much thinner than the channel half-width and there is no effect of the channel Re-number. However, if the penetration depth approaches or exceeds the channel half width, the interaction of the two merging boundary layers influences the stability and turbulence pattern. Application of the same model to the fully developed oscillating channel and pipe flow reproduced the same pattern in the near-wall region at similar Re_{δ_S}, but not so well in the outer region if λ is close to 1. In absence of DNS data or detailed experimental results we present here only few results obtained for a channel and pipe flow at the conditions close to the available experiments.

Fig 4.17 displays the computed wall shear stress and $\overline{uv}$ very close to the wall, together with

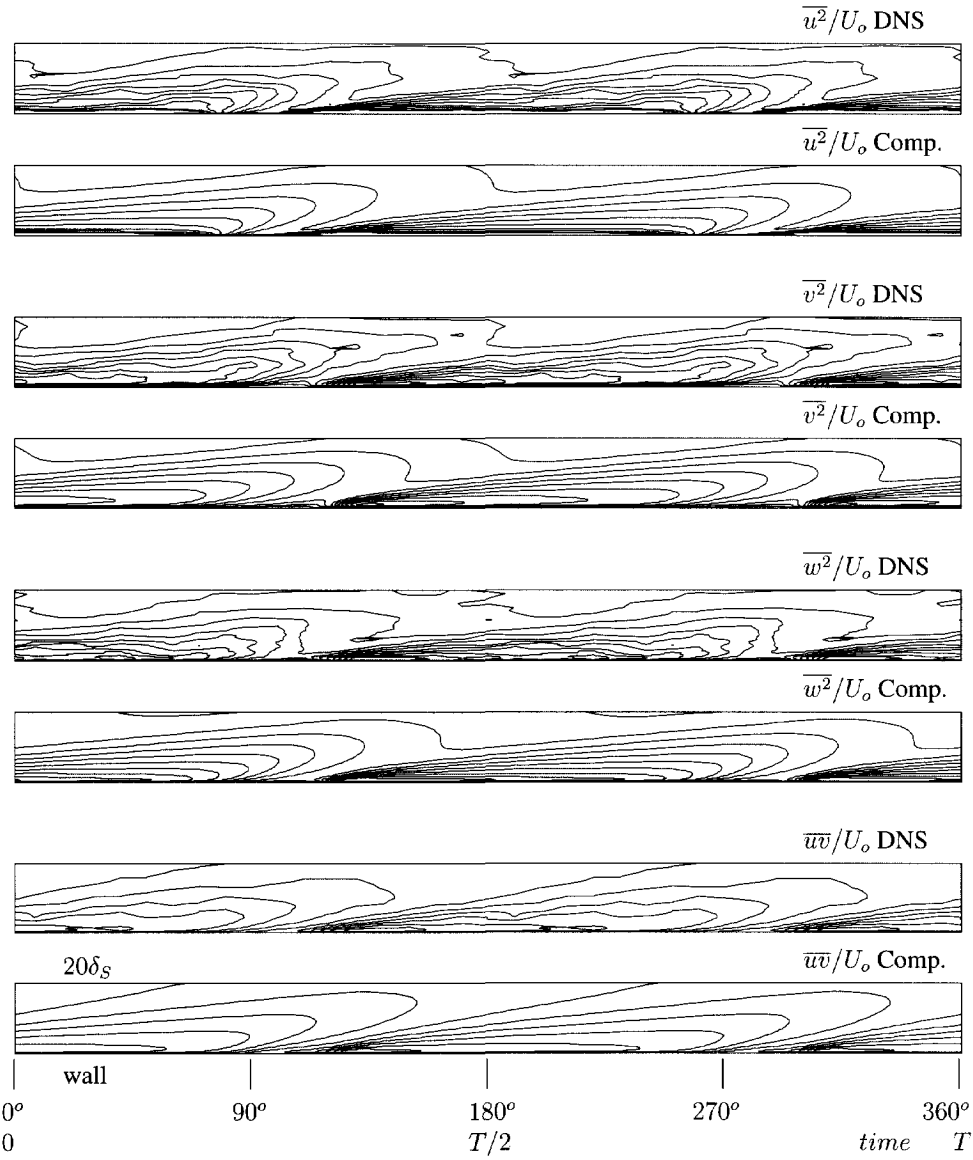

Figure 4.14: Time development of contours of constant turbulent stresses at $Re_\delta = 1000$ for 'steep' variation of free-stream velocity.

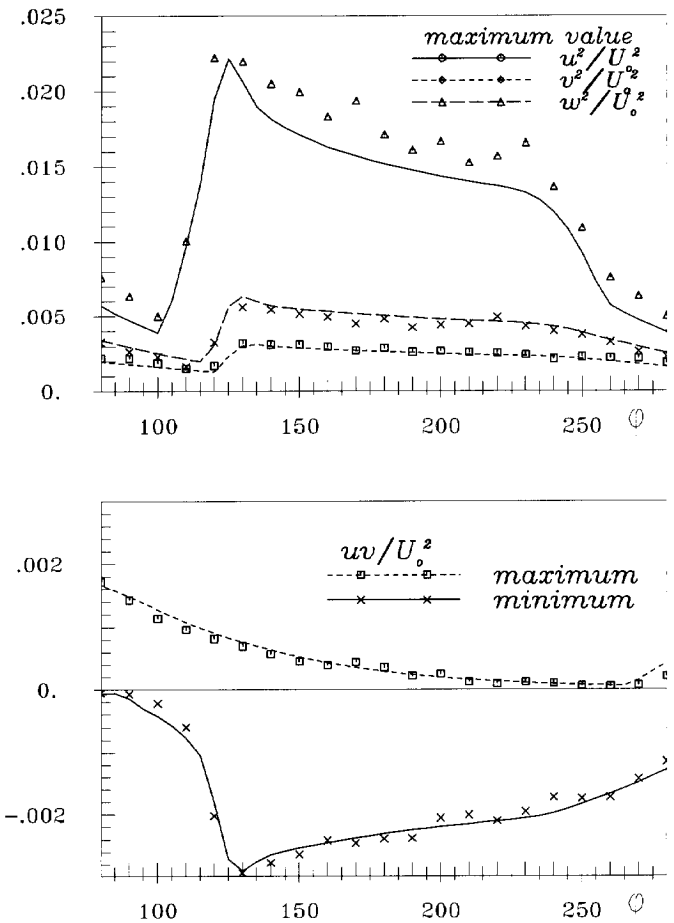

Figure 4.15: Evolution of peak values of all components of Reynolds-stress tensor over a half of the cycle. 'Steep' variation of the pressure-gradient. $Re_{\delta_S} = 1000$. Symbols DNS (Justesen and Spalart 1990), Lines SMC M2.

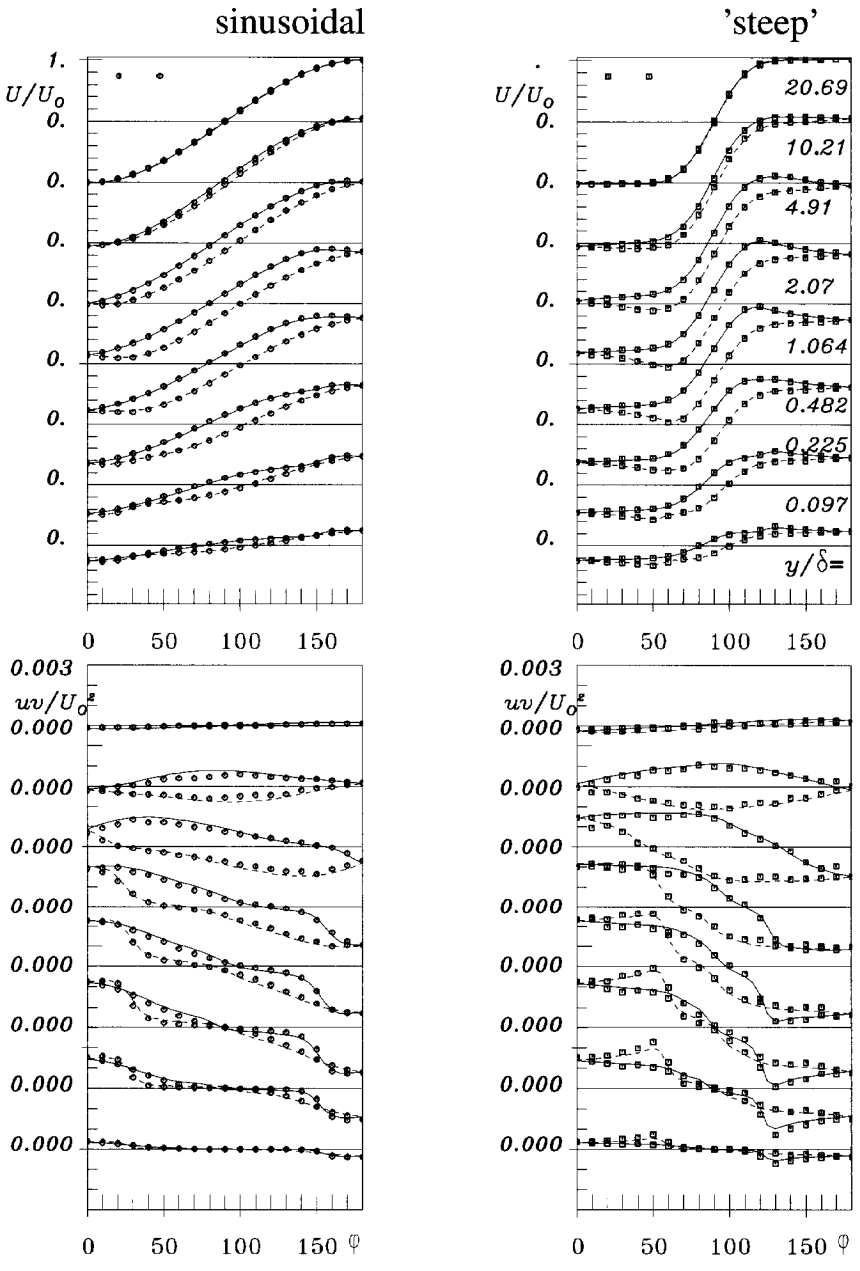

Figure 4.16: Hysteresis in oscillating boundary layers; left: sinusoidal U_∞ DNS (Spalart and Baldwin 1989); right: steep U_∞ DNS (Justesen and Spalart 1990); lines: computation SMC M2; solid lines $\phi = 0^o - 180^o$ and dashed lines $\phi = 180^o - 360^o$.

the experimental data of Hino *et al.* (1983) obtained in a rectangular duct at $Re_{\delta_S} = 876$ and $\lambda = 12.8$.

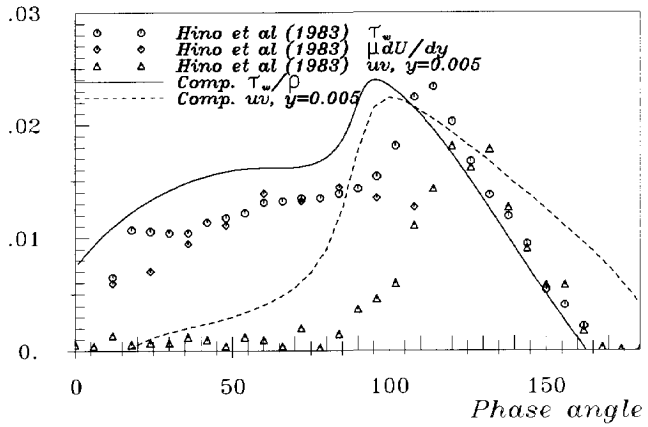

Figure 4.17: Evolution of the shear stress at the wall and at a position in the flow in a plane channel with $Re_{\delta_S} = 876$ and $\lambda = 12.8$.

At this value of λ, one would expect that the flow is essentially of the boundary layer type. The computed and measured profiles of the wall shear stress look similar, but there is a considerable phase difference. The same could be said for the $\overline{uv}$, obtained at $y = 5\ mm$ (Note: $\delta_S = 3.9\ mm$, channel width $H = 100\ mm$). In light of previously shown excellent agreement with the measurements for the same Re_{δ_S} it is difficult to explain these discrepancies. For illustration, Fig 4.18 shows a comparison between the recorded and computed evolutions of the ensemble-averaged velocity at several positions across the flow.

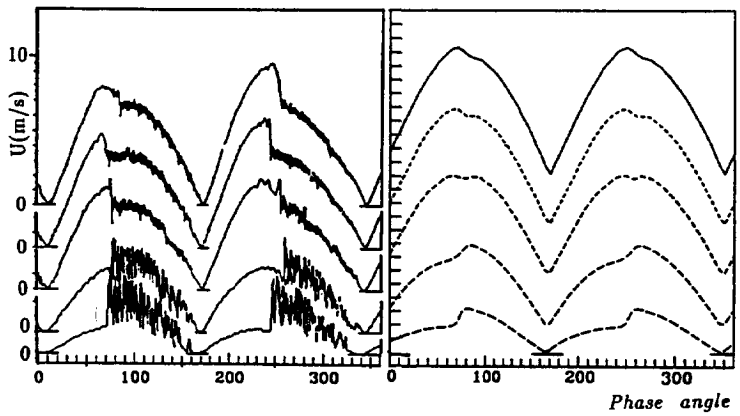

Figure 4.18: Recorded (Hino *et al.* 1983) and computed histograms of the mean velocity at various positions across the channel ($Re_{\delta_S} = 876, \lambda = 12.8$).

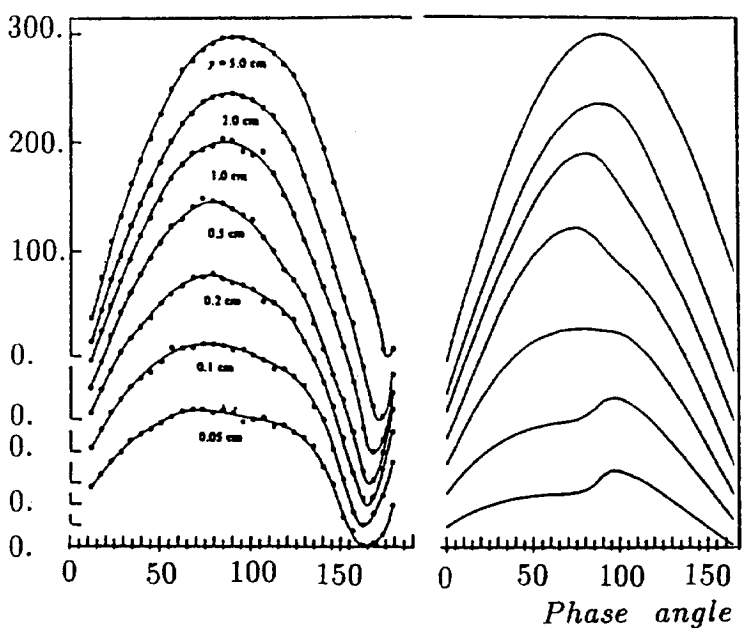

Figure 4.19: Recorded (Hino *et al.* 1989) and computed histograms of the mean velocity at various positions across the pipe ($Re_{\delta_S} = 1530, \lambda = 1.91$).

Except very close to the wall (for y=0.05 and 1 mm), the agreement is satisfactory - both records exhibiting the transition at the start of the deceleration phase. However, the experiments indicate a relatively low level of turbulence despite a large channel Re-number, ($Re = 2.25 \times 10^4$). Much closer agreement is shown with the results of an earlier experiment of Hino *et al.* (1989), Fig 4.19 where the computed velocities at several radial positions are compared with the oscillogram obtained in a pipe at a larger Stokes Re-number, $Re_{\delta_S} = 1530$, but at much smaller channel Re number, $Re = 5830$.

The corresponding lines are obtained at the same non-dimensional distance, normalised with the Stokes thickness δ_S. Both pictures exhibit the same sudden jump in the velocity profiles in the near-wall region and a corresponding sudden decrease in the central region. In this case the Stokes parameter $\lambda = 1.91$ and the instability and transition occur also at the pipe centerline. The phase shift of the velocity maximum is also well reproduced.

Finally Fig 4.20 presents a comparison of the histograms of the bursts in streamwise turbulent fluctuations at three radial position, recorded by (Seume 1988) and SMC results. The resemblance of the signals, both in shape and magnitude, is so striking, in particular at two positions away from the wall, that we considered presenting the results worthwhile, although they were obtained for a frequency about three times smaller than in the experiment (other parameters are the same). The computations at the exactly same conditions produced similar but milder signals. It should be noted that the experiments were carried out in a finite pipe of $L/D = 60$ and that the oscillograms were recorded at $L/D = 44$, whereas our time-marching computations takes no account of the pipe length. The solution of the whole flow domain reproduces the velocity histogram much better (Hadžić and Hanjalić 1995, not shown here).

Oscillating pipe flow

In order to validate the model against the results of other authors, for which more data are available, we consider briefly the flow studied experimentally by Akhavan *et al.* (1991). We selected an oscillating fully developed pipe flow case with $Re_{\delta_S} = 1080$ and $\lambda = 10.6$. As shown in Fig 4.21, the model prediction of the wall shear stress follows closely the experimental results. Note that in this case Re_{δ_S} is marginally larger than in DNS case of Spalart and Baldwin (1989) and since λ is relatively large the influence of the wall is not very pronounced. A slightly slower increase of the wall shear stress than in the boundary layer is observed in the transition phase ($\phi = 60^o - 100^o$).

4.3 Pulsating Pipe Flows

Next flows considered are the two cases of developed pipe flows with imposed sinusoidal oscillation of the bulk flow in a long pipe, investigated experimentally by Tu and Ramaprian (1983) with frequencies of 0.5 and 3.6 Hz and amplitudes of 64 and 15 % respectively. The mean Re-number of 50000 was sufficient to ensure fully turbulent regime over the whole cycle in both cases. Contrary to our expectation, the reproduction of this case appeared to be difficult. Experiments in the low-amplitude high-frequency flow indicated a very small departure of the velocity

fluctuations from the steady flow values close to the wall, as expected, considering that $\lambda >> 1$, and this feature was depicted reasonably well by computations. However, the wall shear stress exhibits a curious modulation, which could not be reproduced by the model, shown in Fig 4.22. The computed wall shear stress remained fully sinusoidal as the imposed pressure variation, with peak values and their phase position in good agreement with experiments.

For the high-amplitude low-frequency case the wall shear stress is reproduced better, apart from positive peaks, which were overpredicted by 13%, as shown in Fig 4.23. The non-linear model of the 'slow' pressure-strain term (with negative coefficient $C_1' = -0.4C_1$, as adopted for some other flows) gave a slight improvement, as shown in both figures. Turbulence fluctuations (Fig 4.24) are reproduced in qualitative agreement with experiments, though better in the deceleration phase than during the acceleration. It should be noted that according to the criterion of Tu and Ramaprian (1983) both flows with $\lambda > 1$ should have a central core which oscillates like a solid body, while the computations showed that the diffusion of unsteady wall disturbances during the deceleration phase extends almost over the complete cross-section.

4.4 Concluding remarks

The low-Re-number second-moment closure model was applied to study the dynamics of mean and turbulence field in broad range of oscillating and pulsating boundary layer and pipe flows at transitional and higher Re-numbers. Jointly with some basic test cases for low Re-number model for which DNS data are available, such as channel and boundary-layer flows, the oscillating boundary layer at $Re_{\delta_S} = 1000$ (DNS by Spalart and Baldwin 1989) was used to select and adjust values and functional form of some low Re-number model coefficients.

Computations of oscillating boundary layers for a range of transitional Reynolds numbers, Re_δ, between 760 and 3460 show a very good agreement with DNS and experimental results. For oscillating flows in pipes and channels for the same Re_δ the transition features are equally well reproduced if $\lambda \gg 1$ and if the duct Reynolds number is higher than the critical value, defined approximately by $Re = 1500\lambda$. It is obvious that these (and probably other) turbulence models cannot simulate the subtle details of non-laminar (or perturbed laminar) pattern at the initiation of instability at the lower transition limit, as found by experiments or DNS, e.g. at $Re_\delta \approx 600$. However, the model seems to be capable of reproducing the conditionally turbulent regime with sudden bursts of turbulence at the start of deceleration phase and subsequent re-laminarization, over a range of transitional Re-numbers. The model requires a minimum of "background" turbulence to be able to reproduce its amplification and eventual transition to the fully turbulent regime. What this minimum is, depends on the choice of the adjustment functions, which have in the past been tuned to satisfy the switch-over from the outer turbulent to the inner viscous regimes in near-wall flows. The SMC model reproduces well the transition dynamics in the corresponding range of Re-numbers, including the form and magnitude of the sudden bursts of turbulence quantities at various positions in the flows.

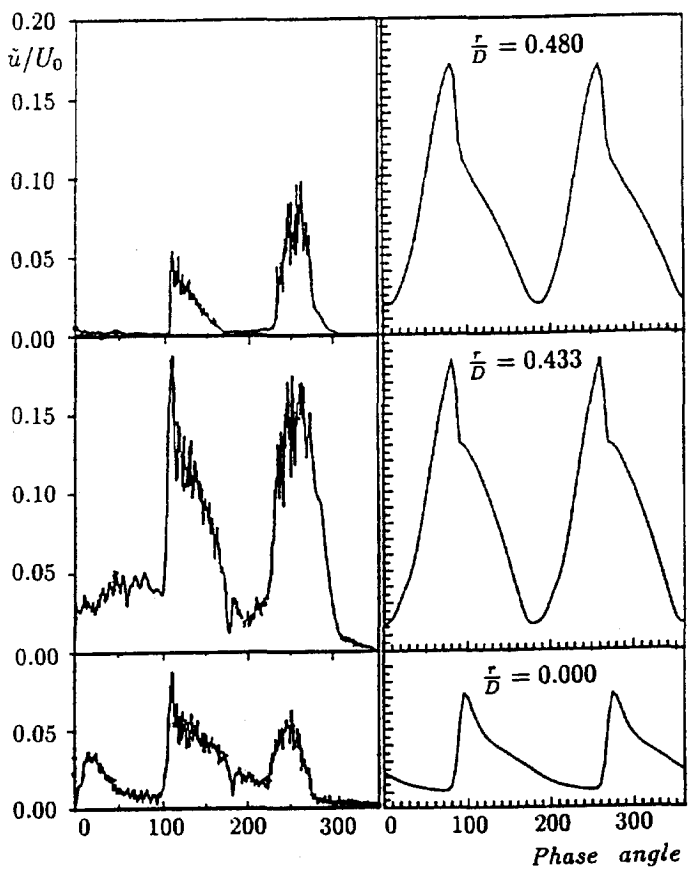

Figure 4.20: Recorded (Seume 1988) and computed histograms of the streamwise velocity fluctuations at three positions across the pipe ($Re_{\delta_S} = 925, \lambda = 6.32$).

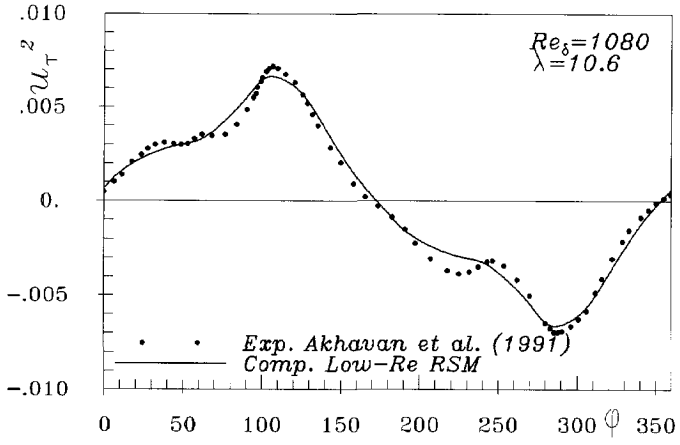

Figure 4.21: Evolution of the wall shear stress in a oscillating pipe flow with sinusoidal pressure variation at $Re_{\delta_S} = 1080$.

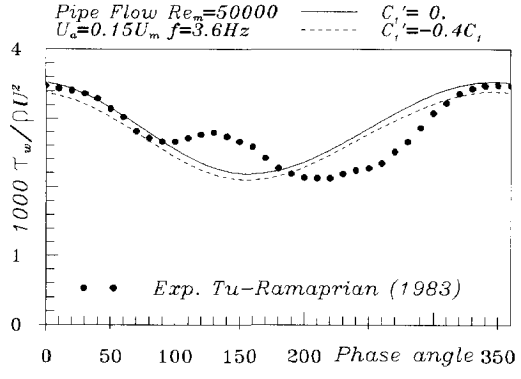

Figure 4.22: High frequency low amplitude pulsating pipe flow.

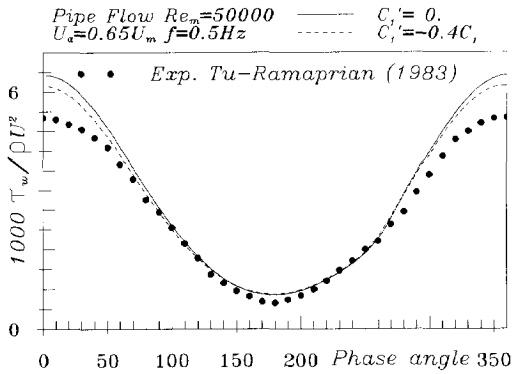

Figure 4.23: High frequency low amplitude pulsating pipe flow.

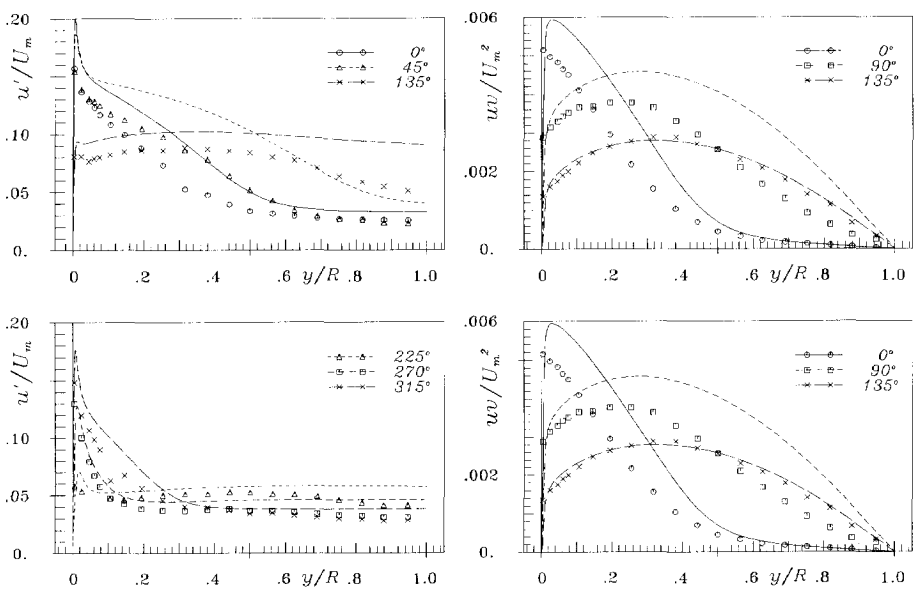

Figure 4.24: Low frequency high amplitude pulsating pipe flow

CHAPTER 5

Bypass and Separation Induced Transition

In this chapter the results of the computation of transitional flows using single-point closure models (linear eddy-viscosity and second moment closure) in several geometries and with several flow-conditions are presented. The first class of the flows considered are the bypass transition flows on the flat-plate with sharp leading edge subjected to several *free-stream turbulence* (FST) intensities, length scales and pressure-gradients. Afterwards, the models have been applied to the separation induced transition on flat-plate with circular leading edge under a range of FST level, and to the separation induced transition on flat wall. The mechanism of transition in these two classes of flows are rather different. In the first case, the transition is induced by free-stream turbulence and the turbulence in the boundary layer is enhanced due to mean rate of strain and presence of the wall. In the separation induced transitional flows, the transition is primarily induced by a separation bubble generated by the adverse pressure gradient. The results of the computations are compared with the experimental and DNS data. The bypass and circular leading edge transitional flows are used as the benchmark in an ongoing collaborative ERCOFTAC[1] project on the capability of turbulence models to predict transitional flows (Savill 1996). All these cases are with relatively high free-stream turbulence level (more than 2%). Because of the importance of reliable and detailed experimental or DNS data for model validation, attention is also given to two cases with separation bubble, for which recent DNS data are available. Results of computation of a case with the transitional sepparation bubble on a flat wall (DNS by Spalart and Strelets 1997) using the SMC model are presented and discussed. In this case, transition is induced by separation, but the incoming boundary layer is virtually laminar. A turbulent separation bubble (DNS by Spalart and Coleman 1997), which resembles the transitional one, was also investigated because more data were available. Although in this case the incoming boundary layer was turbulent, the rapid increase of turbulence within the bubble occurs, similarly as in the transitional sepparation bubble. Finally, an illustration of prediction of a complex and industrially relevant flow using the second moment closure low-Re-number model is presented. It is the flow over the NACA 4412 airfoil at maximum lift, with the incidence angle of 13.87^o, and high Re-number ($Re_c = 1.52 \times 10^6$) (experiments by Coles and Wadcock 1979).

[1] ERCOFTAC stands for European Research Community on Flow, Turbulence and Combustion

5.1 Introduction

Transition from laminar flow to turbulence can be classified in three major groups (Mayle 1991): i) *natural* transition, ii) *bypass* transition, and iii) *separation-induced* transition. The *natural* transition occurs as a consequence of a gradual growth of small perturbations of a laminar flow into two-dimensional waves (so called Tollmin-Schlichting waves) which then, by the non-linear effects, break into turbulence. The expression *bypass* transition, introduced by Morkovin, means that most of development stages in the natural transition is bypassed by some strongly forced disturbances. The bypass transition usually occurs by diffusion of turbulence from the free-stream into a boundary layer. The experiments show that in a boundary layer flow with zero pressure gradient this is the case if FST is larger than 1%. It is possible that a boundary layer separates while still laminar and that at certain conditions the vortices generated by separation reattach to the boundary forming a bubble and generating turbulence within the bubble, which then penetrates into the incoming laminar flow. This kind of transition is called separation-induced transition. This is often the case in flows with adverse pressure-gradients and occurs for example at the leading edge of an airfoil or gas turbine blades.

The mechanism of formation of turbulence in the transitional flows is very complex, and such a process can be studied in details only by means of direct numerical simulation (DNS) which have already been performed for several transitional flows. For example, Spalart and Yang (1987) and Laurien and Kleiser (1989) performed DNS of the boundary-layer type of transition and Spalart and Strelets (1997) performed a DNS of a separation bubble from a flat-plate. This approach, although very expensive, is important for understanding the process of transition and provides essential information for modelling purposes. Large-eddy simulations (LES) have been already applied to computation of transitional flows. Voke and Yang (1995) performed LES for several bypass transition flows and Yang and Voke (1995) performed a LES of the separation-induced transition on a flat plate with circular leading edge.

A number of modelling techniques is currently in use for computation of transitional flows. Possibly the most widely spread ones are in the framework of the RANS modelling. Since the first successful application of low-*Re* $k-\varepsilon$ model to flows with laminarization (Jones and Launder 1972) a substantial progress has been made in the development of turbulence models, expanding gradually their applicability to a wider range of flows including some forms of transition. Progress reports on the activity of the ERCOFTAC Transition Special Interest Group (SIG), (Savill 1993) provide a good overview of the current achievements of single-point closures in modelling the diffusion-controlled bypass transition. Despite substantial efforts, the outcome seems to be inconclusive. Particularly disappointing is the evidence that higher model complexity brought only marginal improvements, and only in some cases. Nevertheless, some conclusions did emerge. The models which use the invariant turbulence parameters, such as the turbulence Re number, perform better than those which use the local wall distance. Satisfying the correct wall limits of the shear stress and of energy dissipation rate was also found to be important for a successful reproduction of the transition. Finally, few contributions with the Reynolds-stress models with low-Re-number modifications all seemed to perform better than two-equation models. Major advantages of the SMC were in the provision to account for anisotropy of the free stream- and of the near-wall stress field, and, particularly in the ability to reproduce the normal-

to-the-wall velocity fluctuations. Another merit is in the exact treatment of the turbulence production and effects of streamline curvature. These features help also in handling other forms of non-equilibrium phenomena frequently encountered jointly with different forms of transition.

Another frequently used technique for modelling transitional flows is the *intermittency approach*. It is assumed that the transitional region is composed of intermittent spots of turbulence in otherwise fully laminar flow. The transitional region is then taken into account by a linear combination of laminar and turbulent solution that is controled by the intermittency γ which is defined as the fraction of time that the flow is turbulent. The intermittency factor γ is determined by experiments for a particular flow. It takes zero value in fully laminar region and unity in the fully turbulent region.

In the framework of linear eddy-viscosity models it is still possible to solve a single set of Navier-Stokes equations while using γ to control transition in computations. The effective eddy-viscosity to be used in momentum equations is

$$\mu_e = \mu + \gamma\mu_t \tag{5.1}$$

where μ_t is the eddy-viscosity obtained from a turbulence model. A major disadvantage of this semi-empirical approach is the need of experimental correlations for γ that limits applicability of this approach to a quite small number of well documented flows.

Although the intermittency models may bring some advantages, particularly for low FST, the gains do not seem to justify the introduction of yet another parameter (and defining equation) which relies heavily on empiricism. Single-point closures have been successfully used to predict intermittent turbulence e.g. at the edge of boundary-layer or free-shear flows without having to define and reproduce this quantity, which remains hidden in the model, just as other information about eddy structure and spectral properties.

5.2 Some basic RANS modelling requirements

Single-point closure models are based on Reynolds averaging, which by its virtue conceals the dynamics of flow disturbances. These models are capable of representing turbulent flows with a relative success and are nowadays widely used for industrial applications. It is generally accepted that the turbulence closures offer more flexibility and better prospects for predicting real complex flows with transitions than any classical linear stability theory. The ability to predict a *change-over* from one regime to another (not necessarily the actual transition mechanism) at appropriate location and under appropriate conditions, and consequent modifications of mean flow parameters, without having to introduce any artificial triggering, will often serve the purpose of computing complex industrial flows involving transition.

Current statistical models can be expected to reproduce transition only when either a continuous source of turbulence exists somewhere in the flow or at its edge from where the turbulence will diffuse (be entrained) into the rest of the non-turbulent flow. Alternatively, the laminar flow must contain some background turbulence, sufficiently weak not to influence the laminar-like mean flow properties but sufficient to amplify itself when the flow deformation or other disturbance is imposed or reaches a sufficient strength to interact with the background turbulence. Such

case is retransition, e.g. in an oscillating turbulent boundary layer at low Re numbers, or in a laminar-like or laminarizing boundary layer subjected to a strong adverse pressure gradient e.g. in compressor cascades. The ability to predict the bypass transition depends on the model of turbulent diffusion, particularly away from the wall, which essentially controls the boundary layer turbulization. In contrast to that, the prediction of laminarization and subsequent re-transition depends on the model's ability to reproduce accurately the process of turbulence decay and production at a low turbulence Re number in a strongly anisotropic field in the near wall region.

The essential requirement on RANS models for the prediction of transitional flows is the integration of the model equations up to the wall (so called low-Re-number models). The low-Re-number modifications have been proposed at different modelling levels, but in the most cases they were tailored to achieve overall damping of turbulence as the wall is approached. In most cases, no distinction is made between the pure viscosity effects, which are of a scalar nature, and non-viscous, directionally biased wall blockage and a consequent pressure reflection. Unlike the viscosity which damps evenly the turbulence fluctuations in all directions, a solid wall imposes a selective damping of the normal-to-the-wall velocity fluctuations and a consequent eddy splatting, resulting in increased turbulence anisotropy, approaching the two-component state very close to the wall. Most low-*Re*-number models treat both effects jointly and often relating the overall damping to the local wall distance. While such a practise can reproduce near wall behaviour in near-equilibrium steady flows similar to those in which the models were tuned, it fails in most cases with complex wall topography, or with a significant departure from equilibrium conditions. In view of the fact that most transitional phenomena are provoked, enhanced or otherwise controlled by sudden changes in boundary or external conditions, it is obvious that such models cannot reproduce a broader variety of transition phenomena.

5.3 By-pass transition on a flat plate

The ability of the HJ low-*Re* SMC had been investigated first in bypass transition on a flat-plate with sharp leading edge with constant and variable pressure. The case is the simplest of all transitional flows considered here.

The transition from a laminar-like mean flow near the wall which is developing at the very beginning of the plate[2] to turbulent boundary layer somewhere downstream is in this case driven by free-stream turbulence. Two cases with constant pressure and with 3% and 6% FST and one case with variable pressure gradient and with 8% FST are considered. Within the ERCOFTAC Transition SIG workshop (Savill 1993) these cases are designated as T3A, T3B and T3C1 respectively. Corresponding free stream mean velocities are 5.2 and 9.6 m/s in T3A and T3B cases, whereas in T3C1 case the free-stream velocity varies between 6 and 8 m/s. In all cases the working fluid is air.

[2]Experiments were carefully controlled to prevent separation at the leading edge.

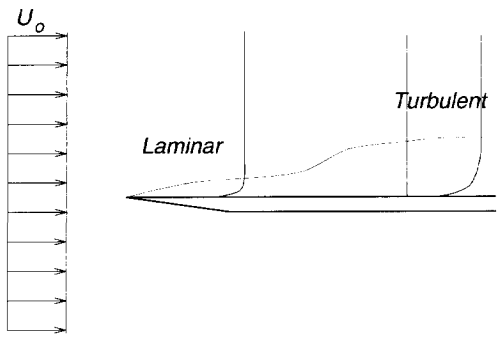

Figure 5.1: Definition sketch of bypass transition on a flat plate with sharp leading edge.

5.3.1 Computational details and inlet conditions

Computations of these cases were performed with a parabolized Navier-Stokes numerical code using the control-volume approach with typically 100 nodes across the flow in a collocated variable arrangement (the same code as for the oscillating boundary layers). The corresponding pressure gradient was specified explicitly and the normal to the wall component of the mean velocity is evaluated from the continuity equation. The parabolic computations started at the leading edge with uniform profiles of all quantities equal to the streamline values supplied by experiments. A validation of the parabolic approach was performed by computing the case T3B by the full (elliptic) Navier-Stokes solver, over a computational domain starting at the leading edge and extending sufficiently downstream to capture in full the transition region. Admittedly, this was not sufficient since the elliptic effect of the leading edge could be detected only by starting the computation ahead of the edge and accounting for the real shape and thickness of the plate. These were ignored in this case, but studied in details in the case of a symmetric round-edged plate, as discussed later. The computational domain is 10 mm wide (which is about 5 times of the maximum boundary-layer thickness) and 2.5 m, 1.5 m and 1.5 m long for these three cases respectively. For the parabolic computations x-step was $\Delta x = 1$ mm which provides grid independent results (tests were done for $\Delta x = 0.5, 1.0$ and 2.5 mm). The elliptic computation of T3B case was performed on an orthogonal grid of 300 CVs in streamwise direction and 120 CVs across the flow. The mesh in direction normal to the wall was made exactly the same as that for parabolic code computation. Since the zero pressure boundary condition was applied in the free-stream, the computational domain in that region was enlarged for 50% of the width used for the parabolic code that was covered with additional 20 CVs. Zero pressure boundary condition was applied also at the down-stream domain boundary. The wall friction factor, which is the most sensitive parameter of the flow behaviour, obtained with these two approaches is shown in Fig 5.2. A small difference between these two results can be addressed to different grids in streamwise direction, to neglecting some terms done in parabolic approach, and to possible effects of pressure variation up to the wall. All results for T3A, T3B and T3C cases presented here are obtained with the parabolic approach.

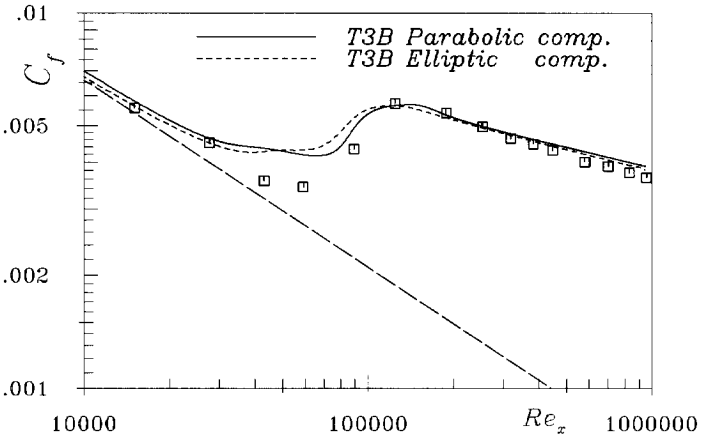

Figure 5.2: Comparison of SMC computations of wall friction factor in T3B case obtained with parabolic and elliptic code on grids of 2500 and 300 CVs in the flow direction respectively.

According to the T3A and T3B case description, provided by the organiser of the ER-COFTAC workshop, the stream-wise normal Reynolds-stress develops as

$$\frac{\sqrt{\overline{u^2}}}{U_0} = C\,(1000 \cdot x + 610)^{-5/7}, \tag{5.2}$$

where x is the stream-wise distance from the leading edge of the plate. For the isotropic turbulence the kinetic energy is

$$k = \frac{3}{2}\,\overline{u^2} = U_0\,C^2\;(1000 \cdot x + 610)^{-10/7}, \tag{5.3}$$

and the dissipation rate is

$$\varepsilon = -U_0\,\frac{dk}{dx} = \frac{15000}{7}\,U_0^3\,C^2\,(1000 \cdot x + 610)^{-17/7}. \tag{5.4}$$

The coefficient C can be evaluated for a particular case using known experimental value of the free-stream turbulence.

Using the model equation for the dissipation rate ε, the development of turbulence kinetic energy in free-stream is given with

$$k = \left[k_0^{1-C_{\varepsilon 2}} + \frac{(1-C_{\varepsilon 2})\,\varepsilon_0}{U_0\,k_0^{C_{\varepsilon 2}}}\;(x - x_0)\right]^{\frac{1}{1-C_{\varepsilon 2}}} \tag{5.5}$$

where x_0 is the position where k_0 is known and x is the position at which k is computed. This expression can be also used to estimate the dissipation at any position (i.e. at inlet) providing

the computed decay of turbulence kinetic energy in accordance with experiments. These two formulae give very close values for inlet dissipation if $C_{\varepsilon 2} = 1.92$ is used.

According to the authors of experiments the free-stream turbulence is isotropic. However, the experimental data at the edge of the boundary layer show some anisotropy (Fig 5.3). Therefore, these data were used to estimate the anisotropy of Reynolds-stresses at the inlet of the computational domain. Computational results of the Reynolds-stresses in the free-stream, obtained with these inlet conditions, are close to experimental data at the edge of the boundary layer. The return to isotropy can be regarded as satisfactory, Fig 5.3.

At inlet ($x = 0.$ m) the turbulence length scales $L_{\varepsilon_i} = k_i^{3/2}/\varepsilon_i$ are 9.9 mm for T3A, 26.6 mm for T3B and 9.8 mm for T3C1. Theses values of ε_i provide the best agreement of the decay of turbulence in free-stream with the experimental data.

Westin and Henkes (1996) showed in detail that different values of dissipation rate in the free-stream as well as in the boundary layer significantly move the position of the transition. In order to reduce the influence of initial conditions, we performed the computations starting at plate's edge with uniform profiles of all variables.

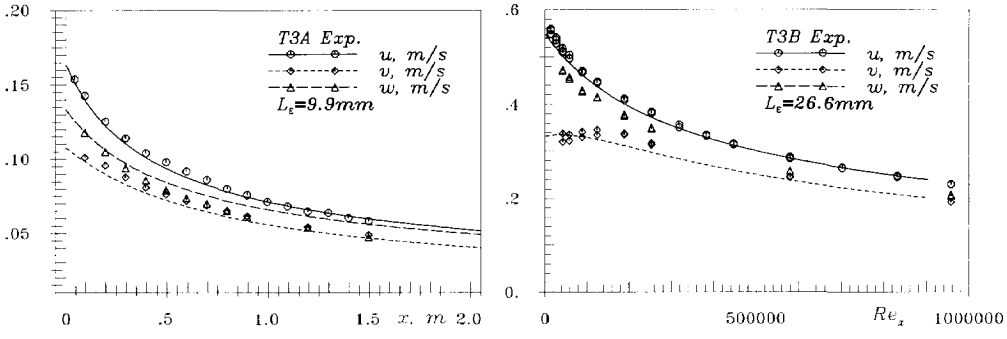

Figure 5.3: Evolution of the Reynolds-stresses in the free-stream computed with SMC model (lines) for the inlet conditions that are described in the text above. Symbols are experiments by Roach and Brierley (1990) at the edge of the boundary layer.

5.3.2 Results and discussion

In the framework of ERCOFTAC workshops the Launder-Sharma low-Re-number eddy-viscosity model has proved to perform the best among all the low-*Re* number eddy-viscosity models in by-pass transition under the influence of free-stream turbulence in the range between 1% and 6%. Fig 5.4 shows the wall-shear stress C_f and the shape factor H obtained with this model for the cases T3A and T3B. The model predicts the transition too early and too suddenly so that the transition region is much shorter than in experiments.

One deficiency of the linear $k - \varepsilon$ model is its inability to reproduce the anisotropy of Reynolds-stress tensor and particularly of the normal components. This is overcome by SMC

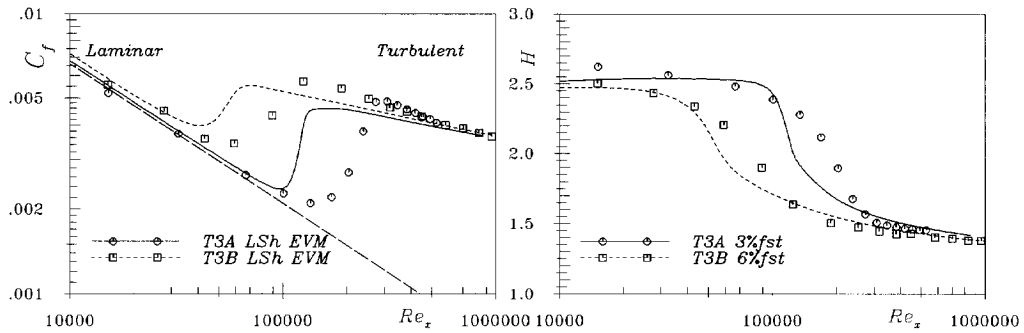

Figure 5.4: Wall-shear stress (C_f) and shape factor (H) computed with the Launder-Sharma low-Re-number EVM for the T3A and T3B cases. Symbols: Experiments by Roach and Brierley (1990).

models solving transport equations for stress components. In these equations the production of the stress is treated exactly while pressure-strain correlation is modelled. This is of significant importance for accounting the dynamics of the stress in the flow. These features are crucial in obtaining generally better results with SMC models compared to eddy-viscosity models. Therefore, it is accepted that SMC models should provide better results in bypass transition flows.

The low-*Re* SMC results for C_f and H are shown in Fig 5.5. The model reproduces the transition including the location of the beginning and the end of transition for T3B case (with FST of 6%) in good agreement with experiments. In the initial phase C_f is over-predicted. As the FST is reduced to 3% the model fails to maintain the turbulence as was measured in experiments. Actually, the position of the beginning of transition is at the same place as in experiments but the transition itself is very slow. These computational results are in accordance with computations of Westin and Henkes (1996) which were performed with the same turbulence model but with slightly different inlet conditions. It was shown by Hanjalić and Hadžić (1995) that a slight decrease in the dissipation rate can significantly improve results for the T3A case, but it does not produce properly the decay of turbulence in the free-stream.

It should be recalled that these results were obtained using Rotta linear model for the slow-part of the pressure-strain correlation with coefficient C_1 given by (2.59). However, by introducing the general nonlinear form of the model (Lumley 1978)

$$\Phi_{ij,1} = -C_1\varepsilon\left[a_{ij} + C_1^{'}\left(a_{ik}a_{kj} - \frac{1}{3}A_2\delta_{ij}\right)\right], \tag{5.6}$$

brings in much improvement as shown in by dashed lines in Fig 5.5. Significant improvement of C_f in the T3A case can also be archived with $C_1^{'} = 0.7$ (not shown here). Excellent agreement with experiments in the T3A case is obtained with $C_1^{'} = 1.2$ (Fig 5.5). This has similar, but not so large, effects on the T3B case that gives now the transition a little too early.

Fig 5.6 and 5.7 show the ability of the model to reproduce the development of the flow during the transition for the T3A and T3B case respectively. Positions at which the profiles are taken are

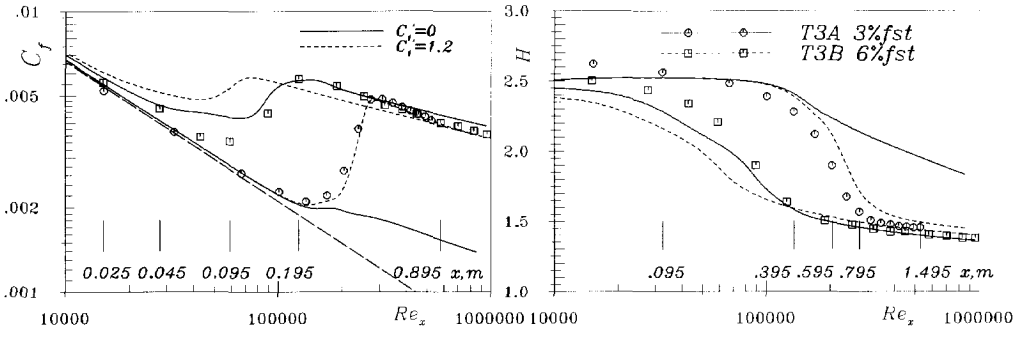

Figure 5.5: Friction factor and shape parameter for bypass transition cases T3A and T3B. Symbols: Experiments by Roach and Brierley (1990). Lines: Computations with SMC.

indicated in Fig 5.5. For both cases the profiles are given at an early stage of development, just before the beginning of transition, in the middle of transitional region, at the end of transition and in the fully developed turbulent boundary layer established after transition. Fig 5.6 shows the computational results for T3A case obtained with non-linear model (equation (5.6)). The velocity is predicted very well in accordance with results for C_f, but the Reynolds stress results deviate from experiments both in value and shape. Before the beginning of the transition and during the transition all normal stresses are under-predicted, and the boundary layer is thiner then experiments show. The production of the stress is much too small. This is primarily due to deficiency in modelling of the dissipation rate rather than due to deficiency in modelling of the redistribution and turbulent diffusion, because already at 0.095 m experiments show a peak of turbulence kinetic energy near the wall which is not reproduced by the model. Fig 5.7 shows results for T3B case obtained with the linear model for Φ_{ij}. This figure confirms that the model reproduces the transition close to the experiments (as seen from the results for C_f). Streamwise velocity and normal stresses are reproduced very well, following the shape and value of experimental results. However, the computed turbulent shear stress exceeds substantially the experimental data at all locations. This finding is strange in view of excellent prediction of the mean velocity and also good results of this model for the zero pressure boundary-layer flow and might be ascribed to an experimental error. The LES of Yang and Voke (1993) shows an overprediction of experimental value of $\overline{uv}$ by about 30% in the flow with about 5% FST and at $Re_x = 130.000$. Experimental and numerical results shown here indicate that it is very important to use the correct anisotropy of the Reynolds-stress tensor at the inlet to be able to compare the experimental and the numerical results.

The third case (T3C) involves variable pressure starting with favourable pressure gradient and reverting to adverse pressure gradient further downstream. The results of the case T3C1, which correspond to 8% free stream turbulence, are presented here. Strong acceleration (see

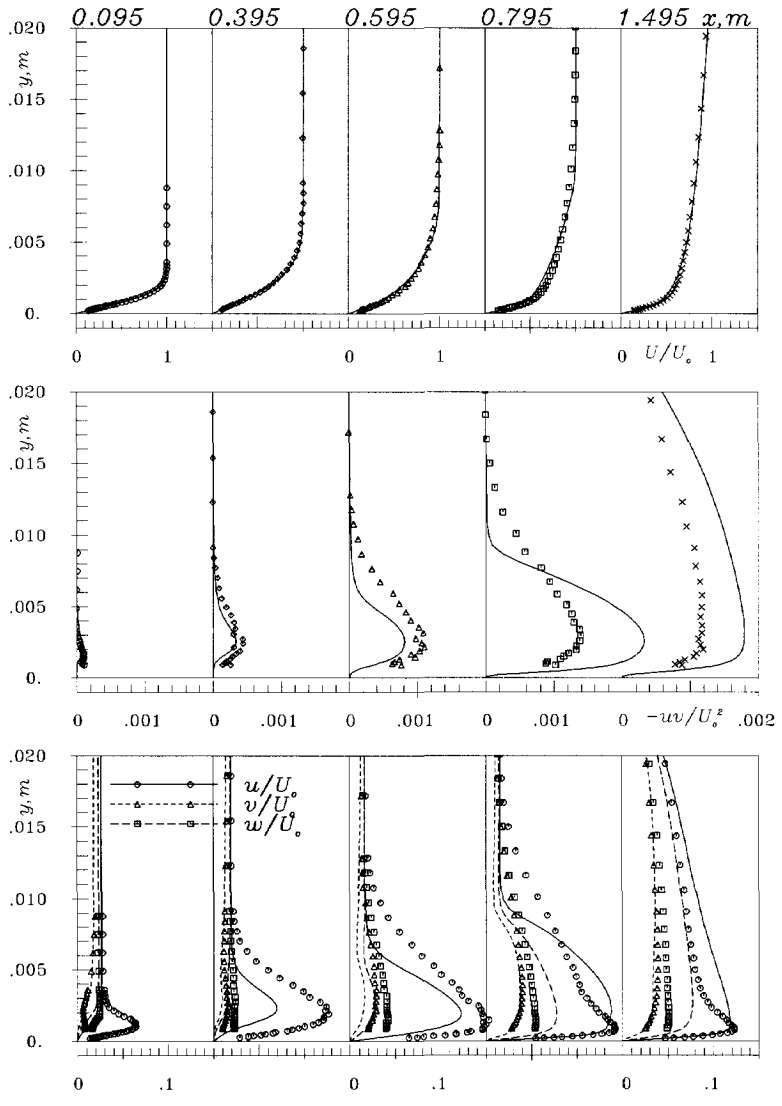

Figure 5.6: Mean velocity and Reynolds-stress profiles in the case T3A (locations indicated in Fig 5.5, right). Symbols: Experiments Rolls–Royce ASL. Lines: Computation with SMC model.

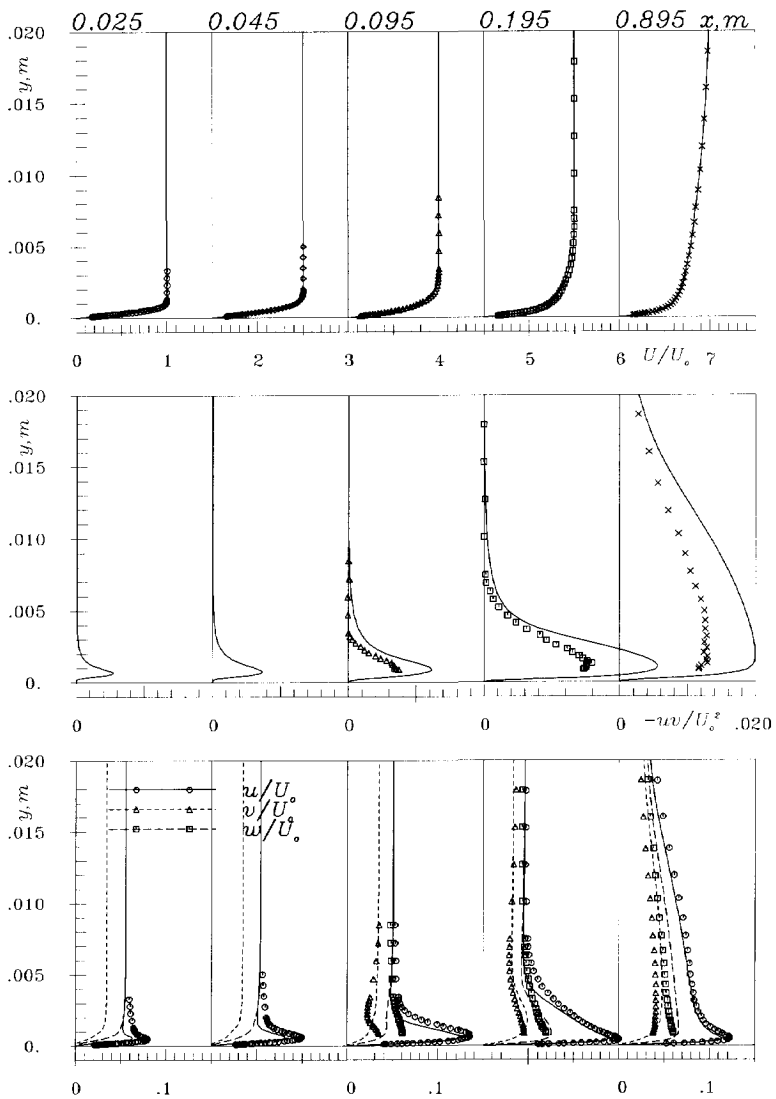

Figure 5.7: Mean velocity and Reynolds-stress profiles in the case T3B (locations indicated in Fig 5.5, left). Symbols: Experiments Rolls–Royce ASL. Lines: Computation with SMC model.

Fig 5.8) in the initial region makes this flow very sensitive to initial conditions. This sensitivity is illustrated by three computed lines in Fig 5.9 corresponding to three slightly different initial dissipation length scales. The chain line obtained with $L_{\varepsilon_i} = 5.0\ mm$ shows no transition: the boundary layer remains laminar throughout the considered flow domain. A small increase to 5.5 mm reproduced the transition reasonably well (full line), though its incipience started somewhat earlier than found by experiments. Further increase in L_{ε_i} moves the transition location back towards the leading edge, but the effect is not very pronounced, as shown by dotted line. It should be noted that an accurate reproduction of the pressure gradient from the experimental data for the free stream velocity variation is difficult and a small change can have a noticeable effect on the predictions.

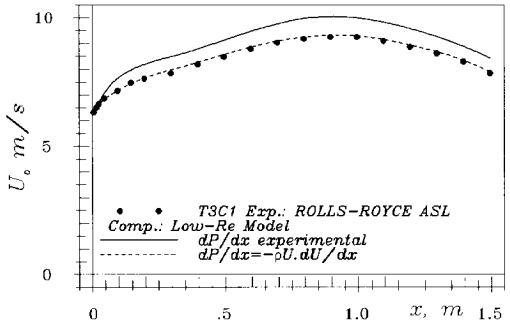

Figure 5.8: Comparison of the experimental end computed mean velocity obtained using $\partial P/\partial x$ given by experiment and computed from the experimental values for the mean velocity.

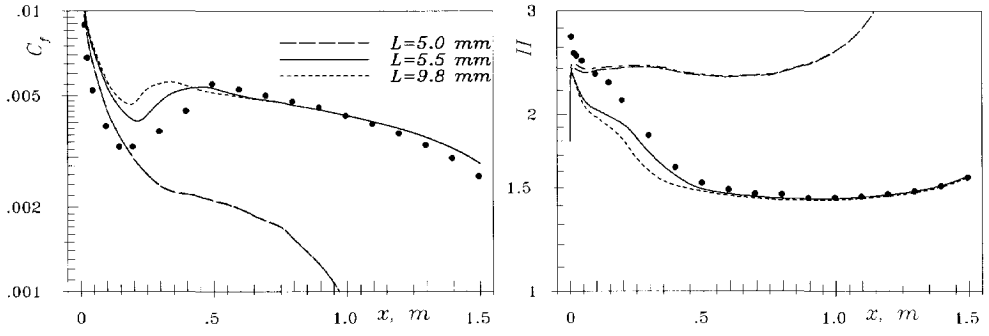

Figure 5.9: Friction factor and shape parameter for bypass transition on a flat plate with variable pressure gradient (free-stream velocity vary as shown in 5.8) and 8% FST. Symbols: Experiments Rolls–Royce ASL. Lines: Computation.

5.4 Transition on a flat-plate with circular leading edge

The transitional flows around a circular leading edge on a flat-plate with several flow conditions, investigated experimentally at Rolls-Royce ASL (Coupland 1995), have been adopted as benchmark test cases for turbulence modelling within the ERCOFTAC Transition SIG The transition in this case is also induced by free-stream turbulence and the experiments indicate that the transition is preceded and enhanced by a thin laminar-like separation bubble which appears at plate just behind the circular edge. This very thin bubble becomes major cause of enhancement of turbulence near the wall. Significant increase of the streamwise normal Reynolds stress was measured in that region. Therefore, the accurate representation of turbulence in the stagnation region as well as in the separation region is of decisive importance for successful computations of such flows.

In last few years several computations of such flows have been reported within the ERCOFTAC Transition SIG (e.g. Chen *et al.* 1994). All of them are based on the eddy-viscosity models. Predicting the correct shape and size of the separation region, which is crucial for predicting correctly the transition, was found to be a major challenge in which most conventional low-*Re*-number models failed.

In this work we applied the Launder-Sharma eddy viscosity model (see Appendix D for the detailed specification of the model) and the HJ low-Re SMC model to bypass transition flows around a circular leading edge in order to investigate the ability of these models to capture separation induced transition. The numerical results are compared to experimental data that include mean velocity and the streamwise normal Reynolds stress. Several cases with different free-stream conditions but in the same geometry were considered. The conditions vary in the mean free-stream velocity and the FST level. Major attention was given to the T3L4 case corresponding to the mean free-stream velocity $U_o = 5\ m/s$ and FST about 5.5%. This case was chosen first because it is the case with the highest level of free-stream turbulence of all six experiments performed.

5.4.1 Computational details

The computational domain was chosen with the inlet located 100 mm upstream from the plate-edge. In order to avoid any influence of the numerical treatment at domain boundaries, the flow-parallel boundary is located 150 mm away from the plate in the free-stream (in experiments the plate is located in the middle of channel with half-height of 218 mm) and the outlet boundary is located 500 mm downstream from the plate-edge. The symmetry boundary conditions are applied in the free-stream and zero-gradient of all variables at outlet. In order to handle easier and more accurate circular leading edge, the computational grid was divided into two blocks, Fig 5.10. The block, which covers the free-stream, contains 184×15 CVs and is not refined because the changes of all variables are not strong in that region. The inner block contains 308×60 control volumes, covers a region of 25 mm near the wall and the grid lines in the direction normal to the wall were highly nonuniformly distributed so that y^+ in the first point to the wall never exceeded the value of 0.3. After grid optimisation the selected grid covered the region of separating bubble (which was predicted only with SMC model) with up to 28 CVs in

the width (negative streamwise mean velocity) and about 55 CVs in the length. The stagnation region was covered with 60 CVs. A grid with the same number of computational points, but distributed in a different manner - being coarser at beginning of the plate and covering the bubble region with only about 25 CVs in the length - was used to assess the sensitivity of the solution to the grid density. The length of the separation bubble is computed on both grids with a difference of about 2%, and the differences in mean velocity and streamwise Reynolds-stress between these two solutions are even smaller, as shown in Fig 5.11.

At the inlet the uniform profiles of all variables were specified. The values are chosen in accordance with experimental data (Coupland 1995) and equation (5.2). In the T3L4 case the free-stream velocity was $U_\infty = 5m/s$ and the isotropic turbulence was defined by $\sqrt{\overline{u^2}}/U_\infty = 0.0627$ and $L_\varepsilon = k^{3/2}/\varepsilon = 27.3\ mm$. These initial conditions provide appropriate decay of turbulence in the free-stream, as can be seen in Fig 5.16 from profiles of u/U_o. It is known that a small anisotropy of free-stream can influence the position of transition, but due to a lack of experimental data for $\overline{v^2}$ and $\overline{w^2}$ the isotropic turbulence at inlet was chosen.

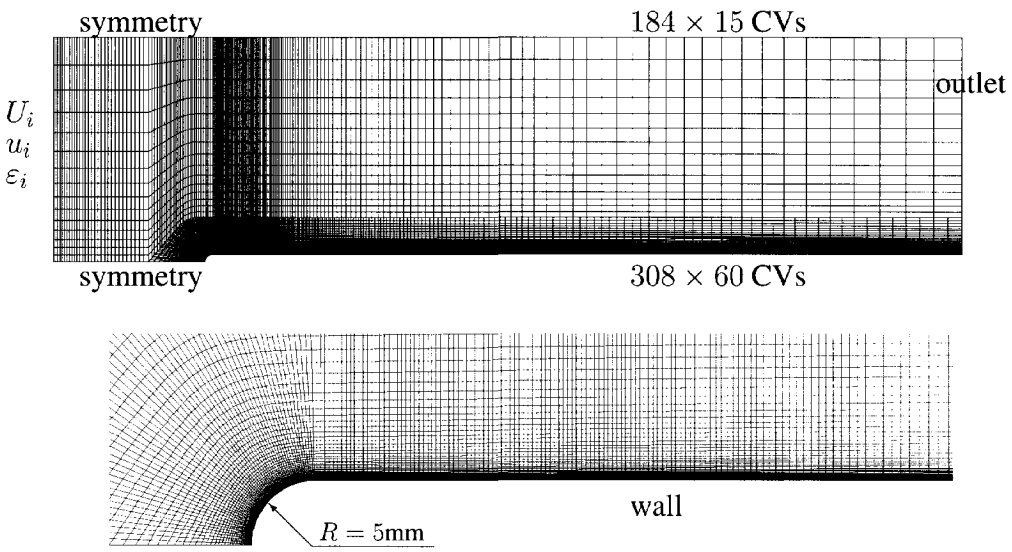

Figure 5.10: Computational domain, boundary condition and numerical grid for T3L4 case.

5.4.2 Results and discussion

As mentioned above, the most popular eddy-viscosity low-*Re*-number model (Launder and Sharma 1974) fails to reproduce the bypass transition in this case. Chen *et al.* (1994) made an ef-

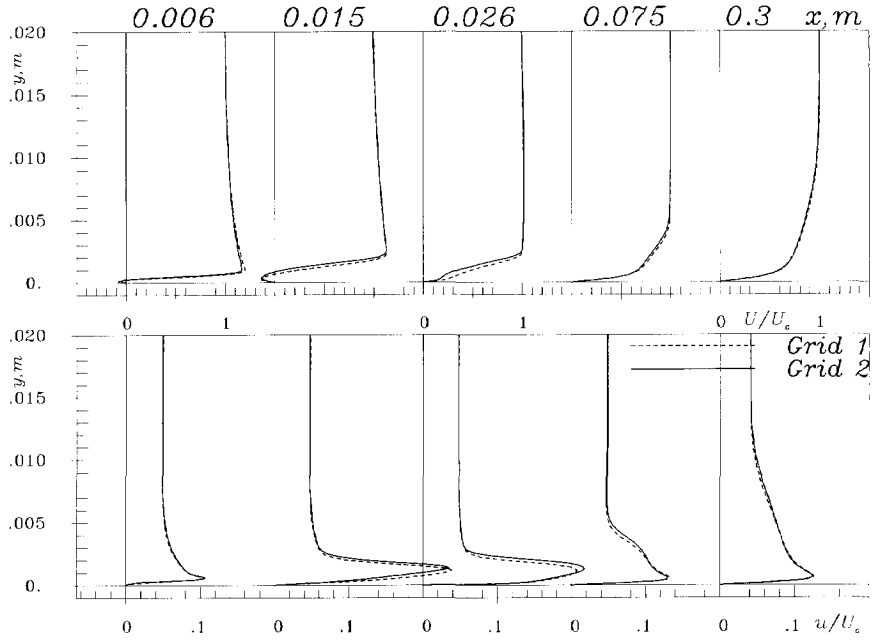

Figure 5.11: Solutions obtained wit SMC on two different grids (`Grid 1` is the coarser grid and `Grid 2` is the finer one shown in Fig 5.10).

fort to improve the results. They reported computations of the case in the same geometry with $U_0 = 29\ m/s$ and $u/U_0 = 0.012$ and did show that the significant improvement can be achieved by modifying the production of kinetic energy as suggested by Kato and Launder (1993) $P_k = C_\mu f_\mu \varepsilon S\Omega$, (where $S = k/\varepsilon \left(S_{ij}S_{ji}\right)^{1/2}$) and $\Omega = k/\varepsilon \left(\Omega_{ij}\Omega_{ji}\right)^{1/2}$)) and also in an *ad-hoc* manner expressing production of k as $P_k = C_\mu f_\mu \varepsilon S \left(0.15S + 0.85\Omega\right)$) obtaining even closer results to experiments.

Fig 5.13 shows calculated stream-lines for the eddy-viscosity and the SMC model. The separation bubble was predicted only with the SMC model and is in close agreement with the experimental results as can be best seen in Fig 5.16 from profiles of mean velocity. The main reason that the EVM does not predict the bubble is that the predicted turbulence kinetic energy is too large in the stagnation region. Fig 5.12 shows the evolution of maximum value of streamwise normal Reynolds stress. The experiments show that the stress increases in the bubble region reaching its maximum near reattachment (the experiments do not give the value of the length of the bubble, but from the mean-velocity profiles it can be concluded that the reattachment point lies between 19 and 21 mm).

The contours of turbulence kinetic energy given in Fig 5.14 illustrate the development of k around leading edge and in the separation bubble. The much too high value of k in the stagnation region predicted with EVM produces too strong mixing and does not allow formation of separation bubble and therefore the real transition cannot be captured. In contrast to this result the SMC

model predicts proper development of turbulence. This is basically due to correct prediction of production and dissipation of turbulence kinetic energy in the stagnation region. Although it is known that the wall reflection model of Gibson and Launder (1978), which is used here in the SMC does not work correctly in the impingement flows such as impinging jet on a flat plate (Craft 1991), in the present case the stagnation region with dominant normal-strain production is rather small. The major effect originates still from shear production in the layer. Also, the curvature of the streamlines is smaller than in the impinging jet.

Fig 5.15 and 5.16 show the streamwise mean velocity profiles and the normal streamwise stress at several positions computed with $k-\varepsilon$ and SMC model. According to the experimental results, the positions at which the results, are compared are located: near the point of separation (x=0.006 m); in the middle of the bubble (x=0.015 m); just behind the point of reattachment (x=0.026 m); in the recovery region (x=0.075 m) and, finally, in the fully developed boundary layer (x=0.300 m). As seen in these figures the results obtained with $k-\varepsilon$ model show poor agreement with experimental data what is a direct consequence of failure to predict the separation bubble. As already said, Launder-Sharma model produces maximum of turbulence kinetic energy in front of the plate. The evolution of the turbulence kinetic energy downstream is shown in Fig 5.12. Because of much too high value of k, the model cannot predict the very thin bubble and, therefore, there is no transition in the bubble region.

In contrast to this result the SMC model reproduces correct value and almost correct shape of maximum of $\overline{u^2}$, though the peak is about 4 mm (20% of the bubble length) behind the experimental one. Fig 5.12 shows the drastic difference in predicting turbulence kinetic energy using EVM and SMC. The SMC calculates the maximum in the middle of the bubble, as indicated by experiments. The SMC results can be regarded as good. Fig 5.16 shows the profiles of the mean velocity and all components of the Reynolds-stress tensor at five selected positions, as said above. The predicted values of $\sqrt{\overline{u^2}}$ show a good development through the flow in accordance with experiments. It should be noted that a possible stress anisotropy in the free-stream can influence the evolution of the flow near the wall as well as the transition itself. The v component of Reynolds-stress exceeds the u component at first three positions, as shown in Fig 5.16, which is most likely a consequence of the assumed isotropic turbulence at the inlet and in the free-stream which may not be realistic. Nevertheless, the stress anisotropy at position $x = 0.3$ m is consistent with the model results of a boundary-layer with zero pressure gradient.

These results are obtained with the second-order discretisation of solved equations (the convective terms in momentum equations were approximated with the QUICK scheme; whereas in the model equations the TVD scheme with UMIST limiter is used). It should be emphasised that the use of the UDS scheme with the SMC model, the predicted bubble was to short (about 6 mm only) and the mean velocity and stress in the recirculation region are far from experimental results as is shown in Fig 3.5, on page 66.

Fig 5.17 shows the values of the coefficients C_1, C_2, C_1^w and C_2^w of the pressure-strain model ϕ_{ij} in the SMC model obtained for the T3L4 case. The results are given at the same positions as the computational results in Fig 5.16. The values of the standard high-Re-number model coefficients, which are constants, are indicated with dashed lines. Strong variation of the model coefficients shows all complexity of the flow. Values of the model coefficients at $x = 300mm$

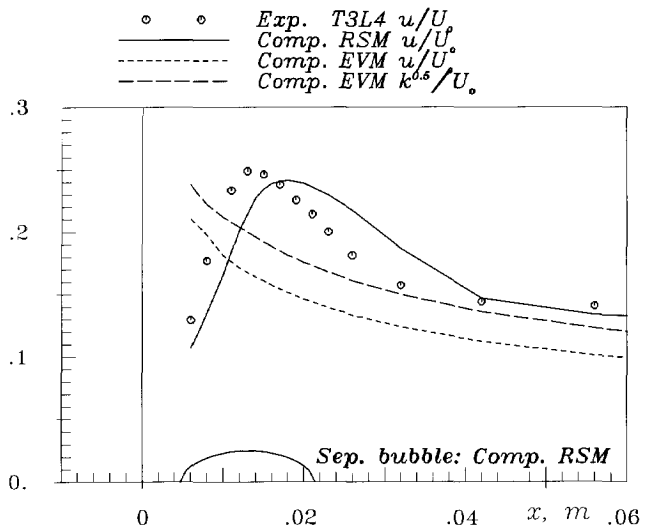

Figure 5.12: Evolution of the maximum of $\overline{u^2}$ in streamwise direction. SMC and EVM results. Separation bubble indicated as predicted with SMC.

which is a well established boundary layer, are very similar to results obtained in a backward-facing step flow at $Re = 5000$ and $x/H = 6$ (which is in the recovery region) as shown in Fig 5.18.

5.5 T3L flows with lower free-stream turbulence

The ERCOFTAC Transition SIG workshop data-bank contains altogether 6 experiments performed in the same geometry as the previous T3L4 case, but with different mean free-stream velocity and different FST level. The case considered above (T3L4) is with 5.5% FST. All other experimental cases are with lower levels of FST. As shown for the by-pass transition on the flat plate with sharp leading edge the SMC model shows some difficulties in predicting the transition correctly if FST is smaller than 3%. A similar tendency is observed in the T3L flows. Two cases were selected to investigate the model ability to predict this kind of flow with lower FST: T3L3 and T3L6 which are both with about 2.5% FST, but T3L3 is with $U_0 = 5m/s$ and T3L6 is with $U_0 = 10m/s$. The same computational domain as in the T3L4 case was used for these two cases. The inlet conditions are selected in accordance with the experiments and are given in Figures 5.19 and 5.20 which show the SMC model results for the stream-lines and the contours of the turbulence kinetic energy k/U_0^2. The largest value of k/U_0^2 and computed separation and reattachment points are indicated in the figure. In both cases the model predicts the separation bubble and the transition to turbulence induced by this bubble. However the predicted separation bubble is in both cases too large in comparison with experiments. This is due to the weakness of the model to predict the transition at a lower level of free-stream turbulence. Nevertheless,

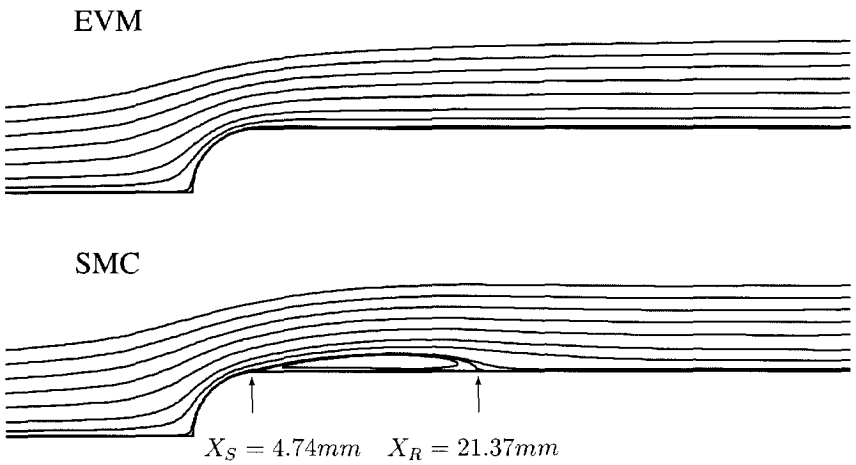

Figure 5.13: Computed stream-lines for T3L4 case obtained with EVM and SMC.

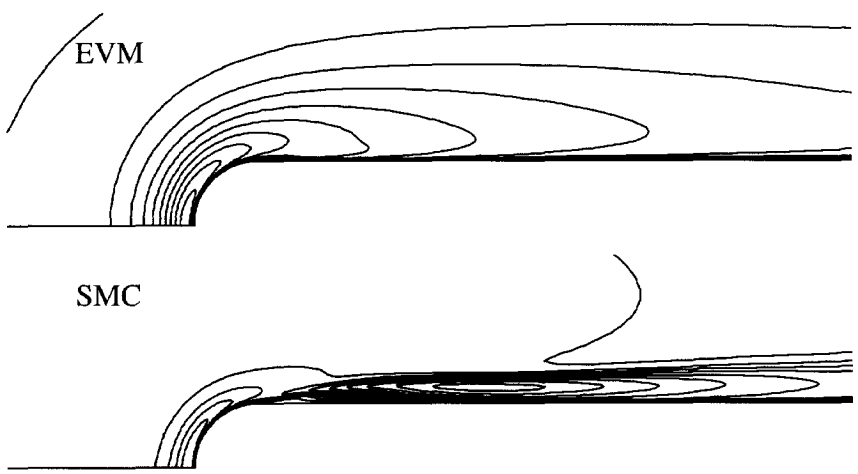

Figure 5.14: Computed turbulence kinetic energy k for T3L4 case obtained with EVM and SMC. For the value of k see Fig 5.12 on page 125.

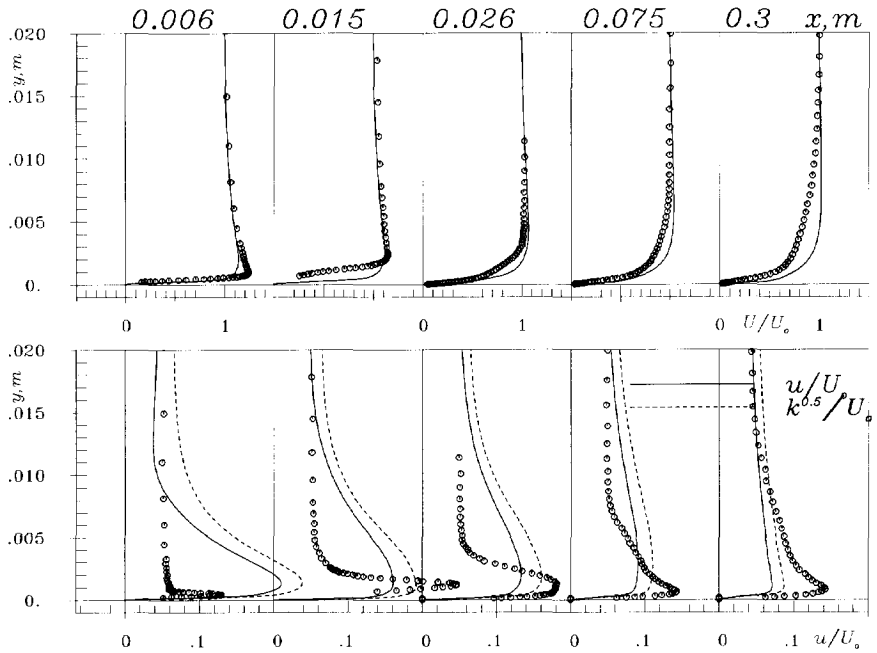

Figure 5.15: T3L4 case. Launder-Sharma EVM model results for U, k and u.

these results are better than any other in the literature (without triggering of turbulence) of which author is aware of.

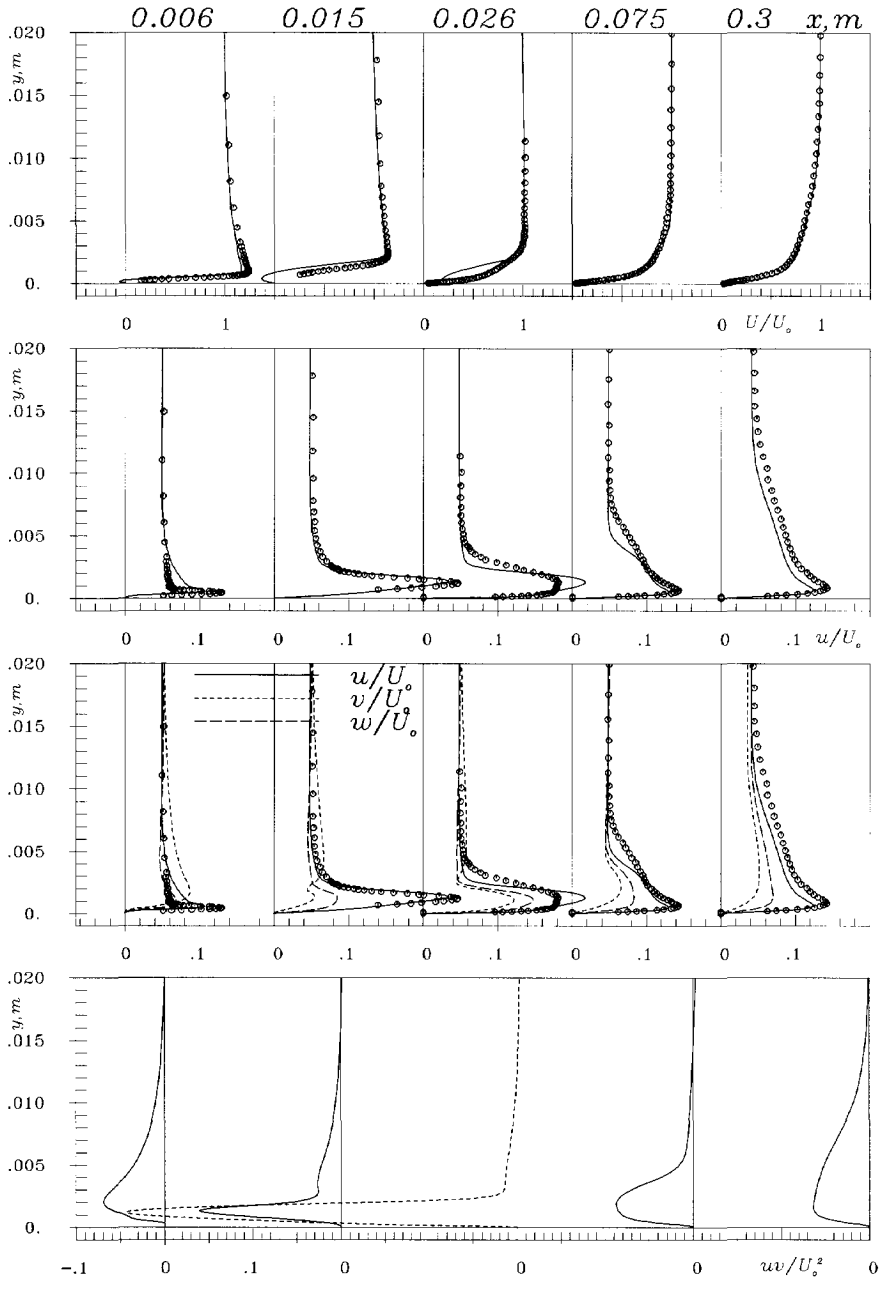

Figure 5.16: T3L4 case. SMC results for the mean velocity U, and all components of the Reynolds-stress tensor.

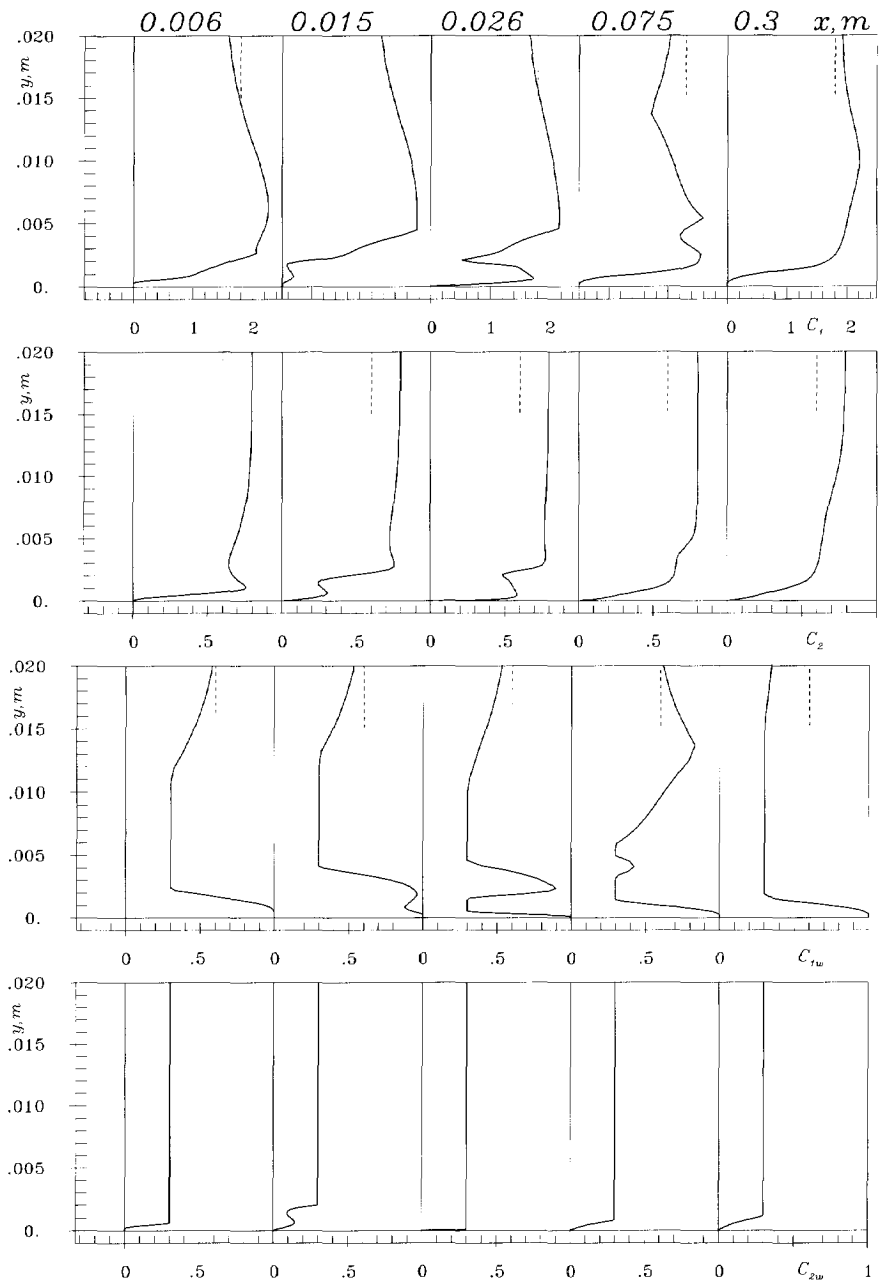

Figure 5.17: The coefficients of the pressure-strain Φ_{ij} term of the low-Re-number SMC in the T3L4 case (solid lines). Dashed lines indicate the values of coefficients of the basic high-Re-number turbulence model $C_1 = 1.8$, $C_2 = 0.6$, $C_1^w = 0.5$ and $C_2^w = 0.3$.

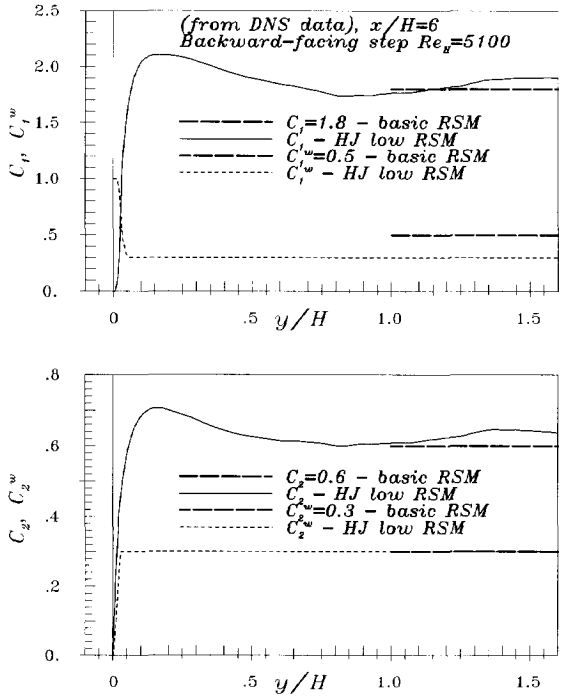

Figure 5.18: The coefficients of the Φ_{ij} term of low-Re SMC evaluated from the DNS data for a backward-facing step flow (Le *et al.* (1997)) at $Re = 5000$ at $x/H = 6$ downstream from the step. (Courtesy of Dr. S. Jakirlić of TU Darmstadt.)

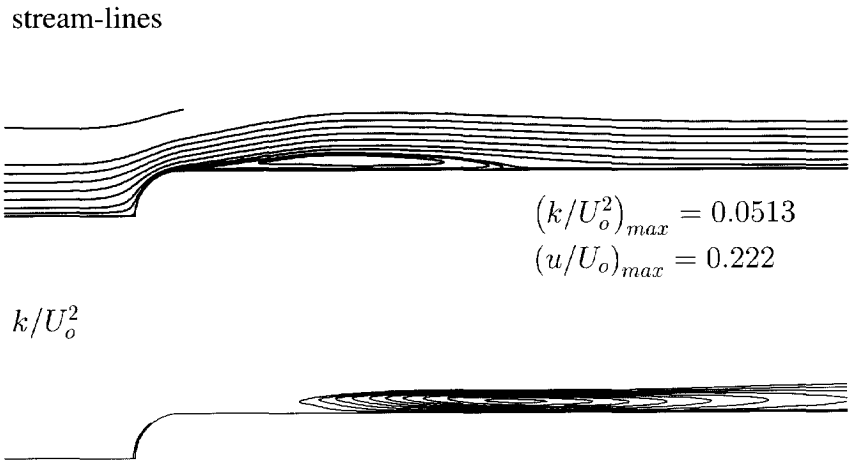

Figure 5.19: T3L3 flow: Computed stream-lines and contours of turbulence kinetic energy k/U_o^2 (contour interval by 0.05) obtained with SMC. Separation point is at $x_S/R = 0.9745$ and reattachment point is $x_R/R = 6.692$. Inlet: $U_o = 5m/s$, $u/U_o = 0.0265$ and $L_\varepsilon = 0.023m$.

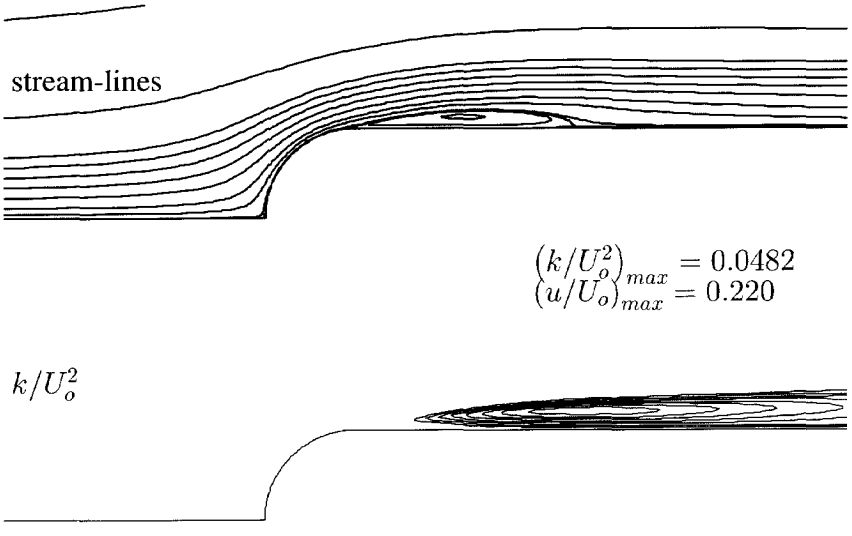

Figure 5.20: T3L6 flow: Computed stream-lines and contours of turbulence kinetic energy k/U_o^2 (contour interval by 0.05) obtained with SMC. Separation point is at $x_S/R = 0.9296$ and reattachment point is $x_R/R = 3.438$. Inlet: $U_o = 10m/s$, $u/U_o = 0.0286$ and $L_\varepsilon = 0.0125m$.

5.6 Turbulent and transitional separation bubble on a plane wall

Separation from a smooth surface and the accompanied recirculation, even if small, have a large influence on the overall flow behaviour especially beyond and downstream of the separation location. The separation bubble is usually a result of adverse pressure gradient and it may appear at leading- or/and trailing-edge of the blades in gas turbines, compressor blades, aerofoils, etc. Due to separation and reattachment, the flow becomes complex, highly curved and usually highly turbulent, with anisotropy of the Reynolds-stress tensor affecting significantly the momentum equation. The success in computation of such flows relies on the correct representation of turbulence anisotropy and the turbulence model's ability to predict large departure from equilibrium. Therefore, the modelling of separation bubble at smooth surface is a challenging task and important for prediction of performances of the associated engineering devices. As shown above, the form of transition within the bubble depends on the structure of the oncoming flow and on the level of the free-stream turbulence as well as on boundary conditions and flow circumstances, such as pressure-gradient, curvature of the wall etc. All these factors strongly influence the shape and the length of the bubble. The laminar separation bubble, accompanied by transition to turbulence, is even more complex than the turbulent one. Therefore, it is more difficult to predict the transitional separation bubble, than the turbulent ones.

Because of the great importance, which the separation induced transitional flows have in many industrial applications, and difficulties for the majority of turbulence models to predict such flows, the next two cases considered are turbulent and transitional separation bubbles on a plane wall. Due to difficulties in measuring, the experimental data for such flows are rare and incomplete. However, several recently published DNS studies of separation bubble flows (Spalart and Coleman 1997; Spalart and Strelets 1997; Na and Moin 1998), offer an excellent opportunity for validation of the models.

The cases considered are:
a) *Turbulent separation bubble*: a 'rapid' separation and reattachment of a turbulent boundary layer on a flat wall created by imposed suction and blowing of the fluid in the free-stream. The DNS were performed by Spalart and Coleman (1997). DNS results for the same case but with slightly different conditions were reported more recently by Na and Moin (1998);
b) *Transitional separation bubble*: a laminar boundary-layer separated from a flat wall by imposed suction of the fluid in the free-stream. Laminar to turbulent transition occurs within the bubble. The DNS of this flow were performed by Spalart and Strelets (1997).

5.6.1 Turbulent separation bubble

In this flow, the separation bubble is created by imposed suction and blowing along the boundary of the computational domain opposite to the wall. An incoming turbulent boundary layer at

$Re_\theta \approx 300$ (according to the authors of DNS, Spalart and Coleman (1997), this is a not perfectly developed boundary layer) separates due to the large adverse pressure gradient (APG) induced by suction and reattaches rapidly under the equally large favourable pressure gradient (FPG) induced by blowing of the fluid at some downstream position. This produces a small separation bubble at the wall in the region between APG and FPG.

The computational domain adopted for the RANS computation is a box of the length L=10 and the width Y=1 (non-dimensional lengths), see Fig 5.22, and is covered with an Cartesian numerical mesh of 100×100 CVs. The mesh is especially refined in the bubble region. The flow inlet is located at X=0 where the DNS data for the mean velocity and the Reynolds-stresses are available and are used to specify the inlet conditions. Since the incoming boundary-layer was not well developed, it posed uncertainties in reproducing the inflow conditions, particularly the dissipation rate profile (which was not provided by DNS) to which the downstream flow pattern is very sensitive (Spalart and Coleman 1997, Dengel and Fernholz 1990). The dissipation ε at the inlet was computed by solving the ε model equation with imposed known DNS data and assuming zero gradients of all variables in stream-wise direction.

The bulk Reynolds-number based on the incoming free-stream velocity and the flow domain is $Re = UY/\nu = 22000$. In accordance with DNS, the top boundary suction and blowing velocity, which is anti-symmetric around $X = 6.6$, is given as

$$V_{(x)} = 0.435 \ \sqrt{2} \ \frac{6.6 - x}{1.22} \ \exp\left[\frac{1}{2} - \left(\frac{6.6 - x}{1.22}\right)^2\right] \tag{5.7}$$

and the zero vorticity

$$\frac{\partial U_{(x)}}{\partial y} = \frac{\partial V_{(x)}}{\partial y} \tag{5.8}$$

boundary condition for the stream-wise mean velocity is imposed in an implicit manner in conjunction with Dirichlet boundary condition. For all turbulence variables the Neumann boundary condition ($\partial\Phi/\partial y = 0$) was imposed. The solution procedure with these boundary conditions did not show any numerical difficulties in the free-stream region. The results for the mean stream-wise velocity component near the top boundary are in excellent agreement with DNS data (see Fig 5.23).

The RANS computations are performed with the HJ low-Re-number second-moment closure with and without the term S_l, yielding similar flow patterns in reasonable agreement with the DNS. However, without S_l the dividing streamline shows an anomalous forward bending in the separation point and backward bending at reattachment. This deficiency of the standard second-moment closure was detected earlier in the studies of backward facing step flow, particularly at low Re numbers (for discussion see Section 2.4). While the use of wall functions and placing the first grid point at a relatively large distance from the wall may conceale the anomaly, it becomes especially visible when using models which allow the integration up to the wall and the

application of finer numerical grids. The introduction of the S_l term into the dissipation equation, which compensates for excessive growth of the length scale in the stagnation zones, eliminates the anomaly both when used in conjunction with the standard high-Re-number second-moment model with wall functions, or with low-Re-number models and integration up to the wall.

The computed separation bubble, Fig 5.22, is somewhat thinner than in DNS, what may be a consequence of inadequate inflow conditions. The streamline anomaly without S_l makes the distance between separation and reattachment shorter. The inclusion of S_l rectifies the anomaly (Fig. 5.22) and extends the bubble length at the wall, though both the separation and reattachment points are predicted somewhat more upstream than in DNS. This is seen in the plot of the friction factor, Fig 5.21, which shows also some discrepancy in the recovery zone. The mean velocity profiles, however, agree very well with the DNS, Fig 5.23. The computed components of turbulence intensity are similar to DNS (see also the contours of kinetic energy, Fig 5.22), though with some discrepancy, which is most noticeable in the profiles of the shear stress.

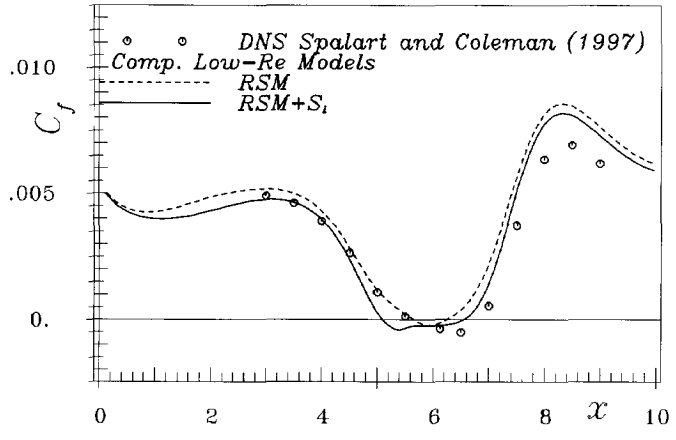

Figure 5.21: Friction factor along the wall in the flow with separation bubble.

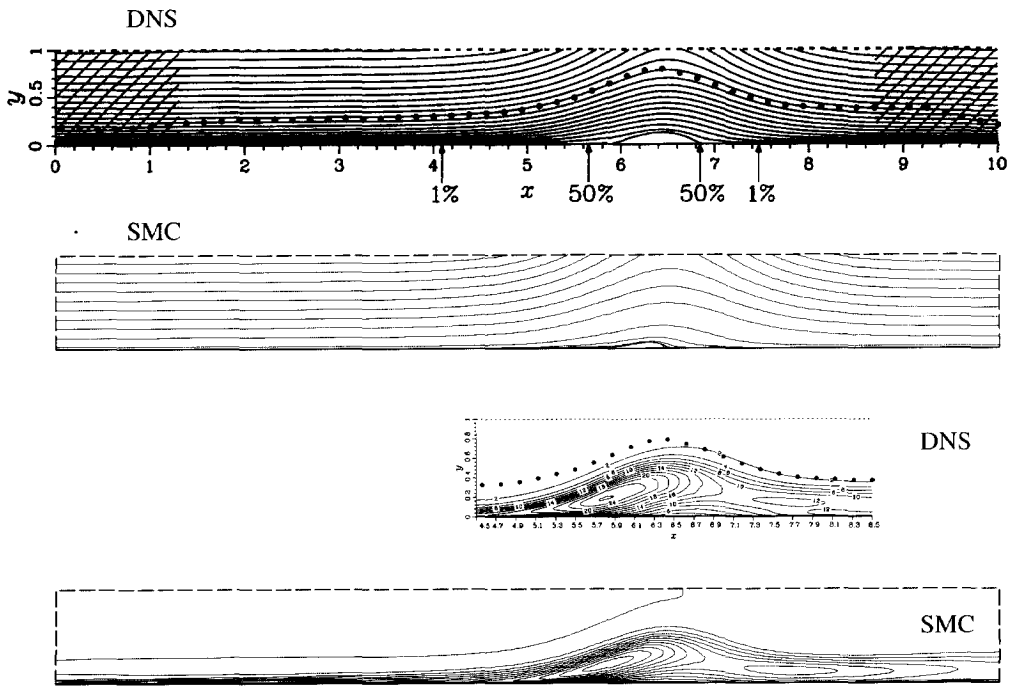

Figure 5.22: Streamlines (a) and kinetic energy contours (b) in a separation bubble. Top figures: DNS Spalart and Coleman (1997) (Courtesy of Dr. P. Spalart of Boeing). Bottom figures: computations low-Re-number SMC.

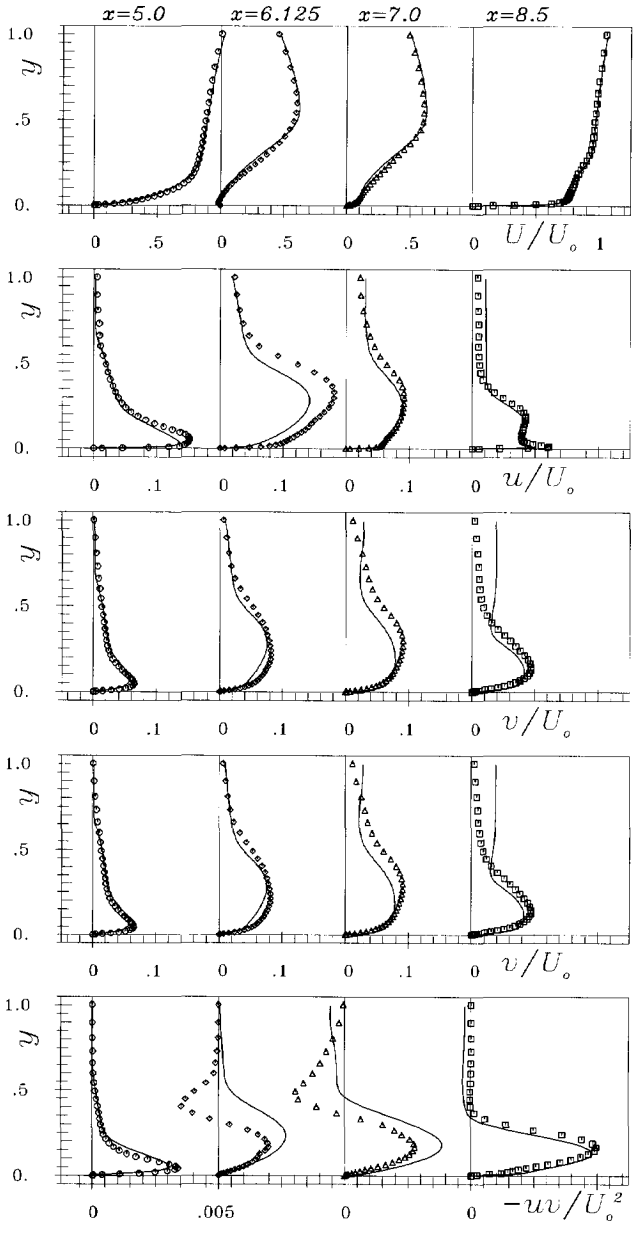

Figure 5.23: Mean-velocity and Reynolds-stress tensor components at characteristic positions ($x = 5$ before separation, $x = 6.125$ in the middle of separation, $x = 7$ just beyond separation and $x = 8.5$ recovery of boundary layer). Symbols: DNS by Spalart and Coleman (1997); Lines: low-Re-number SMC.

5.6.2 Transitional separation bubble

This case, for which DNS were performed recently by Spalart and Strelets (1997), resembles the turbulent bubble discussed in the previous subsection, except that the incoming flow was laminar. The separation of the laminar boundary layer was created by imposed suction along the computational domain boundary opposite to the wall. The flow separates due to the adverse pressure gradient induced by suction and becomes shortly turbulent (within the first half of the bubble). Since the suction is limited to a small part of the domain, the pressure gradient drops to almost zero at the end of the suction region, so that fluid reattaches the wall around that point. The length of the separation bubble is about two flow-domain widths. In this way created bubble becomes highly turbulent, although the incoming boundary layer is laminar. The turbulence generated by bubble penetrates into the laminar part of the flow and is transported downstream by convection. A great challenge for the turbulence models is prediction of coexistence of virtually laminar flow portions and highly turbulent ones without undertaking any outside measures. The peak of the stream-wise normal component of the Reynolds-stress tensor is predicted by the DNS within the separation bubble close to the reattachment point, which is also observed in experiments by Coupland (1995) for T3L cases.

According to Spalart and Strelets (1997) the flow is defined with three non-dimensional parameters: deceleration factor $S = Q_s/(YU_o)$ which is the ratio between the suction flow rate Q_s and the incoming flow rate YU_o; the bulk Reynolds-number $Re_Y = YU_o/\nu$ and the Reynolds-number based on the boundary layer length X, $Re_X = XU_o/\nu$ at which the suction occurs (X is measured from the origin of the boundary-layer). In this particular case $S = 0.3$, $Re_X = 10^5$ and $Re_Y = Re_X/3$ were chosen (Spalart and Strelets 1997) to generate the separation bubble large enough and at a fairly large Reynolds number. In the RANS computations the same boundary conditions sa those of the DNS were imposed. A Blasius laminar boundary layer with $\delta = 6.8639\ 10^{-3}\ Y$ was specified at the inlet and the suction velocity at the top boundary is given as

$$V_{(x)} = \frac{S}{\sigma\sqrt{2\pi}} e^{-1/2(x/\sigma)^2} \tag{5.9}$$

and the zero vorticity (expression (5.8)), as done in the previous case. The suction flow rate is computed as

$$Q_s = \int_0^{10} V_{(x)} dx.$$

Spalart and Strelets (1997) reported that σ does not influence the solution if kept small enough; we used $\sigma = 0.24$.

The computations are performed on numerical meshe of 200x50 CVs. Fig 5.24 shows a comparison of the wall friction factor obtained with the HJ low-Re-number SMC, and the DNS data. The length of the separation bubble is predicted by the model quit well. The model cannot predict the strong acceleration of the reversed flow near the end of the separation bubble. The DNS data show that the bubble has a tendency to "split" into two parts around $X = 3.4$ where the wall shear stress has almost a positive value. Similar under-prediction of C_f is observed in

computations of the back-facing step flow at lower Re-number by Hanjalić and Jakirlić (1998) using the same model, although in that case the flow is fully turbulent and the separation occurs from a sharp edge. Nevertheless, the results for these two rather different separation-bubbles obtained with the SMC are consistent.

Fig 5.25 shows the development of the maximum value of components of the Reynolds-stress tensor along the flows predicted with SMC and compared with DNS data. Although only DNS data for two components are available, the figure indicates that the position of maximum Reynolds-stress obtained with SMC is in good agreement with the DNS data. The model does not capture fully the peak value and the increase in Reynolds-stress components in the transitional region is too sharp. In the recovery region beyond the bubble, where the zero pressure gradient boundary layer develops, the predicted values of stress components are in good agreement with DNS. The peak value of $\sqrt{\overline{u^2}}/U_0$ is about 0.25 which is equal to the value measured by Coupland (1995) for T3L4 case (with 5% FST). The $\sqrt{\overline{u^2}}/U_0$ in the recovery region is about 0.1 which is about 50% lower than measured by Coupland (1995). This is probably a consequence of a high level of free-stream turbulence. In the view of the fact that both laminar and fully turbulent region coexist in the flow, the results can be regarded as pretty good. Fig 5.27 shows the profiles of the mean velocity U and all components of the Reynolds-stress tensor at several positions. Unfortunately, no data are available for comparison.

It needs to be mentioned that the author was not able to obtain a convergent solution with the Launder-Sharma low-Re-number eddy viscosity model.

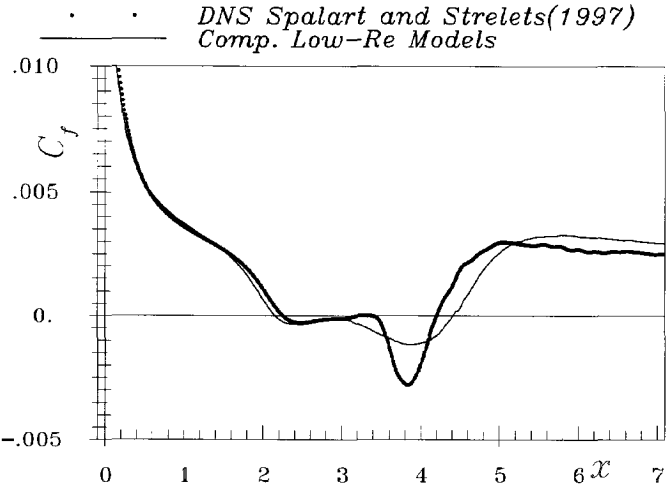

Figure 5.24: Friction factor along the wall in the transitional separation bubble flow. Symbols are DNS data of Spalart and Strelets (1997) and line is SMC model result.

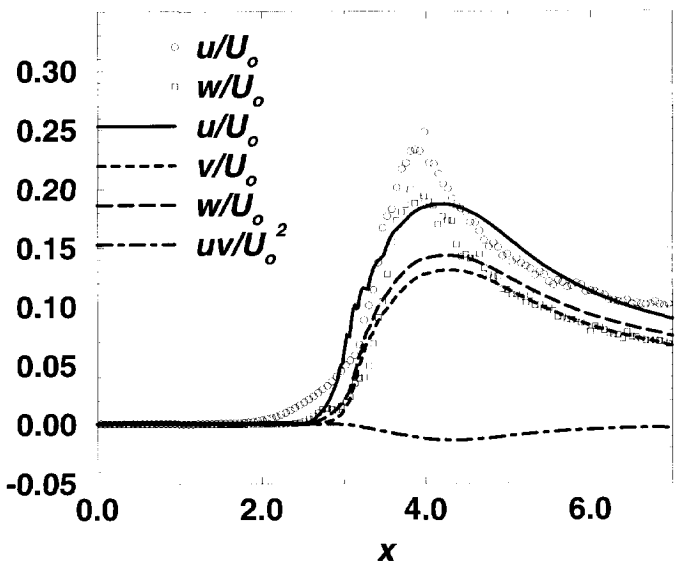

Figure 5.25: Evolution of the maximum value of the Reynolds-stress components across the flow in the flow direction in the transitional separation bubble flow. Symbols are DNS data of Spalart and Strelets (1997) and lines are SMC model results.

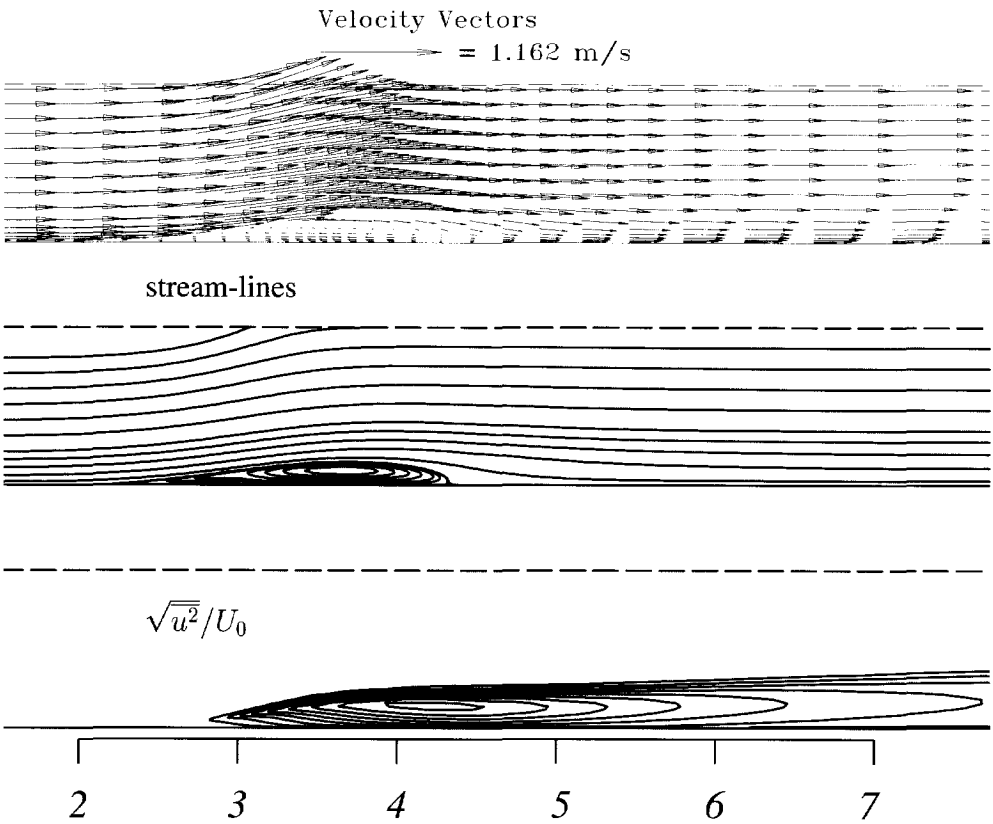

Figure 5.26: Mean velocity vectors, streamlines and contours of $\sqrt{\overline{u^2}}/U_0$ in the transitional separation bubble flow computed with low-Re-number SMC.

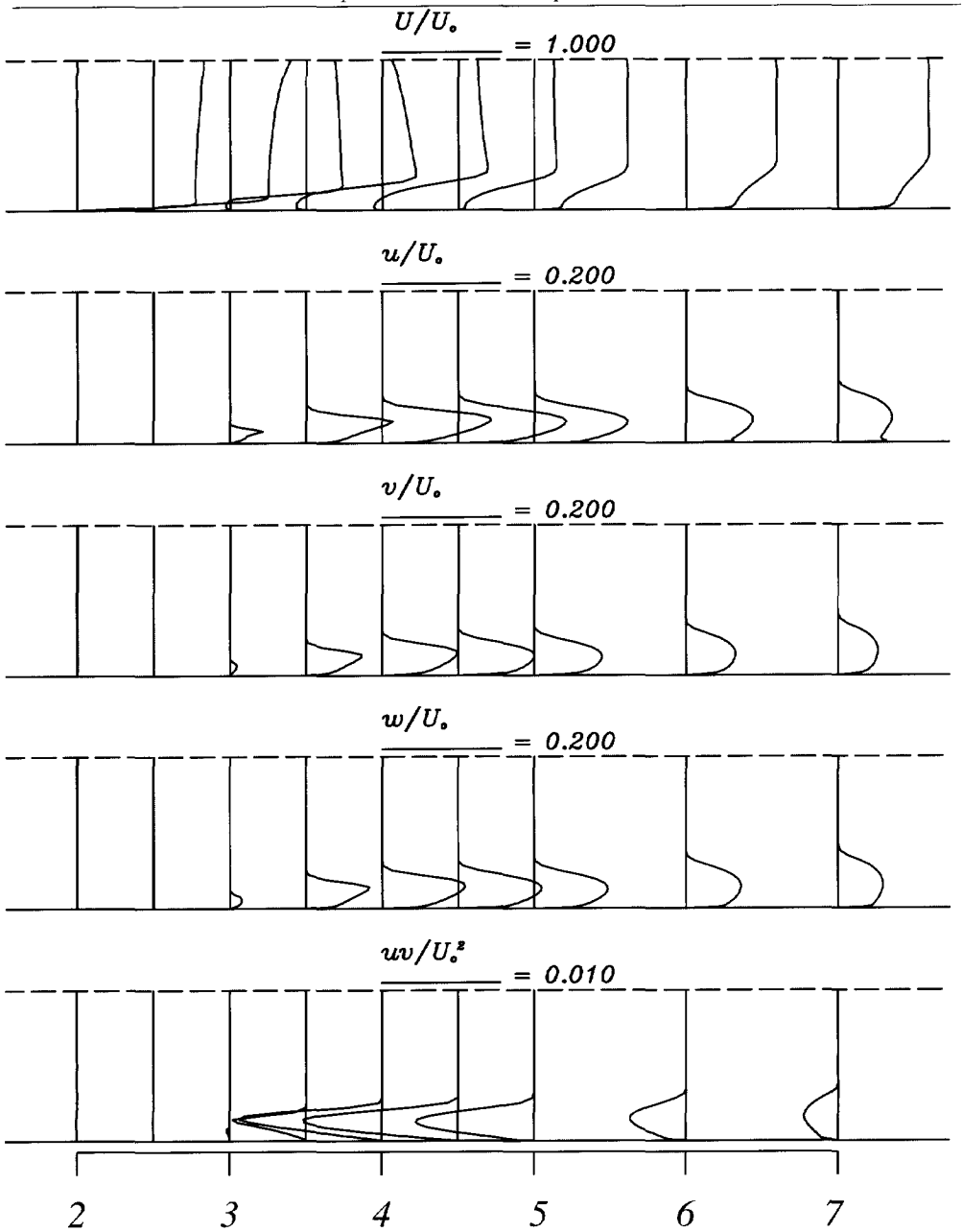

Figure 5.27: Profiles of the mean streamwise velocity and all components of the Reynolds-stress tensor in the transitional separation bubble flow obtained with low-Re-number SMC.

5.7 Airfoil NACA 4412

As an illustration of the prediction of a complex and industrially relevant flow using a second moment closure low-Re-number model, we consider now the flow over the NACA 4412 airfoil at maximum lift, with the incidence angle of 13.87^o, and high Re-number (the chord-based $Re_c = \frac{U_o c}{\nu} = 1.52 \times 10^6$, where c is the chord length) (experiments by Coles and Wadcock 1979). This flow is often used as a test for turbulence modelling. Flows around airfoils involve several important physical phenomena such as: transition to turbulence, laminar separation bubble at leading edge, separation bubble at suction side, curvature of flow, turbulent wake. It is of decisive importance for the wing design to predict such flows accurately. A review of of computations of airfoil flows at high fixed angle of incidence was given recently by Guilmineau *et al.* (1997). Most frequently used turbulence models for computation of airfoil flows at high incidence are eddy-viscosity one- and two-equation models that do not account properly for curvature effects and anisotropy of turbulence and, therefore, perform rather poorly in such configurations. In most computations reported in literature the transition is imposed artificially at the prescribed location adopted from experiment by switching on the turbulence model (or, alternatively, the production of the kinetic energy). The location of transition can have a significant effect on the solution.

In the considered flow around NACA4412 airfoil the transition length is very short and the treatment of the transition proved to have little influence on the overall results. However, predicting the transition location in unknown flows without an empirical input is the major criterion in judging the RANS turbulence model for transitional flows.

Computations were performed with a four-block O-grid with both the high-Re-number and the HJ low-Re-number second-moment closures (398×88 and 398×128 nodes, respectively), *without* imposing any artificial transition. Grid point nearest to the wall was at y^+ between 0.1 and 1.5 for the low-Re model and between 10 and 50 for the high-Re model with wall function. The high-Re-number model gave almost identical results both for 1.5% and for 5% free stream turbulence. Because of the high bulk flow Reynolds number, the application of the low-Re-number model due to a need for a fine and highly non-uniform numerical grid near walls becomes more demanding (slower convergence), particularly with a low free stream turbulence. It should be noted that all computations were performed in a steady mode, what may not be fully suitable, particularly for a low free-stream turbulence.

The computational domain adopted here was as shown in Fig 5.28. The inlet is located at $0.8c$ in front of the airfoil leading edge, the outlet at the distance of about $2c$ beyond the airfoil trailing edge and the top and bottom boundary are located at about $1c$ away from the airfoil. The reason for choosing this domain was twofold: first, the RANS computations with roughly a twice as large domain, show negligible difference in results and, second, the experiments were performed in a wind-tunnel with a cross-section which is in total about $4c$ wide and about $3c$ long (Wadcock 1980). With respect to the experiments, the computational domain for which the results shown here are obtained is located in the middle of the experimental section. There is a doubt that the wind-tunnel walls may have contaminated the results, although it is unlikely that the inner part of the boundary layer will be very sensitive to these effects. Admittedly, it would be more correct to compute this case simulating the whole wind-tunnel section, as done by Rhie

and Chow (1983).

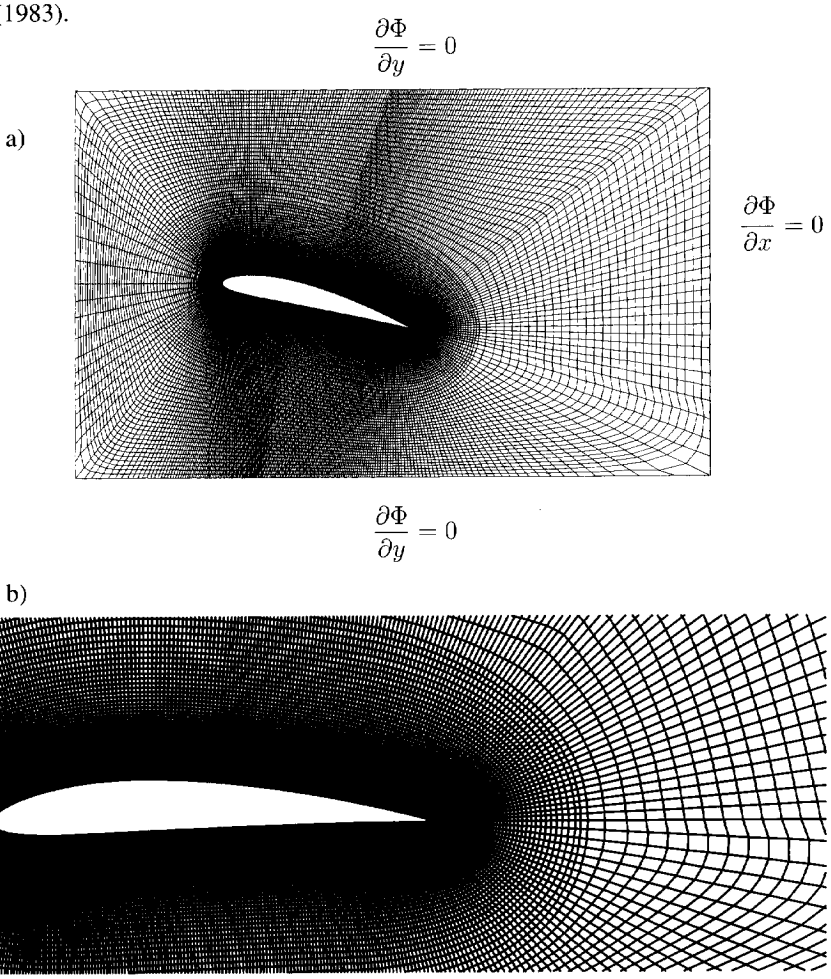

Figure 5.28: NACA 4412 flow: a) computational domain; Numerical mesh of O type consists of four blocks in total 398×88 CVs for the high-Re-number model and 398×128 CVs for the low-Re-number model; b) near wall mesh.

Results obtained with 5% free stream turbulence are presented here. The pressure coefficient obtained by both models agree well with the experiments (Fig. 5.29). A difference between the two sets of results is more visible in the mean velocity- and shear stress profiles, and, particularly, in the size of the separation bubble, Fig. 5.30. Unlike in some fully-turbulent flows (e.g. back-step), where both models result in a similar streamline pattern in the recirculation zone, here the low-Re-number models yield a substantially thinner bubble.

Because of insufficient experimental data it is difficult to judge which streamline pattern is

closer to reality. The mean velocity and shear stress profiles obtained by both models show also close agreement with experiments at most locations along the airfoil, and also in the near wake region, but the low-Re-number model seems to be slightly superior.

In view of the fact that some simpler models such as the zonal $k-\omega$ model of Menter, see Guilmineau *et al.* (1997), can give a reasonable reproduction of available experimental mean flow parameters for a two-dimensional high-load airfoils, this example may not be the most appropriate for illustrating arguments in favour of second-moment closures. In any case, the results obtained with these two second moment closure models are consistently better than those of eddy-viscosity type of models reported by Guilmineau *et al.* (1997), especially for the turbulence quantities. Nonetheless, with this case we demonstrate that the second-moment closures (including their low-Re-number variants with integration up to the wall) may be successfully used to compute complex flows over curved surfaces at high Re numbers and with strong pressure variations. A comparison of results obtained with high and low-Re-number variants of the same basic model, as well as with results obtained with $k-\varepsilon$ and $k-\omega$ models (available in literature) are also believed to provide useful information.

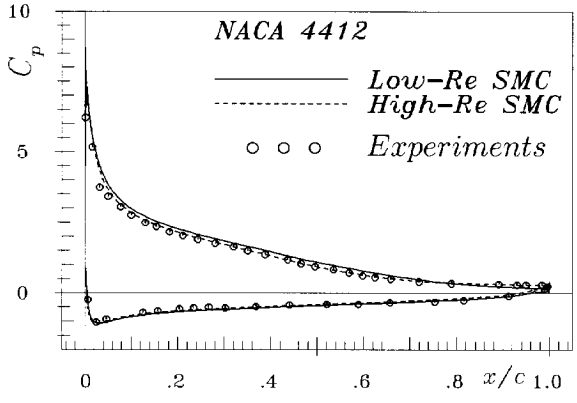

Figure 5.29: NACA 4412 flow: pressure coefficient C_p obtained with low-Re SMC and with high-Re SMC + WF.

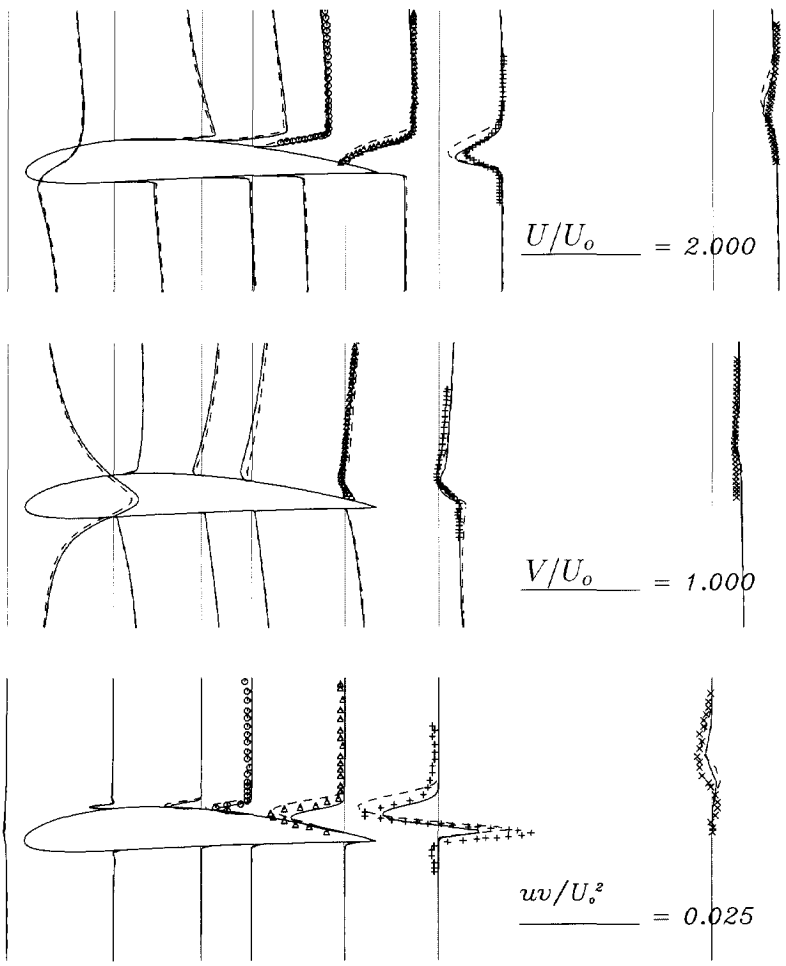

Figure 5.30: NACA 4412 flow: the chordwise mean velocity U/U_o and the perpendicular component of the velocity vector V/U_o and the shear-stress $\overline{uv}/U_o^2$ in the chordwise oriented coordinate system at *x/c = -0.05, 0.25, 0.5, 0.642, 0.908, 1.1747, 1.95146.* Legend as in Fig 5.29.

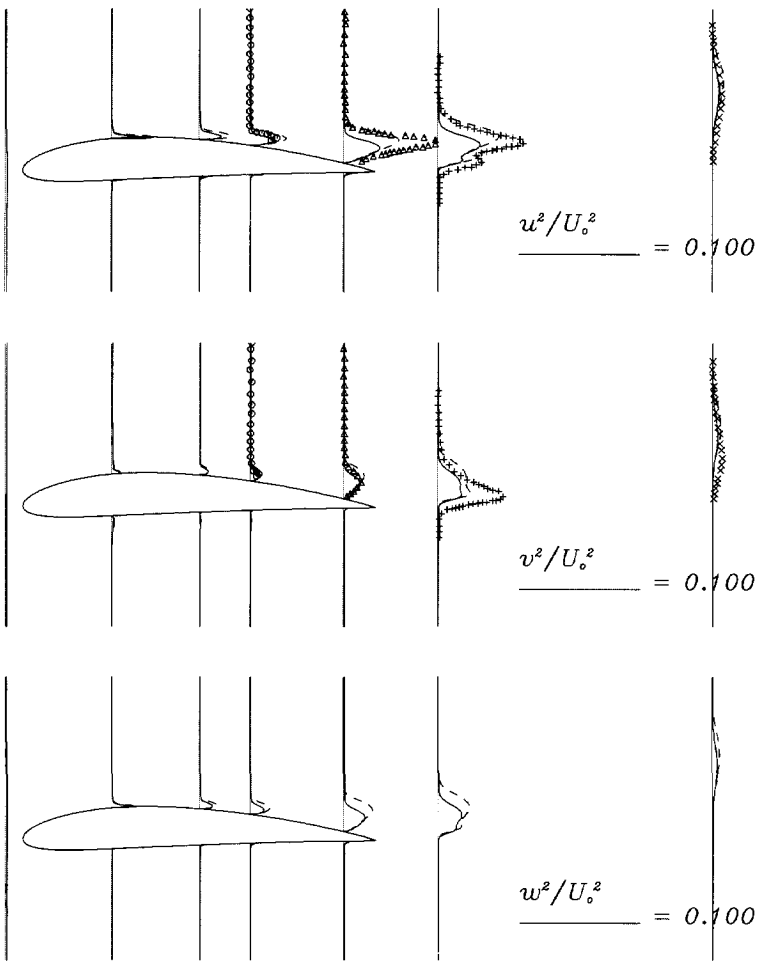

Figure 5.31: NACA 4412 flow: the normal components of the Reynolds-stress tensor in the chordwise oriented coordinate system at *x/c = -0.05, 0.25, 0.5, 0.642, 0.908, 1.1747, 1.95146*. Legend as in Fig 5.29.

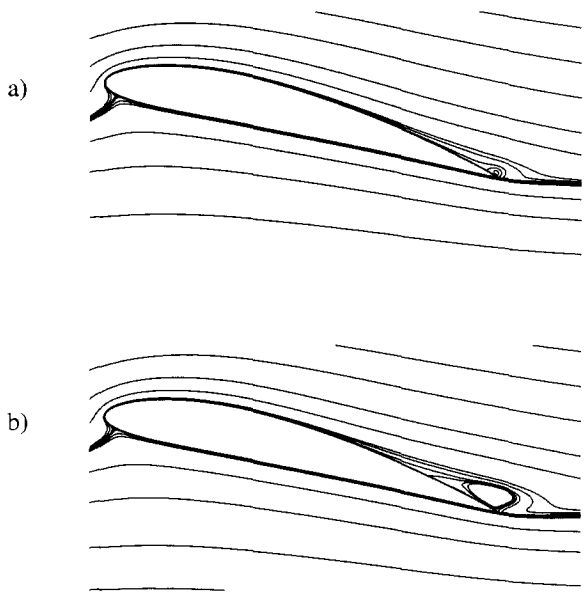

Figure 5.32: NACA 4412 flow: a) streamlines obtained with low-Re SMC and b) with high-Re SMC + WF.

5.8 Concluding remarks

It has been shown here that the low-Re-number SMC is capable of resolving bypass transition for relatively high level of the free-stream turbulence (more than 3%) reasonably well, both for plate with sharp and circular leading edge. Under these circumstances the model predicts the transition location, streamwise mean velocity, Reynolds-stresses, as well as the separation bubble in T3L cases, closely to the experiments. For flows with smaller level of FST this version of the model has difficulty in reproducing the increase of turbulence in the boundary layer at the rate which was found in experiments. Nevertheless, in the T3L case with lower FST the model predicts the separation bubble, and the consequent transition, but the agreement with experiments is not as good as in the case with higher level of FST.

It has been demonstrated that including a nonlinear model for slow-part of the pressure-strain correlation leads to significant improvement of the results for the bypass transition on flat plate with small free-stream turbulence (3%). Unfortunately, this modification does not improve

prediction of the T3L cases with lower FST (virtually, there is no difference in the results).

Although, this SMC model shows some difficulties in predicting the bypass transition at low level of FST, the model is capable of predicting reasonably well the coexistence of virtually laminar and fully turbulent flow regions and separation induced transition on a plane wall, as shown in the case of transitional separation bubble.

It was confirmed that the Launder-Sharma version of the eddy-viscosity model fails to reproduce the transition in the circular-leading edge geometries. In the stagnation region much too high level of turbulence kinetic energy is predicted with this model. This is caused by over-estimation of the production of turbulence kinetic energy (which is always positive due to Boussinesq hypothesis) in that region. In contrast to this result the SMC model predicts proper development of turbulence. This is basically due to the correct prediction of the production and the dissipation of turbulence kinetic energy in the stagnation region. Although the wall reflection model of Gibson and Launder (1978) which is used here in the SMC does not work correctly in impingement flows, in the T3L case the stagnation region is rather small and dominant generation of turbulence is due to shear production and normal-to-the-wall pressure reflection, which is well reproduced by the conventional wall-echo model.

Besides the modelling issues, the accurate representation of convective terms in the transport equations, especially in curved geometries, was shown to be very important for the computation of the bypass transition at flat plate with circular leading edge. It was demonstrated that an advanced numerical strategy, such as multi-block and grid refinement, with accurate discretisation of the model equations in a stable way, offers an opportunity to explore the potential of SMC models in more physically and geometrically complex flows. Application of the low-Re-number model to fairly complex industrially relevant flows, such as NACA 4412 airfoil, does not possess any additional difficulty in comparison to the wall function approach. Although, the low-Re-number approach requires much finer numerical mesh, these more demanding requirements are justified by better performances. The computation of phenomena related to low Re numbers, such as transition, cannot be resolved otherwise.

CHAPTER 6

Conclusions

This thesis has described an investigation of possibilities to model the laminar to turbulence transition in a wide range of conditions using the second moment closure models. In the course of this work a variety of numerical and modelling issues have been examined.

The most important tasks accomplished in the present study are:

- A numerical code for solving the second moment closure turbulence models on two-dimensional, collocated, non-orthogonal, block-structured, body-fitted grids with block-wise grid refinement has been developed. The high accuracy of the procedure is achieved by using QUICK and TVD schemes for discretisation of convective terms in the transport equations solved. The application of higher order schemes was found to be crucial for obtaining accurate solution, especially in more complex geometries involving flow separation. The high stability of the procedure is achieved by introducing, in a specific manner, an isotropic artificial turbulence viscosity in the momentum equations, as well as in the equation for the mean scalar, when applied. This proved to be computationally more robust than any other known approach, and especially as compared to treating second moment gradients as a source term.
- Many of the cases predicted in the present study are at the lower Re-number edge between laminar and turbulent regime and some involve a coexistence of the laminar and fully turbulent flow portions in the same flow domain. In such cases some components of Reynolds stresses are damped more than others and may fully disappear leading to two-component turbulence. Numerical computation of such conditions is sensitive as it may lead to non-physical negative values of essentially positive quantities. Therefore, it is of utmost importance to have a numerical scheme which prevents physically unrealistic solution. This has been achieved here using bounding TVD schemes for discretisation of convection. Of course, adequate modelling, which satisfies the realisability constraint is also of equal importance.
- Since transitional flows are in focus, attention is given to low-Re-number turbulence models with integration up to the wall. Possibilities for modelling of transitional flows with two second moment closure models were investigated: the HJ model and the Durbin elliptic relaxation model. It was found that the latter model is not very stable when the numerical

grid near the wall is very fine ($y^+ < 0.1$). Since it is difficult to control the grid distribution in an unknown situation and, especially, in the transitional flows where the laminar and turbulen flow regions may appear within the same flow, the elliptic relaxation model was not pursued beyond some tentative investigation. Nevertheless the elliptic relaxation modelling of the wall effects on the pressure strain correlation, shows potential for further exploration in computation of turbulent non-equilibrium flows and it is probably a good candidate for a turbulence model aimed at general application.

- Since the HJ model was found to perform satisfactory in a broad range of non-equilibrium flows, this model was further applied to the transitional flows. Jointly with some basic test cases for low Re-number model for which DNS data are available, such as channel and boundary-layer flows, the oscillating boundary layer at $Re_{\delta_S} = 1000$, for which are also DNS data available, was used to select and adjust values and functional form of some low Re-number model coefficients. Such a choice of the model coefficients of the HJ model provides satisfactory results in transitional flows as well as in the fully turbulent wall flows.
- Some alternative routes to modelling of some of the terms have also been explored. A new model for dissipation rate tensor ε_{ij} was proposed. The model is aimed at improving the behaviour of the ε_{ij} in viscous sublayer and provides correct wall limit values. The model is free from the wall topology information and is computationally convenient. Assessment using DNS data shows improvement over the models available in the literature.
- An alternative approach of deriving the pressure-strain correlation models was also proposed. The model is based on modelling the pressure fluctuation using fluctuating and averaged quantities. Instead of Poisson equation for fluctuating pressure as used conventionally, this approach models directly the gradient of the fluctuating pressure which appears in Φ_{ij}. This is done in terms of fluctuating and mean velocity and turbulence time scale by approximating the Navier-Stokes equation for fluctuating motion. The determination of the model coefficients is the same as in the conventional approach.
- A term by term analysis of conventional models of dissipation rate ε equation using DNS data is also proposed with suggestion for possible improvement for non-equilibrium flows.
- The SMC low-Re-number turbulence model was applied to a range of oscillating and pulsating flows at transitional and higher Re number, in bypass transition flows and the separation induced transitional flows in a wide range of conditions. In most of the cases the applied SMC model shows obvious advantages and better performances than any other model available in the literature. It is important to mention here that all transitional flows were predicted *without* prescribing or triggering the transition or any other empirical input, as practised often in models for transitional flows. The ability to predict transition and its location without external trigger is the essential requirement for a general model for complex flows.
- It was demonstrated that an advanced numerical strategy, such as multi-block and local grid refinement, with accurate discretisation of the model equations in a stable way, offers an opportunity to explore the potential of SMC models in more physically and geometrically complex flows and high-Re-number flows. Application of the low-Re-number model to fairly complex industrially relevant flows, such as NACA 4412 airfoil, does not

posses any additional difficulty in comparison to the wall function approach. Although, the low-Re-number approach requires much finer numerical mesh, these more demanding requirements are justified by better performances. Computation of phenomena related to low Re numbers, such as transition, cannot be resolved otherwise.

As compared with conventional and mostly used eddy-viscosity type of models, it has been demonstrated by this thesis that the turbulence modelling in the framework of second moment closure has many advantages: in most cases considered the SMC models performs better than EVMs. It should be recalled that the numerical solution procedure for SMC is slightly more complex than for EVMs, but not so much to discourage a wider use of SMC models. The present author's experience is that the computer demands for SMC are between two (wall functions) and three times (low-Re-models) larger than those for EVM. This is primarily due to complexity of these models and larger number of equations to be solved. However, SMC are physically better founded and offer a larger potential for further improvement. Therefore this author is of opinion that SMC models will play in the near future a more significant role in the industrial CFD than they have had in the past. For more distant future, the RANS my be superseded by LES or DNS. However according to estimation of Spalart *et al.* (1997), as mentioned in Chapter 1, very complex engineering design problems, such as a flow around an airplain wing, will be possible to tackle by LES only in four decades from now.

APPENDIX A

Basic high-Re-number Reynolds-stress model

This appendix displays the basic high-Re-number Reynolds-stress model. The pressure-strain correlation is composed of:
- the return to isotropy (Rotta 1951) model for the slow part,
- the isotropisation of production IP (Noat *et al.* 1973) model for the rapid part,
- Gibson and Launder (1978) model for the wall reflection term.

Dissipation rate tensor is isotropic. Daly and Harlow (1970) model is used for the turbulent diffusion.

$$\frac{D\overline{u_i u_j}}{Dt} = \frac{\partial}{\partial x_k}\left[\left(\nu\delta_{kl} + C_s\frac{k}{\varepsilon}\overline{u_k u_l}\right)\frac{\partial \overline{u_i u_j}}{\partial x_l}\right] + P_{ij} - \frac{2}{3}\varepsilon\delta_{ij} + \Phi_{ij} \tag{A.1}$$

$$P_{ij} = -\left(\overline{u_i u_k}\frac{\partial U_j}{\partial x_k} + \overline{u_j u_k}\frac{\partial U_i}{\partial x_k}\right) \tag{A.2}$$

$$\Phi_{ij} = \Phi_{ij,1} + \Phi_{ij,2} + \Phi^w_{ij,1} + \Phi^w_{ij,2} \tag{A.3}$$

$$\Phi_{ij,1} = -C_1\varepsilon\left(\frac{\overline{u_i u_j}}{k} - \frac{2}{3}\delta_{ij}\right) \tag{A.4}$$

$$\Phi_{ij,2} = -C_2\left(P_{ij} - \frac{2}{3}P_k\delta_{ij}\right) \tag{A.5}$$

$$\Phi^w_{ij,1} = C^w_1 f_w\frac{\varepsilon}{k}\left(\overline{u_k u_m}n_k n_m\delta_{ij} - \frac{3}{2}\overline{u_i u_k}n_k n_j - \frac{3}{2}\overline{u_k u_j}n_k n_i\right) \tag{A.6}$$

$$\Phi^w_{ij,2} = C^w_2 f_w\left(\Phi_{km,2}n_k n_m\delta_{ij} - \frac{3}{2}\Phi_{ik,2}n_k n_j - \frac{3}{2}\Phi_{kj,2}n_k n_i\right) \tag{A.7}$$

$$\frac{D\varepsilon}{Dt} = \frac{\partial}{\partial x_k}\left[\left(\nu\delta_{kl} + C_\varepsilon\frac{k}{\varepsilon}\overline{u_k u_l}\right)\frac{\partial\varepsilon}{\partial x_l}\right] - C_{\varepsilon_1}\frac{\varepsilon}{k}\overline{u_i u_j}\frac{\partial U_i}{\partial x_j} - C_{\varepsilon_2}\frac{\varepsilon^2}{k} \tag{A.8}$$

C_1	C_2	C^w_1	C^w_2	C_s	C_ε	C_{ε_1}	C_{ε_2}
1.8	0.6	0.5	0.3	0.22	0.18	1.44	1.92

APPENDIX B

The low-Re-number second moment closure (HJ)

This appendix gives a summary of the model equations of the Hanjalić-Jakirlić (HJ) low-Re-number Reynolds-stress model. Some unpublished results, obtained in the course of model validation, which are not directly relevant to transitional flows are also shown in this appendix. These results illustrate further the ability of the model to predict non-equilibrium flows. Results are not discussed but figure captions provide necessary informations about the flows.

Performances of this model in a large number of non-equilibrium flows have been published in: Hanjalić, Jakirlić, and Durst (1994), Hanjalić, Jakirlić, and Hadžić (1995), Hanjalić and Hadžić (1995), Jakirlić (1997), Hanjalić and Jakirlić (1998), Hanjalić, Hadžić, and Jakirlić (1998).

B.1 The model equations and coefficients

$$\frac{D\overline{u_i u_j}}{Dt} = \frac{\partial}{\partial x_k}\left[\left(\nu\delta_{kl} + C_s\frac{k}{\varepsilon}\overline{u_k u_l}\right)\frac{\partial \overline{u_i u_j}}{\partial x_l}\right] + P_{ij} + \Phi_{ij} - \varepsilon_{ij} \tag{B.1}$$

$$P_{ij} = -\left(\overline{u_i u_k}\frac{\partial U_j}{\partial x_k} + \overline{u_j u_k}\frac{\partial U_i}{\partial x_k}\right) \tag{B.2}$$

$$\Phi_{ij,1} = -C_1\varepsilon a_{ij} \tag{B.3}$$

$$\Phi_{ij,2} = -C_2\left(P_{ij} - \frac{2}{3}P_k\delta_{ij}\right) \tag{B.4}$$

$$\Phi^w_{ij,1} = C^w_1 f_w\frac{\varepsilon}{k}\left(\overline{u_k u_m}n_k n_m\delta_{ij} - \frac{3}{2}\overline{u_i u_k}n_k n_j - \frac{3}{2}\overline{u_k u_j}n_k n_i\right) \tag{B.5}$$

$$\Phi^w_{ij,2} = C^w_2 f_w\left(\Phi_{km,2}n_k n_m\delta_{ij} - \frac{3}{2}\Phi_{ik,2}n_k n_j - \frac{3}{2}\Phi_{kj,2}n_k n_i\right) \tag{B.6}$$

$$C_1 = C + \sqrt{A}E^2 \qquad C = 2.5AF^{1/4}f \qquad F = \min(0.6; A_2)$$

$$C_2 = 0.8A^{1/2} \qquad C_1^w = \max(1 - 0.7C; 0.3) \quad C_2^w = \min(A; 0.3)$$

$$f = \min\left\{\left(\frac{Re_t}{150}\right)^{3/2}; 1\right\} \quad f_w = \min\left[\frac{k^{3/2}}{2.5\varepsilon x_n}; 1.4\right] \qquad Re_t = k^2/(\nu\varepsilon), \tag{B.7}$$

$$\varepsilon_{ij} = f_s\varepsilon^*_{ij} + (1 - f_s)\frac{2}{3}\delta_{ij}\varepsilon \tag{B.8}$$

$$\varepsilon^*_{ij} = \frac{\varepsilon}{k}\frac{[\overline{u_iu_j} + (\overline{u_iu_k}n_jn_k + \overline{u_ju_k}n_in_k + \overline{u_ku_l}n_kn_ln_in_j)f_d]}{1 + 1.5\,(\overline{u_pu_q}/k)\,n_pn_q\,f_d} \tag{B.9}$$

$$f_s = 1 - \sqrt{A}E^2 \qquad f_d = (1 + 0.1Re_t)^{-1} \tag{B.10}$$

$$\begin{aligned}\frac{D\varepsilon}{Dt} = {} & \frac{\partial}{\partial x_k}\left[\left(\nu\delta_{kl} + C_\varepsilon\frac{k}{\varepsilon}\overline{u_ku_l}\right)\frac{\partial\varepsilon}{\partial x_l}\right] - C_{\varepsilon_1}\frac{\varepsilon}{k}\overline{u_iu_j}\frac{\partial U_i}{\partial x_j} - C_{\varepsilon_2}f_\varepsilon\frac{\varepsilon\tilde{\varepsilon}}{k} \\ & + C_{\varepsilon_3}\nu\frac{k}{\varepsilon}\overline{u_ju_k}\frac{\partial^2U_i}{\partial x_j\partial x_l}\cdot\frac{\partial^2U_i}{\partial x_k\partial x_l} - C_{\varepsilon 4}f_4k\Omega_k\Omega_k + S_l.\end{aligned} \tag{B.11}$$

$$\Omega_i = \epsilon_{ijk}\partial U_j/\partial x_k \tag{B.12}$$

$$S_l = \max\left\{\left[\left(\frac{1}{C_l}\frac{\partial l}{\partial x_j}\right)^2 - 1\right]\left(\frac{1}{C_l}\frac{\partial l}{\partial x_j}\right)^2; 0\right\}\frac{\tilde{\varepsilon}\varepsilon}{k}\,A, \qquad l = k^{3/2}/\varepsilon \tag{B.13}$$

$$f_\varepsilon = 1 - \frac{C_{\varepsilon_2} - 1.4}{C_{\varepsilon_2}}\exp\left[-\left(\frac{Re_t}{6}\right)^2\right] \tag{B.14}$$

$$C_s = 0.22, \quad C_\varepsilon = 0.18, \quad C_{\varepsilon_3} = 0.25, \quad C_l = 2.5.$$

$$\begin{gathered}A_2 = a_{ij}a_{ij}, \quad A_3 = a_{ij}a_{jk}a_{ki}, \quad A = 1 - 9/8(A_2 - A_3) \\ E_2 = e_{ij}e_{ij}, \quad E_3 = e_{ij}e_{jk}e_{ki}, \quad E = 1 - 9/8(E_2 - E_3) \\ a_{ij} = \overline{u_iu_j}/k - 2/3\delta_{ij}, \quad e_{ij} = \varepsilon_{ij}/\varepsilon - 2/3\delta_{ij}.\end{gathered}$$

B.2 Channel flow

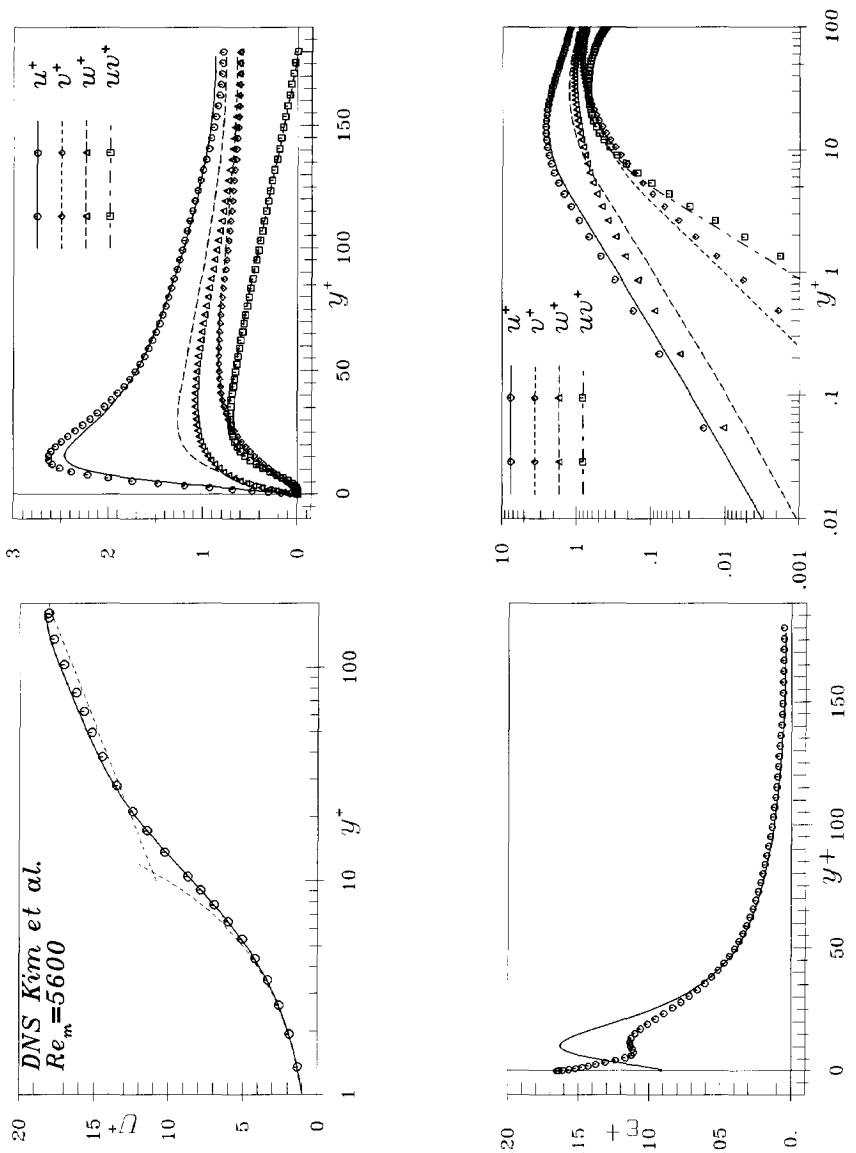

Figure B.1: Results of the HJ low-Re-number Reynolds stress model in a fully developed channel flow at $Re_\tau = 180$. Symbols are DNS data of Kim *et al.* (1987) and lines are the model results.

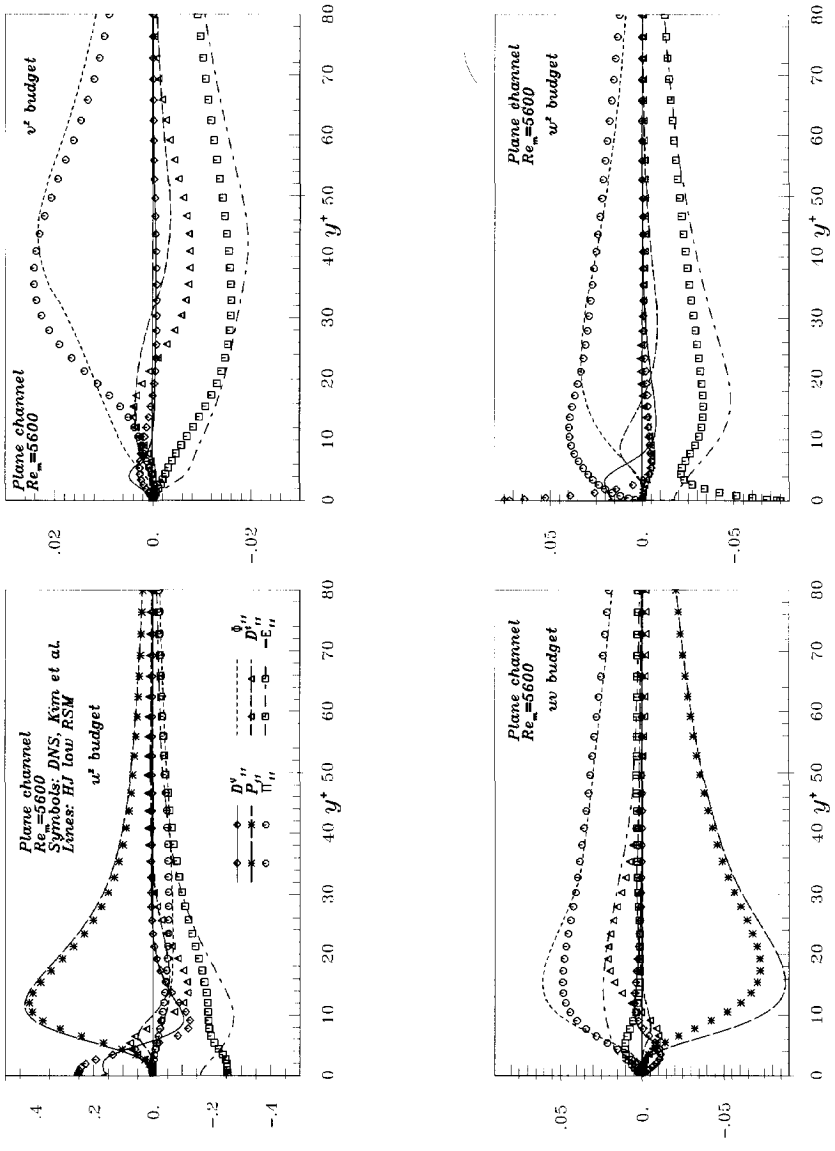

Figure B.2: Budget for transport equations for $\overline{u_i u_j}$ obtained with the HJ low-Re-number Reynolds stress model in a fully developed channel flow at $Re_\tau = 180$. Symbols are DNS data of Kim *et al.* (1987) and lines are the model results. (Courtesy of Dr. S. Jakirlić of TU Darmstadt.)

B.3 Couette flow with a fixed periodical wavy wall

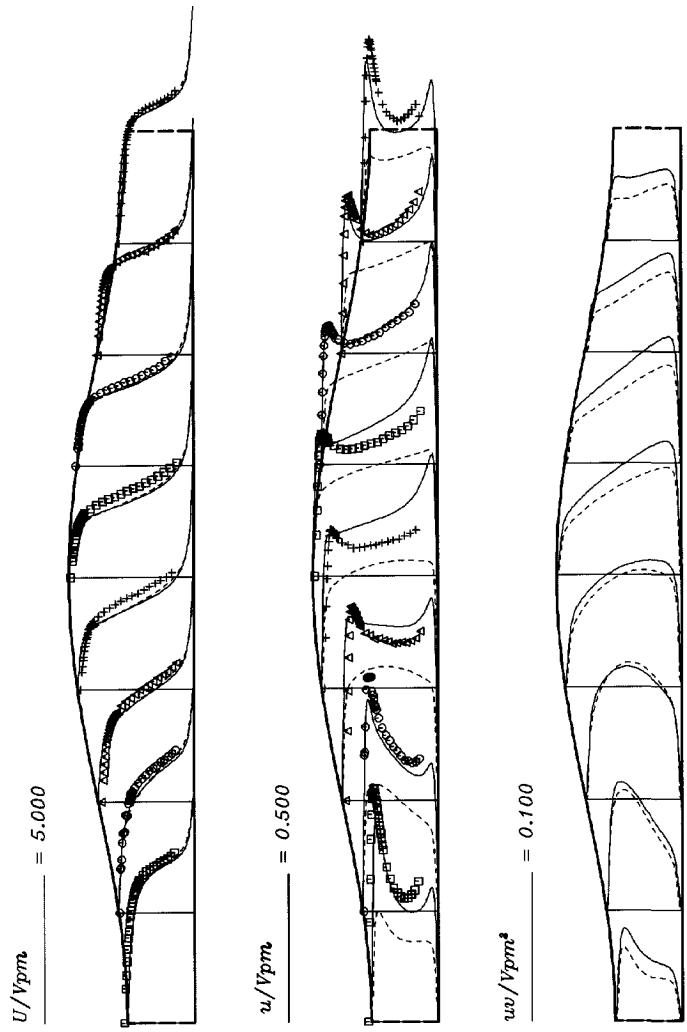

Figure B.3: Profiles of U, $\sqrt{\overline{u^2}}$ and $\overline{uv}$ in a Couette flow with a fixed wavy wall. Symbols: Experiments by Nakabayashi *et al.* (1991). Solid lines: HJ low-Re-number Reynolds-stress model. Dashed lines: Launder-Sharma low-Re-number eddy-viscosity model. ($V_{pm} = 1m/s$). Wavy fixed wall is defined as: $h_{(x)} = 2\delta - e \cos(2\pi x/L)$, where $e = 4.5\ mm$, $2\delta = 15\ mm$ and $L = 1.4m$, $U_w = 7.9m/s$, $Re_w = \dfrac{U_w 2\delta}{\nu} = 4000$.

B.4 Turbulent flow in a channel with a wavy wall

Wavy wall is defined with: $H_{(x)} = H\,[1 + a\cos(2\pi x/B)]$, where $B = 3.84H$, $a = 0.05$ and $Re_m = U_m H/\nu = 4400$ (U_m is the bulk mean velocity). Strong variation of the pressure gradient as well as the wall shear stress is induced by just $0.05H$ amplitude of variation of the top wall boundary.

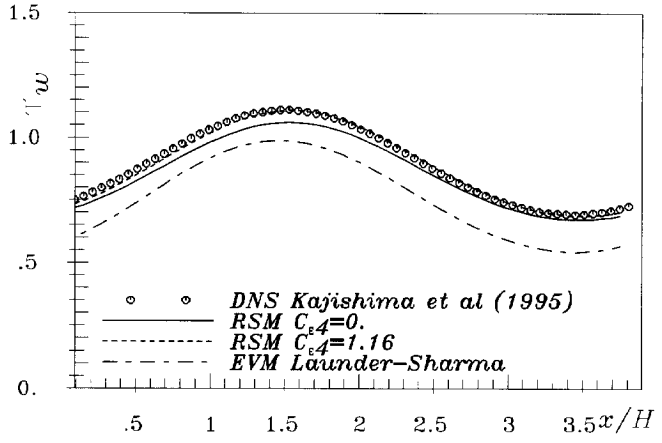

Figure B.4: Wall-shear stress. HJ low-Re number models: $C_{\varepsilon_4} = 0$, solid line; $C_{\varepsilon_4} = 1.16$, dashed line; $k - \varepsilon$ Launder-Sharma model, chain line.

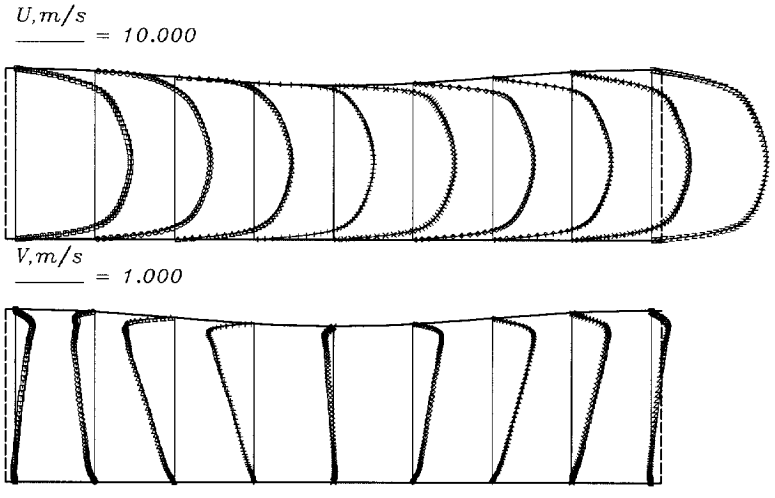

Figure B.5: Figure continues on next page.

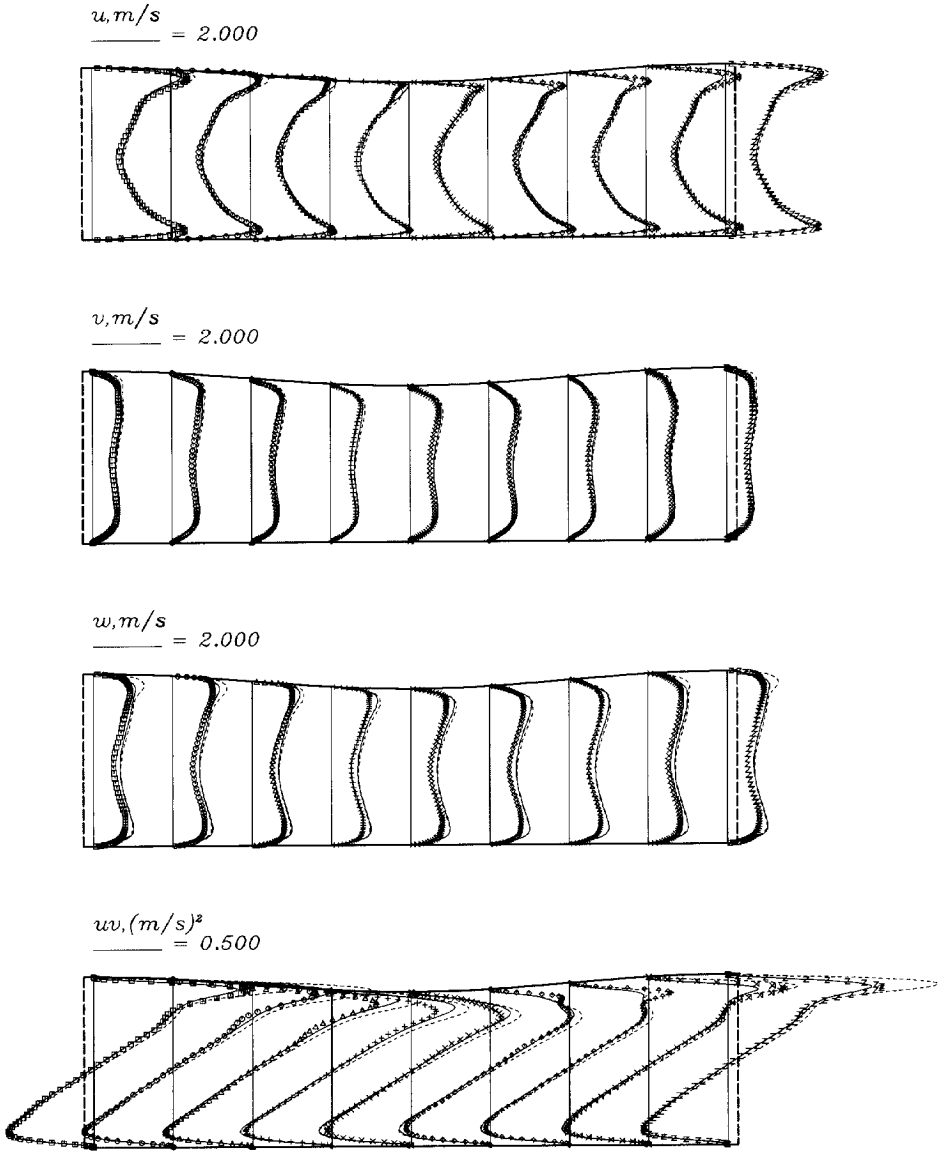

Figure B.6: Lines: Mean velocities and Reynolds-stresses obtained with HJ SMC. Symbols: DNS data of Kajishima *et al.* (1995).

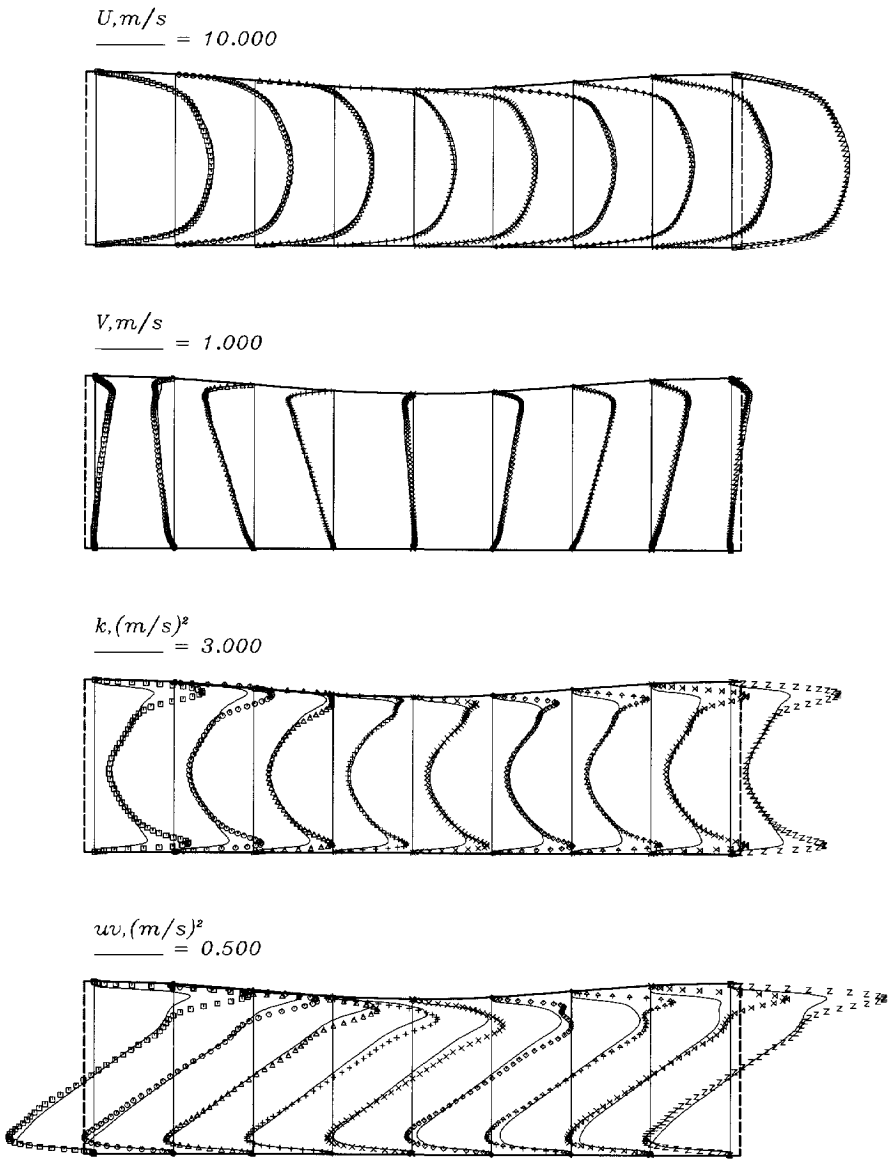

Figure B.7: Lines: Mean velocities and Reynolds-stresses obtained with Launder-Sharma EVM. Symbols: DNS data of Kajishima *et al.* (1995).

APPENDIX C

Durbin's elliptic relaxation model

This appendix gives a summary of the model equations of the Durbin's elliptic relaxation model (ERM) (Durbin 1993) with the wall boundary conditions.

$$\frac{D\overline{u_i u_j}}{Dt} = k\, f_{ij} + P_{ij} - \frac{\overline{u_i u_j}}{k}\varepsilon - \frac{\partial}{\partial x_l}\left(\nu\delta_{lm} + \frac{\nu_{T_{lm}}}{\sigma_k}\right)\frac{\partial \overline{u_i u_j}}{\partial x_m} \tag{C.1}$$

$$\frac{Dk}{Dt} = P_k - \varepsilon + \frac{\partial}{\partial x_l}\left(\nu\delta_{lm} + \frac{\nu_{T_{lm}}}{\sigma_k}\right)\frac{\partial k}{\partial x_m} \tag{C.2}$$

$$\frac{D\varepsilon}{Dt} = \frac{C^*_{\varepsilon_1} P_k - C_{\varepsilon_2}\varepsilon}{T} + \frac{\partial}{\partial x_l}\left(\nu\delta_{lm} + \frac{\nu_{T_{lm}}}{\sigma_\varepsilon}\right)\frac{\partial \varepsilon}{\partial x_m} \tag{C.3}$$

$$-\nabla^2 f_{ij} + \frac{f_{ij}}{L^2} = \frac{f^H_{ij}}{L^2}, \tag{C.4}$$

$$f^H_{ij} = \frac{1-c_1}{kT}\left(\overline{u_i u_j} - \frac{2}{3}k\delta_{ij}\right) - \frac{c_2}{k}\left(P_{ij} - \frac{2}{3}P_k\delta_{ij}\right). \tag{C.5}$$

– turbulent viscosity : $\nu_{T_{ml}} = C_\nu \overline{u_m u_l} T$ (C.6)

– time scale : $T = \mathtt{max}\left(\frac{k}{\varepsilon}, C_T\left(\frac{\nu}{\varepsilon}\right)^{\frac{1}{2}}\right)$ (C.7)

– length scale : $L = C_L\, \mathtt{max}\left(\frac{k^{3/2}}{\varepsilon}, C_\eta\left(\frac{\nu^3}{\varepsilon}\right)^{\frac{1}{4}}\right)$ (C.8)

– $C^*_{\varepsilon_1} = C_{\varepsilon_1}\left(1 + a_1\frac{P_k}{\varepsilon}\right)$ (C.9)

σ_k	σ_ε	C_ν	C_{ε_1}	C_{ε_2}	a_1	C_1	C_2	C_T	C_L	C_η
1.2	1.65	0.23	1.44	1.9	0.1	1.22	0.6	6.0	0.2	80.0

Wall-oundary conditions for f_{ij}

$$f_{11_w} = 0 \tag{C.10}$$

$$f_{22_w} = -20\nu^2 \left(\frac{\overline{v^2}}{y^4}\right)_P \tag{C.11}$$

$$f_{33_w} = -f_{22_w} \tag{C.12}$$

$$f_{12_w} = -20\nu^2 \left(\frac{\overline{uv}}{y^4}\right)_P \tag{C.13}$$

APPENDIX D

Launder-Sharma eddy-viscosity model

This model was published in Launder and Sharma (1974).

$$\frac{\partial k}{\partial t} + \frac{\partial U_j k}{\partial x_j} = \frac{\partial}{\partial x_j}\left[\left(\nu + \frac{\nu_t}{\sigma_k}\right)\frac{\partial k}{\partial x_j}\right] + P_k - \varepsilon \tag{D.1}$$

$$\frac{\partial \tilde{\varepsilon}}{\partial t} + \frac{\partial U_j \tilde{\varepsilon}}{\partial x_j} = \frac{\partial}{\partial x_j}\left[\left(\nu + \frac{\nu_t}{\sigma_\varepsilon}\right)\frac{\partial \tilde{\varepsilon}}{\partial x_j}\right] + C_{\varepsilon 1} P_k \frac{\tilde{\varepsilon}}{k} - C_{\varepsilon 2} f_\varepsilon \frac{\tilde{\varepsilon}^2}{k} + 2\,\nu\,\nu_t \left(\frac{\partial^2 U_i}{\partial x_k \partial x_l}\right)^2 \tag{D.2}$$

$$P_k = \nu_t \left(\frac{\partial U_i}{\partial x_j} + \frac{\partial U_j}{\partial x_i}\right)\frac{\partial U_i}{\partial x_j} \tag{D.3}$$

$$\tilde{\varepsilon} = \varepsilon - 2\,\nu \left(\frac{\partial k^{1/2}}{\partial x_j}\right)^2 \tag{D.4}$$

Wall boundary conditions

$$\tilde{\varepsilon}_w = 0; \quad k_w = 0 \tag{D.5}$$

Model coefficients

$$\nu_t = C_\mu \exp\left[\frac{-3.4}{\left(1 + \frac{\tilde{Re}_t}{50}\right)^2}\frac{k^2}{\tilde{\varepsilon}}\right] \tag{D.6}$$

$$f_\varepsilon = 1 - 0.3 \exp\left[-\tilde{Re}_t^{\,2}\right] \tag{D.7}$$

$$\tilde{Re}_t = \frac{k^2}{\nu\tilde{\varepsilon}} \tag{D.8}$$

$$C_\mu = 0.09, \qquad \sigma_k = 1, \qquad \sigma_\varepsilon = 1.3, \qquad C_{\varepsilon 1} = 1.44, \qquad C_{\varepsilon 2} = 1.92.$$

APPENDIX E

Velocity and Reynolds-stress transformation

This appendix displays the relations of the quantities used within second moment closure modelling, such as the velocity vector components, their gradients, and the Reynolds-stress tensor components in two 2D Cartesian co-ordinate systems: the global system in which a computed flow is defined and a local (e. g. wall-oriented) one. These relations are used within the numerical procedure described in Chapter 3 to impose the wall conditions for the mean velocity and the Reynolds-stresses in the frame work of the wall function approach.

If we define two Cartesian co-ordinate systems (x, y) and (x', y') with the same origin and the positive x'-axis is obtained from the positive x-axis by a counter-clockwise rotation through an angle θ as in Figure E.1 the point M has the co-ordinates in these two systems

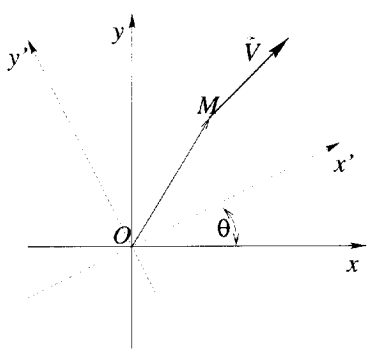

$$x = x' \cos\theta - y' \sin\theta$$

$$y = x' \sin\theta + y' \cos\theta$$

$$x' = x \cos\theta + y \sin\theta$$

$$y' = -x \sin\theta + y \cos\theta$$

Figure E.1: Coordinate transformation.

The components of the velocity vector $\vec{V} = U\,\vec{i} + V\,\vec{j} = U'\,\vec{i}' + V'\,\vec{j}'$ are

$$U = U' \cos\theta - V' \sin\theta$$

$$V = U' \sin\theta + V' \cos\theta$$

$$U' = U\cos\theta + V\sin\theta$$

$$V' = -U\sin\theta + V\cos\theta$$

and the gradients of the velocity components are

$$\frac{\partial U}{\partial x} = \frac{\partial U'}{\partial x'}\cos^2\theta - \left(\frac{\partial V'}{\partial x'} + \frac{\partial U'}{\partial y'}\right)\sin\theta\cos\theta + \frac{\partial V'}{\partial y'}\sin^2\theta$$

$$\frac{\partial U}{\partial y} = -\frac{\partial V'}{\partial x'}\sin^2\theta + \left(\frac{\partial U'}{\partial x'} - \frac{\partial V'}{\partial y'}\right)\sin\theta\cos\theta + \frac{\partial U'}{\partial y'}\cos^2\theta$$

$$\frac{\partial V}{\partial x} = \frac{\partial V'}{\partial x'}\cos^2\theta + \left(\frac{\partial U'}{\partial x'} - \frac{\partial V'}{\partial y'}\right)\sin\theta\cos\theta - \frac{\partial U'}{\partial y'}\sin^2\theta$$

$$\frac{\partial V}{\partial y} = \frac{\partial U'}{\partial x'}\sin^2\theta + \left(\frac{\partial U'}{\partial x'} + \frac{\partial V'}{\partial y'}\right)\sin\theta\cos\theta + \frac{\partial V'}{\partial y'}\cos^2\theta$$

The Reynolds-stress tensor components are

$$\overline{u^2} = \overline{u'^2}\cos^2\theta - 2\overline{u'v'}\sin\theta\cos\theta + \overline{v'^2}\sin^2\theta$$

$$\overline{v^2} = \overline{u'^2}\sin^2\theta + 2\overline{u'v'}\sin\theta\cos\theta + \overline{v'^2}\cos^2\theta$$

$$\overline{w^2} = \overline{w'^2}$$

$$\overline{uv} = \overline{u'^2}\sin\theta\cos\theta + \overline{u'v'}(\cos^2\theta - \sin^2\theta) - \overline{v'^2}\sin\theta\cos\theta$$

$$\overline{u'^2} = \overline{u^2}\cos^2\theta + 2\overline{uv}\sin\theta\cos\theta + \overline{v^2}\sin^2\theta$$

$$\overline{v'^2} = \overline{u^2}\sin^2\theta - 2\overline{uv}\sin\theta\cos\theta + \overline{v^2}\cos^2\theta$$

$$\overline{w'^2} = \overline{w^2}$$

$$\overline{u'v'} = (-\overline{u^2} + \overline{v^2})\sin\theta\cos\theta + \overline{uv}(\cos^2\theta - \sin^2\theta)$$

References

Akhavan, R., R. D. Kamm, and A. H. Shapiro (1991). An investigation of transition to turbulence in bounded oscillatory Stokes flows. Part 1. Experiments. *J. Fluid Mech. 225*, 395–422.

Apsley, D., W.-L. Chen, M. Leschziner, and F.-S. Lien (1997). Non-linear eddy-viscosity modelling of separated flows. *Special Issue of J of Hydraulic Research (to appear).*

Chen, W. L., F. S. Lien, and M. A. Leschziner (1994). Computational modelling of turbulent flow in turbomachine passage with low-Re two-equation models. In *Computational Fluid Dynamics '94*, pp. 517–524.

Chien, K.-Y. (1982). Prediction of channel and boundary layer flows with a low-Reynolds-number turbulence model. *AIAA Journal 20*, 33–38.

Chieng, C. C. and B. E. Launder (1980). On the calculation of turbulent heat transport downstream from an abrupt pipe expansion. *Numer. Heat Transfer, Part B 3*, 189–207.

Chou, P. Y. (1945). On velocity corrlations and the solutions of the equations of turbulent fluctuation. *Quart. of Appl. Math. 3*(1), 38–54.

Ciofalo, M. and M. W. Collins (1989). $k - \varepsilon$ predictions of heat transfer in turbulent recirculating flows using an improved wall treatment. *Numer. Heat Transfer, Part B 15*, 21–47.

Coles, D. and A. J. Wadcock (1979). Flying-hot-wire study of flow past a naca 4412 airforil at maximum lift. *AIAA Journal 17*, 321–329.

Corenflos, K., S. Rida, J. C. Monier, P. D. K. DangTran, and M. Stanislas (1993). Experimental and numerical study of a plane Couette-Poiseuille flow as a test case for turbulence modelling. In W. Rodi and F. Martelli (Eds.), *Engineering Turbulence Modelling and Experiments*. Elsevier Science Publishers B.V.

Coupland, J. (1995). Personal Communication.

Craft, T., B. E. Launder, and K. Suga (1997). Prediction of turbulent transitional phenomena with a nonlinear eddy-viscosity model. *Int. J. Heat and Fluid Flow 18*, 15.

Craft, T. J. (1991). *Second-Moment Modelling of Turbulent Scalar Transport*. Ph. D. thesis, UMIST Manchester, UK.

Craft, T. J. (1997). Computations of separating and reattaching flows using a low-Reynolds-number second-moment closure. In *Proc. of 11th Symp. on Turbulent Shear Flows*.

Craft, T. J. and B. E. Launder (1996). Improvement in near–wall Reynolds stress modelling for compex flow geometries. *Int. J. Heat and Fluid Flow 17*(3), 245–254.

Dafa'Alla, A. A., E. Juntasaro, and M. M. Gibson (1996). Calculation of oscillating boundary layers with the $q - \zeta$ turbulence model. In W. Rodi and G. Bergeles (Eds.), *Engineering Turbulence Modelling and Experiments 3*, pp. 141–150.

Daly, B. J. and F. H. Harlow (1970). Transport equations of turbulence. *Phys. Fluids 13*, 2634–2649.

Davis, S. H. (1972). The stability of time-periodic flows. *Ann. Rev. Fluid Mech. 8*, 57–.

Davydov, B. I. (1960). On statistical dynamics of an incompressible furbulent fluid. *Soviet Physics - Doklady 6*(1), 10–12.

Demirdžić, I., Ž. Lilek, and M. Perić (1992). Fluid flow and heat transfer test problems for non-orthogonal grids: bench-mark solutions. *Int. J. Numer. Methods Fluids 15*, 329–354.

Demuren, A. O. and S. Sarkar (1993). Systematic study of Reynolds stress closure models in the computations of plane channel flows. *J. of Fluid Engineering 115*, 5–12.

Dengel, P. and H. H. Fernholz (1990). An experimental investigation of an incompressible turbulent boundary layer in the vicinity of separation. *J. Fluid Mech. 212*, 615–636.

Drain, L. E. and S. Martin (1985). Two component velocity measurements of turbulent flow in a ribbed-wall flow channel. In *Int. Conference on Laser Anemomotry-Advances and Application*.

Durbin, P. A. (1991). Near-wall turbulence closure modeling without "dumping functions". *Theoretical and Computational Fluid Dynamics 3*, 1–13.

Durbin, P. A. (1993). A reynolds stress model for near-wall turbulence. *J. Fluid Mech. 249*, 465–486.

Durbin, P. A. and C. G. Speziale (1994). Realizability of second-moment closure via stochastic analysis. *J. Fluid Mech. 280*, 395–407.

Ferziger, J. H. and M. Perić (1996). *Computational Methods for Fluid Dynamics*. Springer Verlag Berlin Heidelberg.

Fu, S., B. E. Launder, and D. P. Tselepidakis (1987). Accommodating the effects of high strain rates in modelling the pressure-strain correlation. Technical report, TFD/87/5, Mech. Eng. Dept. UMIST, Manchester, UK.

Fu, S. and C. Wang (1997). Second-moment closure modelling of turbulence in a non-inertial frame. *Fluid Dynamics Research 20*, 43–65.

Gaskell, P. H. and A. K. C. Lau (1988). Curvature-compensated convective transport: Smart, a new boundedness-preserving transport algorithm. *Int. J. Numer. Methods Fluids 8*, 617–641.

Gatski, T. B. and C. G. Speziale (1993). On explicit algebraic stress models for complex turbulent flows. *J. Fluid Mech. 254*, 59–78.

Gibson, M. M. and B. E. Launder (1978). Ground effects on pressure fluctuations in the atmospheric boundary layer. *J. Fluid Mech. 86*, 491–511.

Groth, J. (1991). Description of the pressure effects in the Reynolds stress transport equations. *Phys. Fluids A 3*(9), 2276–2277.

Guilmineau, E., J. Piquet, and P. Queutey (1997). Two-dimensional turbulent viscous flow simulation past airforils at fixed incidence. *Computers and Fluids 26*, 135–162.

Hadžić, I. and K. Hanjalić (1995). On the evolution of turbulence field in a periodic flow in a finite length pipe. In *Proc. of 10th Symp. on Turbulent Shear Flows*, pp. 21.13–21.18.

HaMinh, H., J. R. Viegas, M. W. Rubesin, D. D. Vandromme, and P. R. Spalart (1989). Physical analysis and second-order modelling of an unsteady turbulent flow: The oscillating boundary layer on a flat plate. In *Proc. of 7th Symp. on Turbulent Shear Flows*, pp. 11.5–11.9.

Hanjalić, K. (1994). Advanced turbulence closure models: a view of current status and future prospects. *Int. J. Heat and Fluid Flow 15*(3), 178–203.

Hanjalić, K. and I. Hadžić (1995). Modelling the transition phenomena with statistical turbulence closure models. In R. A. W. M. Henkes and J. L. van Ingen (Eds.), *Transitional Boundary Layers in Aeronautics*, pp. 283–294. North-Holland Amsterdam.

Hanjalić, K., I. Hadžić, and S. Jakirlić (1998). Modellinf turbulent wall flows subjected to strong pressure variations. *ASME J. Fluids Eng.*. acepted for publication.

Hanjalić, K. and S. Jakirlić (1993). A model of stress dissipation in second-moment closures. In F. T. M. Nieuwstadt (Ed.), *Advances in Turbulence IV, Applied Scientific Research 51*, pp. 513–518. Kluwer Academic Publishers.

Hanjalić, K. and S. Jakirlić (1998). Contribution towards the second-moment closure modelling of separating turbulent flows. *Computers and Fluids 27*(2), 137–156.

Hanjalić, K., S. Jakirlić, and F. Durst (1994). A computational study of joint effects of transverse shear and streamwise acceleration on three-dimensional boundary layers. *Int. J. Heat and Fluid Flow 15*(4), 269–282.

Hanjalić, K., S. Jakirlić, and I. Hadžić (1995). Computation of oscillating turbulent flows at transitional re-numbers. *Turbulent Shear Flows 9*, 323–342.

Hanjalić, K., S. Jakirlić, and J. R. Ristorcelli (1996, July 2-5). Alternative approach to modelling the dissipation equation. In S. G. et al. (Ed.), *Advances in Turbulence VI, Proc. of 6th European Turbulence Conference*, pp. 27–30. Lausanne, Switzerland.

Hanjalić, K. and B. E. Launder (1972). A reynolds stress model of turbulence and its aplication to thin shear flows. *J. Fluid Mech. 52*, 609–638.

Hanjalić, K. and B. E. Launder (1976). Contribution towards a reynolds-stress closure for low-reynolds-number turbulence. *J. Fluid Mech. 74*, 593–610.

Hino, M., M. Kashiwayanagi, A. Nakayama, and T. Hara (1983). Experiments on the turbulence statistics and the structure of a reciprocating oscillatory flow. *J. Fluid Mech. 131*, 363–400.

Hino, M., M. Sawamoto, and S. Takasu (1989). Experiments on transition to turbulence in an oscillatory pipe flow. *J. Fluid Mech. 76*, 193–207.

Hirsch, C. (1990). *Numerical Computation of Internal and External Flows*. John Wiley & Sons.

Huang, P. G. and M. A. Leschziner (1985). Stabilisation of recirculating flow computations performed with second-moment closure and third-order discretisation. In *Proc. 5th Symp. on Turbulent Shear Flows*, pp. 20.7–20.12.

Hussain, A. K. M. F. and W. C. Reynolds (1970). The mechanics of an organised wave in turbulent shear flow. *J. Fluid Mech. 41*, 241–258.

Jakirlić, S. Z. (1997). *Reynolds- Spannungs- Modellierung komplexer turbulenter Strömungen*. Ph. D. thesis, University of Erlangen - Nürnberg.

Jensen, B. L., B. M. Sumer, and J. Fredsoe (1989). Turbulent oscillatory boundary layers at high reynolds numbers. *J. Fluid Mech. 206*, 265–297.

Johansson, A. V. and M. Hallbäck (1994). Modelling of rapid pressure strain in reynolds-stress closures. *J. Fluid Mech. 269*, 143–168.

Jones, W. P. and B. E. Launder (1972). The prediction of laminarisation with a two-equation model of turbulence. *Int. J. Heat Mass Transfer 15*, 301–314.

Jones, W. P. and P. Musonge (1988). Closure of the Reynolds stress and scalar flux equations. *Phys. Fluids 31*(12), 3589–3604.

Justesen, P. and P. R. Spalart (1990). Two-equation turbulence modeling of oscillatory boundary layers. *AIAA Paper 41*, 90–0496.

Kajishima, T., Y. Miyake, and T. Ohta (1995). Direct numerical simulation of turbulent flow in a wavy channel. In H. Daiguji and Y. Miyake (Eds.), *Proc. of the Matematical Modelling of Turbulent Flows*, pp. 176–180.

Kato, M. and B. E. Launder (1993). The modelling of the turbulent flow around stationary and vibrating square cylinders. In *Proc. of 9th Symp. on Turbulent Shear Flows*, pp. 10.4–10.10.

Kebede, W., B. E. Launder, and B. A. Younis (1985). Large amplitude periodic flows: a second-moment closure study. In *Proc. of 5th Symp. on Turbulent Shear Flows*.

Kiel, R. and D. Vieth (1995). Experimental and theoretical investigations of the near-wall region in a turbulent separated and reattached flow. *Experimental Thermal and Fluid Sciences 11*, 243–256.

Kim, J. (1990). Technical report. DNS data for channel flow at $Re_\tau = 395$.

Kim, J. (1997). Technical report. DNS data for channel flow at $Re_\tau = 595$.

Kim, J., P. Moin, and N. N. Moser (1987). Turbulence statistics in fully developed channel flow at the low-Reynolds number. *J. Fluid Mech. 177*, 133–166.

Kim, S.-E. and D. Choudhury (1995). A near-wall treatment using wall functions sentized to pressure gradient. In *FED-Vol. 217, Separated and Complex Flows, ASME 1995*, pp. 273–280.

Kuroda, A., N. Kasagi, and M. Hirata (1993). Direct numerical simulation of turbulent plane Couette-Poiseuille flows: effect of mean shear on the near wall turbulence structures. In *TSF9*.

Laufer, J. (1950). Investigation of turbulent flow in a two-dimensional channel. Technical report, NASA TN 2123.

Launder, B. E., G. J. Reece, and W. Rodi (1975). Progress in the development of a re-stress turbulence closure. *J. Fluid Mech. 68*, 537–566.

Launder, B. E. and W. C. Reynolds (1983). Asymptotic near wall stress dissipation rates in a turbulent flow. *Phys. Fluids 26*, 1157–1182.

Launder, B. E. and B. I. Sharma (1974). Application of energy-dissipation model of turbulence to the calculation of flow near a spinning disc. *Lett. Heat Mass Transfer 1*, 131–138.

Launder, B. E. and N. Shima (1989). Second-moment closure for the near-wall sublayer: Development and application. *AIAA J. 27*, 1319–1325.

Launder, B. E. and D. P. Tselepidakis (1991). Progress and paradoxes in modelling near-wall turbulence. *Turbulent Shear Flows 8*, 81–96.

Launder, B. E. and D. P. Tselepidakis (1993). Contribution to the modelling of near-wall turbulence. *Turbulent Shear Flows 8*, 81–96.

Laurence, D., P. A. Durbin, and A. O. Demuren (1995). Modeling near-awll effects in second moment closures by elliptic relaxation. In *TSF10*.

Laurien, E. and L. Kleiser (1989). Numerical simulation of boundary-layer transition and transition control. *J. Fluid Mech. 199*, 403–440.

Le, H., P. Moin, and J. Kim (1997). Direct numerical simulation of turbulent flow over a backward-facing step. *J. Fluid Mech. 330*, 349–374.

Leonard, B. P. (1979). A stable and accurate convective modelling procedure based on quadratic upstream interpolation. *Comput. Methods Appl. Mech. Eng. 19*, 59–98.

Leonard, B. P. (1997). Bounded higher-order upwind multidimensional finite-volume convection-diffusion algorithms. In W. J. Minkowycz and E. M. Sparrow (Eds.), *Advences in Numerical Heat Transfer*, pp. 1–57. Chapter 1.

Lien, F.-S. (1992). *Computational modelling of 3D flow in compex ducts and passages*. Ph. D. thesis, University of Manchester, Institute of Science and Technology.

Lien, F. S. and M. A. Leschziner (1993a). Modelling 2D and 3D separation from curved surfaces with variants of second-moment closure combined with low-Re near wall formulation.

Lien, F. S. and M. A. Leschziner (1993b). Second-moment modelling of recirculating flow with a non-orthogonal collocated finite-volume algorithm. *Turbulent Shear Flows 8*, 205–222.

Lien, F. S. and M. A. Leschziner (1994). A general non-orthogonal collocated finite volume algorithm for turbulent flow at all speeds incorporating second-moment turbulence-transport closure. Part 1: computational implementation. *Comput. Methods Appl. Mech. Engrg. 114*, 123–148.

Lilek, Z., S. Muzaferija, and M. Perić (1997). Efficiency and accuaracy aspects of a full-multigrid SIMPLE algorithm for three-dimensional flows. *Numer. Heat Transfer, Part B 31*, 23–42.

Lumley, J. L. (1975). Pressure-strain correlation. *Phys. Fluids 18*(6), 750–751.

Lumley, J. L. (1978). Computational modelling of turbulent flows. *Adv. Appl. Mech. 18*, 123–176.

Mansour, N. N., J. Kim, and P. Moin (1988). Reynolds-stress and dissipation-rate budgets in a turbulent channel flow. *J. Fluid Mech. 194*, 15–44.

Matsumoto, A., Y. Nagano, and T. Tsuji (1991). Direct numerical simulation of homogeneous turbulent shear flow. In *Proc. of 5th Symp. on Turbulent Shear Flows*.

Mayle, R. E. (1991). The rol of laminar-turbulent transition in gas turbine engines. *Journal of Turbomachinery 113*, 509–537.

Muzaferija, S. (1994). *Adaptive Finite Volume Method for Flow Predictions Using Unstructured Meshes and Multigrid Approach*. Ph. D. thesis, University of London.

Na, Y. and P. Moin (1998). Direct numerical simulation of a separated turbulent boundary layer. *J. Fluid Mech. 370*, 175–201.

Nakabayashi, K., O. Kitoh, and H. Iwata (1991). Turbulent Couette type flow with alternating pressure gradient. In *TSF8*.

Noat, D., A. Shavit, and M. Wolfshtein (1973). Two-point correlation model and the redistribution of Reynolds-stress. *Phys. Fluids 16*, 738–743.

Oberlack, M. (1997). Non-isotropic dissipation in inhomogeneous turbulence. *J. Fluid Mech. 350*, 351–374.

Obi, S. (1991). *Berechnung komplexer turbulenter Strömungen mit einem Reynolds-Spannungs-Modell.* Ph. D. thesis, University of Erlangen.

Obi, S. and H. Hara (1995). An algebraic model od turbulent diffusion. In H. Daiguji and Y. Miyake (Eds.), *Proc. of the Matematical Modelling of Turbulent Flows*, pp. 274–279.

Obi, S., M. Perić, and G. Scheurer (1989). A finite-volume calculation procedure for turbulent flows with second-order closure and collocated variable arrangement. In *Proc. 7th Symp. on Turbulent Shear Flows*, pp. 17.4–17.10.

Parks, S. M., K. Weispfennig, and C. A. Petty (1998). An algebraic preclosure theory for the Reynolds stress. *Phys. Fluids 10*(3), 645–653.

Patankar, S. V. (1980). *Numerical heat transfer and fluid flow.* McGraw-Hill, New York.

Patel, V. C., W. Rodi, and G. Scheuerer (1985). Turbulence models for near-wall and low reynolds number flows: A review. *AIAA Journal 23*, 1308–1319.

Perić, M. (1993). Ein zum Parallelrechnen Geeignetes Finite- Volumen -Mehrgitterverfahren zur Berechnung Komplexer Strömungen auf Blockstrukturierten Gittern mit Lokaler Verfeinerung. Technical report, LSTM, University of Erlangen.

Perot, B. and P. Moin (1995a). Shear-free turbulent boundary layers. Part 1. Physical insights into near-wall turbulence. *J. Fluid Mech. 295*, 199–227.

Perot, B. and P. Moin (1995b). Shear-free turbulent boundary layers. Part 2. New concepts for Reynolds stress transport equation modelling of inhomogeneous flows. *J. Fluid Mech. 295*, 229–245.

Reynolds, O. (1894). On the dynamical theory of incompressible fluids and determination of the criterion. *Philosophical Transactions of the Royal Society 186.*

Reynolds, W. C. (1984). Physical and analytical foundations, concepts and new directions in modelling and simulations. In *Turbulence Models and their Applications*, Volume 2.

Rhie, C. M. and W. L. Chow (1983). A numerical study of turbulent flow past an isolated airfoil with trailing edge separation. *AIAA Journal 21*, 1525–1532.

Roach, P. E. and D. H. Brierley (1990). The influence of a turbulent free stream on zero pressure gradient transitional boundary layer development. Part 1: testcases t3a and t3b. In O. Pironneau, W. Rodi, I. L. Ryhming, A. M. Savill, and T. V. Truong (Eds.), *Numerical simulation of unsteady flows and transition to turbulence*, pp. 319–347.

Rodi, W. and N. N. Mansour (1993). Low Reynolds number $k - -\varepsilon$ modelling with the aid od direct simulation data. *J. Fluid Mech. 250*, 509–529.

Rotta, J. (1951). Statistische Theorie nichthomogener Turbulenz, Part I. *Zeitschrift für Physik 129*, 547–572.

Sana, A. and H. Tanaka (1995). The performance of low reynolds number $k - \varepsilon$ model to analyze an oscillatory boundary layer. In H. Daiguji and Y. Miyake (Eds.), *Proc. of the Matematical Modelling of Turbulent Flows*, pp. 291–296.

Sarkar, A. and R. M. C. So (1997). A critical evaluation of near-wall two equation models against direct numerical simulation data. *Int. J. Heat and Fluid Flow 18*, 197–208.

Savill, A. M. (1993). Some recent progress in the turbulence modelling of by-pass transition. In C. G. S. R. M. C. So and B. E. Launder (Eds.), *Near-Wall Turbulent Flows*. Elsevier Science Publishers B.V.

Savill, A. M. (1996). Transition predictions with turbulence models. In R. A. W. M. Henkes and J. L. van Ingen (Eds.), *Transitional Boundary Layers in Aeronautics*, pp. 311–319. North Holland Amsterdam.

Schlichting, H. (1969). *Boundary-Layer Theory*. McGraw-Hill, New York.

Seume, J. R. (1988). *An Experimental Investigation of Transition in Oscillating Pipe Flow*. Ph. D. thesis, University of Minnesota.

Shih, T.-H. and J. L. Lumley (1985). Modeling of pressure correlation terms in reynolds stress and scalar flux equations. Technical report, FDA-85-3, Cornell University, Ithaca, USA.

Shima, N. (1993). Prediction of turbulent boundary layers with a second-moment closure: Part I - Effects of periodic pressure gradient, wall transpiration and free-stream turbulence. *J. Fluid Eng. 115*, 56–69.

Shima, N. (1995). Modeling of asymptotic near-wall behavior of the Reynolds-stress dissipation. In *Proc. of 10th Symp. on Turbulent Shear Flows*, pp. 2.13–2.18.

Shir, C. C. (1973). A preliminary numerical study of atmospheric turbulent flow in the ideallized planetary boundary layer. *Journal of Atmospheric Sciences 30*, 1327.

Spalart, P. R. and B. S. Baldwin (1989). Direct simulation of a turbulent oscillating boundary layer. *Turbulent Shear Flows 6*, 417–440.

Spalart, P. R. and G. N. Coleman (1997). Numerical study of a separation bubble with heat transfer. *Eur. J. Mech., B./Fluids 16*, 169–189.

Spalart, P. R., W.-H. Jou, M. Strelets, and S. R. Allmaras (1997). Comments on the feasibility of les for wings, and on hybrid rans/les approach. In *First AFOSR Int. Conf. on Direct Numerical Simulation and Large Eddy Simulation*.

Spalart, P. R. and M. K. Strelets (1997). Direct and Reynolds-averaged numerical simulations of a transitional separation bubble. In *Proc. of 11th Symp. on Turbulent Shear Flows*.

Spalart, P. R. and K. S. Yang (1987). Numerical study of ribbon-induced transition in Blasius flow. *J. Fluid Mech. 178*, 345–365.

Speziale, C. G., R. Abid, and P. A. Durbin (1994). On realizability of Reynolds stress turbulence closures. *Journal of Scientific Computing 9*(4), 369–403.

Speziale, C. G., S. Sarkar, and T. B. Gatski (1991). Modelling the pressure-strain correlation of turbulence: an invariant dynamical systems approach. *J. Fluid Mech. 227*, 245–272.

Suga, K. (1997). Nonlinear eddy viscosity modeling with a transport equation for Lumley's stress flatness parameter. In *Proc. of 11th Symp. on Turbulent Shear Flows*, pp. 13.18.

Tavoularis, S. and S. Corrsin (1981). Experiments in nearly homogeneous turbulent shear flow with a uniform mean tempe rature gradient. Part 1. *J. Fluid Mech. 104*, 311–347.

Tu, S. W. and B. R. Ramaprian (1983). Fully developed periodic turbulent pipe flow. Part 1. Main experimental results and comparison with predictions. *J. Fluid Mech. 137*, 31–58.

van Leer, B. (1974). Towards the ultimate conservative difference scheme. V. A second-order sequel to Godunov's method. *J. Comput. Phys. 32*, 101–136.

Voke, P. R. and Z. Yang (1995). Numerical study of bypass transition. *Phys. Fluids 7*(9), 2256–2264.

Wadcock, A. J. (1980). Two-dimensional stalled airfoil. In S. J. Kline, B. J. Cantwell, and G. M. Lilley (Eds.), *The 1980-81 AFOSR-HTTM-Stanford Conference on Complex Turbulent Flows*, Volume 1, pp. 234–252.

Westin, K. J. A. and R. A. W. M. Henkes (1996). Prediction of by-pass transition with differential reynolds stress models. Technical report, Delft University of Technology, Faculty of Aerospace Engineering.

Yang, Z. and P. R. Voke (1993). Large-eddy simulation of transition under turbulence. Technical report, University of Surrey. ME-FD/93.12.

Yang, Z. and P. R. Voke (1995). Large-eddy simulation of boundary layer transition on a flat plate with semi-circular leading edge. In *TSF10*.

Yap, C. R. (1987). *Turbulent heat and momentum transfer in recirculating and impinging flows.* Ph. D. thesis, UMIST Manchester, UK.

Summary

Second-Moment Closure Modelling of Transitional and Unsteady Turbulent Flows

Statistical modelling of turbulent fluid flows, based on Reynolds-averaging of the fluctuating flow quantities, aims at determining the averaged quantities which are needed for computation, analysis and design of a variety of industrial, environmental and biological flows. Among several statistical modelling techniques, the second-moment closure (SMC) is the approach which has the best physical foundation and still remains simple and applicable for solving real problems. This becomes particularly important in predicting transitional and other low-Re-number turbulent flows. Although most flows in engineering and nature are highly turbulent, there are many situations of practical relevance where the viscosity effects play important role and cannot be ignored. Such flows often undergo laminar-to-turbulent and reverse transition and some involve a simultaneous coexistence of the laminar and fully turbulent regime in the flow domain of interest. Low-Re-number effects are also always present in near-wall regions in all wall bounded turbulent flows. The Reynolds-averaging approach conceals, by its virtue, the dynamics of the flow disturbances and, therefore, is not capable of predicting the actual transition mechanism. However, this modelling technique is capable of predicting the transition to turbulence when even a small source of turbulence exists in the flow or at its edge, as for example the by-pass transition in wall bounded flows, separation induced transition and oscillating wall flows. The ability to predict a change-over from one regime to another at appropriate location and under appropriate conditions, and consequent modifications of mean flow parameters, without having to introduce any artificial triggering, serve the purpose of computing complex industrial flows involving transition.

This thesis deals with computational modelling of the wall-bounded fluid flows in arbitrary geometries at transitional and higher Re-numbers using SMC statistical turbulence models. The two main objectives of this study are: *i*) to investigate possibilities for modelling of transitional wall flows by second-moment closure modelling, to provide a comparative and critical analysis of the existing models, and to contribute to their improvement and validation; *ii*) to establish a reliable, accurate and efficient numerical solution procedure for solving the second-moment closure transport models for arbitrary two-dimensional flow domains with applying both the wall functions and integration of the model equations up to the wall with applying the exact wall boundary conditions.

Chapter 2 presents the rationale of high- and low-Re-number second-moment closures. Because transitional flows are in focus, attention is given to low-Re-number turbulence models with integration up to the wall. Possibilities for modelling of transitional flows with two second-moment closure models were investigated: the Hanjalić-Jakirlić (HJ) model and the Durbin elliptic relaxation model. It was found that the latter model is not very stable when the numerical grid near the wall is very fine. Because it is difficult to control the grid distribution in an unknown situation and, especially, in the transitional flows where the laminar and turbulent flow regions may appear within the same flow, the elliptic relaxation model was not pursued beyond some tentative investigation. Nevertheless the elliptic relaxation modelling of the wall effects on

the pressure strain correlation, shows potential for further exploration in computation of turbulent non-equilibrium flows and it is probably a good candidate for a turbulence model aimed at general application.

Alternative routes to modelling of some of the terms in the transport equations for the Reynolds-stresses have also been explored. A new model of the dissipation rate tensor ε_{ij} was proposed. The model, aimed at improving the behaviour of ε_{ij} in the viscous sublayer, provides correct wall limit values and is free from the wall topology information. It proved also to be computationally convenient. An alternative approach of deriving the pressure-strain correlation models was also proposed. The model is based on modelling the pressure fluctuations using fluctuating and averaged quantities. Instead of the Poisson equation for fluctuating pressure, as used conventionally, this approach models directly the gradient of the fluctuating pressure which appears in the velocity-pressure/gradient correlation. This is done in terms of fluctuating and mean velocity, and turbulence time scale by approximating the Navier-Stokes equation for fluctuating motion. The determination of the model coefficients follows the same procedure as in the conventional approach. A term by term analysis of the conventional models of the dissipation rate equation using results from direct numerical simulation (DNS) is also proposed with suggestion for possible improvement for non-equilibrium flows.

Chapter 3 presents the essential features of the numerical approach used for solving modelled equations with the wall functions and with the exact wall boundary conditions. Special attention is given to obtaining accurate solution and providing sufficient stability of the numerical solver in order to enable application of the SMC models in geometrically and physically complex flows. A numerical code for solving SMC models on two-dimensional, collocated, non-orthogonal, block-structured, body-fitted grids with block-wise grid refinement has been developed. The high accuracy of the procedure is achieved by using QUICK and TVD schemes for discretisation of the convective terms in the transport equations. The application of higher order schemes was found to be crucial for obtaining accurate solution, especially in more complex geometries involving flow separation. The high stability of the procedure is achieved by introducing, in a specific manner, an isotropic artificial turbulent viscosity in the momentum equations.

Since the HJ model was found to perform satisfactory in a broad range of non-equilibrium flows, this model was further applied to the transitional flows. Jointly with some basic test cases for low Re-number model, such as channel and boundary-layer flows, the optimisation of the model coefficients was done using available DNS and experimental data for oscillating boundary layer flows at transitional Re-number. Such a choice of the model coefficients of the low-Re-number SMC model provides satisfactory results in transitional flows as well as in the fully turbulent wall flows.

Subsequent two chapters present applications and model validation in two major classes of transitional flows. In Chapter 4 attention is focussed on the oscillating and pulsating flows at transitional and higher Re-numbers. Chapter 5 presents results of the model validation and its application to transitional flows involving bypass transition and the separation induced transition in a range of conditions. In most of the cases the SMC model shows obvious advantages and better performances than any other model available in the literature. It is important to mention here that all transitional flows were predicted *without* prescribing or triggering the transition or any other empirical input, as often practised in models for transitional flows. The ability

to predict transition and its location without external trigger is the essential requirement for a general model for complex flows.

Samenvatting

Tweede-orde sluitingsmodellering van transitionele en instationaire turbulente stromingen

Statistisch modelleren van turbulente stromingen, gebaseerd op Reynolds-middeling van de fluctuerende stromingsgrootheden, richt zich op de bepaling van de gemiddelde grootheden die nodig zijn voor de berekening, analyse en het ontwerp van een keur aan industriële, milieu-technische en biologische stromingen. Temidden van verschillende statistische modelleringstechnieken, is tweede-orde sluiting (SMC) de benadering die de meest hechte fysische onderbouwing heeft en desondanks eenvoudig en toepasbaar blijft voor het oplossen van reële problemen. Dit wordt voornamelijk belangrijk bij het voorspellen van transitionele stromingen en andere turbulente stromingen bij lage Reynoldsgetallen. Hoewel de meeste stromingen in de techniek en in de natuur sterk turbulent zijn, zijn er ook vele praktisch relevante gevallen waar de effecten van viscositeit een belangrijke rol spelen en niet veronachtzaamd kunnen worden. Dergelijke stromingen ondergaan vaak omslag van laminair naar turbulent en omgekeerd en sommige bevatten gelijktijdig het laminaire en het volledig turbulente regime in het beschouwde stromingsdomein. Lage-Reynolds effecten zijn ook altijd aanwezig in gebieden nabij een wand in wandgebonden turbulente stromingen. De aanpak met behulp van Reynolds-middeling verbergt van nature de dynamica van verstoringen in de stroming en is derhalve niet geschikt voor het voorspellen van het eigenlijke omslagmechanisme. Desalniettemin is deze modelleringstechniek in staat om de omslag naar turbulent te voorspellen wanneer slechts een kleine bron van turbulentie in de stroming of aan de rand aanwezig is, zoals bijvoorbeeld in het geval van bypass-transitie bij wandgebonden stromingen, loslating geïnduceerde omslag en oscillerende wanden. De mogelijkheid om de overgang van het ene naar het andere regime te voorspellen op de juiste plaats en onder de juiste voorwaarden, en de daaruitvolgende wijzigingen van gemiddelde stromingsparameters, zonder het introduceren van kunstmatig triggeren, heeft tot doel om complexe industriële stromingen met omslag te berekenen.

Dit proefschrift behandelt de numerieke modllering van wandgebonden stromingen in willekeurige geometrieën rond transitionele en hogere Reynoldsgetallen met behulp van SMC statistische turbulentiemodellen. De twee belangrijkste doelen van deze studie zijn: i) om de mogelijkheden te onderzoeken voor de modellering van transitionele wandstromingen met behulp van tweede-orde sluitingsmodellering, om een vergelijkende en kritische analyse te verschaffen van de bestaande modellen, en om bij te dragen aan de verbetering en validatie daarvan; ii) om een betrouwbare, nauwkeurige en efficiënte numerieke oplosprocedure te verkrijgen voor het oplossen van SMC transportmodellen voor willekeurige twee-dimensionale stromingsdomeinen onder het toepassen van zowel wandfuncties als het doorintegreren van de modelvergelijkingen tot op de wand met de exacte randvoorwaarden aan de wand.

Hoofdstuk 2 behandelt de basis van tweede-orde sluitingsmodellen voor hoge en lage Reynoldsgetallen. Omdat de nadruk ligt op transitionele stromingen, wordt er aandacht geschonken aan lage-Reynolds turbulentiemodellen, met integratie tot op de wand. De mogelijkheden voor het modelleren van transitionele stromingen met twee SMC modellen zijn onderzocht: het model van Hanjalić-Jakirlić (HJ) en het elliptische relaxatiemodel van Durbin. Dit laatste model is niet

erg stabiel gebleken wanneer het rekenrooster bij de wand zeer fijn is. Omdat het moeilijk is om de verdeling van de gridpunten te controleren in onbekende situaties en vooral in transitionele stromingen waar laminaire en turbulente gebieden kunnen voorkomen in dezelfde stroming, is het elliptische relaxatiemodel slechts verkennend onderzocht. Desondanks laat de elliptische relaxatiemodellering van de wandeffecten op de pressure-strain correlatie mogelijkheden zien voor nader onderzoek naar de berekening van turbulente niet-evenwichtsstromingen en is het waarschijnlijk een goede kandidaat voor een turbulentiemodel dat is gericht op algemene toepassingen.

Alternatieven voor de modellering van sommige termen in de transportvergelijkingen voor de Reynoldsspanningen zijn ook onderzocht. Een nieuw model voor e dissipatie-snelheidstensor ϵ_{ij} is voorgesteld. Het model, gericht op de verbetering van het gedrag van ϵ_{ij} in de visceuze sublaag, verschaft de correcte limietwaarden bij de wand en is vrij van informatie over de wandtopologie. Het bleek ook numeriek geschikt te zijn. Een alternatieve aanpak voor het afleiden van de pressure-strain correlatiemodellen is ook voorgesteld. Het model is gebaseerd op de modellering van drukfluctuaties met gebruik van zowel fluctuerende als gemiddelde grootheden. In plaats van de Poisson-vergelijking voor de fluctuerende druk, zoals meestal gebruikt, modelleert deze aanpak direct de gradient van de fluctuerende druk die verschijnt in de correlatie tussen de snelheid en de drukgradient. Dit is gedaan in termen van fluctuerende en gemiddelde snelheid en turbulente tijdsschaal door het benaderen van de Navier-Stokes vergelijking voor fluctuerende bewegingen. Het bepalen van de modelcoëfficiënten volgt dezelfde procedure als in de conventionele aanpak. Tevens is een termsgewijze analyse van de conventionele modellen voor de dissipatie-snelheid vergelijking voorgesteld met gebruik van directe numerieke simulaties (DNS) en suggesties voor mogelijke verbeteringen bij niet-evenwichtsstromingen.

Hoofdstuk 3 behandelt de essentiële punten van de numerieke aanpak die is gebruikt voor het oplossen van de gemodelleerde vergelijkingen met wandfuncties en met de exacte randvoorwaarden op de wand. Speciale aandacht is gegeven aan het bereiken van een nauwkeurige oplossing en het verschaffen van voldoende stabiliteit van de numeriek oplossingsmethode om de toepassing van de SMC-modellen mogelijk te maken in geometrisch en fysisch complexe stromingen. Er is een numerieke rekencode ontwikkeld voor het oplossen van SMC-modellen op twee-dimensionale, gecolloceerde, niet-orthogonale, blok-gestructureerde, body-fitted grids met bloksgewijze gridverfijning. De grote nauwkeurigheid van de procedure is bereikt door het toepassen van QUICK en TVD-schema's voor de discretisatie van de convectieve termen in de transportvergelijkingen. Het toepassen van hogere-orde schema's is cruciaal gebleken voor het bereiken van nauwkeurige oplossingen, vooral in meer complexe geometrieën waar loslating van de stroming optreedt. De grote stabiliteit van de procedure is verkregen door het op een specifieke wijze introduceren van een isotrope kunstmatige turbulente viscositeit in de impulsvergelijkingen.

Omdat het HJ-model bleek te voldoen in een breed spectrum van niet-evenwichtsstromingen, is dit model verder toegepast op de transitionele stromingen. Tesamen met enige standaard testgevallen voor lage-Reynolds modellen, zoals kanaal- en grenslaagstromingen, is de optimalisatie van de modelcoëfficiënten uitgevoerd met behulp van beschikbare DNS-data en experimentele data voor oscillerende grenslaagstromingen bij transitionele Reynoldsgetallen. Een dergelijke keuze voor de modelcoëfficiënten van het lage-Reynolds SMC model verschaft bevredigende

resultaten in transitionele stromingen en in volledig turbulente wandstromingen.

De hieropvolgende twee hoofdstukken behandelen toepassingen en modelvalidatie in twee belangrijke klassen van transitionele stromingen. In hoofdstuk 4 wordt de aandacht gericht op de oscillerende en pulserende stromingen rond transitionele en hogere Reynoldsgetallen. Hoofdstuk 5 behandelt de resultaten van modelvalidatie en de toepassing op transitionele stromingen, met bypass-transitie en door loslating geïnduceerde omslag in een reeks condities. In de meeste gevallen laat het SMC model duidelijke voordelen en betere prestaties zien dan ieder ander in de literatuur beschikbaar model. Het is belangrijk om hier te vermelden dat alle transitionele stromingen zijn voorspeld *zonder* het voorschrijven of triggeren van transitie of enige andere empirische input, zoals vaak wordt gedaan bij modellen voor transitionele stromingen. De mogelijkheid om omslag en de locatie daarvan te voorspellen zonder uitwendige trigger is een essentiële eis aan algemene modellen voor complexe stromingen.

Acknowledgement

The research for this thesis I performed at the Institute of Fluid Mechanics (LSTM) of the University of Erlangen-Nürnberg, Germany, and the Heat Transfer Section of the Delft University of Technology, The Netherlands.

In the first place, I would like to express my gratitude to my supervisor, Professor Kemal Hanjalić, for his invaluable advice, guidance and encouragement throughout of my studies.

I am especially thankful to Prof. Dr. Dr. h. c. Franz Durst, the head of LSTM, for providing the work conditions and financial support for a large colony of the exile Bosnian researchers, including myself. I greatly acknowledge the financial support of the International office of the Forschungszentrum Jülich, Germany, and of the Max-Plank award to Professors F. Durst and K. Hanjalić, that made my stay in Germany possible.

Professor Milovan Perić of the University of Hamburg kindly gave me a version of a computer code he developed, which was an essential basis for my research. I am also very thankful to him for his guidance and encouragement while I was familiarising myself with this code and the numerical techniques.

I am grateful to the members of the thesis committee for valuable comments on the manuscript of this thesis.

I would like to thank Dr. P. Spalart of Boing, Dr. T. Kajishima of the Osaka University, Dr. E. Guilmineau of the Ecole Centrale de Nantes and Dr. J. Coupland of the Rolls-Royce ASL for providing me with the DNS and experimental data that I used in the course of this study.

My thanks also go to Dr. Suad Jakirlić, Prof. Dominique Laurence, Prof. Shinnosuke Obi and Prof. Nikola Stošić for numerous discussions on the turbulence modelling and its numerical aspects. I want to express my gratitude to Professor Ismet Demirdžić and Dr. Samir Muzaferija who were my first teachers in the fluid mechanics.

I would like to thank to those people who have been my colleagues in my research during all these years, particularly to Dr. Mirek Weclas, Johan Volkert, Dr. Anne Cadiou, Dr. Henri Pascal, Robbert Verweij, Bojan Ničeno, Dr. Stefan Heinz, Kržištof Stawiarski. I owe a great debt of thanks to those people who have provided long and steady support in area of great interest and importance to me: Enes Đedović, Suad Ganibegović, Midhat Hajrović, Dr. Basim Abu Jdail, Nedžad Malkić. I would like to thank Margaret van de Loo and Dr. Theo van der Meer for their assistance at many occasions that made my stay in Holland more pleasant, Jaap Bekman for his engagement to keep the computing facilities running properly and Bram Starke for translating some parts of this thesis into Dutch.

I would like to thank my parents, my sisters and my brother for their love, support and encouragement during my studies. My special thanks go to Enisa for her support and patience.

Some of computations were carried out on the CRAY-computers of the Computing center München and of the Stichting Academisch Rekencentrum Amsterdam (SARA).

Ibrahim Hadžić

About the author

1 February 1968	Born in Dubrave Donje, district Živinice, Bosnia-Herzegovina (BH)
1982 - 1986	Technical High School of Mechanical Engineering in Tuzla, BH
1986 - 1991	Studied mechanical engineering at the Faculty of Mechanical Engineering Sarajevo of the University of Sarajevo, BH
1991 - 1992	Research assistant at Faculty of Mechanical Engineering, University of Sarajevo
1992 - 1995	Research assistant at Institute of Fluid Mechanics (LSTM), University of Erlangen-Nürnberg, Germany
1995 -	Research assistant, Section Thermofluids, Faculty of Applied Sciences, Delft University of Technology, Delft, The Netherlands